A NUMERICAL AND EXPERIMENTAL STUDY

OF WINDBACK SEALS

A Dissertation

by

CHAE HWAN LIM

Submitted to the Office of Graduate Studies of
Texas A&M University
in partial fulfillment of the requirements for the degree of

DOCTOR OF PHILOSOPHY

May 2009

Major Subject: Mechanical Engineering

A NUMERICAL AND EXPERIMENTAL STUDY

OF WINDBACK SEALS

A Dissertation

by

CHAE HWAN LIM

Submitted to the Office of Graduate Studies of
Texas A&M University
in partial fulfillment of the requirements for the degree of

DOCTOR OF PHILOSOPHY

Approved by:

Chair of Committee,   Gerald L. Morrison
Committee Members, J. C. Han
                                Luis San Andres
                                Hamn-Chin Chen
Head of Department, Dennis L. O'Neal

May 2009

Major Subject: Mechanical Engineering

ABSTRACT

A Numerical and Experimental Study of Windback Seals.

(May 2009)

Chae Hwan Lim, B.S., Sungkyunkwan University;

M.S., Texas A&M University

Chair of Advisory Committee: Dr. Gerald L. Morrison

Windback seals work similarly to labyrinth seals except for the effect of helical groove. These seals are essentially a tooth on stator or tooth on rotor labyrinth seal where the grooves are a continuous helical cut like a thread. Windback seals are used in centrifugal gas compressor to keep oil out of the gas face seal area. These face seals cannot be contaminated by oil. A purge gas is applied to the seal to help force the oil back into the bearing area.

The windback seal should be designed to prevent any oil contamination into the supply plenum and to reduce purge gas leakage. The CFD simulations have been performed with the effect of clearance, tooth width, cavity shape, shaft rotation, eccentricity, and tooth location on the seal leakage performance and the flow field inside the seal. The leakage flow rate increases with increasing the pressure differential, rotor speed, radial clearance, cavity size, and shaft diameter and with decreasing the tooth width. The eccentricity has a minimal effect for the windback seal. From oil simulations, the windback seal with 25% rotor eccentricity has some of the journal bearing action and drives back flow into the gas plenum. However the windback seal can be used to force

the oil back into the bearing side before starting the compressor by applying a purge gas flow since the positive axial velocity inside the cavity is larger than the negative axial velocity. $\dot{m}/\rho A_{cav} Rw$ is constant for varying shaft rotation since the leakage flow rate for the windback seal increases linearly as the the rotor speed increases. The leakage flow rate for the windback seal increases as the groove size increases due to the pumping action of the windback seal. A windback seal design based upon the numerical simulations that minimize gas leakage and help prevent gas face seal oil contamination was optimized.

The windback seal has two leakage flow paths. Since the leakage flow rate under teeth of windback seals is the same as for a similar geometry labyrinth seal, the flow under the teeth can be predicted by two-dimensional labyrinth seal analysis. An empirical model for the leakage rate through the cavity has been developed which fits the data with a standard deviation of 0.12.

DEDICATION

This work is dedicated to my wife Soyoung, my son Alex and my parents.

ACKNOWLEDGMENTS

TABLE OF CONTENTS

LIST OF TABLES

NOMENCLATURE

A	Leakage area of seal πDc [m^2]
A_{cav}	Seal cavity area [m^2]
c	Radial seal clearance [m]
C_d	Discharge coefficient
D	Shaft diameter [m]
DP	Differential pressure across seal [kPa]
h	Seal cavity depth [m]
i, j	index notation (1,2,3 representing x, y and z directions)
k	Gas specific heat ratios
L	Seal length [m]
$\dot{m}$	Total leakage mass flowrate [kg/s]
$\dot{m}_{cav}$	Leakage mass flowrate through the seal cavity [kg/s]
$\dot{m}_{utooth}$	Leakage mass flowrate under the tooth [kg/s]
n	Equivalent number of teeth L/s
P	Static pressure [Pa]
$\dot{Q}$	Air volumetric flowrate [m^3/s]
$\dot{Q}_{cavity}$	Air volumetric flowrate through the seal cavity [m^3/s]
$\dot{Q}_{total}$	Total air volumetric flowrate [m^3/s]
$\dot{Q}_{undertooth}$	Air volumetric flowrate under the tooth [m^3/s]

R	Air constant [J/(kg.K)]
Re	Axial Reynolds number $\dot{m}/\pi D\mu$
Re$_{cir}$	Circumferential Reynolds number $\rho\Omega Dc/(2\mu)$
s	Tooth pitch [m]
t	Tooth thickness [m]
T	Temperature [K$^\circ$]
Ta	Taylor number $\mathrm{Re}_{cir}^2(2c/D)$
x, y, z	Rectangular coordinate direction
r,θ,x	Cylindrical coordinate direction

Greek symbols

ρ	density [kg/m^3]
μ	Dynamic viscosity [Pa.s]
Ω	Rotor speed [rpm]
κ	Turbulence kinetic energy [m^2/s^2]
α	Flow coefficient
γ	Kinetic energy carry over coefficient
ψ	Expansion coefficient or Pressure function
ν	Specific Volume [m^3/kg]
ε	Turbulent dissipation rate [m^2/s^3]

Subscripts

i   Inlet condition

e   Exit condition

Abbreviations

CFD   Computational fluid dynamics

TOS   Tooth on Stator

TOR   Tooth on Rotor

rpm   Revolution per minute

INTRODUCTION

Non-contacting seals are primarily used to reduce the fluid leakage inside systems such as pumps, compressors, and gas and steam turbines. Labyrinth seals are usually used in rotating machines. When the fluid enters a seal, it is forced through the small clearance of the first tooth and some of the pressure drop is converted into kinetic energy. The large portion of this kinetic energy is dissipated by turbulent viscous loss in the chamber downstream. The higher velocities have greater dissipation and increased turbulence generation. Each tooth of a labyrinth seal converts a portion of the available pressure head into mean flow kinetic energy, some of which is dissipated within the cavity immediately downstream. The design tool of seals can be developed by providing a highly dissipative flow path between high and low pressure regions.

Cetrifugal gas compressors use windback seals to keep oil out of the gas face seal area. These face seals can not be contaminated by oil. The geometry of windback seals is very similar to that of labyrinth seals. These seals are essentially a tooth on stator or tooth on rotor labyrinth seal where the grooves are a continuous helical cut like a thread. Windback seals work similarly to labyrinth seals except for the effect of helical groove. A gas purge is applied to the seal to help force the oil back into the bearing area. The helical groove of windback seal has the pumping action through the groove and this pumping action can be used by applying a purge gas flow.

This dissertation follows the style of the *ASME Journal of Fluid Mechanics*.

The most important application for the windback seal inside a gas compressor is how it works when oil is inside the seal. A smooth annular seal with rotor eccentricity may produce a pressure field which forces oil into the gas face seal area. Oil leaks to both the bearing side and gas compressor side. The helical groove of a windback seal reduces this pumping action by diminishing the journal bearing action.

The windback seal should be designed to prevent any oil contamination into the supply plenum (high pressure side) and to reduce purge gas leakage. The geometry of the seal has several effects on the seal leakage performance and the flow field inside the seal. Therefore, this study considers clearance, tooth width, cavity shape, shaft diameter, and tooth location (tooth on stator or tooth on rotor) to develop a windback seal design.

LITERATURE REVIEW

Windback seals have rarely been studied. However, windback seals are geometrically similar to labyrinth seals. Various studies have been performed for labyrinth seals. Therefore, a literature review of labyrinth seals will be presented in this section.

Most of the previous labyrinth seal work was performed to develop empirical and numerical relationships between the leakage rate, pressure drop, seal geometry, and shaft speed. Martin (1908) developed one of the first leakage models for labyrinth seals. He assumed isothermal flow of ideal gas through a series of orifices. He also assumed that all kinetic energy in each throttling chamber was completely dissipated from one throttling to another.

Egli (1935) improved the leakage characteristics of labyrinth seals in Martin's (1908) labyrinth formula. He developed an empirical method to predict the performance of both straight through and staggered labyrinth seals with constant leakage area. He stated that the staggered labyrinth seal clearly was a better seal than the straight through seal but it was more difficult to manufacture and more expensive than the straight through seal. He began his analysis by examining an isentropic expansion of compressible fluid through a single ideal orifice. His method presented the effect of kinetic energy carry-over from one throttling into the next as a function of the number of throttles and the clearance to pitch ratio. The results showed that the kinetic energy carry-over increased as the clearance to pitch ratio and the number of throttles increased.

The leakage equation was a function of upstream fluid conditions, flow coefficient, leakage area of throttling, expansion coefficient, and carry-over coefficient. It is given by

$$\dot{m} = A\alpha\psi\gamma\sqrt{\frac{P_i}{v_i}} \tag{1}$$

$$\psi = \sqrt{\frac{1-(P_e/P_i)^2}{n+\ln(P_i/P_e)}} \tag{2}$$

where α is flow coefficient, ψ is expansion coefficient, and γ is carry-over coefficient. The flow coefficient and expansion coefficient were presented empirically and graphically and were based on the number of throttles, pressure ratio, and clearance to tooth width ratio. His experimental results indicate that the flow coefficient is constant when the clearance to tooth width ratio is more than 3.5. For values less than 3.5, the flow coefficient increases as the clearance decreases. He also considered the pressure drop in each chamber of the seal, but not the effect of shaft rotation and variable area.

Hodkinson (1939) accounted for the kinetic energy carry-over with fluid mechanics instead of the previously used thermodynamics. He represented the leakage in a labyrinth seal as flow passing through a series of perfect nozzles. He modeled the carry-over coefficient as a function of the number of throttles and the clearance to pitch ratio. It is given by

$$\gamma = \sqrt{\dfrac{1}{1 - \dfrac{n-1}{n} \cdot \dfrac{c/s}{c/s + 0.02}}}$$

(3)

where n is number of throttles, c is clearance, and s is tooth pitch. He stated, based upon experiment, that the effects of shaft rotation were negligible on leakage. The results of his analysis were within about 5% of the experimental data.

Zabriskie and Sternlieht (1959) presented a method for calculation of labyrinth seal leakage. This prediction utilizes a friction factor as a function of Reynolds number which is then related to the mass rate of the flow and the pressure ratio across the seal. He considered the clearance, overall pressure ratio, and entrance pressure and temperature as the primary factors for controlling the leakage. The results were within 20% accuracy of actual test data. This method can be used for staggered and straight through seals but there are some limitations for various tooth configurations due to the lack of friction factor data.

Heffner (1960) studied the leakage problem through labyrinth seals by reasoning the basic equation that describes the flow is the same as the flow through single orifices. He also compared theoretical criterion and experimentally determined the critical pressure ratio. He established the flow coefficient using the empirical data. The flow coefficient was presented graphically and was based on the Reynolds number, mass flow rate, and clearance. Using this approach, the results were within 3% accuracy of actual test data. He considered velocity carry-over for straight-through seals but not the effect of shaft rotation.

Stoff (1980) investigated incompressible flow in seals using a numerical study based upon computational fluid mechanics. The computer code, based on the TEACH program, was used to solve the Reynolds averaged Navier-Stokes equations using a k-ε turbulence model. Experimental measurements obtained by using Laser-Doppler anemometry were compared with the numerical predictions. His measurements and predictions of mean swirl velocity were within about 7%.

Cogan (1982) compiled investigations of previous existing prediction analyses for leakage in labyrinth seals. He summarized the leakage prediction methods from Martin's (1908) formula up to the open literature in 1972. The leakage data for straight through seals investigated and analyzed have been non-dimensionalized. He used Egli's (1935) equation for his analysis. The effects of clearance, tooth width, tooth height, shaft rotation, and number of throttles were compared with the experimental data. Table 1 shows a summary of his analysis in straight through labyrinth seals. Cogan's summary can differ if seals have different flow conditions such as higher pressure drop and small clearance.

Rhode and Hibbs (1993) studied the clearance effect on annular and labyrinth seal leakage. They developed a previous Reynolds averaged Navier-Stokes equation based finite difference computer code to predict seal leakage directly from given upstream and downstream reservoir pressures. Their predictions were in excellent agreement within 8% of previous measurements. They found that annular seals leaked 20% more than labyrinth seals for various clearances.

Table 1 Effect of flow conditions and seal geometry for leakage in the labyrinth seal

	Flow coefficient, α	Remark
Clearance ↑	↑	For very small clearance, clearance ↓, α ↑
Tooth width ↑	↑	
Tooth height ↑	Constant	
Shaft rotation ↑	↓	Small effect
# of throttles ↑	↓	
Eccentricity		No significant effect

Liquid-lubricated bearings with spiral grooves were investigated by Boostma (1975). He theoretically studied load capacity, frictional losses, and stability of spiral groove journal bearings. A liquid lubricated self-sealing bearing with a spiral groove was studied experimentally. This experiment was mainly performed with the bearing having a free boundary. In an eccentrically operating self-sealing spiral groove journal bearing the bearing gap was filled completely with a lubricant in the middle. His experimental data were in good agreement with the theory for a self-sealing herringbone journal bearing at various eccentricities. He found that leakage starts at a lower speed of shaft rotation than in conditions of concentric operation in a bearing with a static load, but at a higher speed of shaft rotation in a bearing with imbalance load.

Gansle and Childs (1996) measured leakage for helically-grooved annular gas seals. He tested three grooved seals with helix angles of 0°, 15°, and 30° against shaft

rotation. The helix angle varies from zero (circumferential grooving) to 90° (axial grooving). Leakage test comparison between helically grooved seals, a smooth seal, and a honeycomb-stator seal was performed without any analytical or computational development. The results showed that the 15° helix groove seal, 30° helix groove seal and smooth seal leaked about 1.66, 2.2 and 2.3 times more than the honeycomb-stator seal.

There were no significant effects of seal shaft eccentricity upon labyrinth seal leakage for incompressible fluid flow as indicated by Yeh and Cochran (1970), and Nikitin and Ipatov (1973). Marquette and Childs (1997) studied the rotor eccentricity effects on the rotordynamic coefficient and the leakage flow rate. The leakage flow rate increased slightly with increasing rotor eccentricity, increases with increasing pressure drop, and decreases with increasing shaft rotation speed. When the rotor eccentricity ratio was changed from 0 to 0.5, the leakage flow rate increased about 4%.

Al-Ghasem (2007) numerically and experimentally studied the seal leakage and flow field for the windback seal. He used the FLUENT (2005) CFD program to perform numerical simulations. He presented the effect of clearance, tooth pitch, cavity depth and the tooth number of starts on the leakage flow rate. The leakage flow rate increased slightly with increasing the rotor speed, increased with the seal clearance, increased with increasing the cavity depth, increased with increasing the tooth pitch, and increased with increasing the number of starts. The measurements were in excellent agreement within 5% of the predictions. The simulations adequately predicted shaft rotation effects. This will allow subsequent experimental results to simulations.

OBJECTIVES

The main purpose of seals in turbomachinery is to prevent and minimize internal leakage from a region of high pressure to a region of lower pressure. However, this is a secondary purpose for windback seals. Their main purpose inside compressors is to isolate oil from gas face seals. From the literature review, numerical and experimental studies of labyrinth seals have been conducted for many years. There is a large database for labyrinth seals on the open literature. However, there is very little published information for windback seals.

The purpose of this study for windback seals is to provide useful information that can be applied to improve the seal design. In order to develop a better design for windback seals, the effects of tooth width, cavity shape, cavity depth, tooth location (tooth on stator or tooth on rotor), and the direction of shaft rotation are investigated. Then, seal design can be improved. The study emphasizes as the following:

1. physical modeling of the transport phenomenon in windback seals
2. preventing gas face seal oil contamination
3. minimizing gas leakage
4. increasing seal durability

NUMERICAL PROCEDURE

Computational fluid dynamics is used to investigate seal performance before a seal is constructed. The numerical simulations will provide information about the leakage, pressure distribution, and fluid motion. The computer simulation is performed using the program FLUENT (2005) version 6.1.22. FLUENT (2005) solves unstructured, structured and hybrid grids and has the ability to adaptively modify the grid. FLUENT (2005) solves the time averaged conservation of mass and Navier-Stokes equations, written in Cartesian.

$$\frac{\partial \rho}{\partial t} + \frac{\partial}{\partial x_i}(\rho u_i) = 0 \tag{4}$$

$$\frac{\partial}{\partial t}(\rho u_i) + \frac{\partial}{\partial x_j}(\rho u_i u_j) = \tag{5}$$

$$-\frac{\partial p}{\partial x_i} + \frac{\partial}{\partial x_j}\left[\mu(\frac{\partial u_i}{\partial x_j} + \frac{\partial u_j}{\partial x_i} - \frac{2}{3}\delta_{ij}\frac{\partial u_i}{\partial x_i})\right] + \frac{\partial}{\partial x_j}(-\rho\overline{u_i' u_j'})$$

These equations are called the Reynolds-averaged Navier-Stokes equations.

In the standard k-ε model, Reynolds stresses are modeled using the Boussinesq hypothesis

$$-\rho\overline{u_i'u_j'} = \mu_t\left(\frac{\partial u_i}{\partial x_j} + \frac{\partial u_j}{\partial x_i}\right) - \frac{2}{3}\left(\rho\kappa + \mu_t\frac{\partial u_i}{\partial x_i}\right)\delta_{ij} \qquad (6)$$

$$\mu_t = \rho C_\mu \frac{k^2}{\varepsilon} \qquad (7)$$

where the turbulent viscosity, μ_t, is computed by combining turbulent kinetic energy, k, and its rate of dissipation, ε.

The turbulence kinetic energy, k, and its rate of dissipation, ε, are obtained from the following transport equations:

$$\frac{\partial}{\partial t}(\rho k) + \frac{\partial}{\partial x_j}(\rho u_i k) = \frac{\partial}{\partial x_j}\left[(\mu + \frac{\mu_t}{\sigma_k})\frac{\partial k}{\partial x_j}\right] + G_k - \rho\varepsilon \qquad (8)$$

and

$$\frac{\partial}{\partial t}(\rho\varepsilon) + \frac{\partial}{\partial x_j}(\rho u_i \varepsilon) = \frac{\partial}{\partial x_j}\left[(\mu + \frac{\mu_t}{\sigma_\varepsilon})\frac{\partial\varepsilon}{\partial x_j}\right] + C_1\frac{\varepsilon}{k}G_k - C_2\rho\frac{\varepsilon^2}{k} \qquad (9)$$

where G_k is the generation of turbulent kinetic energy due to mean velocity gradients and is given by

$$G_k = -\rho\overline{u_i'u_j'}\left(\frac{\partial u_i}{\partial x_j}\right) \qquad (10)$$

The model constants C_1, C_2, C_μ, σ_k, and σ_ε have the following values:

$$C_1 = 1.44, \quad C_2 = 1.92, \quad C_\mu = 0.09, \quad \sigma_k = 1.0, \quad \sigma_\varepsilon = 1.3$$

The turbulent heat transport is modeled using Reynolds analogy to turbulent momentum transfer. The energy equation is given by the following:

$$\frac{\partial}{\partial t}(\rho E) + \frac{\partial}{\partial x_j}(u_i(\rho E + p)) = \frac{\partial}{\partial x_j}\left[k_{eff}\frac{\partial T}{\partial x_j} + u_i \tau_{ij}\right] + S_h \qquad (11)$$

where E is the total energy, k_{eff} is the effective thermal conductivity, τ_{ij} is the deviatoric stress tensor and S_h includes the heat of the reaction and any other volumetric heat source. The term involving τ_{ij} represents the viscous heating.

For compressible flows, the ideal gas law is as following:

$$\rho = \frac{P_{op} + P}{\dfrac{R}{M_w}T} \qquad (12)$$

where R is the universal gas constant, M_w is the molecular weight of the gas, and $P_{op}+P$ is the local absolute pressure.

The k-ε turbulence model is widely used for the solution of turbulent flows in engineering applications. In this simulation, the standard k-epsilon model is considered with enhanced wall treatment. Enhanced wall treatment is one of the near wall modeling

methods and has a near wall formulation that can be used with a fine mesh (low Reynolds number). Comparison of leakage predictions using the standard wall treatment and enhanced wall treatment was performed. The enhanced wall treatment provided more accurate results. It required that the node nearest to the wall be located at $y^+ < 10$.

Table 2 Baseline labyrinth seal geometry

Cavity Shape	Rectangular
Shaft Diameter	116.84 mm
Radial Clearance	0.1016 mm
Tooth Pitch	3.556 mm
Tooth Width	0.7874 mm
Tooth Height	2.9464 mm
Seal Length	22.327 mm
# of teeth	7

The study commences with the simulation of an axisymmetric smooth seal and a tooth on stator labyrinth seal using a two-dimensional seal geometry. There are some reasons for performing two-dimensional flow simulations. Two-dimensional annular and labyrinth seals are much easier to analyze than three-dimensional windback seals. Two-dimensional simulations can provide information on the effect of the tooth width, the

cavity shape, the clearance, and the grid patterns. Then, three-dimensional simulations for windback seals can be performed with the same two-dimensional cross-section geometry and axial-radial grid patterns.

The baseline labyrinth seal used has a tooth on stator with rectangular groove, approximately 25% pitch of tooth width, and 116.84 mm (4.6 in) shaft diameter. Table 2 shows the geometry of the baseline seal.

The shaft diameter was selected since it coincides with the shaft diameter in an existing experimental facility (Kaul (1999)).

The fluid flow for the windback seals has two leakage paths.

$$\dot{Q}_{total} = \dot{Q}_{cavity} + \dot{Q}_{undertooth} \qquad (13)$$

The $\dot{Q}_{cavity}$ flow is produced by the helical groove of the windback seal. The analysis of how the flow is split between through cavity and under tooth flow is evaluated for windback seals and compared to the under tooth flow present in the labyrinth seal.

Simulations are compared with three different radial clearances (0.0508, 0.1016, and 0.1524 mm), three different tooth widths (25%, 50%, and 75% of the pitch), three different cavity shapes (rectangular, semi-circular deep, and semi-circular shallow), 33% of the pitch with semi-circular shallow cavity, three different shaft diameters (116.84, 203.2, and 304.8 mm) and tooth locations (TOS and TOR). The baseline design has a tooth width which is approximately 25% of the tooth pitch. The effect of tooth width on the performance of windback seals is investigated. Simulations for three different cavity shapes are conducted to study how air and oil behave over the top of the seal teeth. The effect of tooth width upon hydrodynamic generated pressure fields (journal bearing

effect) must be determined. The semi-circular deep groove has the same baseline seal geometry except that the bottom of the groove is a complete semi-circle. Semi-circular shallow groove has only a semi-circle profile of the entire groove region. These seals have a stronger tooth than the baseline design and a smaller groove cross sectional area for the $\dot{Q}_{cavity}$ flow.

The study provides detailed information about how oil migrates from the bearing side to the gas seal plenum by simulating a smooth annular seal, straight-through labyrinth seals, and windback seals that are totally filled with oil. The important concern is the pumping effect of the seal with air and oil. The dynamics of the flow field change significantly since oil has much higher viscosity than air. In practice, simulations for two component flow should be performed because in reality air and oil are present inside seal. However, a smooth annular seal, straight-through labyrinth seals, and windback seals which are either full of air or full of oil were simulated to obtain information about the area and magnitude of oil migration and the precise transport phenomenon due to the journal bearing action and the pumping action of the helical groove. A smooth annular seal with rotor eccentricity produces a pressure which forces oil into the gas face seal area. Oil will be pumped into the high pressure side and low pressure side. It leaks out both sides of the seal. The spiral groove of a windback seal reduces this pumping action and help to destroy the journal bearing action. The pressure of centered and rotor eccentric windback seals may be generated over the supply pressure if oil is inside the seal.

Table 3 CASES simulated for labyrinth seals with two-dimensions of flow conditions

	Clearance (mm)	Pitch (mm)	Tooth width (mm)	Shaft Diameter (mm)	Cavity Shape	
BASELINE	0.1016	3.556	0.7874	116.84	Rectangular	⊓
CASE L1	0.0508	3.556	0.7874	116.84	Rectangular	⊓
CASE L2	0.1524	3.556	0.7874	116.84	Rectangular	⊓
CASE L3	0.1016	3.721	1.8605	116.84	Rectangular	⊓
CASE L4	0.1016	3.883	2.912	116.84	Rectangular	⊓
CASE L5	0.1016	3.556	0.7874	116.84	Semi-circular deep	⌢
CASE L6	0.1016	3.556	0.7874	116.84	Semi-circular shallow	⌢
CASE L7	0.1016	3.620	1.2067	116.84	Semi-circular shallow	⌢
CASE L8	0.1016	3.556	0.7874	203.2	Rectangular	⊓
CASE L9	0.1016	3.556	0.7874	304.8	Rectangular	⊓
CASE S	0.1016	-	-	116.84	Smooth	—

Table 4 CASES simulated for seals with three-dimensions of flow conditions

|	Clearance (mm)	Pitch (mm)	Tooth width (mm)	Shaft Diameter (mm)	Cavity shape		Journal Eccentricity ratio
BASELINE1	0.1016	3.556	0.7874	116.84	Rectangular	⌐⌐	0
BASELINE2	0.1016	3.556	0.7874	116.84	Rectangular	⌐⌐	0.25
CASE W1	0.0508	3.556	0.7874	116.84	Rectangular	⌐⌐	0
CASE W2	0.1524	3.556	0.7874	116.84	Rectangular	⌐⌐	0
CASE W3	0.1016	3.721	1.8605	116.84	Rectangular	⌐⌐	0.25
CASE W4	0.1016	3.890	2.9600	116.84	Rectangular	⌐⌐	0.25
CASE W5	0.1016	3.556	0.7874	116.84	Semi-circular deep	⌒	0.25
CASE W6	0.1016	3.556	0.7874	116.84	Semi-circular shallow	⌒	0.25
CASE W7	0.1016	3.620	1.2070	116.84	Semi-circular shallow	⌒	0.25
CASE W8	0.1016	3.556	0.7874	203.2	Rectangular	⌐⌐	0.25
CASE W9	0.1016	3.556	0.7874	304.8	Rectangular	⌐⌐	0.25
CASE W10	0.1016	3.556	0.7874	116.84	Tooth on Rotor	⊔	0
CASE S	0.1016	-	-	116.84	Smooth	—	0.25
CASE L	0.1016	3.556	0.7874	116.84	Rectangular	⌐⌐	0.25

In order to determine how the spiral groove will effectively destroy the journal bearing affect, simulations for centered and rotor eccentric windback seals were performed. Therefore, two-dimensional models with 0% rotor eccentricity and three-dimensional models with 25% rotor eccentricity were simulated. Some three-dimensional models were simulated with centered windback seals.

Tables 3 and 4 show the cases that were simulated numerically for two-dimensional flow seals and smooth seal and three-dimensional flow seals. These simulations are based on the tooth on stator except CASE S and CASE W10.

Operating conditions considered for the smooth, labyrinth and windback seals are three differential pressures (34.47, 68.95, and 103.42 kPa) across the seal using air and oil as the working fluid. Four different rotor speeds (0, 5000, 10000, and 15000 rpm) are also considered in these simulations.

EXPERIMENTAL APPARATUS

The test rig and instrumentation are described in this section. The leakage measurements were made on the seal test facility at the Turbomachinery Laboratory, Texas A&M University. The experimental setup consists of the seal test rig, its instrumentation, and data acquisition system.

Seal test rig and instrumentation

The measurements are made using the seal test rig for static test shown in Figure A1. Al-Ghasem (2007) showed that CFD can accurately predict shaft rotation rate effects upon windback seals. This effect was small so a non-rotating facility is used in this study. This facility is oriented vertically and used to study the flow performance of windback seal. Air is used as the working fluid. Air enters vertically through the bottom and encounters the windback seal through two hoses. Figure A2 shows the windback seal and aluminum plate. The aluminum plate is used to hold the windback seal. The windback seal is made from brass. The test seal geometry is shown in Figure A3. There are six locations in each cavity for pressure tap holes access into the flow field. These locations were designed to be drilled at the center of the cavity. Table 5 describes the test seal geometry from the drawing. The number of the teeth defines the seal length divided by the seal pitch.

Figures A4 shows the control system to supply air into seal test rig. The air first enters into test facility room. It then passes through a pressure regulator, a safety release

valve, an air filter, a Rosemount absolute pressure transducer, a turbine flowmeter, and an air flow rate control valve.

Table 5 Test seal geometry

Cavity Shape	Semi-circular shallow
Shaft Diameter	116.81 mm
Radial Clearance	0.1143 mm
Tooth Pitch	3.621 mm
Tooth Width	1.207 mm
Tooth Height	1.207 mm
Seal Length	22.327 mm
# of teeth	6.28

Figure A5 shows a pressure regulator, a high pressure safety release valve, and an air filter. The pressure regulator is used to reduce the supply pressure into the test facility room below 689 kPa. The maximum pressure for the safety release valve is 1034 kPa (150 psi). The air filter removes solid particulates to the extent of 10 μm.

The Rosemount pressure transducer shown in Figure A6 is installed upstream of the turbine flow meter. It can measure 1034 kPa absolute pressure (150 psia). In order to calculate the air mass flow rate, the absolute pressure and temperature upstream of the

turbine flow meter must be measured using the Rosemount absolute pressure transducer and T-type thermocouple.

The air turbine flow meter and the signal conditioner shown in Figure A7 are used to measure mass flow rate. The range of turbine flow meter is from 0.00051 to 0.0049 m^3/s. The signal conditioner is used to convert the signal of the turbine flow meter to voltage.

An inlet pressure gage for the seal and a low pressure safety release valve are shown in Figure A8. The seal inlet pressure is controlled by the air flow rate control valve and measured by a high accuracy pressure gage. The maximum pressure of the low pressure safety release valve is 207 kPa (30 psig).

In order to determine the inlet pressure and the axial pressure distribution along the axis of the seal, the pressure transducers shown in Figure A9 are used to record the pressures of the inlet plenum and six cavities. The range of the pressure transducers is between 0 to 207 kPa (30 psig). The air supply and seal surface temperature are measured by thermocouples.

Data acquisition system

A data acquisition system for this experiment consists of PCMCIA data acquisition card, USB-1616FS, and USB-TC connected to a notebook computer. The data acquisition of this experiment was performed using the program LabVIEW version 7.1.

Figure A10 shows the PC-card DAS 16/16 AO data acquisition system. The PC-card DAS 16/16 AO is a control board for a computer with PCMCIA type-2 slots. The heart of the board is an analog to digital converter. It has a reduced set of four digital I/O lines rather than eight. It provides either 16 single ended or 8 differential analog inputs with sample rate up to 200 kS/s, and a resolution of 16 bit. It has four different input ranges (± 10 V, ± 5 V, ± 2.5 V, and ± 1.25 V). ± 1.25 V input range with the absolute accuracy of ± 0.19 mV was set for this experiment. Seven differential input channels were used to measure one inlet pressure of the seal and six pressures located in the center of each groove along the axis of the seal.

Figure A11 shows the USB-1616FS and USB-TC acquisition boards. The USB-1616FS provides 16 simultaneously sampled 16-bit analog inputs with sample rates up to 50 kS/s per channel. It also provides one 32-bit counter and 8 bits of digital I/O. It has four different input ranges (± 10 V, ± 5 V, ± 2 V, and ± 1 V). ± 10 V input range with the absolute accuracy of ± 5.66 mV was set for this experiment. Three channels were used to measure an absolute supply pressure from the Rosemount pressure transducer, air flow rate from turbine flow meter, and supply voltage of the pressure transducers (Figure A8).

The USB-TC is a USB-based temperature measurement device that provides eight thermocouple temperature inputs with 24 bit resolution and 2 S/s sampling rate per channel. It also provides eight digital I/O bits and supports J, K, R, S, T, N, E, and B type thermocouples. For this experiment, T-type thermocouples are used to measure the air supply temperature upstream of the turbine flow meter, inlet temperature, and seal surface temperature. The maximum error of T-type thermocouple measurement is ± 1.717 C° for a temperature range of -200 C° to 0 C° and ± 0.713 C° for a temperature range of 0 C° to 600 C°.

TWO-DIMENSIONAL FLOW SIMULATIONS

Two-dimensional flow simulations are considered with a straight through smooth annular seal and labyrinth seals. Many researchers have investigated the effects of modifying the geometric dimensions such as clearance, tooth width, tooth height, and groove shape. Operating conditions were considered for two-dimensional seals with the pressure drop across the seal being set to 0.34, 0.68, and 1.02 atm with an exit pressure of 1 atm. Shaft speeds of 0, 5,000, 10,000, and 15,000 rpm were considered. Pressure plenums were located upstream and downstream of the seal with the rotor running the entire length of the seal and through the plenums along the bottom.

Seal grid and geometry

These simulations are to determine which grid patterns provide acceptable results and to produce grids that have the minimum number of nodes necessary to produce the same result provided by grids with many more nodes. The grid pattern used in the two-dimensional flow simulations have many highly non-uniform regions in the x and y directions. Figure B1 and B2 show the overall layout grid and geometry for the smooth annular and baseline tooth on stator labyrinth seal. It is set to the high pressure on the left side. The two large rectangles are the inlet and exit plenums, bottom is the rotor surface, and outside and top walls have constant pressure boundary conditions. The number of nodes for the initial case (34.47 kPa pressure differential, and no shaft rotation) is about 6,400 for the baseline design case. It increases by grid adaption to meet

the same static pressure and velocity magnitude gradients for all conditions. The number of nodes for the final grid (103.42 kPa pressure differential, and 15,000 rpm) is about 8,000 for the baseline design case.

Figures B3 and B4 show how the leakage flow rate varies as the number of nodes is increased using adaptive gridding based upon the static pressure and velocity magnitude gradients. Adaptive grid refinement is performed to efficiently reduce the numerical error with minimal gridding nodes in FLUENT (2005) solution. These simulations are used with curvature approach which multiplies the undivided Laplacian of the selected solution variable by a characteristic length scale. The gradient function is given by the following equation (FLUENT (2005)):

$$\left| e_{i2} \right| = (A_{cell})^{\frac{r}{2}} \left| \nabla^2 f \right| \tag{14}$$

where e_{i2} is the error indicator, A_{cell} is the cell area, r is the gradient volume weight, and $\nabla^2 f$ is the undivided Laplacian of the desired field variable (f).

As the static pressure gradient decreases from 0.045 to 0.005, the leakage flow rate increases 2% while the number of nodes increases from 6,400 to 7,700. For the velocity magnitude gradient, the leakage flow rate does not affect decreasing the velocity magnitude gradient from 0.001 to 0.0002 while the number of nodes increases from 6,400 to 8,100. Therefore, the static pressure and velocity magnitude gradients used in the two-dimensional simulations were selected to be 0.03 and 0.0009, respectively.

Figures B5 and B6 show a closed up of the refined grid in the entrance region to the seal. Pressure and velocity contour plots for the entire length of the annular and labyrinth seals will be shown in this section. Since the effect for two-dimensional seals may be applied to three-dimensional windback seals, the effect of clearance, tooth width, cavity shape and shaft diameter for the leakage performance of two-dimensional seals are also studied in this section.

Effect of clearance on labyrinth seal performace

Baseline, CASE L1, and CASE L2 from Table 3 were simulated with clearances of 50.8, 101.6, and 152.4 μm, respectively. Figure B7 presents the effects of clearance on the leakage mass flow rate as the differential pressure varies for the tooth on stator labyrinth seal operated at rotor speeds of 0 and 15,000 rpm. These data show that as the differential pressure increases, the leakage mass flow rate increases steadily. Table 6 provides detailed information for the effect of shaft rotation of the labyrinth seal with three differential pressures. The shaft rotation effects are maximum at the minimum clearance and minimum at the maximum clearance as the leakage flow rate decreases as the shaft rotation increases from 0 to 15,000 rpm.

Table 6 Rotation effect of the labyrinth seal for three different clearances

Pressure differential	Leakage decrease % (from 0 to 15,000 rpm)		
	C=0.0508 mm	c=0.1016 mm	c=0.1524 mm
34.47 kPa	7.96%	3.03%	2.71%
68.95 kPa	4.16%	1.43%	1.37%
103.42 kPa	2.86%	1.06%	1.49%

Figure B8 shows that the maximum increase of the leakage mass flow rate as the clearance increases from 0.0508 to 0.1524 mm is at the lowest differential pressure (34.47 kPa) with the rotor speed of 15,000 rpm and minimum increase is at the highest differential pressure (103.42 kPa) with no shaft rotation. Many researchers have

analyzed labyrinth seals and found that shaft rotation will not affect leakage mass flow rate significantly. There are two factors that affect shaft rotation rate dependence in seal leakage. These factors are the differential pressure and the seal clearance. In general, increasing the shaft rotation rate will result in a decrease of the mass flow rate. Shaft rotation for the lowest differential pressure (34.47 kPa) has a greater effect than for the highest pressure. The small clearance (0.0508 mm) also increases the effect of shaft rotation. The maximum of the shaft rotation effect was 8% decrease at the lowest differential pressure with the clearance of 50.8 μm and the minimum was around 1% decrease at the highest differential pressure with the clearance of 152.4 μm.

Figure B9 presents the pressure distributions along the rotor surface for three different clearances at the maximum rotor speed of 15,000 rpm. These plots show that the inlet pressure drop increases as the clearance increases. The pressure inside the cavity is almost constant indicating very little pressure recovery from the throttling process. The flow under the tooth produces the uniform pressure drop. The pressure drop across the tooth is converted to kinetic energy and thermal energy. Due to this kinetic energy, the axial velocity increases into the next tooth. These plots have a similar trend except the magnitude of inlet and tooth edge pressure drops.

Figures B10 to B17 gives full details of the flow field inside the seals. These pressure and velocity contour plots for three different labyrinth seals simulated operating at minimum and maximum pressure drops and shaft rotation speeds were plotted within one figure. The colors of the contours correspond to the magnitude of the pressure and velocities. To help provide detailed information in the flow field, the same contour

amplitude scales were used in a figure. Since it is very difficult to analyze the flow field in the clearance region, it was zoomed in the radial direction in the region below each figure part.

Figures B10 and B11 present the pressure contour plots for the three different clearances. The pressure contour plots show that the pressure slowly decreases in the axial direction. These plots show that there is no shaft rotation effect for the three clearances as the shaft rotation increases from 0 to 15,000 rpm. Figures B12 and B13 show the axial velocity contours for the three different clearances. The axial velocity slowly increases as the flow progresses in the axial direction due to the pressure drop across the tooth decreasing the air density. The maximum axial velocities existing in the clearance region are 65, 75, and 85 m/s for 0 rpm and 45, 75, and 85 m/s for 15,000 rpm as the seal clearance increases from 50.8 to 152.4 μm at 34.47 kPa. This indicates that increasing the shaft rotation rate from 0 to 15,000 rpm decreases the maximum axial velocity for the minimum clearance. Increasing the seal clearance increases the magnitude of the axial velocity. There is no negative axial velocity in the clearance region. The negative axial velocity only exists inside the seal cavity generating the circulation in the counter clockwise direction.

The radial velocity contour plots for three different clearances at 0 and 15,000 rpm are shown in Figures B14 and B15. Shaft rotation has a negligible effect as the shaft rotation rate increases from 0 to 15,000 rpm. As the seal clearance increases, the magnitude of the radial velocity increases. The radial velocities have ranges of -5 to 10, -10 to 20, and -15 to 25 m/s for the rotor speeds of 0 and 15,000 rpm. The flow going

through under the tooth generates the vortex existing in the cavity. The radial velocity contours and Figure B16 give more detail information about the vortex generated by the maximum axial velocity in the clearance region. These contours clearly indicate the presence of a vortex inside the cavity. Figure B16 shows the magnitude of the vorticity at 0 and 15,000 rpm as the seal clearance increases. It is clear that the vortex strength increases with increasing clearance and for the small clearance of 50.8 μm, the vortex strength is much smaller than for the clearances of 101.6, and 152.4 μm. The tangential velocity at the inlet is confined to the region very close to the rotor surface. However, the effect of rotor reaches all the way across the seal by the exit. Figure B17 shows the tangential velocity contours for three clearances at 15,000 rpm. In the labyrinth seal, as the seal clearance decrease, the interaction of the fluid flow in the cavity is much smaller. As the clearance increases, the effect of the rotor speed decreases in that the tangential velocity along the centerline of the clearance decreases.

Effect of tooth width on labyrinth seal performance

The effect of tooth width upon the seal performance was investigated for CASE L3 and CASE L4 from Table 3. The baseline design has a tooth width which is approximately 25% of the pitch. This is modified to 50%, and 75% of the pitch. CASE L3 and L4 have the 50% and 75% of the pitch, respectively. These seals have a same clearance of 101.6 μm, and a rectangular groove. Figure B18 shows that as tooth width increases from 25% to 75% of the pitch with pressure differentials of 34.47, 68.95, and 103.42 kPa, the leakage mass flow rate decreases. The 75% wide tooth is clearly mechanically stronger and has an average of 17% less leakage than the baseline tooth width (25% tooth width). The maximum decrease percent in the leakage mass flow rate is 15% at the pressure differential of 34.47 kPa and rotor speed of 15,000 rpm, while the minimum decrease percent is 8.5% at the pressure differential of 103.41 kPa with no shaft rotation. This trend is opposite to that compiled by Cogan (1982). This implies that the effect of tooth width on leakage flow rates is different for high differential pressures.

Figure B19 presents the effect of tooth width as the pressure differential increases from 34.47 kPa to 413 kPa. This plot shows how increasing to higher pressure differentials affects the leakage rate. As the pressure differential across the seal increases to 275.79 kPa, the leakage mass flow rate dependence upon tooth width switches. The leakage flow rate increases for pressure differentials above 275.79 kPa as the tooth width increases from 25% to 75%. For the effect of shaft rotation, the leakage rate decreases as the shaft rotation rate increases from 0 to 15,000 rpm. However the effect is minimal with only a small decrease in the leakage rate.

Figure B20 presents the pressure distributions along the rotor surface for three different tooth widths at the maximum rotor speed of 15,000 rpm. This plot shows that the inlet pressure drop decreases as the tooth width increases. For CASE L4 (75% tooth width seal), the uniform pressure drops under the teeth are not clearly shown and the axial pressure drop under the tooth expands gently down to the next cavity due to the wide tooth. As the tooth width increases from 75% to 100% of the pitch, the axial pressure distribution will gradually transform to that of the annular seal. A 100% of the pitch represents the smooth annular seal.

As discussed earlier, the pressure and velocity contours provide full details of the flow field inside the seal. These pressure and velocity contour plots for three different labyrinth seals simulated operating at minimum pressure drops and maximum shaft rotation speed were plotted within one figure. These conditions were selected since the effects of changing parameters are maximized. The clearance region was expanded in the radial direction.

Figure B21 presents the pressure contour plots for the three different tooth widths. The pressure contour plots show that the pressure slowly decreases along the axial direction. Since there is negligible shaft rotation effect for the these contour plots with three tooth widths as the shaft rotation increases from 0 to 15,000 rpm, the 15,000 rpm case is selected. Figures B22 to B25 show the velocity contours for three different tooth widths. The axial velocity slowly increases as the flow progresses in the axial direction due to the pressure drop decreasing the air density. The narrow tooth width seal has a much larger maximum axial velocity under the teeth in the clearance region than

the wide tooth width seal. Increasing tooth width decreases axial velocity, radial velocity, and vortex strength generated inside the seal cavity. There is no effect on the magnitude of the tangential velocity shown in Figure B25 as tooth width increases. However, the wide tooth seal (75% tooth width) has less interaction of the fluid flow inside the seal cavity than the narrow tooth seals.

Figure B26 illustrates the flow pattern in the cavity of the 75% tooth width seal with four different rotor speeds. When the tangential velocity is large compared to the axial velocity, a second recirculation zone forms inside the cavity. Since the 75% tooth seal has relatively smaller axial velocity than the other tooth width seals, a secondary vortex forms inside the cavity in the 75% tooth seal at the rotor speeds of 10,000 and 15,000 rpm. There was no evidence of the secondary recirculation zone for the 25% and 50% tooth width seals. Figure B27 shows the secondary vortex formation for varying pressure differentials. Since the axial velocity at the highest pressure differential is larger than at the lowest pressure differential, the second recirculation zone is largest at the lowest pressure differential.

Effect of cavity shape on labyrinth performance

The effect of cavity shape upon the labyrinth seal performance was investigated by modifying the groove geometry. The original design of cavity shape has a rectangular groove. One design for the cavity shape is simulated by replacing the square top with a complete semi-circle. Another design of the cavity shape was compared with where the entire groove region is a semi-circular profile. The second modification also reduces the tooth height. The first modification is called semi-circular deep. The second modification is called a semi-circular shallow. The third design has the same groove shape with the second design but the 25% of the pitch of the second design is replaced with 33% of the pitch. Since the cavity of the second and third modification has only a complete semi-circle profile, tooth heights for these designs are decreased to the radius of the complete semi-circle. The air leakage of these four different cavity shapes (rectangular, semi-circular deep, 25% tooth width semi-circular shallow, and 33% tooth width semi-circular shallow) are compared for three different pressure drops at the rotor speed of 15,000 rpm in Figure B28.

In general, decreasing the seal cavity shape moderately decreases the seal leakage rate for the labyrinth seal. The modification of the cavity shape affects the strength of the vortex which converts the kinetic energy issuing from each tooth into internal energy. The important parameters for the modification with the cavity shape are the cavity width and depth. These parameters can be considered to the tooth width of pitch and tooth height. Many researchers have observed that the height of teeth does not have as great an effect on the leakage rate as does the cavity width. Figure B28 shows

the effect of cavity shape on leakage mass flow rate. The effect of the semi-circular deep groove modification is negligible with small decrease (below 1%) in the leakage due to the small decrease in the area of the groove. The effect of another modification to semi-circular shallow groove results in an average 3% decrease in the leakage. The small effect is due to about 50% decrease of the tooth height. Third modification to semi-circular groove with 33% of the pitch leaks 7% less than the baseline design seal due to the decrease in the cavity depth and width. The change in cavity width increases the tooth width which also causes a decrease in leakage as shown in the previous section. The wall pressure distribution for three different cavity shapes is shown in Figure B29. The effect of cavity shapes is negligible for the pressure distribution. The pressure and velocity contours are compared with four different cavity shapes in Figures B30 to B34. Similarly there is no effect for the pressure contours. Since the rectangular and semi-circular deep shapes have the same tooth height, there is minimal difference with axial and radial velocity contours.

The axial and radial velocity for the semi-circular shallow groove seal with 25% of the pitch shows no change in the clearance region but the cavity flow has been greatly reduced. The modification to the semi-circular shallow with 33% of the pitch results in small decrease in the axial velocity in the clearance region due to wide tooth and short tooth height. Figure B33 illustrates that the vorticity magnitude inside the seal cavity for the semi-circular shallow design is larger than the other designs. This is due to modifying the entire groove to the complete semi-circle. This plot explains why the cavity shape of three-dimensional windback seal should be changed. Since the semi-circular shallow groove seals have a smaller axial and radial velocity than the rectangular groove seal, the vortex strength should be decreased. However, the vorticity magnitude was increased by the semi-circular groove. The tangential velocity contours shown in Figure B34 have the same trend in the clearance region. Shaft rotation affects the tangential velocity inside the entire seal cavity for the semi-circular shallow design more than the other designs. The magnitude of tangential velocity inside the cavity for the semi-circular shallow designs is larger than the other designs.

Effect of shaft diameter on labyrinth seal performance

The effect of shaft diameter on the seal performance was investigated with increasing the shaft diameter. The baseline seal has the shaft diameter of 116.8 mm with 101.6 μm clearance. It is modified to 203.2 and 304.8 mm shaft diameter. This modification for the seal geometry has same geometry with the baseline seal. Figure B35 and B36 are for air with shaft diameters of 116.8, 203.2, and 304.8 mm with radial clearance of 0.101 mm. Three differential pressures (5, 10, 15 psi) are used. There is a linear increase in leakage with seal diameter. The ratio of the mass flow rate to the shaft diameter is almost constant with the shaft diameter. In other words the mass flow rate for the labyrinth seals show a linear relationship with shaft diameter. For no shaft rotation, both were within 0.1% difference with increasing from 116.8 to 203.2 mm and from 116.8 to 304.8 mm, respectively. For the rotor speed of 15,000 rpm, it was within 5% maximum difference of baseline seal diameter.

Figure B37 to B41 show the pressure and velocity component contours for the effect of the shaft diameter at the pressure differential of 34.47 kPa and the rotor speed of 15,000 rpm. The axial and radial velocity decrease and tangential velocity increases as the shaft diameter increases from 116.8 to 304.8 mm. Since the axial and radial velocities decreases with increasing the shaft diameter, the vortex strength decreases.

THREE-DIMENSIONAL FLOW SIMULATIONS WITH AIR

Three-dimensional flow simulations include the centered windback seal, the 25% rotor eccentric windback seal, the 25% rotor eccentric labyrinth seal, and the 25% rotor eccentric annular seal. Three-dimensional flow simulations of the performance for a windback seal were investigated with modifying the seal geometry such as clearance, tooth width of pitch, cavity shape, shaft diameter, and tooth location (TOS and TOR). These simulations are also compared with labyrinth and smooth annular seals with 25% rotor eccentricity.

Operating conditions are considered with pressure drops across the seal set to 0.34, 0.68, and 1.02 atm with an exit pressure of 1 atm. Shaft speeds of 0, 5,000, 10,000, and 15,000 rpm are considered. Pressure plenums are located upstream and downstream of the seal with the rotor running the entire length of the seal and through the plenums. Air was used as a working fluid in the simulation.

Seal grid and geometry

The grid pattern used in these simulations is based on the two-dimensional labyrinth seal grid. In these simulations, the seal can be meshed with the small number of nodes around the circumference since the velocity gradients in the circumferential direction are smaller than in the axial direction and much smaller than in the radial direction. The number of nodes around the circumference is 52. The number of nodes for the initial case (34.47 kPa pressure differential, and no shaft rotation) is about 370,000 for the baseline design case. It is increased by grid adaption to meet the same static pressure and velocity magnitude gradients for all conditions. The number of nodes for the final grid (103.42 kPa pressure differential, and 15,000 rpm) is about 810,000 for the baseline design case.

How varying the static pressure and velocity magnitude gradient affect the calculated mass flow rate in these simulations are presented in Figure C1 and C2. The trend is very similar to the two-dimensional simulations. As the static pressure gradient decreases from 1.02 to 0.05, the leakage flow rate increases less than 1% while the number of nodes increases from 390,000 to 640,000. The leakage flow rate does not vary with decreasing velocity magnitude gradient from 0.01 to 0.001, while the number of nodes increases from 390,000 to 780,000. Therefore, static pressure and velocity magnitude gradients used in the two-dimensional simulations were 0.2 and 0.005, respectively.

Figure C3 shows the cross section of the grid and geometry for the baseline windback seal. The same geometry and grid pattern used for the two dimensional labyrinth seal are applied in these simulations. The grid pattern used for the two dimensional labyrinth seal provided appropriate results. In order to reduce the number of nodes required to produce the same result provided by grids with many more nodes, a large compression ratio was used on the regions near the surface in these simulations. The high pressure of the seal is located on the left side of the grid. The two large rectangles at each end are the inlet and exit plenums, the bottom is the rotor surface, and the outside and top walls have constant pressure boundary conditions. The rotor surface rotates in the same direction of the helical groove to produce flow from the high pressure to low pressure regions. Figure C4 shows a closed up of the refined grid in the entrance region to the seal and first groove.

The seal geometries in these CFD simulations are calculated in three-dimensional Cartesian coordinate systems.

It is transformed to a cylindrical coordinate system from the following equations are used;

$$x = x \tag{15}$$

$$V_x = V_x \tag{16}$$

$$r = \sqrt{y^2 + z^2} \tag{17}$$

$$V_r = V_z \sin\theta + V_y \cos\theta \tag{18}$$

$$\theta = \tan^{-1}(z/y) \tag{19}$$

$$V_\theta = V_z \cos\theta - V_y \sin\theta \tag{20}$$

The effect of clearance, tooth width, cavity shape and shaft diameter for the leakage performance of the windback seals are studied in this section.

Pressure and velocity flow fields

The CFD simulations give full details of the flow field inside a windback seal. These data can be examined to evaluate how the varying parameters change the flow field and hence the overall leakage rate. Figure C5 shows three-dimensional pressure contour plots for the baseline windback seal. The groove starts along the positive y axis. The pressure decreases along the helical groove due to the pressure loss under the tooth and friction in the cavity. The detailed information about the flow field inside the seal is not readily apparent in this plot. To analyze the seal performance for the varying parameters about the flow field, planes were sliced in four radial cross section angles. Figure C6 and C7 present the four angles viewed for the centered and 25% rotor eccentric windback seals. The helical groove starts in the 240° and 270° region and ends in the 90° and 120° region. The maximum and minimum clearance for the 25% rotor eccentric windback seal shown in Figure C7 are in the 270° and 90° sliced planes. To compare the flow field in the groove starting region and to obtain information of the flow field under the teeth, the clearance region in the 270° sliced plane was expanded in the radial direction. Color contours of the pressure and velocities are presented on these planes. To compare the seal performance with the varying parameters in the flow field, the same contour levels are displayed in the figures.

Figure C8 and C9 present the pressure contours for the baseline windback seal with no shaft eccentricity, 0.106 mm clearance, and 34.47 kPa differential pressure at 0 and 15,000 rpm. These plots are very similar to the pressure contour plots obtained for the two-dimensional labyrinth seal. The pressure inside the seal cavity slowly decreases

along the helical groove direction. Shaft rotation effect is not apparent in these contour plots as the shaft rotation rate increases from 0 to 15,000 rpm. There is a large pressure drop across the each tooth. Figure C10 shows the axial pressure distribution along the middle of the clearance for various pressure differentials (34.47, 68.95, and 103.42 kPa) at the rotor speed of 0, and 15,000 rpm in the 0° nominal clearance sliced plane. The axial pressure distributions in the 0° sliced plane shows that there is no shaft rotation effect and the pressure inside cavity is almost constant. This plot has the same trend as the two-dimensional labyrinth seal which was explained in the previous section. The flow under the tooth produces the perpendicular pressure drop. This pressure drop across the tooth is converted to kinetic energy and thermal energy. Due to this kinetic energy, the axial velocity increases into the next tooth. Since the kinetic energy increase in the axial direction, the tooth inlet effect also increases. Therefore, the maximum of the axial velocity is generated under the last tooth of the seal.

Figures C11 and C12 present the contour plots for the axial velocity for the rotor speeds of 0 and 15,000 rpm with a differential pressure of 34.47 kPa.. There is no shaft rotation effect as the difference of the maximum axial velocity as the rotor speed increases from 0 to 15,000 rpm is negligible. The axial velocity increases as the flow passes through the seal due to the air density decreasing with decreasing pressure. The maximum velocity for the two different rotor speeds is around 90 m/s. A negative axial velocity is shown inside the cavity. The negative axial velocity existing inside the cavity indicates the presence of a vortex caused by the axial velocity accelerated under the tooth and the viscous force between it and the fluid inside the cavity. The axial velocity

under the tooth is accelerated due to the pressure differential across a tooth. After passing under the tooth the axial velocity decreases in magnitude as it expansions into the seal cavity. The flow passes under the next tooth and the axial velocity increases under the tooth by the flow contraction due to the small clearance area. This is shown in the following plots.

Figure C13 shows the axial velocity distribution for the four sliced angle views along the middle of clearance. Since the 0° sliced plane has a different number of cavities and the grooves of the 90° and 270° sliced planes were open to the downstream and upstream plenums, these plots show different axial velocity distribution for the four sliced angle views. There is no negative axial velocity at the seal inlet for the four different sliced angle views. Since the air density decreases as the pressure inside the seal decreases in the axial direction, the axial velocity increases as the flow progresses through the seal.

Figures C14 and C15 show the radial velocity contours for rotor speeds of 0 and 15,000 rpm. The radial velocity contours are almost identical at 0 and 15,000 rpm. The presence of a vortex inside each cavity is clearly shown in these plots. Each vortex is represented by the positive and negative radial velocities inside the cavity. They are generated in the counter clockwise direction. The vortex strength inside the cavity increases as the axial velocity increases. In other words, the vortex strength increases due to increase in pressure drop as the flow passes through the seal.

Figures C16 and C17 show the circumferential velocity contours. The circumferential velocity changes greatly with increasing shaft rotation at speed.

Increasing the rotor speed from 0 to 15,000 rpm increases the circumferential velocity inside the seal cavity and in the clearance region. For no shaft rotation, the maximum circumferential velocity exists inside the seal cavity and increases in the axial direction as the flow passes through the seal. For the rotor speed of 15,000 rpm, the circumferential velocity not only increases gradually in the axial direction, but also along with the direction of helix angle. It decreases in the radial direction from rotor surface for the clearance region. Since the V_θ boundary layer barely reaches all the way across the seal clearance, the flow proceeds through the seal cavity due to the flow resistance under the tooth.

The fluid flow for the windback seal has two leakage paths, under the teeth and through the cavity. Figure C18 and C19 show the leakage flow rate under the tooth and through the cavity along the axial direction of the seal at the 270° sliced plane. Since the first cavity is open with upstream plenum, the leakage flow rate for the first cavity is excluded in this plot. The leakage flow rate through the seal cavity, $\dot{m}_{cav}$, increases significantly with increasing the rotor speed. $\dot{m}_{cav}$ is almost constant along the seal length for the lowest pressure differential while there is a small increase in $\dot{m}_{cav}$ at the middle cavity for the highest pressure differential. This is interesting in that V_θ increases significantly in the downstream direction due to rotor drag and density reduction. This all balances out to maintain a constant mass flow rate in the cavity. The mass flow rate under the teeth is almost ten times larger than the cavity flow rate and is not dependent upon the shaft speed. These values are within 3% of the flow inside the labyrinth seal.

Figures C20 to C22 demonstrate the magnitude of the velocities inside the seal with increasing rotor speeds at a pressure difference of 34.47 kPa. Shaft rotation does not have an effect on the axial and radial velocities as the rotor speed increases from 0 to 15,000 rpm. For the circumferential velocity contours shown in Figure C22, increasing the rotor speed increases V_θ inside the seal cavity and in the seal clearance region. V_θ increases as the flow progress through the seal. With no shaft rotation, the circumferential velocity in the clearance region is negligible. With shaft rotation, the rotor effect due to the viscous force has a small effect since the V_θ boundary layer barely reaches across the seal clearance by the exit. Therefore, the maximum V_θ for no shaft rotation exists inside the seal cavity, while it exists in the clearance region near the rotor surface for the all cases. As the rotor speed increases from 0 to 15,000 rpm, the maximum V_θ inside the seal cavity increased from 36.2 to 54.9 m/s. Hence, the circumferential velocity increases by the rotor speed affects the leakage flow rate through the seal cavity.

Effect of clearance on windback seal performance

Three centered windback seals were simulated with radial clearances of 50.8, 101.6, and 152.4 μm. The dependence of the leakage rate for the windback seals was compared with differential pressures of 34.47, 68.95, and 103.42 kPa, and rotor speeds of 0, 5,000, 10,000, and 15,000 rpm.

Figure C23 presents the effects of clearance on the leakage mass flow rate as the differential pressure varies for the windback seal operated at rotor speeds of 0 and 15,000 rpm. These data show that as the differential pressure increases, the leakage mass flow rate increases steadily. For labyrinth seals, the leakage mass flow rate decreases as the rotor speed increases from 0 to 15,000 rpm. However, increasing the rotor speed slightly increases the leakage mass flow rate for windback seals. This is due to the helical groove of windback seal in the same direction of the shaft rotation acting as a pump much in the same manner as addressed for the helical cut bearing studied by Boostma (1975).

Table 7 gives detailed information for the effect of shaft rotation on the windback seal with three differential pressures. The shaft rotation effects on the total leakage flow rate, $\dot{m}_{tot}$, are maximum at the minimum clearance with the lowest differential pressure and minimum at the maximum clearance with the highest differential pressure as the shaft rotation increases from 0 to 15,000 rpm. The shaft rotation effect on the leakage flow rate through the cavity, $\dot{m}_{cav}$, are maximum at the maximum clearance with the lowest differential pressure and minimum at the minimum clearance with the highest differential pressure. $\dot{m}_{cav}$ decreases with increasing the seal

clearance and $\dot{m}_{cav}$ increases with increasing the rotor speed. This illustrates that $\dot{m}_{cav}$ depends on the rotor speed and clearance. The leakage flow rate under the tooth for the windback seal, $\dot{m}_{utooth}$, decreases and $\dot{m}_{cav}$ greatly increases with increasing the rotor speed.

Table 7 Shaft rotations on mass flow rate of windback seals for three different clearances

| ΔP (kPa) | Leakage increase % (from 0 to 15,000 rpm) | | | | | | | | |
| | c=0.0508 mm | | | c=0.1016 mm | | | c=0.1524 mm | | |
	$\dot{m}_{tot}$	$\dot{m}_{cav}$	$\dot{m}_{utooth}$	$\dot{m}_{tot}$	$\dot{m}_{cav}$	$\dot{m}_{utooth}$	$\dot{m}_{tot}$	$\dot{m}_{cav}$	$\dot{m}_{utooth}$
34.47	13.8%	64.7%	-1.4%	5.4%	85.6%	-1.4%	2.3%	90.0%	-1.3%
68.95	8.5%	42.2%	-1.0%	3.6%	56.6%	-1.0%	1.4%	54.3%	-0.9%
103.42	6.0%	32.6%	-1.2%	2.6%	41.3%	-0.8%	1.1%	43.9%	-0.8%

Therefore increasing the clearance from 0.0508 to 0.1524 mm decreases the shaft rotation at speed effect in the total leakage flow rate and increases leakage flow rate in the cavity.

Table 8 and Figure C24 show the dependence of leakage mass flow rate of the windback seal upon three differential pressures with varying rotor speed as the radial clearance increases from 0.0508 to 0.1524 mm. When the radial clearance increase from

0.0508 to 0.1016 mm, and from 0.1016 to 0.1524 mm, the maximum percent increases in the leakage mass flow rate is at the lowest differential pressure (34.47 kPa) and with no shaft rotation; while the minimum increase percent is at the highest differential pressure (103.42 kPa) with a rotor speed of 15,000 rpm. The increase percent in the leakage rate for the radial clearance increase of 0.0508 to 0.1016 mm is much larger than for the 0.1016 to 0.1524 mm clearance seals.

Table 8 Effect of clearance upon the leakage rate for windback seal with three differential pressures and four rotor speeds

Clearance (mm)	Pressure differential	Leakage increase %			
		0 rpm	5000 rpm	10000 rpm	15000 rpm
from 0.0508 to 0.1016	34.47 kPa	141%	133%	128%	123%
	68.94 kPa	131%	127%	124%	120%
	103.41 kPa	119%	117%	115%	112%
from 0.1016 to 0.1524	34.47 kPa	68.5%	67.4%	65.5%	63.5%
	68.94 kPa	67.6%	66.0%	65.3%	64.1%
	103.41 kPa	66.2%	65.4%	64.6%	63.9%

Shaft rotation for the lowest differential pressure (34.47 kPa) has a greater effect on seal leakage than for the highest differential pressure. A smaller clearance (0.0508 mm) also has a greater effect for the shaft rotation. As discussed earlier, $\dot{m}_{cav}$ for the maximum clearance and the lowest pressure differential has a great dependence on

shaft rotation at speed and $\dot{m}_{utooth}$ has a small dependence for shaft rotation. However, since $\dot{m}_{cav}$ for the clearances of 0.0508 mm, 0.1016 mm, and 0.1524 mm are 26%, 10%, and 5% of the total leakage flow rate, respectively, the minimum clearance has a greater effect for the shaft rotation than the maximum clearance.

The fluid flow for the windback seal has two leakage paths, under the teeth and through the cavity. Figures C25 and C26 show the leakage rate for the two leakage paths with three clearances. Increasing the radial clearance decreases the leakage flow rate through the cavity. As the rotor speed increases, the leakage flow rate inside the seal cavity increases but the leakage flow rate under the teeth decreases. This trend for leakage flow rate under the teeth is very similar to that of a labyrinth seal.

Figure C27 presents the axial pressure distribution along the middle of the clearance for varying pressure differentials (34.47, 68.95, and 103.42 kPa) at rotor speeds of 15,000 rpm in the 0° sliced plane. These plots show that the inlet pressure drop increases as the clearance increases and pressure inside the cavity is almost constant. The flow under the tooth produces the perpendicular pressure drop. The pressure drop across the tooth is converted into kinetic energy and thermal energy. Since the viscous drag for the minimum clearance is larger than for the maximum clearance, the axial velocity for minimum clearance is smaller than for the maximum clearance and the pressure drop near the inlet plenum is also smaller. These plots show a similar trend as with the labyrinth seals.

Figure C28 presents the pressure contour plots for the 270° sliced plane for the three different clearances with the differential pressure of 34.47 kPa at the rotor speed of

15,000 rpm. The pressure contour plots for all seals with different clearances show that the pressure slowly decreases in the axial direction and there is no shaft rotation effect for the three clearances as the shaft rotation increases from 0 to 15,000 rpm.

Figure C29 show the axial velocity contours on the 270° sliced plane for three different clearances. The axial velocity increases as the flow progresses downstream in the axial direction due to the decrease in the air density. Since the air density decreases in the axial direction and the mass flux under tooth is constant, the maximum axial velocity is generated under the last tooth of the seal. As the first groove is open to the inlet plenum on the 270° sliced plane, the axial velocity under the first tooth is larger than the middle tooth of the seal. Increasing the seal clearance increases the magnitude of the axial velocity. The maximum axial velocities under the teeth are 45, 65, and 85 m/s for the rotor speed of 15,000 rpm as the seal clearance increases from 50.8 to 152.4 μm at 34.47 kPa. The axial velocity for the three seals does not change with varying rotor speed. The axial velocity inside the seal cavity increases about 30% as the clearance is increased. Figure C33 presents the axial velocity distribution for four different angular planes along the middle of clearance with the pressure differential of 34.47 kPa at the rotor speed of 15,000 rpm. The average maximum axial velocity for four different angular planes increases by 40% as the clearance increases from 0.0508 to 0.1016 mm while it increases by 22% as the clearance increases from 0.1016 to 0.1524 mm. There is no negative axial velocity in the clearance region. The negative axial velocity only exists inside the seal cavity generating the circulation in the counter clockwise direction.

The flow passing under the tooth generates the vortex existing in the cavity. The vortex generated by the axial velocity under the teeth is indicated by the radial velocity contours shown in Figure C30. These contours clearly indicate the presence of a vortex inside the cavity except for the minimum clearance. The vortex strength for the minimum clearance (0.0508 mm) is smaller than for the others. Since the same contour level for three different clearances was used, the vortex for the minimum clearance is not clearly shown. Shaft speed has a negligible effect for the radial velocity as the shaft rotation rate increases from 0 to 15,000 rpm. As the seal clearance increases, the magnitude of the radial velocity and the vortex strength increase due to the larger axial velocity in the clearance region driving the vortex by the shear layer between the cavity and the through flow.

Figures C31 and C32 show the circumferential velocity contours for a pressure differential of 34.47 kPa at the rotor speed of 0 and 15,000 rpm.

The maximum V_θ for no shaft rotation exists inside the seal cavity, while for the rotor speed of 15,000 rpm it exists in the clearance region near the rotor surface. As the clearance increases, V_θ decreases. For the minimum clearance (0.0508 mm), since the effect of rotor reaches all the way across the seal by the exit, V_θ inside the cavity is affected by the rotor speed. For 0.1016 mm clearance, the boundary layer on the rotor surface barely reaches across the seal by the exit, V_θ inside the cavity is not much affected by the rotor surface. For the maximum clearance, the rotor surface does not affect V_θ inside the cavity since the boundary layer does not reach all the way across the seal by the exit. Therefore, as the clearance increases, the effect of the rotor decreases in that the circumferential velocity along the centerline of the clearance decreases. As discussed earlier in Table 7 and 8, since the cavity leakage flow rate are affected by the rotor speed and the clearance, increasing the clearance decreases the flow resistance under the tooth and the flow for the minimum clearance goes to the seal cavity. Hence, $\dot{m}_{cav}$ for the minimum clearance seal is larger than $\dot{m}_{cav}$ for the maximum clearance.

Effect of rotor eccentricity on windback seal performance

   The effect of rotor eccentricity upon the seal leakage rate of the windback seals was investigated with journal eccentricities of 0 and 0.25. Figure C34 and Table 9 show the leakage rate for a centered and a 25% rotor eccentric windback seals with three differential pressures as the rotor speed increases from 0 to 15,000 rpm. The rotor eccentric windback seal leaks slightly more than the centered windback seal. The increase in the leakage rate was below 1%. The maximum increase in the leakage rate was at the lowest differential pressure (34.47 kPa) and no shaft rotation, while the minimum increase was at the highest differential pressure and the rotor speed of 15,000 rpm.

Table 9 Carry over coefficient for different seal with 25% rotor eccentric windback seal

Rotor eccentricity	Pressure differential	Leakage increase %			
		0 rpm	5000 rpm	10000 rpm	15000 rpm
	34.47 kPa	0.91%	0.88%	0.80%	0.66%
from 0 to 0.25	68.94 kPa	0.89%	0.85%	0.86%	0.75%
	103.41 kPa	0.68%	0.64%	0.64%	0.58%

   Figure C35 presents the pressure distribution for centered and 25% rotor eccentric windback seals along the middle of clearance along the 0° angle sliced plane at rotor speeds of 15,000 rpm. Since the 25% rotor eccentric windback seal at the 0° and

180° angular planes has the same clearance as the centered windback seal, there is no difference for the seal performance and pressure and velocity components also show no change. However, the pressure drop and axial velocity for 25% rotor eccentric windback seal in the maximum clearance region (270° section) is larger than that for the centered windback seal. For the minimum clearance region, the axial velocity and pressure drop for 25% rotor eccentric windback seal are smaller than the centered windback seal. Figure C36 shows the effect of a rotor eccentricity upon the axial velocity distribution. The maximum axial velocity for the 25% rotor eccentric windback seal in the maximum clearance region is 15% larger than the centered windback seal, while in the minimum clearance region (90° plane) the maximum axial velocity for the 25% rotor eccentric seal with the minimum clearance is 10% smaller than the centered seal.

The remaining studies will be for 25% rotor eccentric seals since the overall leakage rates are not appreciably effected by rotor eccentricity. This will allow direct comparison to oil filled seals operating at the same rotor eccentricity. For the oil filled seals, hydrodynamic generated pressure fields can be present and a comparison to the same seal operating with just air is desired.

Effect of tooth width on windback seal performance

The effect of tooth width upon the windback seal's performance was investigated by increasing the tooth width while keeping a constant pitch. The baseline design has a tooth width which is approximately 25% of the pitch length. This is modified to 50%, and 75% of the pitch. These seals have the same clearance of 101.6 μm, 25% rotor eccentricity, and a rectangular groove.

Figure C37 shows the leakage flow rate for the windback for three pressure differentials of 34.47, 68.95, and 103.42 kPa at the rotor speeds of 0 and 15,000 rpm as the tooth width of pitch increases from 25% to 75%. The leakage mass flow rate decreases with increasing the tooth width of pitch. This is the same trend observed for labyrinth seals operating under the same conditions except rotor eccentricity. The 75% of the pitch is clearly mechanically stronger and has an average of 17% less leakage than the baseline tooth width (25% tooth width). As the shaft rotation increases from 0 to 15,000 rpm, the leakage flow rate for baseline windback seal increases, while the leakage flow rate for the wide tooth decreases. It is responding like a labyrinth seal. In other words, as the tooth width of pitch increases, the leakage flow rate decreases but the effect of helical groove also decreases.

Figure C38 shows how the windback seal differs from labyrinth seal. The labyrinth seal data were added in the Figure C37. The windback seals leak 13% for 25% tooth width, 10% for 50% tooth width, and 6% for 75% tooth width more than the labyrinth seals.

Table 10 presents the shaft rotation effect of the total, cavity, and under tooth leakage difference for three differential pressures with shaft speed increasing from 0 to 15,000 rpm.

Table 10 Shaft rotation effect of windback seals for three different tooth widths

ΔP (kPa)	Leakage increase % (from 0 to 15,000 rpm)								
	25% toot width			50% tooth width			75% tooth width		
	$\dot{m}_{tot}$	$\dot{m}_{cav}$	$\dot{m}_{utooth}$	$\dot{m}_{tot}$	$\dot{m}_{cav}$	$\dot{m}_{utooth}$	$\dot{m}_{tot}$	$\dot{m}_{cav}$	$\dot{m}_{utooth}$
34.47	6.1%	79.5%	-0.7%	3.0%	92.7%	-1.6%	-1.3%	120.8%	-3.2%
68.95	3.6%	49.4%	-0.6%	1.6%	62.0%	-1.5%	-0.6%	90.0%	-2.0%
103.42	2.9%	39.1%	-0.4%	1.7%	49.4%	-0.8%	-0.8%	73.1%	-1.9%

The shaft rotation effects on the total leakage flow rate, $\dot{m}_{tot}$, are maximum, 6.1%, at the 25% tooth width seal with the lowest differential pressure while $\dot{m}_{tot}$ for the 75% tooth width seal decreases with increasing the rotor speed. As the tooth width of pitch increases, the percent of the leakage increase for the leakage flow rate through the cavity, $\dot{m}_{cav}$, increases. The leakage flow rate under the tooth for the windback seal, $\dot{m}_{utooth}$, decreases with increasing the rotor speed. The maximum increase percent for

$\dot{m}_{cav}$ is at the lowest pressure differential with the 75% tooth width. However, since

$\dot{m}_{cav}$ for the 75% tooth width seal is a much smaller portion of the total leakage flow rate

than for the 25% tooth width, the 25% tooth width seal has a great effect for the shaft

rotation.

Table 11 presents the shaft rotation effect of $\dot{m}_{utooth}$ for the windback seal and the

leakage for the labyrinth seal. The trend for $\dot{m}_{utooth}$ is very similar to the labyrinth seal.

The comparison between these two leakages will be discussed later.

Table 11 Shaft rotation effect of leakage rate for windback and labyrinth seals for three
different tooth widths

ΔP (kPa)	Leakage increase % (from 0 to 15,000 rpm)					
	25% toot width		50% tooth width		75% tooth width	
	Labyrinth	$\dot{m}_{utooth}$	*Labyrinth*	$\dot{m}_{utooth}$	*Labyrinth*	$\dot{m}_{utooth}$
34.47	-1.4%	-0.7%	-2.5%	-1.6%	-4.1%	-3.2%
68.95	-1.2%	-0.6%	-1.4%	-1.5%	-2.1%	-2.0%
103.42	-1.0%	-0.4%	-1.0%	-0.8%	-1.5%	-1.9%

Figure C40 and Table 12 present the effect of tooth width for the difference of

leakage flow rate as the tooth width of pitch increase from 25% to 50%, and from 50%

to 75% respectively. There is almost a linear decrease in leakage flow rate with increasing tooth width. The decrease in the leakage flow rate for increasing from 25% to 50% tooth width is larger than that for increasing from 50% to 75% since the baseline seal design has actually 22% of the pitch. The maximum decrease in the leakage mass flow rate is 14.2% at the pressure differential of 34.47 kPa and rotor speed of 15,000 rpm, while the minimum decrease is 4.3% at the pressure differential of 103.42 kPa with no shaft rotation. In a previous section, as the pressure differential increased much higher, the leakage flow rate for tooth width resulted in an opposite trend. This also represents that the effect of tooth width on leakage flow rates may cause a different result for high differential pressure like labyrinth seals.

Table 12 Effect of tooth width upon the leakage rate for windback seal with three differential pressures and four rotor speeds

Tooth width of pitch	Pressure differential	Leakage decrease %			
		0 rpm	5000 rpm	10000 rpm	15000 rpm
from 25% to 50%	34.47 kPa	11.7%	12.2%	13.2%	14.2%
	68.95 kPa	9.9%	10.3%	11.0%	11.6%
	103.42 kPa	9.2%	9.3%	9.8%	10.3%
from 50% to 75%	34.47 kPa	7.8%	8.7%	9.8%	11.6%
	68.95 kPa	5.9%	6.5%	7.1%	8.0%
	103.42 kPa	4.3%	5.2%	5.8%	6.6%

The fluid flow for the seal has two leakage paths, under the teeth and through the cavity. Figures C41 and C42 show the leakage rate for the two leakage paths. Increasing the tooth width decreases the leakage flow rate inside the cavity. The percent of the leakage inside the seal cavity to the total leakage flow rate are 10.5% for 25% tooth width, 6.4% for 50% tooth width, and 2.2% for 75% tooth width. As the rotor speed increases, the leakage flow rate inside the seal cavity increases but the leakage flow rate under the teeth decreases. This trend for leakage flow rate under the teeth is very similar with labyrinth seal. Figures C43 and C44 show a direct comparison of the leakage flow rate for the labyrinth seal and the under the tooth leakage for the windback seal. The leakage data are in good agreement with three different tooth width seals. The leakage data for the labyrinth seal were on the average within 3.8% of the leakage rate under the tooth for the windback seal. If the tooth width of pitch is increased, the flow under the teeth for the windback seals can be predicted by two-dimensional labyrinth seal analysis. Since the windback seals for these data have a 25% rotor eccentricity, the difference of leakage data can be reduced if the labyrinth seal has a 25% rotor eccentricity. Figure C45 shows another comparison for leakage data of labyrinth seal and under the teeth for windback seal with both at a 25% rotor eccentricity. The difference of leakage flow rate was less than 2%.

Figure C46 presents the pressure distributions along the middle of the clearance for three different tooth widths at the maximum rotor speed of 15,000 rpm. This plot shows that the inlet pressure drop decreases as the tooth width increases while near the exit it increases. For the 75% of the pitch, the pressure distribution at the lowest

differential pressure (34.47 kPa) is operated like the smooth seal and the axial pressure drop under the tooth expands gently down to next cavity. The pressure drop increases as the flow goes in the axial direction. This is due to kinetic energy generated under the tooth by the pressure drop which is gradually increased by the pressure drop under next tooth. Therefore, the maximum axial velocity occurs under the last tooth of the seal.

Sliced angular contour plots except the circumferential contour plot are almost identical as the shaft rotation increases from 0 to 15,000 rpm. Figure C47 presents the pressure contour plots of 270° sliced plane for the three different tooth widths with the differential pressure of 34.47 kPa at the rotor speed of 15,000 rpm. The pressure for three seals slowly decreases in the axial direction and has a minimal radial variation. The radial pressure variation for the 75% tooth seal is 50% smaller than for the narrower tooth seals. The differences of the radial pressure between the top of cavity and the clearance region are 150 Pa for the 25% and 50% tooth seal, and 75 Pa for the 75% tooth seal.

Figure C48 shows the axial velocity contours of 270° sliced plane for three different tooth widths. The axial velocity slowly increases as the flow goes in the axial direction due to decreasing pressure (density). These plots clearly show that the maximum axial velocity exists in the clearance region of the last tooth. Increasing the tooth width of pitch decreases the axial velocity. The maximum axial velocity under the teeth is decreased from 85 to 65 m/s for the lowest differential pressure with the rotor speed of 15,000 rpm as the tooth width of pitch increases from 25% to 75%.

Figure C51 presents the axial velocity distribution for four different angular planes along the middle of clearance with the pressure differential of 34.47 kPa at the rotor speed of 15,000 rpm. The average maximum axial velocity for four different angular planes decreases by 19% as the tooth width of pitch increases from 25% to 50% while it decreases by 14% as the tooth width increases from 50% to 75%. The negative axial velocity is not shown in these plots. The negative axial velocity only exists inside the seal cavity generating the vortex in the counter clockwise direction.

As the flow goes through under the tooth a vortex is generated inside the cavity. The vortex generated by the axial velocity under the teeth is shown in Figures C48 and C49. For the widest tooth, the narrow cavity has two vorticies stacked inside it as was above for the labyrinth seal. The radial contours clearly show the presence of vortex inside the cavity. Increasing the tooth width of pitch decreases the vortex strength. As the tooth width increases, the magnitude of the radial velocity also decreases. For 75% tooth width, the vortex strength is smaller than the others. For 50% and 25% tooth widths, the vortex is clearly shown by the positive and negative radial velocity inside the seal cavity. Shaft rotation has a negligible effect on the radial velocity.

Figure C50 shows the circumferential velocity contours with the pressure differential of 34.47 kPa at the rotor speed of 15,000 rpm. Shaft rotation effect starts at the rotor surface. V_θ decreases in the radial direction from rotor surface. As the tooth width increases, V_θ inside the seal cavity decreases. The maximum circumferential velocity with no shaft rotation exists inside the seal cavity, while for the rotor speed of 15,000 rpm it exists in the clearance region near the rotor surface. The maximum value of V_θ inside the cavity are 48 m/s for 25% tooth width, 40 m/s for 50% tooth width, and 30 m/s for 75% tooth width. These values explain that the rotor effect due to the viscous drag for varying tooth width are the same near the rotor surface but the wide tooth seal (75% tooth width) has less interaction of the fluid flow inside the seal cavity than the narrow tooth seals due to the decrease in the cavity size.

Therefore increasing the tooth width decreases the circumferential velocity inside the cavity and $\dot{m}_{cav}$ for the 25% tooth width seal is much larger than $\dot{m}_{cav}$ for the 75% tooth width seal.

Effect of cavity shape on windback seal performance

The effect of cavity shape upon the seal performance was investigated by modifying the groove geometry. Modifying the cavity shape for the windback seals was simulated following the same procedure for the labyrinth seal. The original design of the cavity shape was a rectangular groove. One design for the cavity shape is simulated by replacing the square top with a complete semi-circle. Another design of the cavity shape was compared with where the entire groove region is only the semi-circle profile. The second modification also reduces the tooth height. The third design has the same groove shape as the second design but the 25% of the pitch of the second design is replaced with 33% of the pitch. Since the cavity of the second and third modification has only a complete semi-circle profile, tooth heights for these designs are decreased to the radius of the complete semi-circle. The air leakages of four different cavity shapes (rectangular, semi-circular deep, 25% tooth width semi-circular shallow, and 33% tooth width semi-circular shallow) are compared for three different pressure drops at the rotor speeds of 0 and 15,000 rpm.

For the labyrinth seals discussed in the previous section, modifying the seal cavity shape did not affect seal leakage rate according to the two-dimensional simulation in this study. However, the modification of the cavity shape affected the strength of the vortex which converts the kinetic energy issuing from each tooth into internal energy. The height of the teeth did not have as great an effect on the leakage rate as did the cavity width.

Figures C52 to C54 show the effect of cavity shape upon the leakage rate for the windback and labyrinth seals. The semi-circular deep groove windback seal leaks 2.3% less than the baseline windback seal. In the two-dimensional simulation for the labyrinth seal the difference of leakage was less than 1% due to the small decrease in the area of the groove.

For the labyrinth seal, the second design, semi-circular shallow groove, leaked 3% less than the baseline design, while for the windback seal, it leaked 14% less than the baseline design. This means that the labyrinth seal possesses a small effect for the tooth height in the leakage data while the windback seal has a larger leakage rate dependence upon the tooth height due to the decrease in flow area in the cavity to accommodate $\dot{m}_{cav}$.

For the labyrinth seal, the third design, semi-circular shallow groove with 33% of the pitch, leaked 6% less than the baseline design seal, while for the windback seal it leaked 16% less than the baseline design. The leakage flow rate for the third modification for the windback seal is affected by the tooth width of pitch, cavity size reduction, and cavity shape. Therefore, the leakage flow rate for the windback seal decreases with reducing the cavity size.

Table 13 presents the effect of shaft rotation with varying the cavity shape (see the Table 10 for the baseline design). The baseline design and first modification have a small dependence (3-6%) upon shaft rotation, while the second and third modifications possesses as much smaller dependence (1-3%). This is due to the smaller cavity area which reduces $\dot{m}_{cav}$. Since $\dot{m}_{cav}$ is the leakage effected by the shaft rotation which is enhanced by the tangential velocity, the substantially reduced $\dot{m}_{cav}$ does not greatly

change $\dot{m}_{total}$ with the rotor speed. $\dot{m}_{utooth}$ for the three modifications is minimally

affected by shaft rotation.

Table 13 Shaft rotation effect of windback seals for three different cavity shapes

ΔP (kPa)	Leakage increase % (from 0 to 15,000 rpm)								
	First Modification			Second Modification			Third Modification		
	$\dot{m}_{tot}$	$\dot{m}_{cav}$	$\dot{m}_{utooth}$	$\dot{m}_{tot}$	$\dot{m}_{cav}$	$\dot{m}_{utooth}$	$\dot{m}_{tot}$	$\dot{m}_{cav}$	$\dot{m}_{utooth}$
34.47	6.3%	89.5%	-0.6%	3.1%	368%	-1.4%	2.7%	494%	-1.0%
68.95	4.2%	53.6%	0.5%	1.8%	254%	-1.3%	1.4%	358%	-1.0%
103.42	3.3%	44.9%	0.2%	1.0%	208%	-1.5%	1.0%	293%	-0.9%

Figures C55 and C56 show the leakage flow rate for the two leakage paths. As

the rotor speed increases, the leakage flow rate inside the seal cavity increases but the

leakage flow rate under the teeth decreases. Since the baseline and semi-circular deep

designs have the same effect due to the small area change between two, the performance

for the leakage data has the same trend. For the baseline and semi-circular deep designs

the leakage flow rates inside the cavity were 10% and 9% of the total leakage flow rate,

while for the semi-circular shallow designs were only 3% and 2% of the total leakage

flow rate. This means that the increase percent of $\dot{m}_{cav}$ for four different cavity shapes is

maximum at the third design with the lowest pressure differential but $\dot{m}_{cav}$ does not greatly affect $\dot{m}_{tot}$.

As discussed earlier, modifying the cavity shape has a small effect on the windback seal and a great effect for the cavity depth while the labyrinth seal has a negligible effect for cavity shape and a small effect for the cavity depth.

Table 14 Leakage difference between $\dot{m}_{lab}$ and $\dot{m}_{utooth}$ with three differential pressures and four rotor speeds

Rotor speed (rpm)	Leakage difference % between $\dot{m}_{lab}$ and $\dot{m}_{utooth}$								
	First Modification			Second Modification			Third Modification		
	ΔP (kPa)			ΔP (kPa)			ΔP (kPa)		
	34.5	68.9	103.4	34.5	68.9	103.4	34.5	68.9	103.4
0	1.0%	3.3%	2.9%	1.1%	0.1%	0.1%	1.2%	1.2%	2.4%
5,000	1.2%	3.5%	3.2%	1.4%	0.3%	0.4%	1.3%	1.3%	2.9%
10,000	1.7%	3.8%	3.4%	1.6%	0.1%	0.04%	1.9%	1.2%	2.7%
15,000	1.5%	4.9%	4.2%	1.5%	0.6%	0.3	1.5%	0.8%	2.5%

Table 14 presents the leakage difference of the labyrinth seals and $\dot{m}_{utooth}$ of the windback seals. The leakage data are in good agreement with the modifications of the

cavity shape. The leakage rate for the labyrinth seal were within 2.9% on the average for the first design, 0.5% for the second design, and 0.8% for the third design of $\dot{m}_{utooth}$ for the windback seal. Therefore, $\dot{m}_{utooth}$ for the windback seal with four different cavity designs can be predicted by two dimensional labyrinth seal analysis. This allows simple two dimensional labyrinth seal simulations to be used to predict the leakage under the tooth of windback seals. The remaining task is how to determine the leakage through the cavity.

Table 15 presents the reduction of $\dot{m}_{cav}$ with the cross sectioned cavity area. As the cross sectioned area of the cavity reduces, the $\dot{m}_{cav}$ decreases 14% for the first modification, 78% for the second modification, and 85% for the third modification.

Table 15 Reduction of $\dot{m}_{cav}$ with the reduction of the cross sectioned cavity area

$\dot{m}_{cav}$ Reduction %					
First Modification		Second Modification		Third Modification	
$\dot{m}_{cav}$	% Area	$\dot{m}_{cav}$	% Area	$\dot{m}_{cav}$	% Area
14 %	10 %	78%	63 %	85%	72%

The axial pressure distributions along the middle of the clearance for four different cavity shapes are shown in Figures C57 and C58. In these figures, S-cir D, S-

cir S, and t represent semi-circular deep, semi-circular shallow, and tooth width, respectively. The effect of cavity shapes was negligible for the pressure distribution in the labyrinth seal. There is a small effect for the windback seal due to the reduction of the cavity size. The first modification, semi-circular deep, shows a similar response as the baseline seal for the pressure distribution (see the pressure contour in Figure C59). For the semi-circular shallow groove seals, the pressure drop at the inlet of each tooth except the first and last teeth is smaller than the baseline design due to the decrease in cavity depth, while the pressure drop under first and last teeth is larger than the baseline design. This effect can help force the oil back into the bearing area since the axial velocity is accelerated by the larger pressure drop generated under the first and last tooth. Increasing the tooth width decreases this effect.

The velocity contours on the 270 degree sliced plane are compared for the four different cavity shapes in Figures C60 to C62. The operating condition is 15,000 rpm and 34.47 kPa. From the axial velocity contour (Figure C60) and the axial velocity distributions along the middle of clearance in the four different angle planes (Figure C63), V_x under each tooth except the first and last tooth for the baseline seal design is larger than the other designs while V_x under the first and last teeth is smaller than the semi-circular shallow seal with the 25% tooth width. As discussed Figures C57 and C58 the semi-circular shape seal with the 25% tooth width has a larger pressure drop under the first and last teeth than the baseline design. The axial velocity distributions in the four different sliced planes (Figure C63) demonstrate this effect. Figure C61 shows the radial velocity contours in the 270° sliced plane. As the cavity size reduces, the

magnitude of the radial velocity decreases and the strength of the vortex inside the cavity decreases. These values range from -12.5 to 21.6 m/s for the baseline, -9.5 to 17.6 m/s for the first modification, -7.7 to 9.0 m/s for the second modification, and -6.6 to 8.7 m/s for the third modification. It is due to the reduction of cavity size. The third design, the semi-circular shallow seal with 33% of the pitch, also produces a decrease in the axial and radial velocity due to the reduction of the cavity size. Figure C62 presents the circumferential velocity contours for different cavity shapes. For the first modification, the semi-circular deep seal, V_θ inside the seal cavity increases since V_θ in the clearance region is larger than the baseline design. For the second modification, the semi-circular shallow seal, V_θ inside the seal cavity also increases since V_θ in the clearance region is larger than the baseline design and there is less fluid in the cavity to accelerate by the viscous drag. V_θ inside the seal cavity for the second design is larger than the first design. The baseline and first modification seals have the same geometry except the top of the cavity. However the modification to the semi-circular shapes increases the circumferential velocity. Therefore, the circumferential velocity varies with the different configurations and operating condition. This affects the cavity flow. For the third modification, semi-circular seal with 33% tooth width, since increasing the tooth width from 25% to 33% increases the wall friction in the clearance region, V_θ in the clearance region and hence, inside the seal cavity decreases.

Effect of shaft diameter on windback seal performance

The effect of shaft diameter on the seal performance was investigated by increasing the shaft diameter. It is evaluated how the seal diameter affects the leakage rate for the baseline windback seal. The baseline seal has a shaft diameter of 116.8 mm with 0.1016 mm clearance. It was modified to 203.2 and 304.8 mm shaft diameter. Since the number of grid nodes was increased in the circumferential direction due to increase of the shaft diameter, the final total number of nodes was increased to 1,100,000 for the shaft diameter of 203.2 mm and 1,600,000 for the shaft diameter of 304.8 mm. Figure C64 shows the leakage flow rate for the three differential pressures with shaft diameters of 116.8, 203.2, and 304.8 mm and a radial clearance of 0.1016 mm. There is a linear increase in leakage with seal diameter which expected since the leakage area increases linearly with shaft diameter. However, the ratio of the mass flow rate to the shaft diameter shown in Figure C65 is not constant. For no shaft rotation, this ratio decreases 5.1% and 1.7% while increasing from 116.8 to 203.2 mm and from 203.2 to 304.8 mm, respectively. For the rotor speed of 15,000 rpm, it decreases 5.5% and 3.2%.

Figures C66 and C67 show the leakage for the two leakage paths of the fluid flow for the windback seals. As the shaft diameter increases, the leakage flow rate inside the cavity decreases with no shaft rotation but increases with shaft rotation due to the V_θ boundary layer crossing the clearance and increasing $\dot{m}_{cav}$ by viscous drag. The percent of the cavity leakage flow rate to the total leakage flow rate decreases with increasing the shaft diameter. As the rotor speed increases, the leakage flow rate inside the seal cavity increases but the leakage flow rate under the teeth decreases. The cavity flow rate

decreases with the shaft diameter. Since the length of the cavity increases with increasing shaft diameter much the same as increasing a pipe length decrease the flow rate. However, shaft rotation effects increase with shaft diameter since V_θ on the shaft surface increases with increasing shaft diameter producing more viscous drag pulling the fluid through the cavity.

Figure C68 presents how the seal diameter affects the leakage flow rate under the teeth for the windback seal. The ratio of mass flow rate under the tooth to the shaft diameter is almost constant with no shaft rotation, but it decreases 5% at the lowest differential pressure and 4% at the highest differential pressure with the shaft rotation. For no shaft rotation, the leakage data under the tooth can be predicted by simple calculation.

Figures C69 and C70 show a comparison of the leakage data for the labyrinth seal and under the tooth windback seal at the rotor speeds of 0 and 15,000 rpm. $\dot{m}_{utooth}$ for the windback seals with three different shaft diameters were within 3.5% of the leakage data in the labyrinth seal on the average. The flow rate under the tooth for the windback seal can be analyzed with simple two-dimensional labyrinth seal analysis and the effects of the windback seal cavity flow are additive to the labyrinth seal leakage.

The pressure distribution and pressure contour plots shown in Figures C71 and C72 show little effect of the shaft diameter. The axial and radial velocities in Figures C73 and C74 decrease as the shaft diameter increases. The vortex strength inside the cavity also decreases with increasing the shaft diameter. The under the tooth cross sectional area (πDc) increases with increasing the shaft diameter and the pressures inside the seal are almost same for the three different shaft diameters as the flow progresses through the seal. Therefore, increasing the shaft diameter decreases the axial velocity and radial velocity due to the decrease of the under the tooth cross sectional area and the vortex strength also decreases. The axial velocity distributions along the middle of clearance in the four angular planes shown in Figure C76 demonstrate details of the axial contour plot. Figure C75 shows that the circumferential velocity increases with increasing the shaft diameter due to shaft rotation effect. Since the circumferential velocity increases with increasing the shaft diameter, the circumferential velocity inside cavity also increases due to larger viscous drag from shaft acting on the cavity fluid.

Effect of tooth location on windback seal performance

The effect of the tooth location on the seal leakage performance was investigated with tooth on stator (TOS) and tooth on rotor (TOR) designs. The windback seals simulated so far in this study have a tooth on stator. The TOR windback seal has the same geometry as the baseline TOS windback seal. In general, the labyrinth seal with tooth on stator leaks more than that with tooth on rotor. The maximum difference in the leakage data for baseline seals was within 3%. TOS and TOR labyrinth seals have the same effect with varying the rotor speed except for the lowest differential pressure.

The simulations for the TOR windback seal were performed with no rotor eccentricity. Figures C77 and C78 show the leakage flow rate for tooth locations of windback seal with three differential pressures at the rotor speed of 0, and 15,000 rpm. The TOS windback seal leaks an average of 4.8% more than the TOR windback seal. The maximum difference in the leakage flow rate was 7% at the lowest differential pressure with no shaft rotation, while the minimum difference was 3.8% at the highest differential pressure with the rotor speed of 15,000 rpm. For the lowest differential pressure, as the rotor speed increases from 0 to 15,000 rpm, TOS increases by 5% while TOR increases by 8%.

These data explain that TOR windback seal has a greater effect for a helical groove. This is due to the enhanced pumping action caused by the increased rotor surface area.

The pressure distributions for these two seals along the middle of the clearance with the rotor speed of 15,000 rpm are shown in Figure C79. The inlet and exit pressure drop for TOR windback seal is much larger than TOS. This indicates that the kinetic energy generated by the pressure drop under the first and last teeth for TOR windback seal is larger than that for TOS.

The axial velocity distribution along the seal clearance shown in Figure C80 supports the analysis of the pressure distribution. The axial velocity under the first and last teeth for the TOR seal is much larger than that for the TOS. This is due to large pressure drop in the TOR seal.

A further study of how the windback seal with the tooth on rotor works with varying the clearance, rotor eccentricity, tooth width, cavity size, and shaft diameter should be performed experimentally and analytically in a future study.

Summary

The primary objective in this study is how a windback seal can isolate bearing oil from the gas face seal in a gas compressor. A secondary objective is to minimize gas leakage. The optimal design should be satisfied with these objectives in mind.

The windback seal leaks more than the equivalent labyrinth seal. The leakage flow rate for labyrinth seals decreases with increasing the rotor speed. However, increasing the rotor speed increases the leakage flow rate for windback seals. This is due to the helical groove producing a pumping action from the high to low pressure regions.

The pressure distribution for windback seals decreases along the axial and helical groove directions. The pressure inside the seal cavity is almost constant. There is no shaft rotation effect for the pressure, axial velocity, and radial velocity while the circumferential velocity has a great effect. The pressure drop under each tooth increases V_x. V_x increases as the flow progresses through the seal due to the decrease in the air density. The axial velocity and viscous interaction at the cavity through flow interface causes the vortex inside the seal cavity. The vortex strength increases with increasing the pressure differential and rotor speed. Since V_θ is very dependent on the viscous drag of the rotor rotation surface, V_θ increases with increasing the rotor speed. The leakage flow rate through the cavity increases with increasing V_θ due to the increase in the rotor speed.

Increasing the seal clearance increases the total leakage flow rate and decreases the leakage flow rate through the seal cavity. As the seal clearance increases, the axial and radial velocities increase, the circumferential velocity decreases, and the vortex strength increases. The windback seal with the minimum clearance (0.0508 mm) leaks

less than the 0.1016 mm and 0.1524 mm seals but has the weak vortex inside the seal cavity. The swirling motion of the fluid and the magnitude of the tangential velocity inside the cavity directly affect the gas ability to remove oil from the seal. Since these value are low in the 0.0508 mm seals it will not be as effective as the larger clearances at preventing oil contamination. Increasing the seal clearance from 0.1016 to 0.1524 mm increases the leakage flow rate and vortex strength. However, since these two seals have the similar characteristics in the flow field inside the seal, the optimal clearance in this study is 0.1016 mm.

Increasing the tooth width decreases the total and cavity leakage flow rates. The 25% tooth width seal leaks 11% and 17% more than the 50% and 75% tooth width seals, respectively. As the rotor speed increases, the leakage flow rate increases for the 25% and 50% tooth seals while it decreases for the 75% tooth seal. The 75% tooth width seal has a minimal groove effect. The axial, radial, and circumferential velocities inside the seal cavity decrease as the tooth width increases. The vortex strength also decreases. The wide tooth width seal has two vorticies inside the cavity and decreases the helical groove effect. Hence the optimal tooth width is appropriate between 25% and 50% tooth width in terms of the leakage.

For the cavity shape cases, windback seals with four different cavity sizes were considered by decreasing the cavity size and modifying the cavity shape since the modification of the cavity shape affects the vortex strength. Decreasing the cavity size decreases the total and cavity leakage flow rate. These modifications result in leakage data reduction of 2% for the first modification, 14% for the second modification, and

16% for the third modification from the baseline seal with the rectangular cavity shape. Decreasing the cavity size decreases the vortex strength. However, the axial velocity under the first and last tooth for the semi-circular shallow designs is as large as the baseline design. This can help force the oil back to the bearing side. The semi-circular shallow design with the 33% tooth width is mechanically stronger and has an average of 16% less leakage than the baseline design (rectangular cavity shape and 25% tooth width and has the maximum increase percent for the cavity flow leakage as the rotor speed increases.

Hence, the optimal windback seal design in the air simulations is the semi-circular shallow shape with a 33% tooth width and 0.1016 mm clearance. This seal satisfies the effect of the clearance, tooth width, and cavity shape and minimizes gas leakage rate.

The rotor eccentric windback seal has a negligible effect on the leakage flow rate. The rotor eccentricity ratio of 0.25 was selected for direct comparison to oil filled seals.

THREE-DIMENSIONAL SIMULATIONS - OIL

This section provides detailed information on how oil might migrate from the bearing side of the seal to the gas seal plenum. The important objective is to determine if it is possible for a windback seal to transfer oil from the oil lubricated bearing side of the seal into the gas seal side by means of pressure fields generated by the viscous drag of oil inside an rotor eccentric seal (i.e. hydrodynamic lubrication). If the hydrodynamic generated pressure is large enough, it will induce an oil flow into the gas plenum. For this study, the seals are totally filled with oil. Future studies should include two component studies where gas and oil are simultaneously present within the seal. The present simulations include annular, labyrinth, and windback seals with 25% rotor eccentricity ratio and 0.1016 mm radial clearance. The flow under these conditions is considered to be laminar based upon the Reynolds number of the oil filled annuli. The properties of the oil are : $\rho = 889$ kg/m^3, $\mu = 1.06$ kg/(m s).

Oil leakage flow rate

Figures D1 and D2 show the net oil leakage flow rate for smooth, labyrinth and the baseline windback seal for differential pressures of 34.47 and 103.42 kPa. The y-axis was changed to a logarithm scale due to the large variance present. The windback seal shows a three order of magnitude increase in the leakage flow rate as the rotor speed increases from 0 to 15,000 rpm. This is due to the pumping action of the helical groove as was observed by Bootsma (1975) for a spiral grooved bearing. The rotating shaft causes a large tangential velocity due to the increased viscous drag of the oil compare to air. This in turn causes the oil to move through the helical cavity channel producing a net leakage flow rate through the seal. The labyrinth seal having discrete cavity rings only leaks about three times more than the smooth seal. There is no leakage dependency upon the rotor speed for the smooth or the labyrinth seal. For the annular, labyrinth, and windback seals without shaft rotation, there is a linear increase in leakage with the pressure differential and the ratio of the leakage flow rate to the pressure differential is almost constant. With shaft rotation, the leakage flow rate for the annular and labyrinth seals increases linearly with increasing the pressure differential, while the leakage flow rate for the windback seal does not change for the three differential pressures.

Pressure and velocity flow field

Figure D3 presents the pressure contours along the middle of the clearance for the smooth seal with 25% rotor eccentricity operating with the oil at the pressure differential of 103.42 kPa, and the rotor speed of 15,000 rpm. The maximum and minimum clearances are located in positive y and negative y directions, respectively. The results are consistent with a finite length journal bearing analysis. This study is assuming the oil will not cavitate due to the extremely low pressures predicted. The goal of this part of the study is to illustrate that hydrodynamic effects can cause undersigned oil flow into the gas seal plenum and to determine how the groove in the windback seal may decrease the effect. The pressure contour plot shown in Figure D4 was sliced in four radial cross section angles. The maximum and minimum clearances are located in 270° and 90° sliced plane, respectively. To obtain exact information in the flow field, the clearance regions for all planes were expanded along the radial direction.

The pressure contour for the 25% rotor eccentric smooth seal shown in Figure D3 shows the azimuthal pressure variance on the rotor surface. The result is that of a finite length journal bearing when the seal is filled with oil. The magnitude of the pressure generated is 145 times more than the operating pressure differential. The range of positive and negative pressures is $\pm 1.5 \times 10^7$ Pa. This low pressure would cause cavitation of the oil if the seal was operated at these conditions. The purpose of this simulation was to show how the hydrodynamic action can generate pressure fields which may cause oil to flow into the gas plenum. This pressure field explains how the fluid can be pushed outside the seal into the gas plenum and pulled inside the seal from the bearing area.

Similarly, large positive and negative pressures in the clearance regions of 0° and 180° sliced planes are clearly shown in Figure D4.

Figures D5 and D6 show the axial velocity contour plots for a pressure differential of 103.42 kPa and the rotor speed of 15,000 rpm. There are positive and negative axial velocities inside the seal whose range is ±2.5 m/s. This indicates that the fluid overcomes the purge gas pressure field to move into the gas seal plenum. This is represented by the negative axial velocity. Figure D6 demonstrates that the fluid is pushed out both sides of the seal in the 0° slice plane while pulled inside both sides of the seal on the 180° slice plane. Thus if a smooth annular seal was used to isolate the gas plenum from the bearing, any oil contamination could set up journal bearing type pressure fields which may pull oil in on the suction side from the bearing and inject oil into the gas plenum on the pressure side. Figures D7 show the circumferential velocity contours for a pressure differential of 103.42 kPa and the rotor speed of 15,000 rpm. The circumferential velocity does not change in the axial direction, but decreases in the radial direction from rotor surface for the clearance region.

The next step is to evaluate how a labyrinth seal changes the flow fluid inside the seal when oil is present. Are the grooves sufficient to destroy the hydrodynamic induced pressure field? Figure D8 presents the pressure contours on the middle of clearance for the labyrinth seal with 25% rotor eccentricity operating with oil at the pressure differential of 103.42 kPa and the rotor speed of 15,000 rpm. The pressure generated by the hydrodynamic effect ranges in values ±120 kPa, a hundred times smaller than for the smooth seal. Figure D9 shows that the pressure at the four angular slice planes is greatly

decreased compared to the 25% rotor eccentric smooth seal. However, the labyrinth seal with 25% rotor eccentricity still has some of the journal bearing action but the pressure generated by the oil is greatly decreased.

Figure D10 and D11 show that the magnitude of the axial velocity inside the seal has decreased and ranges ±0.3 m/s inside the seal cavity near the clearance. If the negative axial velocity under the tooth on the high pressure side of the seal is present, the oil will contaminate the gas plenum. The axial velocity distribution on the middle of the clearance for the 25% rotor eccentric labyrinth seal in the four different angle planes shown in Figure D18 presents that the negative axial velocity exists on the gas plenum side.

Oil contamination in a labyrinth seal cannot be easily removed from the cavities once it is present. A windback seal provides a means of removal by the continuous cavity path back to the bearing area. Given sufficient purge gas pressure, the oil can be eliminated before the compressor is started. This section will determine if the pressures generated in an oil flooded windback seal which is operating at speed will purge back to the bearing or contaminate the gas plenum.

Figures D13 and D14 present the pressure contours for the 25% rotor eccentric windback seal operating with oil at the pressure differential of 103.42 kPa and the rotor speed of 15,000 rpm. The 25% rotor eccentric windback seal produces pressures up to 200 kPa inside the seal. This may be sufficient to cause oil flow into the gas plenum. It is generated by the journal bearing action but the pressure generated by the oil is greatly diminished compared to the smooth seal but slightly larger than for the labyrinth seal.

Since the groove region in the 270° and 90° sliced plane is open with the gas plenum side and bearing side, respectively, the positive and negative pressures generated in the groove region open near the gas plenum side and bearing side are larger than the 25% rotor eccentric labyrinth seal.

Figures D15 and D16 show the axial velocity contours. The same contour levels are used for direct comparison with the 25% rotor eccentric labyrinth seal. Both the labyrinth and windback seal with 25% rotor eccentricity have a small amount of negative axial velocity inside the seal. The axial velocity for the windback seal ranges from -0.4 to 0.4 m/s except in the open groove regions near the inlet and exit plenums in the 90° and 270° sliced planes. The axial velocity in the open groove regions reaches -4.8 m/s. The windback seal is also very effective at destroying the journal bearing affect as was the labyrinth seal. The magnitude of the pressure and axial velocity for the 25% rotor eccentric windback seal is larger than the 25% rotor eccentric labyrinth seal but has a smaller level of pressure variance and negative axial velocity in the seal except near the starting and ending groove region than the labyrinth seal. This is demonstrated by Figure D18. The axial velocity distributions along the middle of clearance for four different angles are plotted. To analyze the magnitude of the axial velocity for direct comparison, the scale was decreased to -0.4 to 0.4 m/s. The negative axial velocity for the 25% rotor eccentric windback seal is larger in magnitude than that for 25% rotor eccentric labyrinth seal. For the 270° section, the negative axial velocity for windback seal in the open groove region with the inlet plenum is shown. Since the groove starts between 240° and 270° and this groove region was open with upstream plenum, the negative axial velocity

is generated in this region. This means that the 25% rotor eccentric windback seal drives backflow into the gas plenum side more than the 25% labyrinth seal. However, once the flow progresses from the starting groove region, the positive axial velocity inside the cavity shown in the Figure D16 is larger than the negative axial velocity due to the continuous helical groove. Therefore, the windback seal can be used to force the oil back into the bearing side before starting the compressor by applying a purge gas flow. This will cause the oil to flow into the bearing region. It may be necessary to apply a larger purge gas pressure before startup to make sure all oil is purged. Once the purge is completed, a smaller purge gas pressure can be used to help keep oil out of the windback seal. A labyrinth seal will not easily clean itself with a gas purge before the compressor startup due to the lack of a flow path for the oil rugged in the labyrinth cavity. A further study of how this startup purge works and how much the pressure differential is required should be performed experimentally and analytically in a future study.

Effect of tooth width

The effect of increasing the tooth width for the 25% rotor eccentric windback seals operating with oil was investigated. The reason for this study is to determine how increasing the tooth width, and hence the ruggedness of the seal, influences the oil migration. The leakage flow rate, pressure, and axial and tangential velocities are presented to allow detailed information about the flow field to be obtained. The axial contour plots use the same contour levels as before for direct comparison.

Figure D19 and D20 present the oil leakage flow rate for three tooth widths. The leakage flow rate does not change as the pressure differential increases from 34.37 to 103.42 kPa. There is a linear increase as the rotor speed increases from 0 to 15,000 rpm. For three tooth width seals, the leakage rate increases by 100% for three differential pressures as the rotor speed increases by 100%. The flow is due to the pumping action of the helical seal and the leakage flow rate increases as the groove size increases. This shows that normal purge gas pressures have no effect upon the leakage when only oil is present.

The pressure contour plot for the 25% rotor eccentric windback seal with the 50% of the pitch is shown in Figure D21. The pressure generated by the hydrodynamic effect for the 50% tooth width seal is twice as large as the baseline design but pumps 53% less fluid. The range of the pressure is -400 to 500 kPa. The positive and negative pressures are located in 0° and 180° sliced planes. The large pressure is generated inside the first cavity in the 270° sliced plane near where the groove starts, between 240° and 270°. This region is open to the inlet plenum. Some of the journal bearing action exists

in the clearance region. The oil cavity leakage flow rate is much larger than the under the tooth leakage flow rate. Increasing the tooth width increases the journal bearing action. This decreases the oil leakage flow rate. The tangential velocity inside the cavity decreases with increasing the tooth width. This is due to the viscous effect.

Figure D22 shows that a small amount of the axial velocity is produced inside seal. The magnitude of axial velocity is -0.45 to 0.45 m/s except the open groove region near the inlet and exit plenum in the 90° and 270° sliced planes. The axial velocity in the open groove regions reaches -7 m/s (see Figure D26).

Figure D24 and D25 show the pressure and axial velocity contours for the 25% rotor eccentric windback seal with the 75% of the pitch. The journal bearing affect is clearly shown. The pressure generated by the hydrodynamic effect for the 75% tooth width seal is seven times as large as the baseline design but pumps 85% less fluid. The pressure variance increases to ±1,400 kPa. There is both positive and negative axial flow present. The magnitude of the axial velocity is ±0.8 m/s except in the open groove regions near the inlet and exit plenums in the 90° and 270° sliced planes. The axial velocity in the open groove regions reaches -8 m/s (see Figure D26).

The circumferential velocity contours for the 25% rotor eccentric windback seal with varying tooth width are shown in Figure D17, D23, and D27. V_θ decreases in the radial direction from rotor surface. As the tooth width increases, V_θ inside the seal cavity decreases but is not affected by the rotor surface.

The 50% and 75% tooth width seals possesses the journal bearing action. The pressures for the 50% and 75% tooth width seals are 2 and 7 times as large as the 25% tooth width seal and the axial velocities increases to 12% and 100% compared to the 25% tooth width seal. Therefore, as the tooth width increases, the journal bearing action increases and the axial velocity also increases. Increasing the tooth width of pitch enhances the journal bearing affect and increases the magnitude of axial velocity and pressure inside the seal. Therefore, the optima seal from the three different tooth width seals is the 25% tooth width when the seal is filled with oil.

Effect of cavity shape

The effect of cavity shape upon the seal performance for the 25% rotor eccentric windback seals operating with the oil was investigated with different cavity shapes. Oil leakage flow rates for different cavity shapes are shown in Figure D28 and D29 and have a linear increase as the rotor speed. There is no differential pressure dependence in leakage flow rate except for the no shaft rotation case. The rectangular shape leaks 2.6%, 38.5%, and 52.3% more than the semi-circular deep, semi-circular shallow with 25% tooth width, and semi-circular shallow with 33% tooth width, respectively as the cavity sizes decrease by 10%, 63%, and 71%.

In these simulations of the four different cavity shapes, there are the differences for the cavity regions between 240° and 270° (groove starting region), and 90° and 120° (groove ending region) near the inlet and exit plenums. The groove in these regions for the rectangular and semi-circular deep shape designs is open with the inlet and exit plenum while for the semi-circular shape designs, only the clearance region is open.

Figures D30 and D31 show the pressure and velocity contours for the 25% rotor eccentric windback seal with semi-circular deep shape and 25% of the pitch. The pressure ranges from -200 to 200 kPa. It also has the journal bearing action. The axial velocity distribution for the semi-circular deep shape seal has the same trend as the baseline design seal. The magnitude of the axial velocity is -0.4 to 0.4 m/s except the open groove region near the inlet and exit plenum in the 90° and 270° sliced planes. The axial velocity in the open groove regions reaches -4.8 m/s (see Figure D38). The semi-

circular deep seal has the same values for the axial velocity inside the seal as the baseline seal.

Figures D33 and D34 show the pressure and velocity contours for the 25% rotor eccentric windback seal with semi-circular shallow shape and 25% of the pitch. The magnitude of pressure ranges from -800 to 600 kPa. It also has the journal bearing action. The axial velocity ranges from -2.8 to 2.8 m/s except in the region near the inlet and exit plenum in the 90° and 270° sliced planes. The axial velocity in the open clearance regions reaches +10 m/s (see Figure D38). This large positive axial velocity is present in the regions which are open to the clearance with the inlet and exit plenum. Hence, this effect represents that the large negative axial velocity that is generated when the groove is open with the plenums, and the large positive axial velocity is produced when the clearance region is open with the plenums.

The pressure and axial velocity contour for semi-circular shallow groove seal with 33% of the pitch is shown in Figures D36 and D37. The pressure span generated by the oil has increased to -1000 to 800 kPa. It also has the journal bearing action. The axial velocity ranges from -1 to 1 m/s except the region near the inlet and exit plenum in the 90° and 270° sliced planes. The axial velocity in the open groove regions reaches +10 m/s (see Figure D38).

Figure D32, D35, and D39 show the circumferential velocity contours for varying the cavity shape with the pressure differential of 103.42 kPa at the rotor speed of 15,000 rpm. V_θ decreases in the radial direction from rotor surface. V_θ inside the seal cavity for semi-circular deep groove seal with 25% of the pitch is not much affected by

the rotor surface. However V_θ inside the seal cavity for semi-circular shallow groove seals is affected by the rotor surface due to the height of the teeth.

The next step is to investigate how the flow field inside the seal changes when the groove region is open to the inlet and exit plenum for the semi-circular shallow seal. Figures D40 to D42 illustrate the effect of the flow filed for the modified semi-circular shallow design. The pressure variation generated by the oil was increased to -1200 to 800 kPa. It also has the journal bearing action. The axial velocity ranges from -1 to 1 m/s except the region near the inlet and exit plenum in the 90° and 270° sliced planes. The axial velocity in the open clearance regions reaches -15 m/s (see Figure D42). The axial velocity distribution shown in Figure D42 has the same trend in the 0° and 180° planes while the large axial velocity near the inlet and exit plenum in the 90° and 270° planes has the different values.

Therefore, the modification to semi-circular deep design has the same effect with the baseline design except the small decrease in the leakage and the modification to semi-circular shallow does not affect to destroy the journal bearing affect and increases the magnitude of the axial velocity.

Summary

The oil simulations in this section help to evaluate which design protects the gas face seal from the oil contamination due to hydrodynamic action when the oil is present in the windback seal. The windback seal with 25% rotor eccentricity has some of the journal bearing action but the pressure generated by the viscous drag of oil is greatly diminished compared to a journal bearing. The maximum magnitude of the pressure and axial velocity for the 25% rotor eccentric windback seal is larger than the 25% rotor eccentric labyrinth seal. However, smaller pressure and negative axial velocity is generated over most of the windback seal except in the region near the inlet and exit plenum when compared to the 25% labyrinth seal.

The leakage flow rate does not change as the pressure differential increases when the oil is present in the windback seal. From Figure D20 and D29, $\dfrac{\dot{m}}{\rho A_{cav} R w}$ is constant for all rotor speeds. This means that the leakage flow rate has a linear increase as the rotor speed increases. As the groove size increases, the leakage flow rate increases due to the pumping action of the windback seal.

For three different tooth width seals, the optimal design is the 25% tooth width seal due to lower back flow and journal bearing action. For four different cavity shape seals, the optimal design also is the semi-circular deep design. However, as discussed earlier, the axial velocities inside the seal groove starting and ending regions near the inlet and exit plenum have the large negative and positive values near the open regions (groove or clearance) with the plenum. From Figure D42, large positive axial velocities

are produced when the only clearance region is open to the plenums, while large negative axial velocities are produced when the groove is open to the plenums. Therefore, the large negative velocity generated due to the open groove region can be decreased by moving the groove starting region to a tooth width size into the downstream and the groove ending region to a tooth width size into the upstream plenum. Then the flow enters and exit only through the clearance region from the inlet and exit plenum. However, this design does not allow for the purge gas to push the oil through the channel without going over a tooth.

A further study for how the windback seal design generates the flow field by modifying various seal configuration in the open region to the plenums should be performed experimentally and analytically in a future study.

EXPERIMENTAL RESULTS FOR WINDBACK SEAL

The main objective of the experimental work is directed to the verification of the theoretical and numerical analyses. An improved windback seal design based upon the numerical simulations that minimizes gas leakage and helps prevent gas face seal oil contamination was manufactured.

In practice, experiments and simulations for two phase flow should be performed because in reality air and oil are present inside seal. However, in order to obtain information about the area and magnitude of oil migration and the precise transport phenomenon due to the journal bearing action and the pumping action of the helical groove, the simulations for a smooth annular seal, straight-through labyrinth seals, and windback seals which are either full of air or full of oil were performed in this study.

As discussed in previous section, the windback seal can be used to force the oil back into the bearing side before starting the compressor by applying a purge gas flow. In the oil simulation, the best design was the semi-circular deep seal. However, since the working fluid in this experimental work is air and the windback seal should be operated with a purge gas flow, the best design in the air simulations was selected. The improved windback seal designed based upon the numerical simulation was tested with the semi-circular shallow groove, 33% of the pitch, shaft diameter of 116.81 mm, and radial seal clearance of 0.1143 mm. Since the shaft rotation for windback seal has a minimal with gas effect, a static test was performed. The working fluid is air. Compressed air enters into a plenum and exits to atmosphere (101.325 kPa). The pressure difference across the

seal and the mass flow rate are measured. Pressure transducers are used to measure the pressure distribution inside each cavity for the windback seal.

The numerical simulation for the windback seal with 33% of the pitch, semi-circular shallow groove, and radial clearance of 0.1143 mm is compared with the experimental data in this section. Experimental data include the pressures inside the seal cavity at different locations and the mass flow rate.

Uncertainty analysis

The uncertainty analysis in calculating the leakage mass flowrate is based on Kline and McClintock (1953). The density from the ideal gas law is as following:

$$\rho = P / RT \tag{21}$$

Ignoring the uncertainty in R (Universal gas constant), the uncertainty in air density simplifies to

$$\frac{\delta\rho}{\rho} = \sqrt{(\frac{\delta P}{P})^2 + (\frac{\delta T}{T})^2} \tag{22}$$

The mass flow rate is calculated using

$$\dot{m} = \rho Q \tag{23}$$

The uncertainty in the mass flowrate is calculated using the following equation:

$$\frac{\delta\dot{m}}{\dot{m}} = \sqrt{(\frac{\delta\rho}{\rho})^2 + (\frac{\delta Q}{Q})^2} \tag{24}$$

The total uncertainty for the mass flow rate can be calculated with the uncertainty of the instruments and the measurement error obtained by the data acquisition system. The uncertainties of the instruments are 0.075% of the range for the Rosemount absolute pressure transducer, 0.3% of the range for the pressure transducer, and 0.11% of the measurements for the turbine flow meter. Table 16 shows the total uncertainty for the windback seal.

Table 16 Total uncertainty calculations for the windback seal

P_{in} (kPa)	$\delta\rho$ (kg/m^3)	$\delta\dot{m}$ (kg/s)
34.5	0.022	0.000017
68.9	0.021	0.000026
103.4	0.021	0.000036

Leakage mass flow rate

Figure E1 shows the leakage mass flow rate for the measurements and predictions with varying the pressure differentials of 34.47, 68.95, and 103.42 kPa. The leakage flow rate increases linearly as the differential pressure increases from 34.47 to 103.42 kPa. The measurements for the leakage mass flow rate are an average of 12.3% higher than the prediction data.

The leakage data for the windback seal can be non-dimensionalized according to the equations by Egli (1935), and Hodkinson (1939). The carry over coefficient, γ, found

in the equation for the flow coefficient explains the effect of kinetic energy carry over. The flow coefficient can be calculated in Equations (1), (2), and (3).

P_{in} and P_{out} are the absolute inlet and outlet pressure, n is the number of throttles and ψ is the expansion coefficient. Al-Ghasem (2007) found that the carry over coefficient for the windback seal differs Hodkinson (1939)'s labyrinth seal study. Hodkinson defines the carry over coefficient as a function of the divergence angle to exit from under the tooth to the cavity. This angle represents the dissipation of the kinetic energy. Hodkinson assumed that the divergence angle is constant as the pressure differential ranges from 2 to 6 atm. However, Al-Ghasem showed that the divergence angle decreases up to 50% as the pressure differential increases from 0.34 to 1.02 atm. Hodkinson uses a constant divergence angle of 1.15 degree while the divergence angle observed by Al-Ghasem varies from 3.71 to 68.57 degree. The dissipation of the kinetic energy inside the seal cavity increases as the divergence angle is increased. The differences between Hodkinson and Al-Ghasem studies are the pressure drop across the seal and the flow leakage inside the cavity since Hodkinson's data are obtained for much larger differential pressure compared to Al-Ghasem's data. Additionally the windback seal has the cavity leakage due to the continuous helical groove.

Figure E2 shows the variation of the flow coefficient as P_{out} / P_{in} increases. Increasing the pressure ratio decreases the flow coefficient. This plot gives same information with Figure E1.

Figure E3 presents the flow coefficient versus the axial Reynolds number. Reynolds number defines $Re = \dot{m} / \pi D \mu$. D is the shaft diameter, and μ is the dynamic

viscosity of air. From the equation, higher *Re* increases the mass flow rate. Therefore, the flow coefficient also is increased.

Pressure distribution

Static pressure data from the pressure transducers were obtained along with the seal length inside the seal cavities at six different locations. When air enters into the seal inlet through the plenum, the inlet effect due to the contraction in inlet area causes a larger pressure drop than present in the next contraction. This pressure drop increases the kinetic energy and the axial velocity under the teeth. The pressure inside the seal cavity is almost a constant value inside the cavity and then as the flow passes under the next tooth, a pressure drop is generated. Figure E4 presents the pressure distribution for measurement and prediction for three differential pressures of 34.47, 68.95, and 103.42 kPa. The pressure distribution matches well except in last two cavities since the seal tooth in the downstream side of the last cavity is much narrower than the other teeth.

Summary

The measurements for the leakage mass flow rate are an average of 12.3% higher than the prediction data. However, there is the difference between the prediction and measurement in the seal groove configuration. For the numerical simulation the seal groove is open to the inlet and exit plenum between 240° and 270° while for the experiment the open groove region with the plenums varies with the circumferential direction. Since for the numerical simulation the open groove case leaks 3.4% more than the closed groove case, it may be the different result if the open groove region is changed as an actual seal.

EMPIRICAL LEAKAGE MODEL

This section will investigate the applicability of an empirical leakage model for the windback seal leakage. The empirical study starts with the evaluation of performance information for two dimensional labyrinth seals since the leakage under the teeth of windback seals is the same as for a similar geometry labyrinth seal. Then the difference for three dimensional windback seals from the labyrinth seal is analyzed. The empirical study is based upon the numerical simulation data.

The leakage data through the seal cavity is normalized to the discharge coefficient used in the orifice flow meter according to the following equation:

$$C_d = \alpha\gamma\psi = \frac{\dot{m}_{cav}}{\pi Dc\sqrt{\rho_{in}(P_{in} - P_{out})}} \tag{25}$$

The discharge coefficient, C_d, is the combined to the product of the flow coefficient, carry over coefficient, and expansion coefficient. C_d has the dependence upon the seal clearance, tooth width, cavity size, shaft diameter, pressure ratio, and rotor speed. The empirical model for the cavity flow starts with the baseline windback seal and it will be developed by including the additional effects of the tooth width, cavity size, clearance, and shaft diameter from the baseline empirical model.

The first step is to determine the empirical model for the cavity leakage flow rate with the baseline windback seal design.

$$C_{d1} = \cfrac{1}{A_1 + \cfrac{B_1}{\ln\left[\dfrac{P_{in}}{P_{out}}\right]} + C_1 \Omega} \qquad (26)$$

$A_1 = 35.846513$, $B_1 = -1.7437772$, $C_1 = -0.00074219168$ [1/rpm]

where C_{d1} is the discharge coefficient for the baseline windback seal, Ω is the rotor speed (rpm). This empirical model fits the leakage data with the standard deviation of 0.038. However it can be improved with more complicated equation with the standard deviation of 0.00068.

The second step is to add the effects of tooth width and the cavity shape from the baseline empirical model.

$$C_{d2} = C_{d1}\left(A_2 + B_2 (A_{cav})^{1.5} + C_2 \sqrt{\Omega}\right) \qquad (27)$$

$A_2 = -0.0612325$, $B_2 = 0.00013323193$, $C_2 = 0.12627436$

where A_{cav} is the cavity area. This empirical model, C_{d2}, fits the leakage data with the standard deviation of 0.138.

The third step is to add the effect of the clearance from the second step empirical model.

$$C_{d3} = C_{d2}\left(A_3 + \frac{B_3}{c} + \frac{C_3}{\frac{P_{in}}{P_{out}}} \right) \tag{28}$$

$A_3 = -0.390606$, $B_3 = 0.00013323193$, $C_3 = 0.12627436$

$$C_{d4} = C_{d3}\left(A_4 + B_4\Omega^{2.5} + C_4\Omega^3 \right) \tag{29}$$

$A_4 = 0.97261272$, $B_4 = 2.2944203\times10^{-11}$, $C_4 = -1.7532893\times10^{-13}$

where c is the seal clearance. This empirical model, C_{d3}, fits the leakage data with the standard deviation of 0.122. The shaft rotation effect was included in C_{d4} of the curve fit from C_{d3}. The curve fit follows the leakage data with the standard deviation of 0.121.

The final step is to add the effect of the shaft diameter from C_{d4}. However, the dependence upon the shaft diameter is not modeled well due to large variation in the cavity leakage with increasing rotor speed.

Figure E5 shows the comparison of C_d obtained from the numerical simulations and C_d calculated from the final empirical model. This final empirical model, C_{d4}, includes the all effects for the seal geometry except the shaft diameter cases. However, there are some outliers in the final curve fit. These values exist at 0 rpm in the semi-circular shallow seals since the values are much smaller than the others. This is due to much smaller cavity flow resulted from the small cavity size.

SUMMARY AND CONCLUSIONS

The main objective of this study is to improve the windback seal design based upon the numerical simulations. The present study investigated the seal performance on smooth, labyrinth, and windback seals for the pressure differentials of 34.47, 68.95, and 103.42 kPa and the rotor speeds of 0, 5000, 10,000, and 15,000 rpm by presenting CFD simulations. This work investigated: (1) the effect of clearance, (2) the effect of tooth width, (3) the effect of cavity shape, (4) the effect of shaft diameter, (5) the effect of eccentricity, and (6) the effect of tooth location. The information obtained from the current investigation provides a more clear understanding of windback seal characteristics. The following summary and conclusions are made from the investigation of this study.

Flow field

1. The windback seal leaks more than the equivalent labyrinth seal due to the helical groove producing a pumping action from the high to low pressure regions.

2. The pressure distribution decreases in the axial and along the helical groove direction. The pressure inside the seal cavity is almost constant.

3. There is no shaft rotation effect for the pressure, axial velocity, and radial velocity.

4. The axial velocity increases as the flow progresses through the seal due to the decrease in the air density.

5. The vortex strength increases with increasing the pressure differential and rotor speed.

6. The circumferential velocity and the leakage flow rate through the cavity increase with increasing the rotor speed since the circumferential velocity has the great effect for the cavity flow.

Effect of clearance

1. The leakage flow rate increases with increasing the radial clearance.

2. The leakage flow rate through the seal cavity decreases with increasing the radial clearance due to the decrease in the flow resistance under the tooth.

3. Increasing the pressure differential increases the leakage flow rate.

4. As the rotor speed increases, the leakage flow rate decreases for labyrinth seals and increases for windback seals. However, the shaft rotation does not affect the leakage flow rate significantly. The shaft rotation has a great effect at the minimum clearance and the lowest differential pressure.

5. Increasing the seal clearance increases the inlet pressure drop, axial velocity, radial velocity, and the vortex strength.

Effect of tooth width

1. The leakage flow rate decreases with increasing the tooth width.

2. For labyrinth seal, at the higher differential pressure (275.79 kPa) the leakage flow rate increases with increasing the tooth width. The simulation for windback

seal for the higher differential pressure was not performed, but the same result is expected.

3. The leakage flow rate increases with increasing the pressure differential.

4. For windback seals, as the rotor speed increases, the leakage flow rate increases for 25% and 50% tooth width seals and decreases for 75% tooth width seal. Hence, the helical groove effect decreases with increasing the tooth width.

5. For labyrinth seals, increasing the rotor speed decreases the leakage flow rate.

6. Increasing the tooth width decreases the inlet pressure drop, axial velocity, radial velocity, and the vortex strength.

Effect of cavity shape

1. First modification for the seal cavity shape (rectangular to semi-circular deep) has a small effect in the leakage flow rate.

2. For windback seal, second modification to semi-circular shallow with same tooth width results in decrease in the leakage flow rate due to decrease in the cavity depth.

3. For labyrinth seal, second modification has a small decrease in the leakage flow rate. Decreasing the cavity depth does not have a great effect in the leakage flow rate.

4. For windback seal, third modification to semi-circular groove with 33% tooth width results in decrease in the leakage flow rate due to decrease in the cavity depth and increase in the tooth width.

5. For labyrinth seal, third modification results in decrease in the leakage flow rate due to increase in the tooth width.

6. The baseline design has a greater shaft rotation effect than other modifications. However it is small effect.

7. Decreasing the cavity size decreases the vortex strength.

8. The axial velocity under the first and last tooth for semi-circular shallow designs is as large as the baseline design.

Effect of shaft diameter

1. Increasing the shaft diameter increases the leakage flow rate.

2. For windback seal, there is a linear increase in leakage with the seal diameter but the ratio of the leakage flow rate to shaft diameter is not constant while for labyrinth seal, the ratio is almost constant.

3. As the shaft diameter increases the axial and radial velocity decreases while the circumferential velocity increases.

Effect of eccentricity

1. Increasing the rotor eccentricity from 0 to 0.25 results in small increase in leakage flow rate. The difference of leakage flow rate is within 1%.

Effect of tooth location

1. For windback seal, TOS seal leaks average 4.8% more than TOR seal.

2. For labyrinth seal, TOS seal leaks 3% more than TOR seal.

3. As the rotor speed increases, TOS seal increases by 5% while TOR seal increases by 8%.

Numerical simulation - oil

1. 25% rotor eccentric labyrinth seal is more effective at destroying the journal bearing action than 25% rotor eccentric windback seal.

2. 25% rotor eccentric windback seal generates smaller axial negative velocity than 25% rotor eccentric windback seal except the open regions to the inlet and exit plenums.

3. The windback seal leaks 1000 times more than the labyrinth and smooth seal with shaft rotation.

4. There is no leakage dependency upon the rotor speed for the smooth and labyrinth seal.

5. The leakage flow rate for the windback seal does not change for three differential pressures with shaft rotation.

6. Since the leakage flow rate for the windback seal increases linearly as the the rotor speed increases, $\dfrac{\dot{m}}{\rho A_{cav} Rw}$ is constant for varying shaft rotation.

7. The leakage flow rate for the windback seal increases as the groove size increases due to the pumping action of the windback seal.

8. Increasing the tooth width of pitch is not effective at destroying the journal bearing affect.

9. The modification to semi-circular shallow does not affect to destroy the journal bearing affect.

Experimental verification

1. The measurements for the leakage mass flow rate are an average 13% difference of the prediction data.

2. The pressure distribution matches well except last two cavities.

This study provided detailed information about seal performance by simulating a smooth seal, straight through labyrinth seals and windback seals which are either full of air or full of oil. The windback seal has two leakage paths. One is the leakage under the seal teeth and other is the leakage through the seal cavity. The cavity leakage has a small portion of the total leakage flow rate. The leakage under the seal teeth can be predicted by two dimensional labyrinth simulations. The empirical model for the cavity flow was developed with the standard deviation of 0.12.

The optimal designs for the air and oil simulation are the semi-circular shallow cavity shape seal with the 33% tooth width and the semi-circular deep cavity shape seal, respectively. For the oil simulation the pressure generated in the semi-circular shallow cavity shape seal is much larger than the operating pressure differential. This seal has a journal bearing affect. This pressure field may pull oil in on the suction side from the

bearing and inject oil into the gas plenum on the pressure side. However, the positive axial velocity inside the cavity is larger than the negative axial velocity due to the continuous helical groove. Due to this reason the windback seal can be used to force the oil back into the bearing side before starting the compressor by applying a purge gas flow. A further study of (1) how this startup purge works and how much the pressure differential is required (2) how the windback seal works when gas and oil are simultaneously present in the seal, (3) how the windback seal design generates the flow field by modifying various seal configuration in the open region to the plenums (4) how the windback seal with the tooth on rotor works with varying the clearance, eccentricity, tooth width, cavity size, and shaft diameter should be performed experimentally and analytically in a future study.

REFERENCES

Al-Ghasem 2007 Windback seal design for gas compressors; numerical and experimental study. Ph.D. Dissertation, Texas A&M University, College Station.

Bell, K. J., & Bergelin, O. P. 1957 Flow through annular orifices. *Transactions of the ASME*, **79**, 593-601.

Bootsma, J. 1975 Liquid – lubricated spiral – groove bearings. Ph.D. Dissertation, Technology University Delft, Delft, Netherlands.

Cogan, K. C. 1982 Leakage prediction of incompressible fluids in labyrinth seals. M.S. Thesis. Texas A&M University, College Station.

Dollin, F., & Brown, W. S. 1937 Flow of fluids through openings in series. *Engineer*, **164**, (4259), 223-224.

Egli, A. 1935 The leakage of steam through labyrinth seals, *Trans. ASME*, **57**, 115-122.

FLUENT 6 User's Guide, 2005 Jan, FLUENT Incorporated, Centrerra Resource Park, 10 Cavendish Court, Lebanon, NH 03766.

Gansle, A., & Childs, D. 1996 Experimental leakage and rotordynamic results for helically grooved annular gas seals. *ASME Trans. Journal of Engineering for Gas Turbines and Power*, **118**, 389-393.

Heffner, F. E. 1960 A general method for correlating labyrinth seal leak-rate data, *Trans. ASME. Journal of Basic Engineering*, Series D, **82**, (2), 265-275.

Hodkinson, B. 1939 Estimation of the leakage through a labyrinth gland, *Proceedings of the Institute of Mechanical Engineers.* **141**, 283-288.

Kaul, A. 1999 Design and development of a test setup for the experimental determination of the rotordynamic and leakage characteristics of annular bushing oil seals. M.S. Thesis. Texas A&M University, College Station.

Kline, S. J., & McClintock, F. A. 1953 Jan Describing uncertainties in single-sample experiments. *Mechanical Engineering*, 3-8.

Komotori, K., & Miyake, K. 1977 Leakage characteristics of labyrinth seals with high rotating speed, *Proceedings of Tokyo Joint Gas Turbine Congress*, 371-380.

Marquette, O. R., & Childs, D. W. 1997 Eccentricity effects on the rotordynamic coefficients of plain annular seals: theory versus experiment, *Journal of Tribology*, **119**, 443-448.

Martin, H. M. 1908, Jan 10. Labyrinth packings, *Engineer*, **85**, 35-38.

Nikitin, G. A., & Ipatov, A. M. 1973 Design of labyrinth seals in hydraulic equipment, *Russian Engineering Journal*, **53**, (10), 26-30.

Rhode, D. L., & Hibbs, R. I. 1986 A comparative investigation of corresponding annular and labyrinth seal flow fields, ASME Paper No. 89-GT-195.

Sneck, H. J. 1974 Labyrinth seal literature survey, *Journal of Lubrication Technology*, **96**, 579-582.

Stocker, H. L. 1975 Advanced labyrinth seal design performance for high pressure ratio gas turbines, ASME Paper 75-WA/GT-22.

Stodola, A. 1927 *Steam and Gas Turbines*, McGraw-Hill, 189-194.

Stoff, H. 1980 Incompressible flow in a labyrinth seal, *ASME Journal of Engineering for Gas Turbines and Power.* **100**, 817-829.

Waschka, W., Wittig, S., & Kim, S. 1992 Influence of high rotational speeds on the heat transfer and discharge coefficients in labyrinth seals, *ASME Journal of Turbomachinery*, **114**, 462-468.

Willenborg, K., Kim, S., & Wittig, S. 2001 Effects of Reynolds number and pressure ratio on leakage loss and heat transfer in a stepped labyrinth seal, *ASME Journal of Turbomachinery*, **123**, 815-822.

Yeh, F. C., & Cochran, R. P. 1970, Feb. Comparison of experimental and ideal leakage flows through labyrinth seals for very small pressure difference, *NASA TMX-1958*.

Yucel, T., & Kazakia, J. Y. 2001 Analytical predictions techniques for axisymmetric flow in gas labyrinth seals, *ASME Journal of Engineering for Gas Turbines and Power*, **123**, 255-257.

Zabriskie, W., & Sternlieht, B. 1959 Sept Labyrinth seal leakage analysis, *Journal of Basic Engineering, Trans. ASME*, Series D, **81**, (3), 332-340.

Zimmermann, H., & Wolff, K. H. 1998 Air system correlations, part 1: labyrinth seals, ASME Paper 98-GT-206.

APPENDIX A

Appendix A contains the photographs and diagrams of the experimental apparatus.

Figure A1. Test Rig
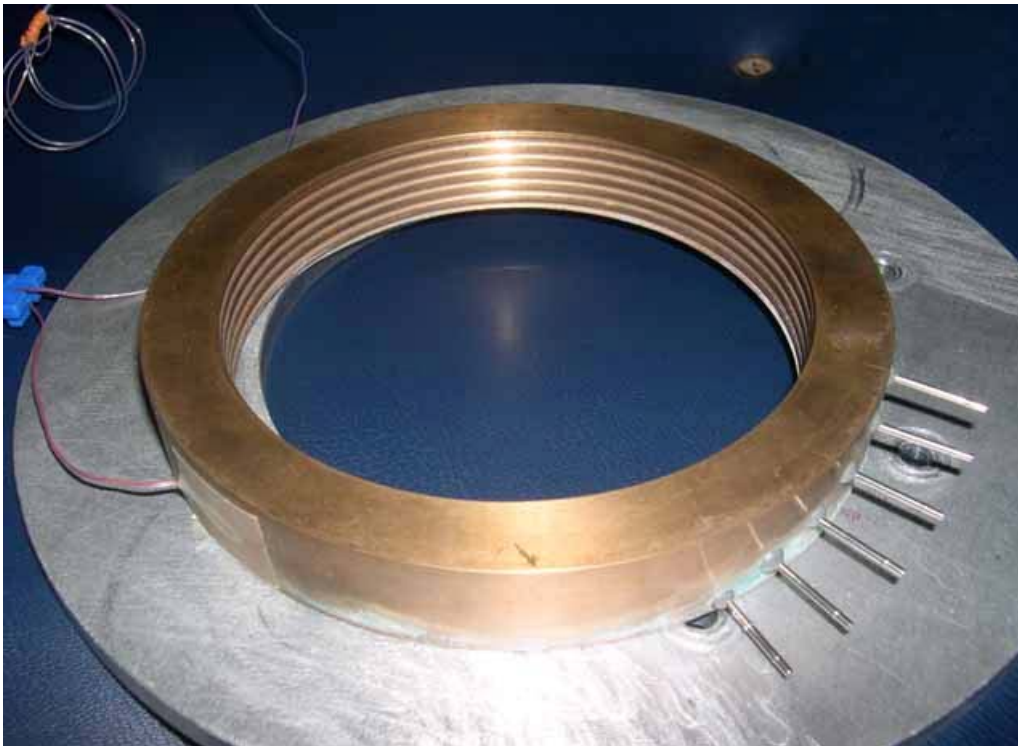
Figure A2. Windback Seal and Holding Aluminum Plate
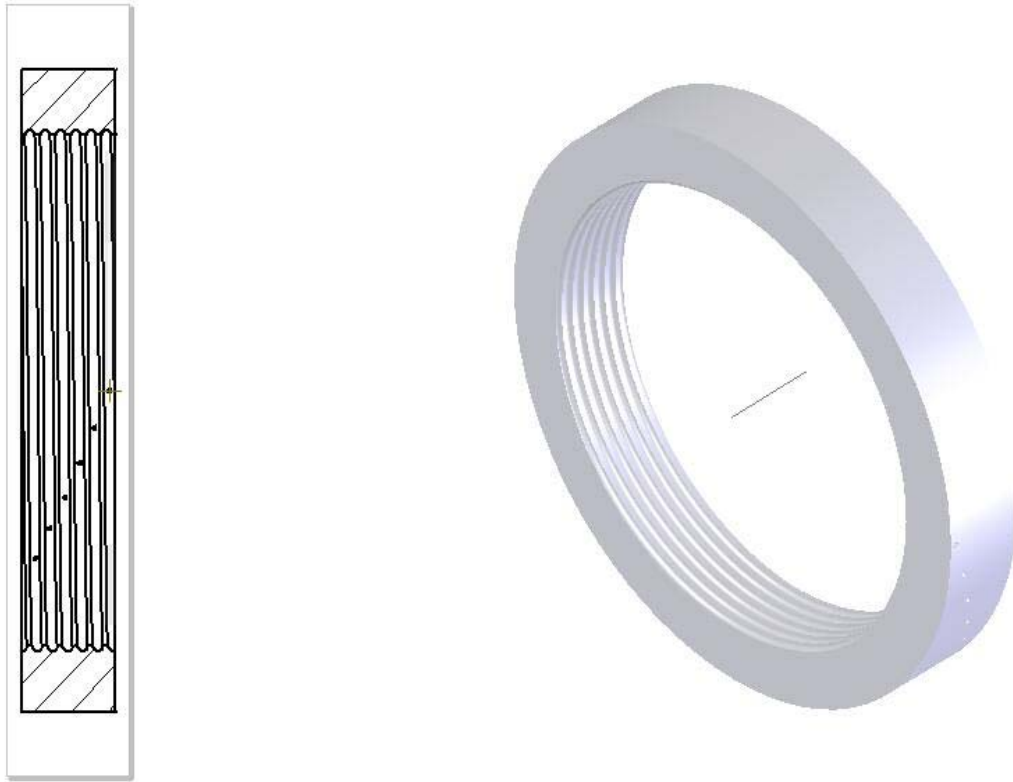
Figure A3. Drawing for Windback Seal

Figure A4. Air control system

Figure A5. Regulator, Safety Release Valve, and Air Filter

Figure A6. Rosemount Pressure Transducer

Figure A7. Air Turbine Flow meter and Signal Conditioner

Figure A8. Air Flow Rate Control Valve, Inlet Pressure Gage, and Safety Release Valve
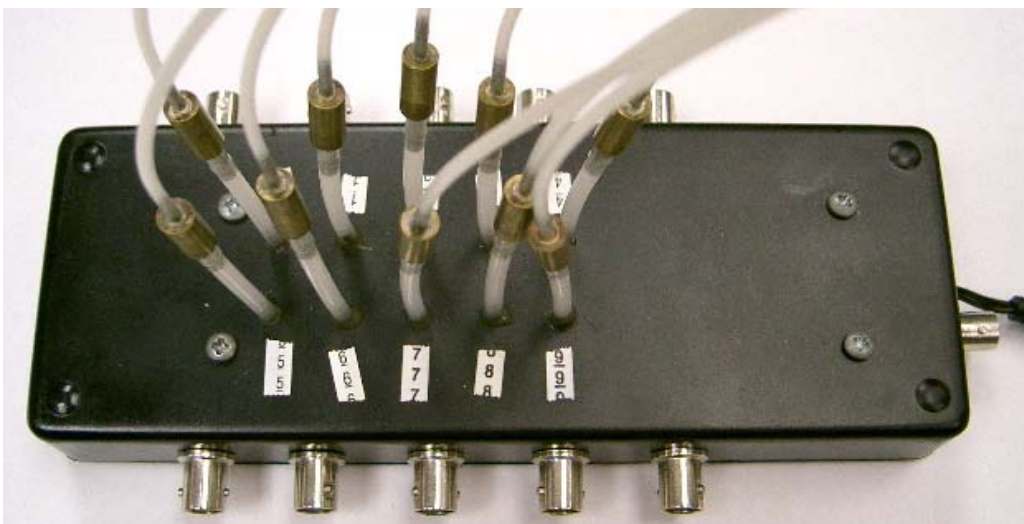
Figure A9. Pressure Transducer
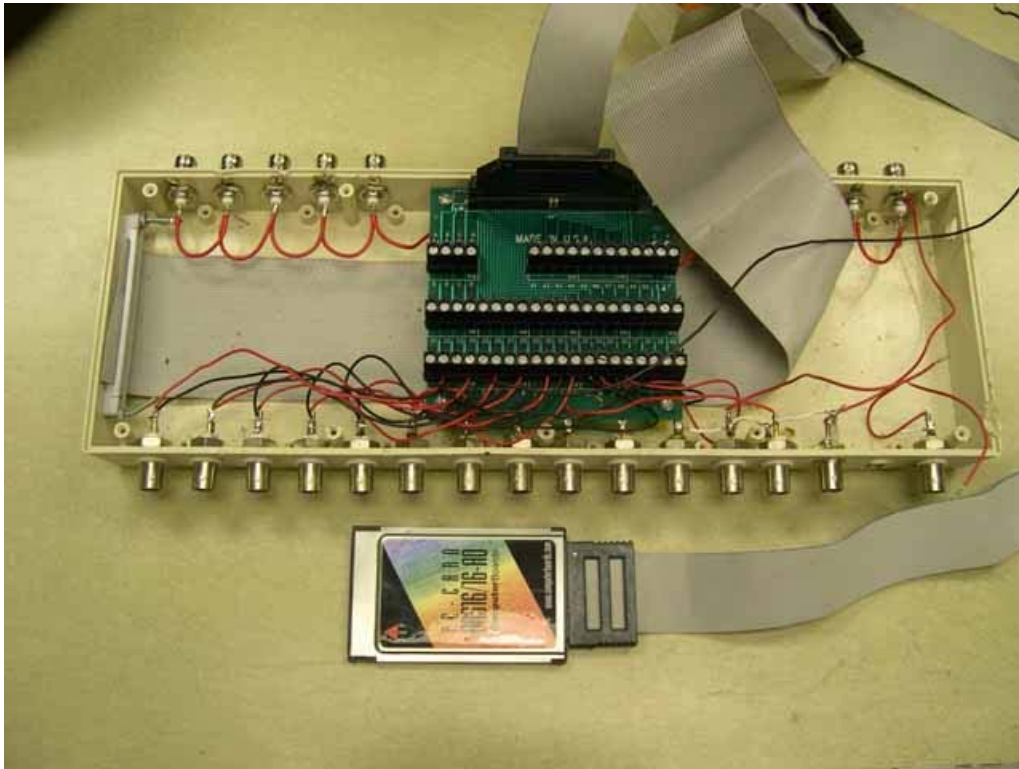
Figure A10. PC card DAS 16/16 AO
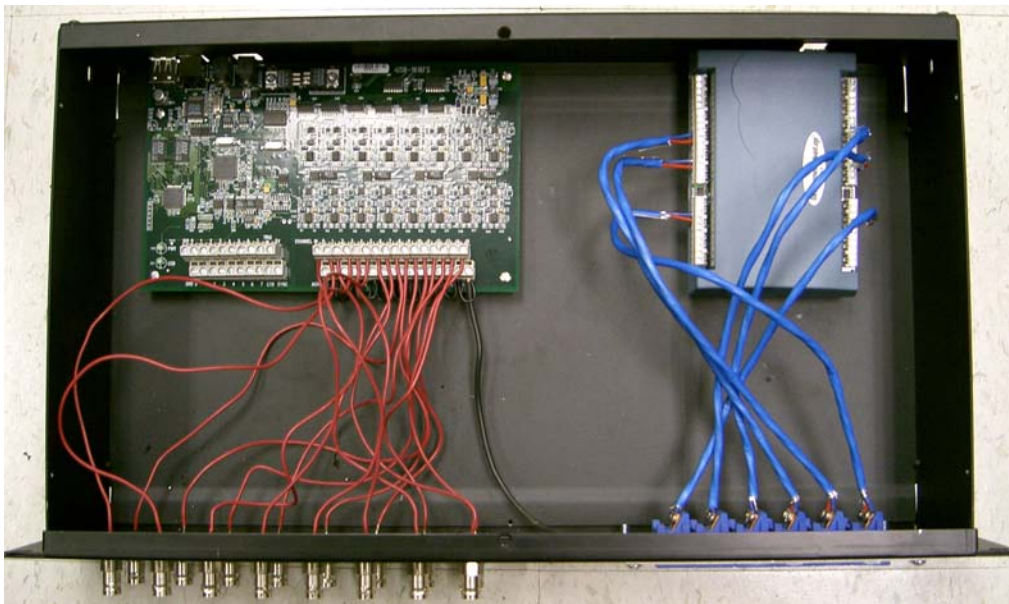
Figure A11. USB-1616 FS and USB-TC

APPENDIX B

Appendix B contains the plots of the leakage, pressure distribution, and velocity components for the two dimensional simulations.
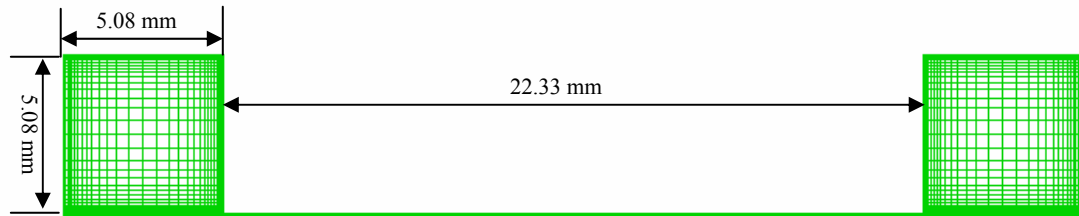
Figure B1. Overall layout annular seal grid and geometry
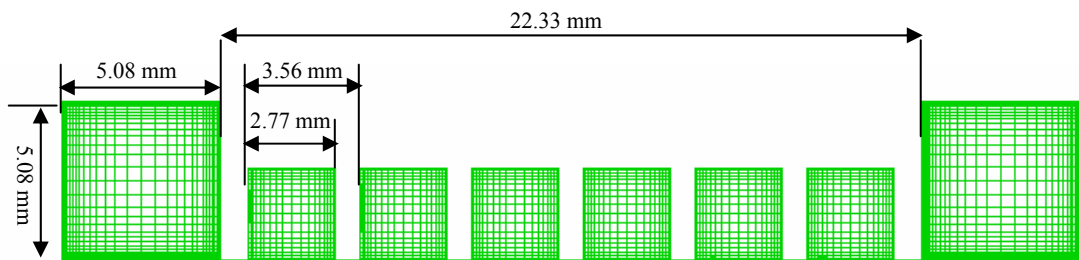
Figure B2. Overall layout labyrinth seal grid and geometry
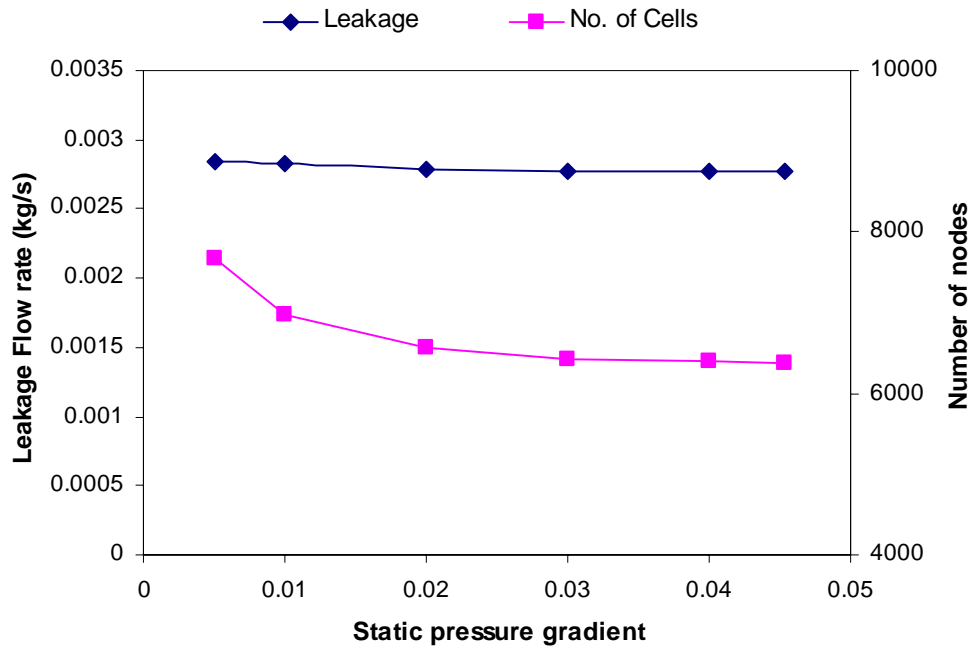
Figure B3. Leakage flow rate and number of nodes vs. static pressure gradient in the two-dimensional baseline seal
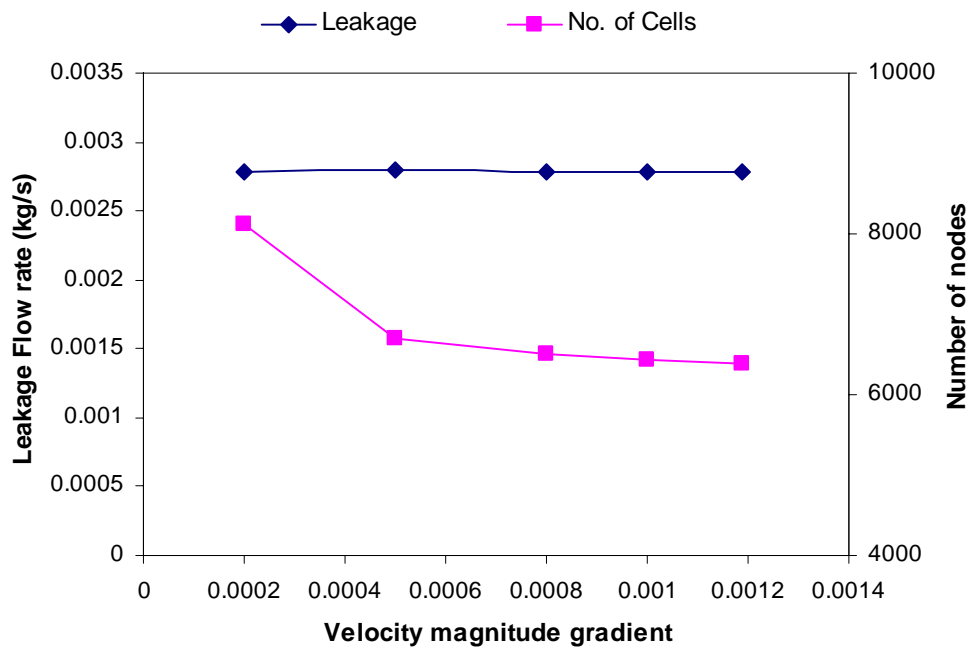
Figure B4. Leakage flow rate and number of nodes vs. velocity magnitude gradient in the two-dimensional baseline seal
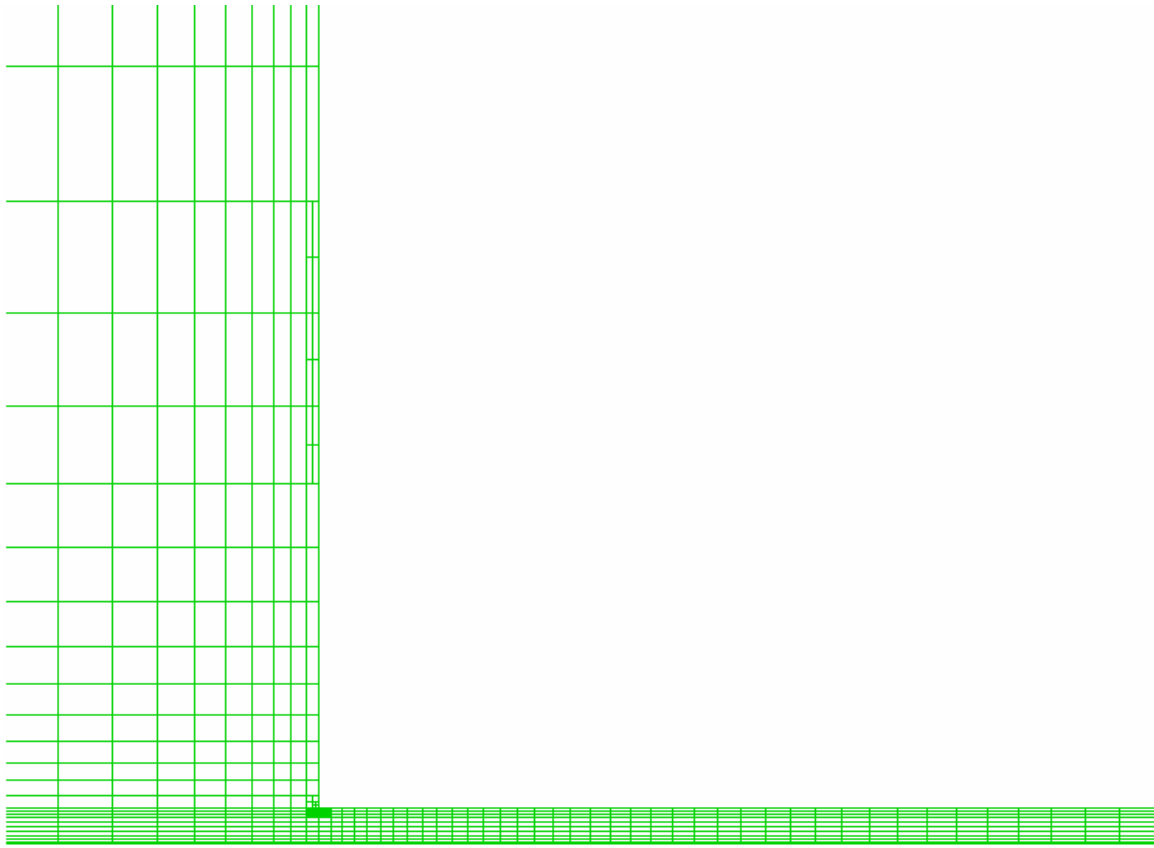
Figure B5. Grid refinement in the entrance region of annular seal
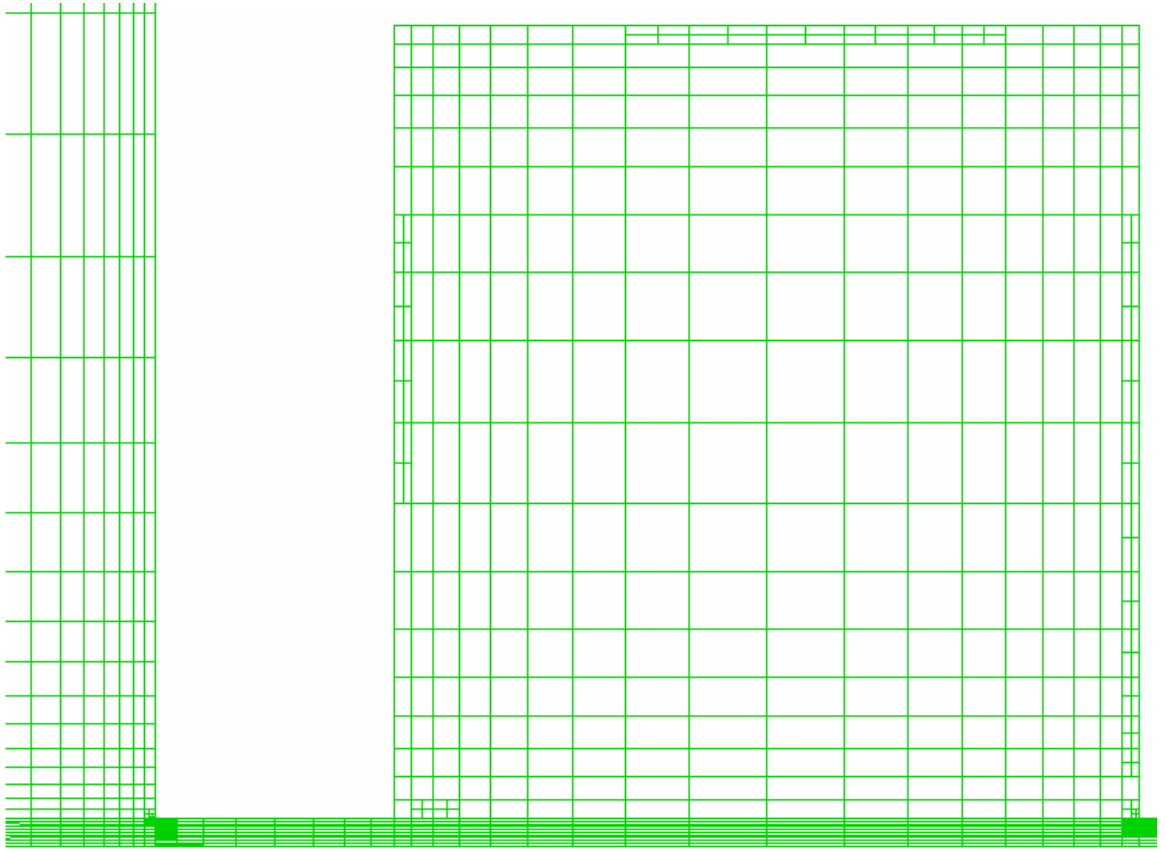
Figure B6. Grid refinement in the entrance region and first groove of labyrinth seal
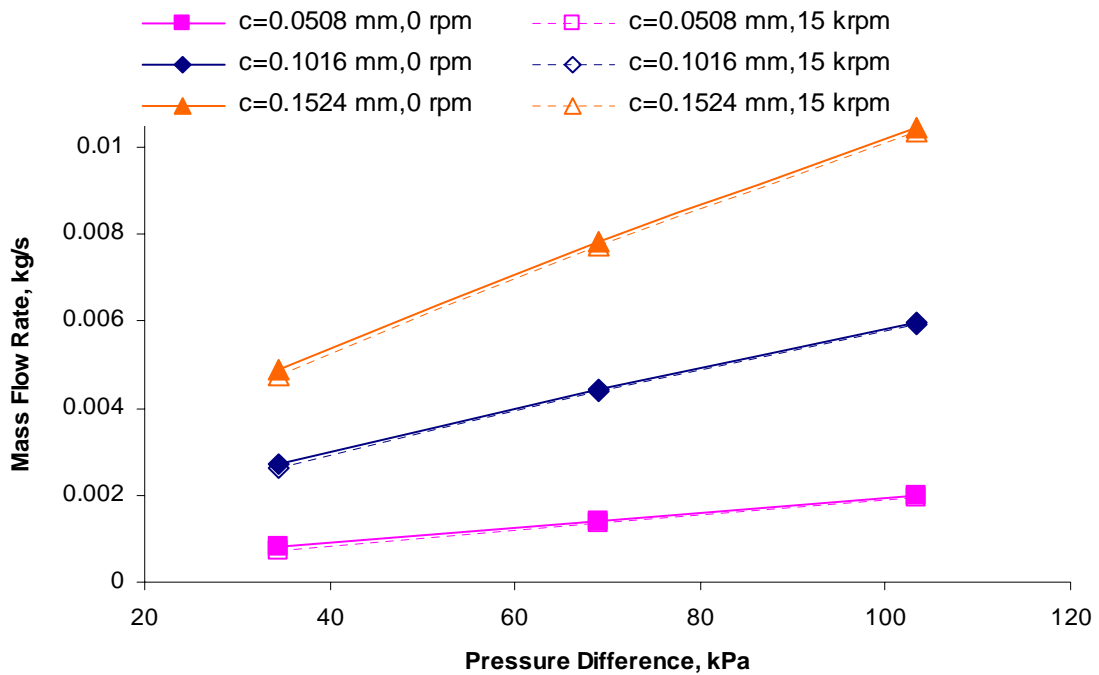
Figure B7. Air leakage flow rate vs. differential pressure for labyrinth seals with three different clearances at rotor speeds of 0 rpm, and 15,000 rpm
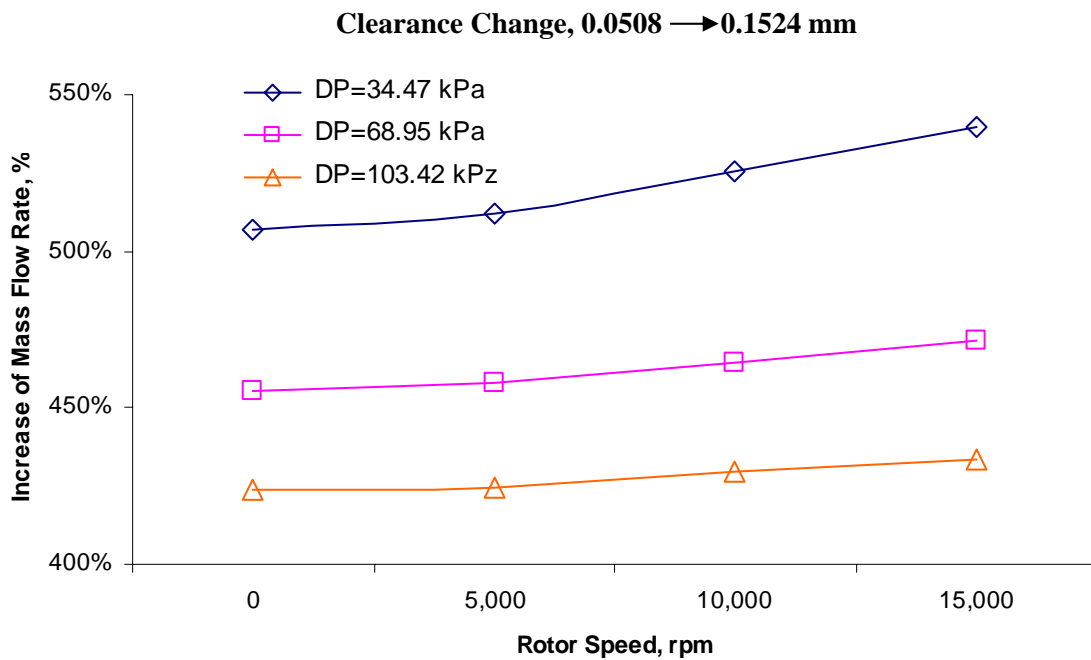
Figure B8. Increase percent of air leakage mass flow rate due to clearance change with varying the rotor speed for labyrinth seals
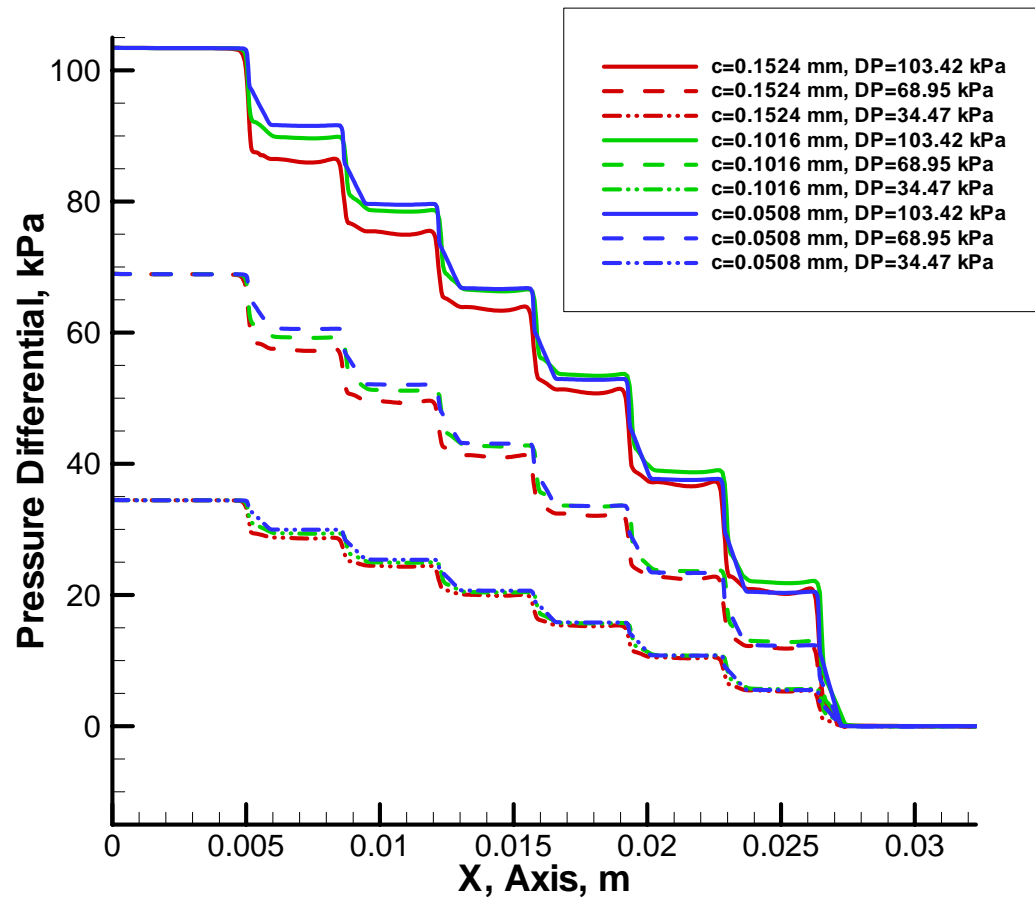
Figure B9. Pressure distribution on rotor surface for three different clearances, air, Ω=15,000 rpm
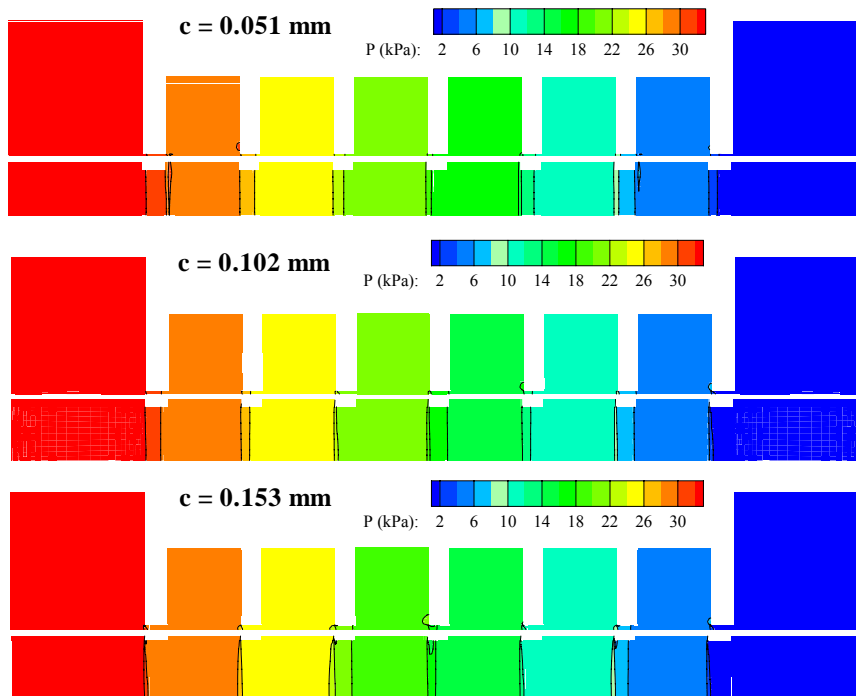
Figure B10. Pressure contours of labyrinth seals with three different clearances, Ω=0 rpm, ΔP=34.47 kPa
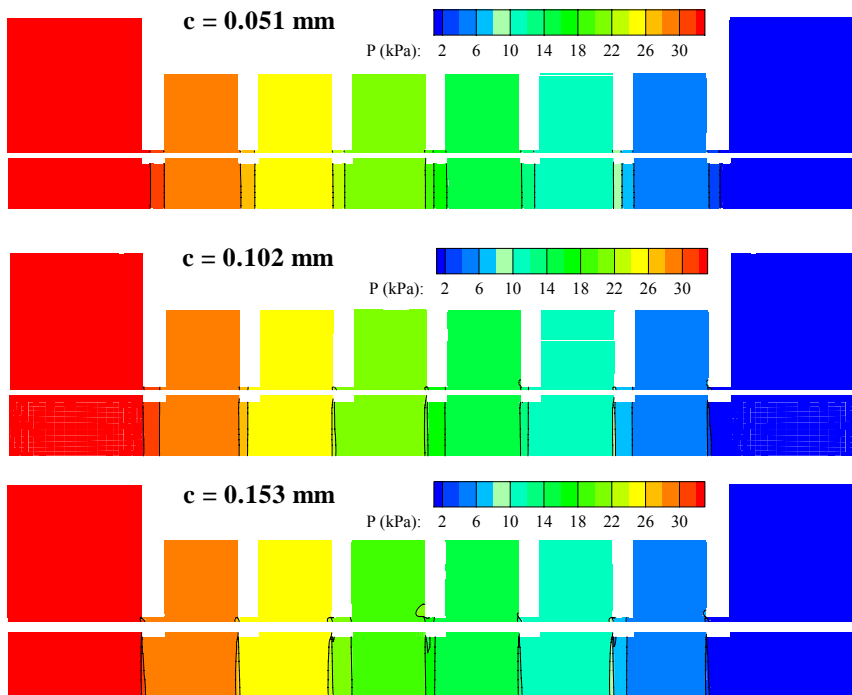
Figure B11. Pressure contours of labyrinth seals with three different clearances, Ω=15,000 rpm, ΔP=34.47 kPa
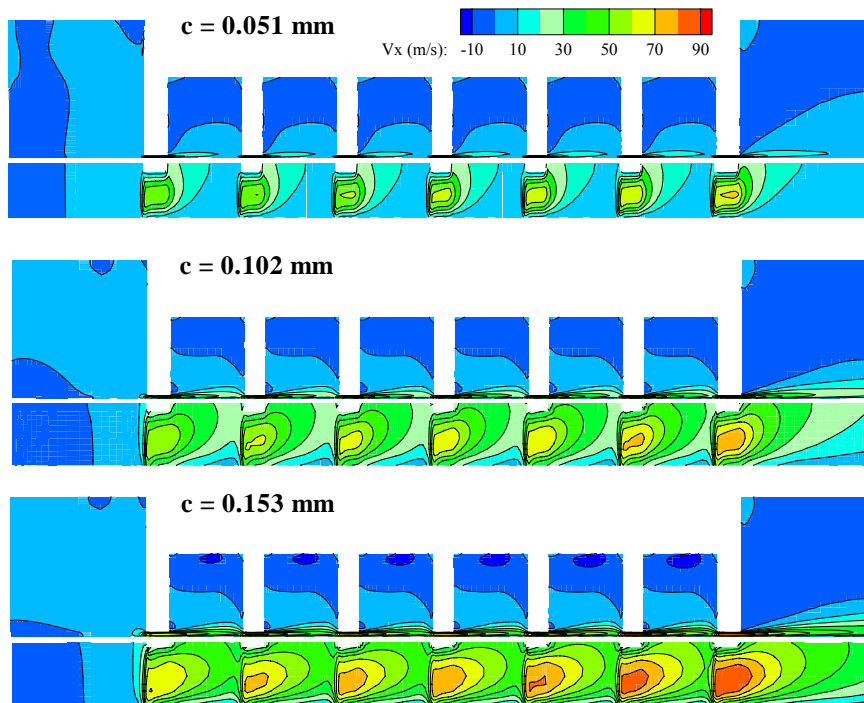
Figure B12. Axial velocity contours of labyrinth seals with three different clearances, Ω=0 rpm, ΔP=34.47 kPa
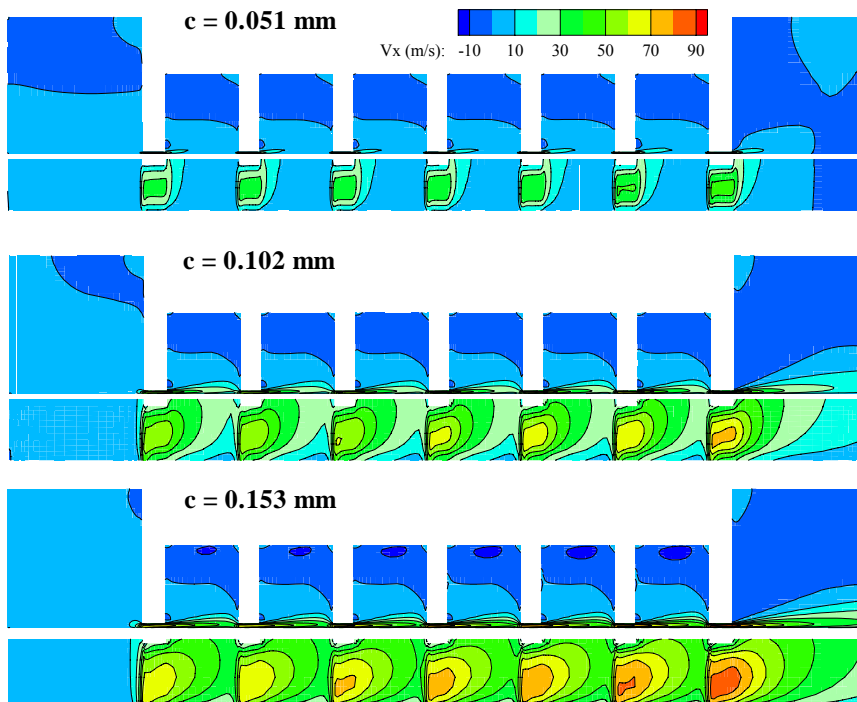
Figure B13. Axial velocity contours of labyrinth seals with three different clearances, Ω=15,000 rpm, ΔP=34.47 kPa
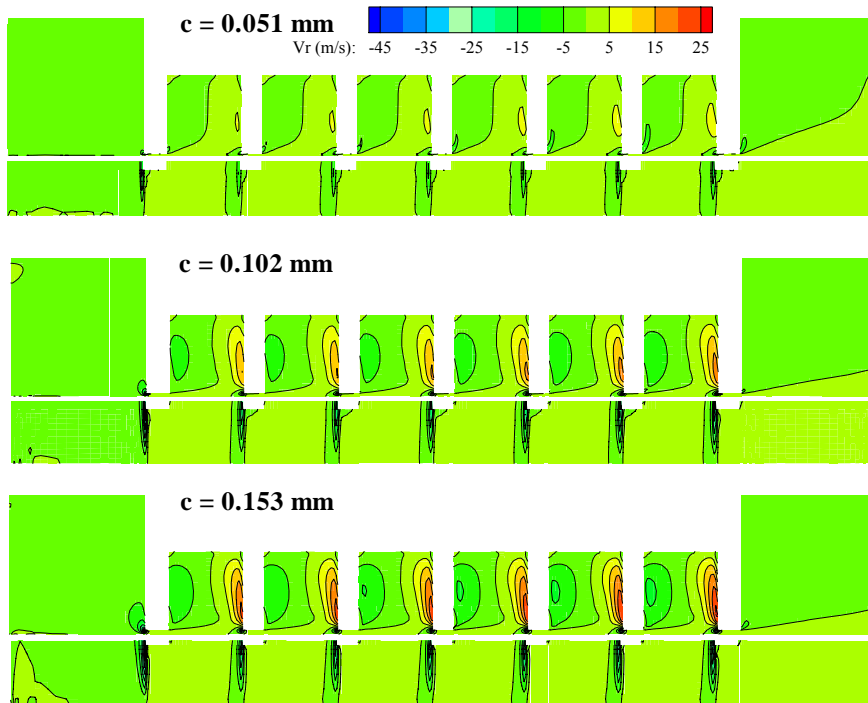
Figure B14. Radial velocity contours of labyrinth seals with three different clearances, Ω=0 rpm, ΔP=34.47 kPa
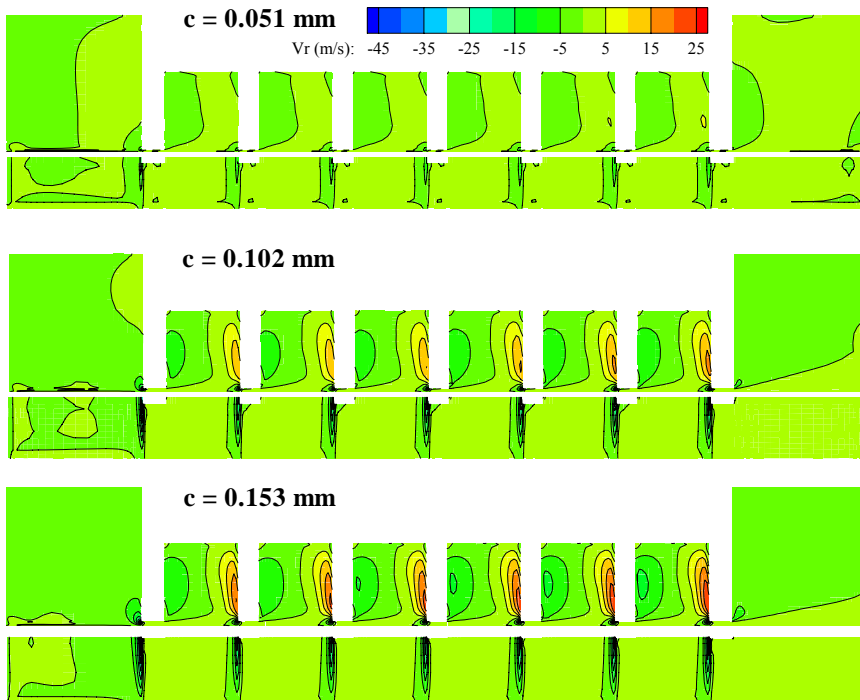
Figure B15. Radial velocity contours of labyrinth seals with three different clearances, Ω=15,000 rpm, ΔP=34.47 kPa
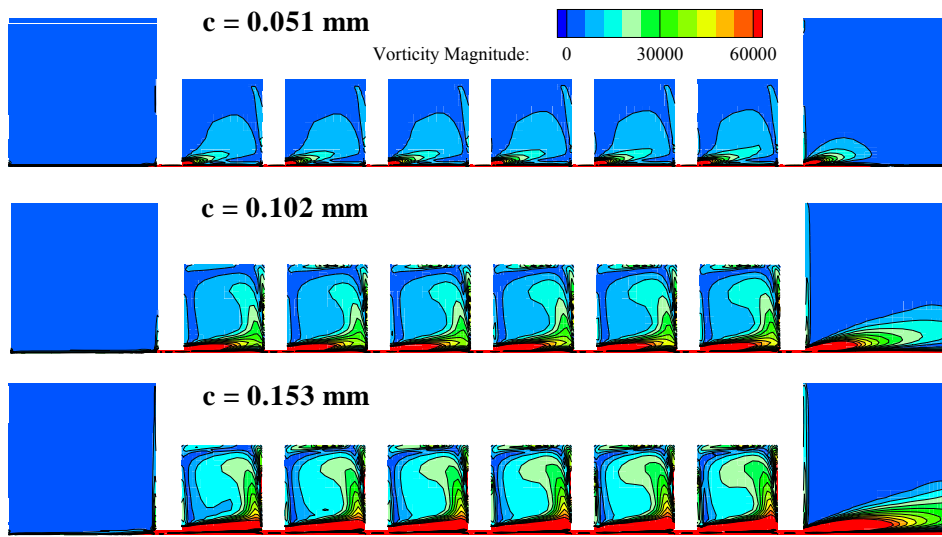
Figure B16. Vorticity magnitude contour plot of the labyrinth seal with three different clearances, Ω=15,000 rpm, ΔP=34.47 kPa
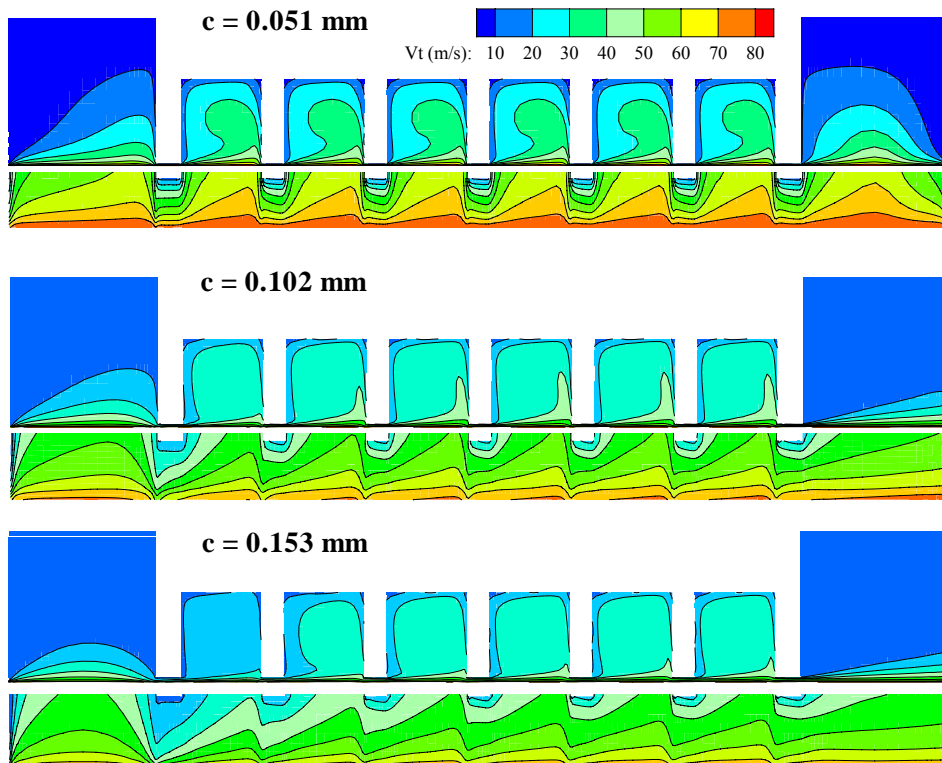
Figure B17. Tangential velocity contour plots of the labyrinth seals with three different clearances, Ω=15,000 rpm, ΔP=34.47 kPa
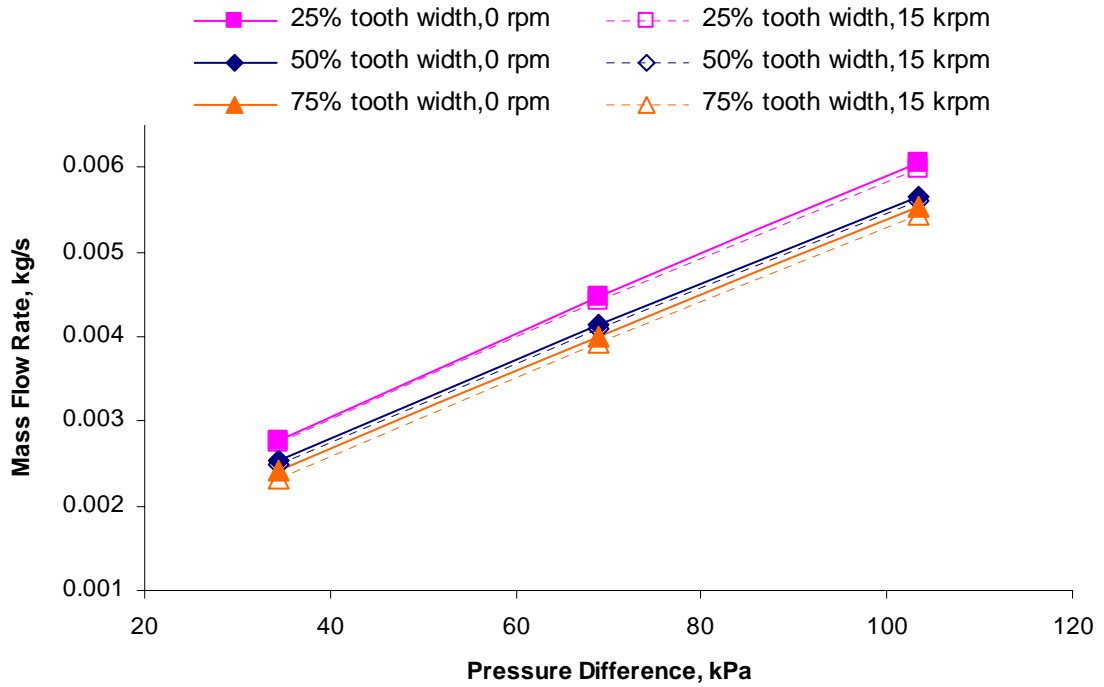
Figure B18. Leakage mass flow rate vs. differential pressure for labyrinth seals with three different tooth widths at rotor speeds of 0 rpm, and 15,000 rpm, c=0.1016 mm
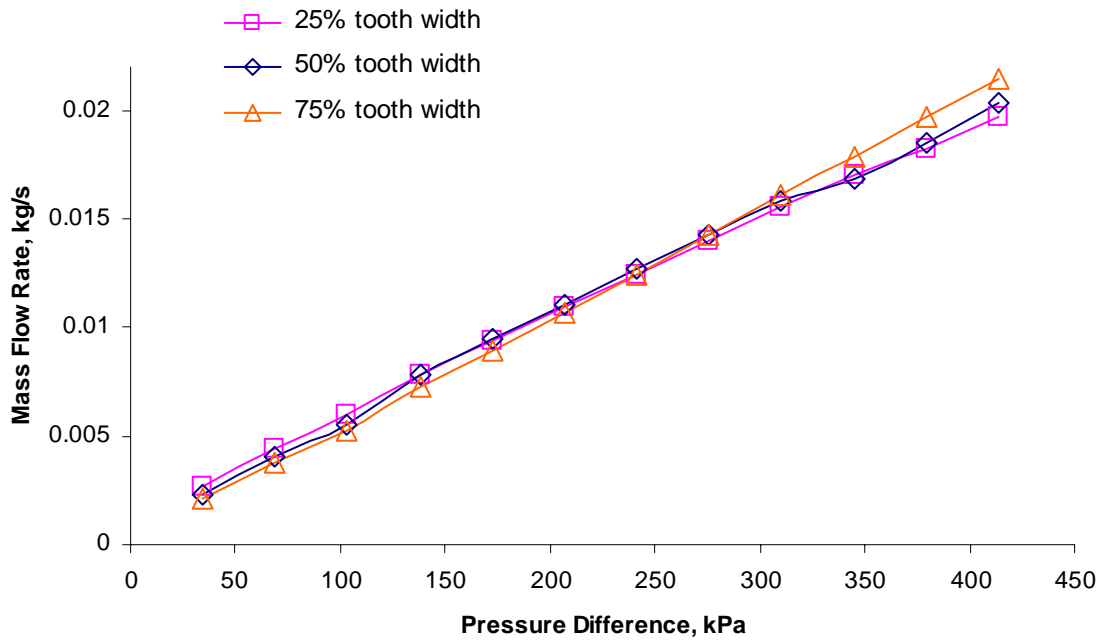
Figure B19. Effect of tooth width for high pressure differential for straight through labyrinth seals at rotor speed of 0 rpm
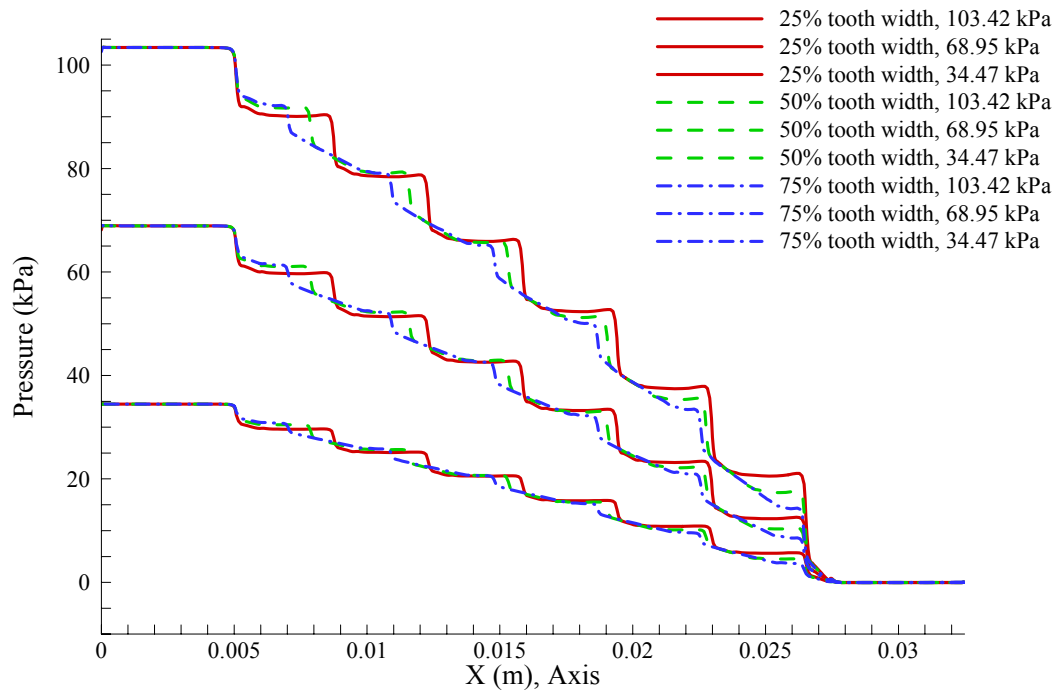
Figure B20. Axial pressure distribution of rotor surface for three different tooth widths, c=101.6 µm, Ω=15,000 rpm
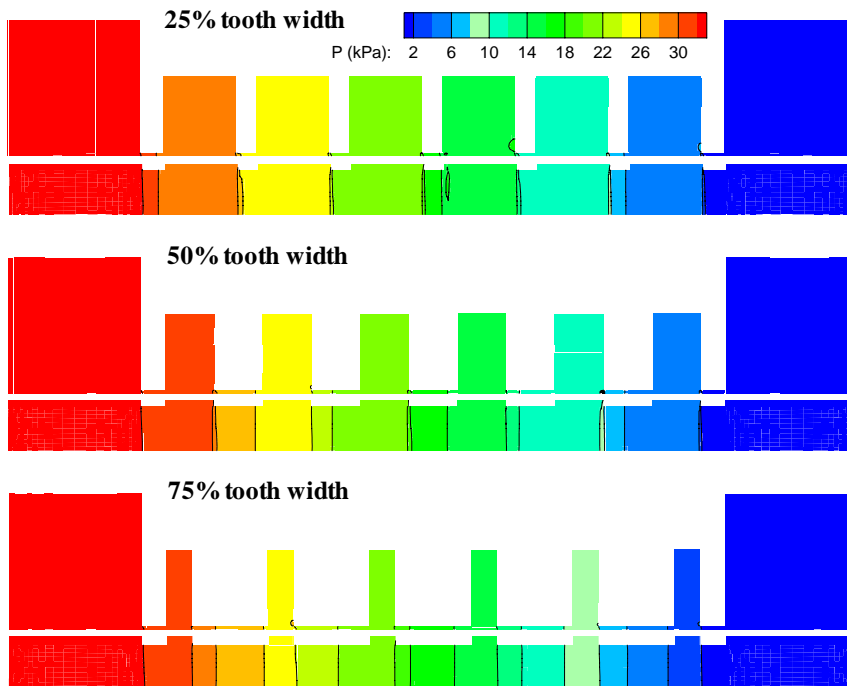
Figure B21. Pressure contours of labyrinth seals with three different tooth widths, c=101.6 µm, Ω=15,000 rpm, ΔP=34.47 kPa
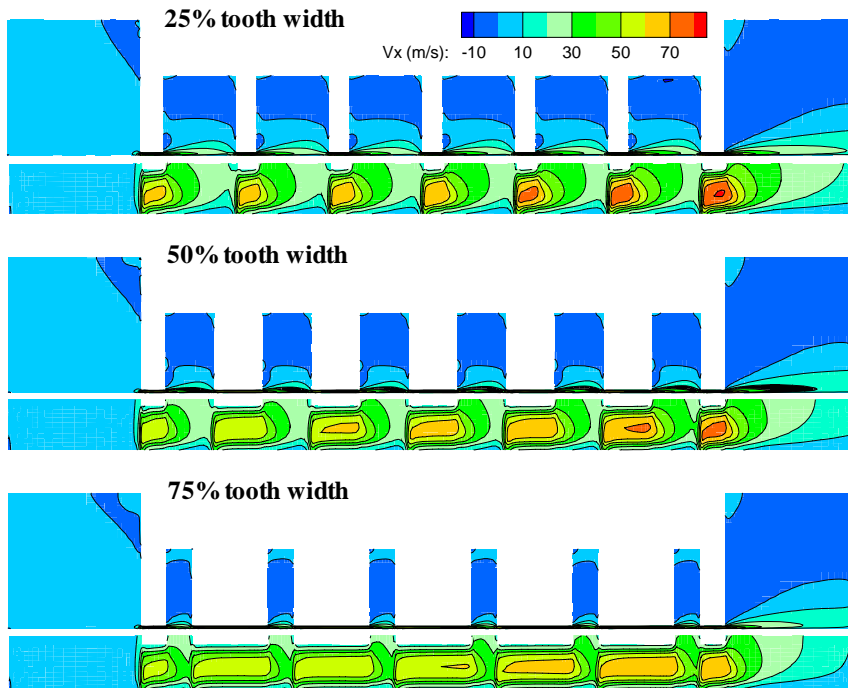
Figure B22. Axial velocity contours of labyrinth seals with three different tooth widths, c=101.6 μm, Ω=15,000 rpm, ΔP=34.47 kPa
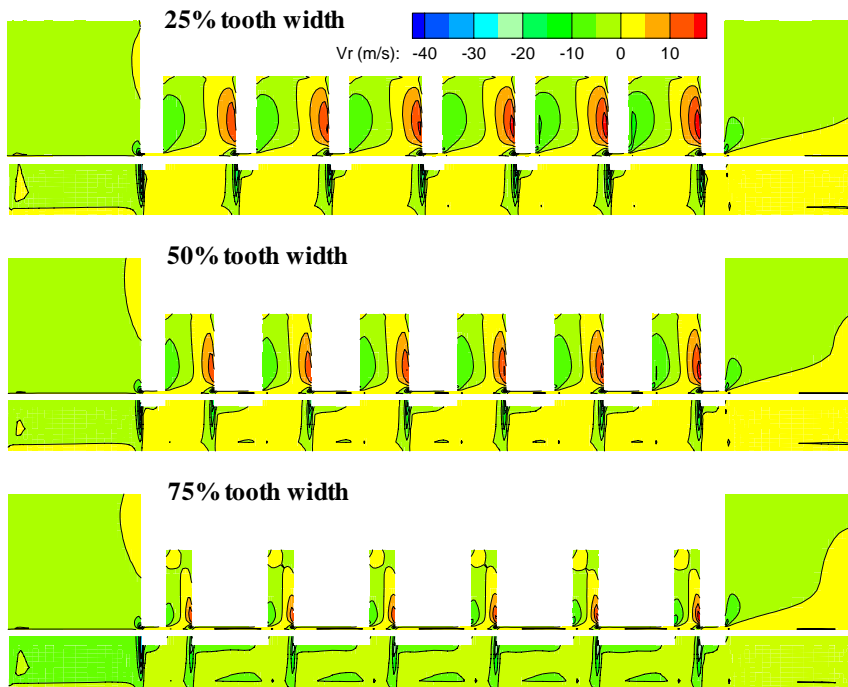
Figure B23. Radial velocity contours of labyrinth seals with three different tooth widths, c=101.6 μm, Ω=15,000 rpm, ΔP=34.47 kPa
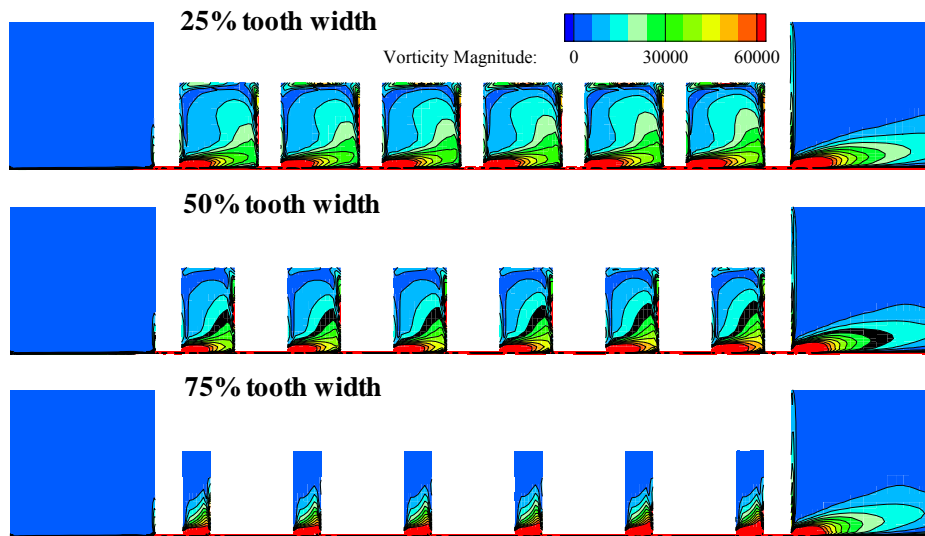
Figure B24. Vorticity magnitude contours of labyrinth seals with three different tooth widths, c=101.6 μm, Ω=15,000 rpm, ΔP=34.47 kPa
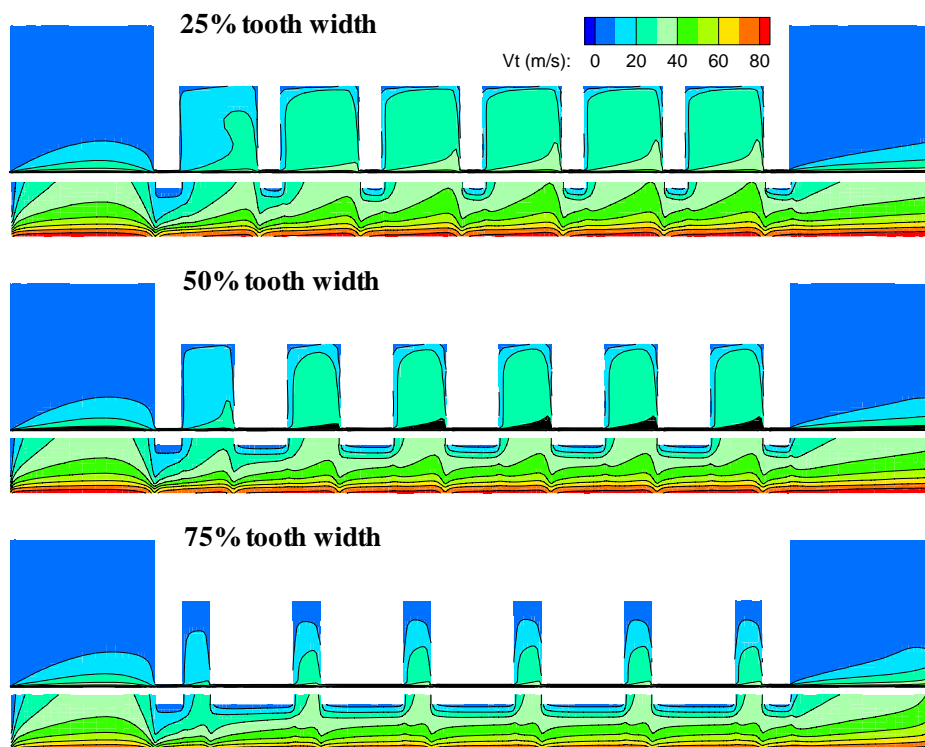
Figure B25. Tangential velocity contours of labyrinth seals with three different tooth widths, c=101.6 μm, Ω=15,000 rpm, ΔP=34.47 kPa

0 rpm   **5000 rpm**   **10000 rpm**   **15000 rpm**
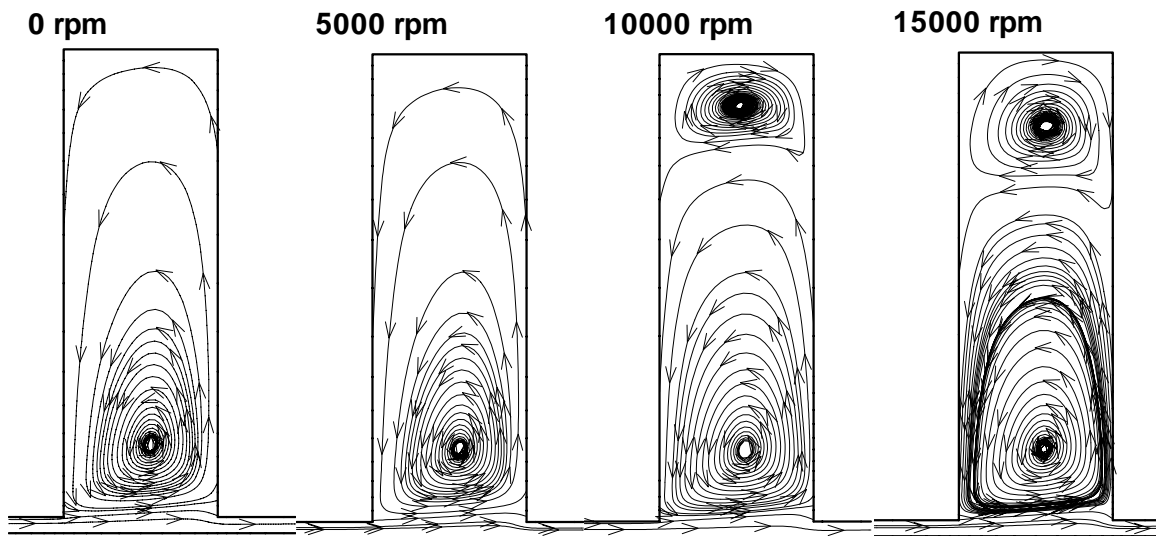
Figure B26. Appearance of secondary vortex in labyrinth seal with 75% tooth width, c=101.6 μm, ΔP=34.47 kPa

34.47 kPa   **68.95 kPa**   **103.42 kPa**
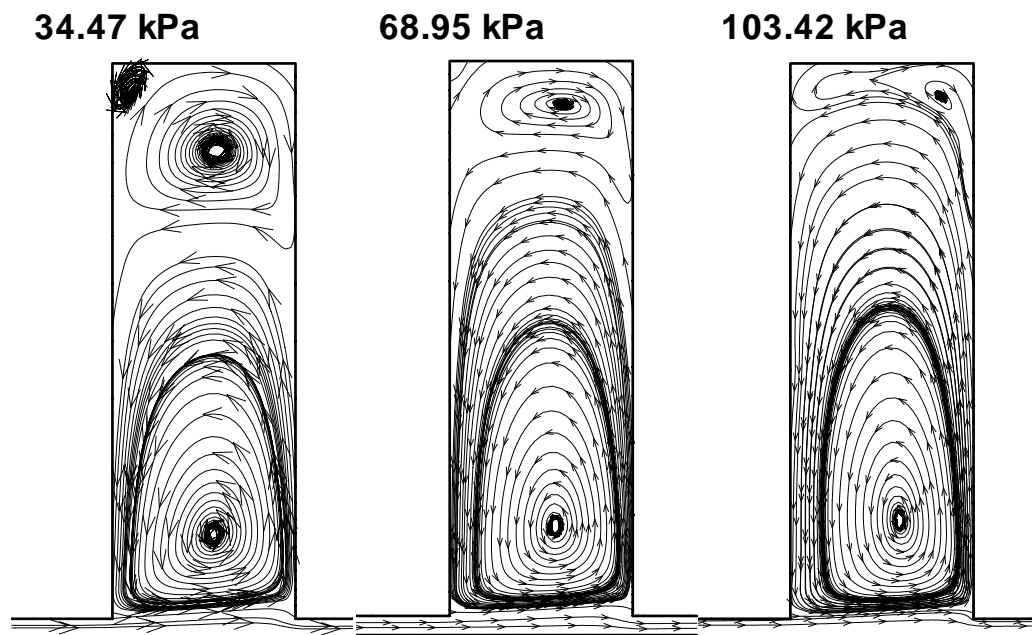
Figure B27. Appearance of secondary vortex in labyrinth seal with 75% tooth width at various differential pressures, Ω=15,000 rpm, c=101.6 μm

Cavity Shape, Tooth width, Shaft speed

- rectangular,25%,0 rpm
- rectangular,25%,15 krpm
- semi-circular deep,25%,0 rpm
- semi-circular deep,25%,15 krpm
- semi-circular shallow,25%,0 rpm
- semi-circular shallow,25%,15 krpm
- semi-circular shallow,33%,0 rpm
- semi-circular shallow,33%,15 krpm
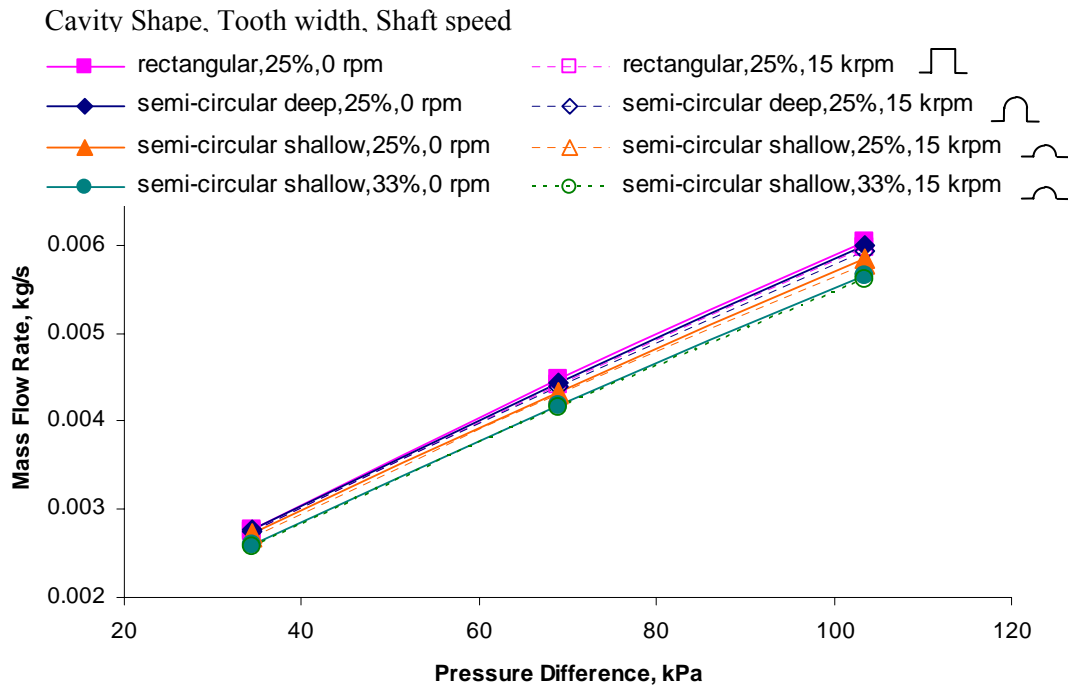
Figure B28. Leakage mass flow rate vs. differential pressure for various cavity shapes in the labyrinth seals at rotor speeds of 0 rpm, and 15,000 rpm

Rectangular, 103.41 kPa
Rectangular, 68.94 kPa
Rectangular, 34.47 kPa
Semi-circular deep, 103.41 kPa
Semi-circular deep, 68.94 kPa
Semi-circular deep, 34.47 kPa
Semi-circular shallow, 103.41 kPa
Semi-circular shallow, 68.94 kPa
Semi-circular shallow, 34.47 kPa
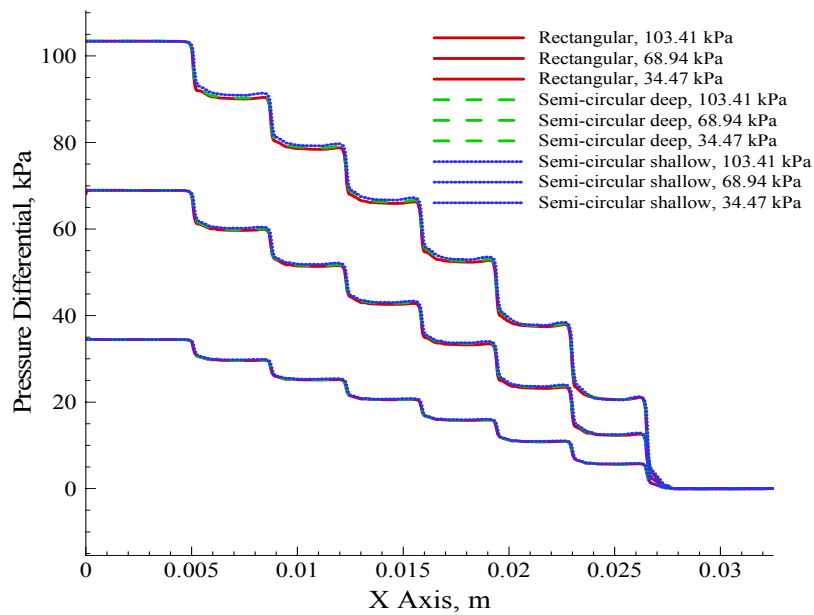
Figure B29. Axial pressure distribution of rotor surface for three different cavity shapes,c=101.6 μm, Ω=15,000 rpm
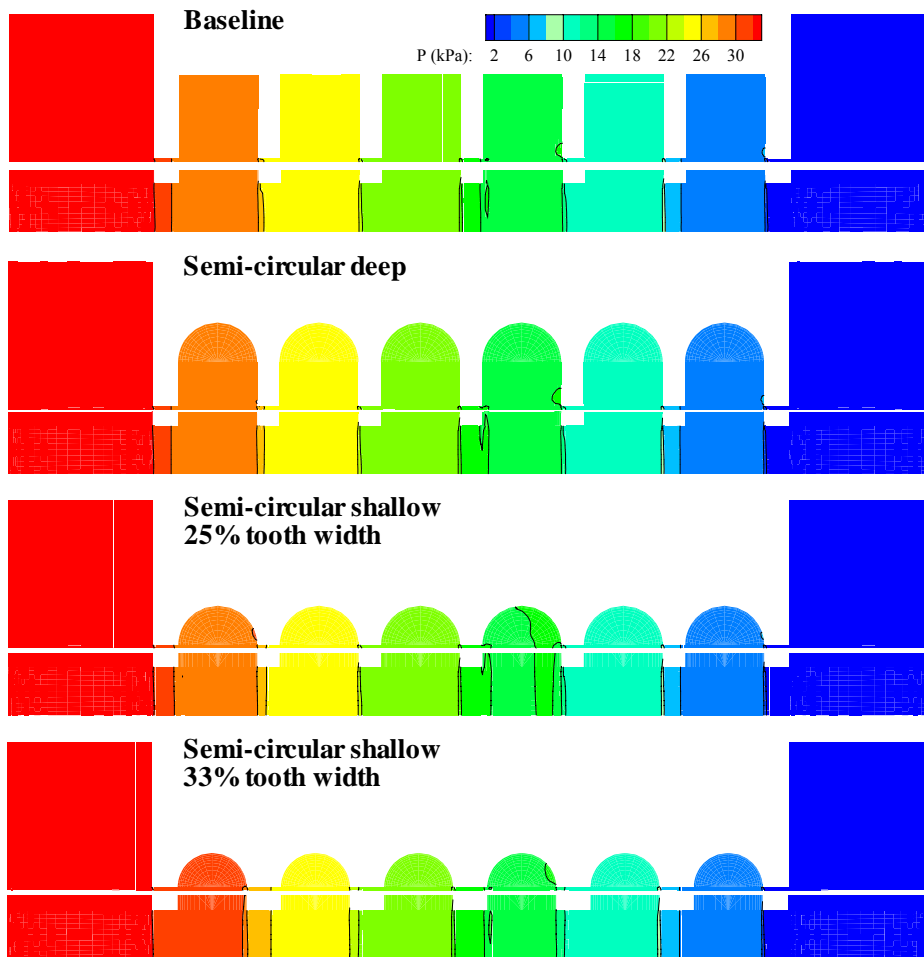
Figure B30. Pressure contours of labyrinth seals with three different cavity shapes, c=101.6 µm, Ω=15,000 rpm, ΔP=34.47 kPa
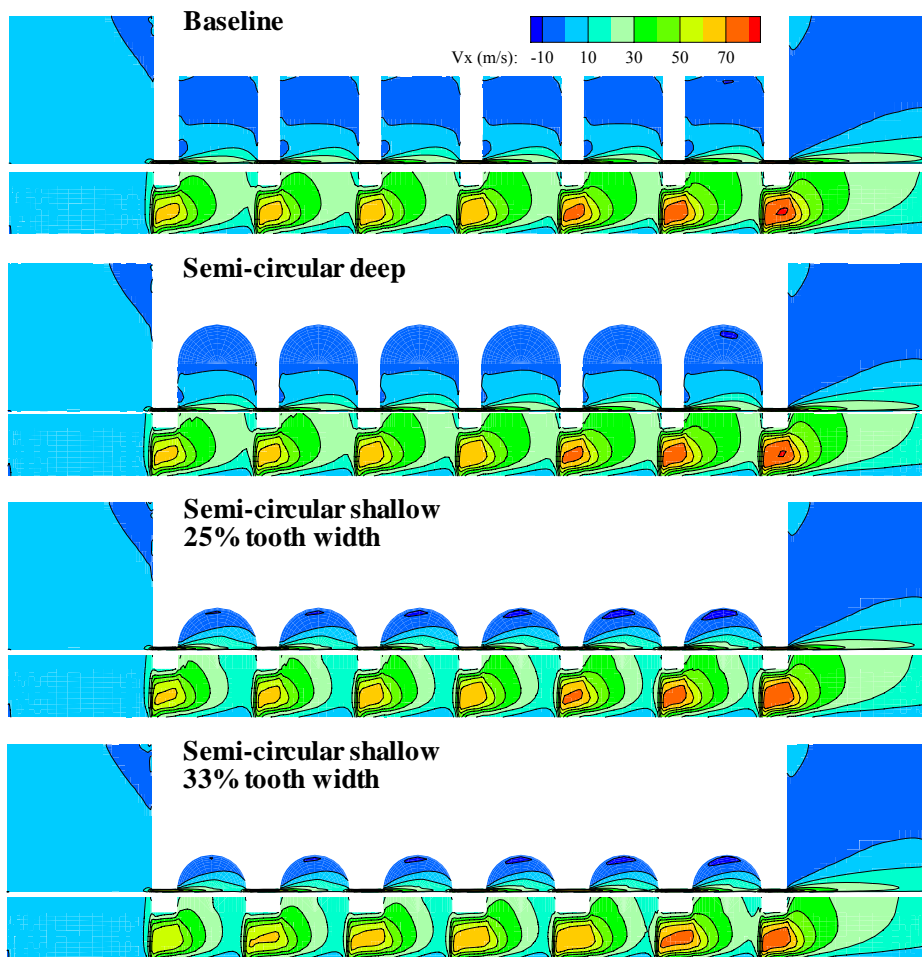
Figure B31. Axial velocity contours of labyrinth seals with three different cavity shapes, c=101.6 μm, Ω=15,000 rpm, ΔP=34.47 kPa
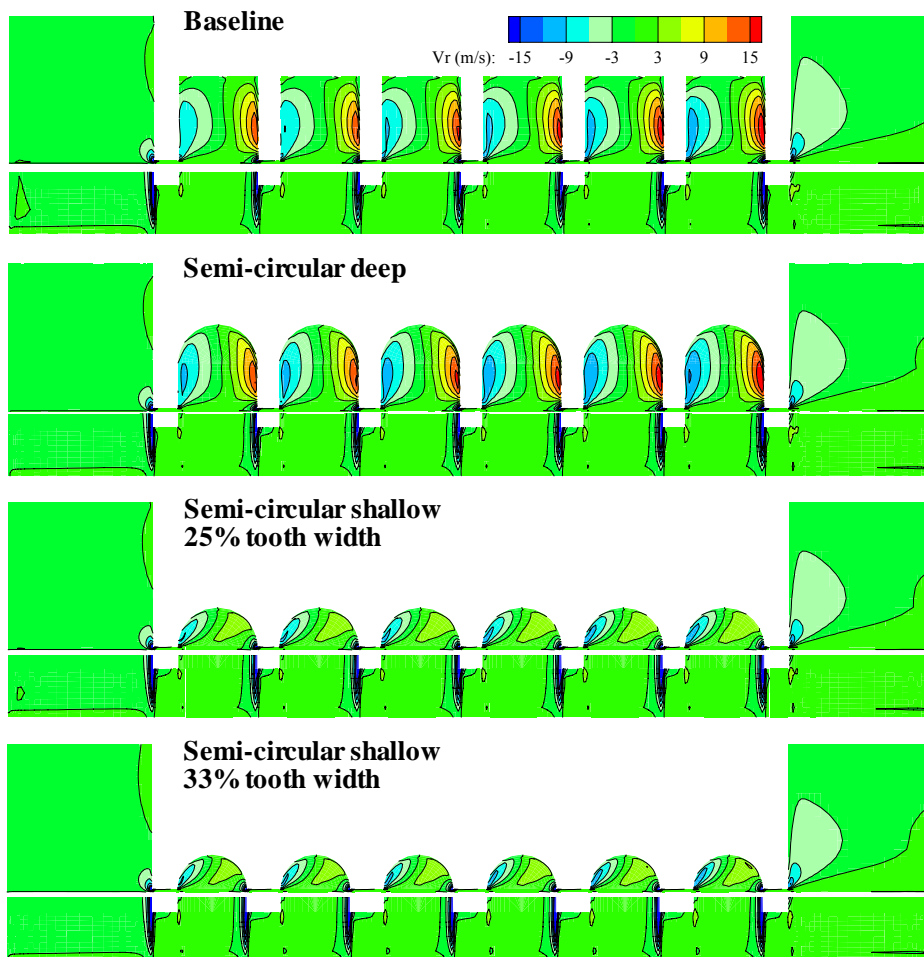
Figure B32. Radial velocity contours of labyrinth seals with three different cavity shapes, c=101.6 μm, Ω=15,000 rpm, ΔP=34.47 kPa
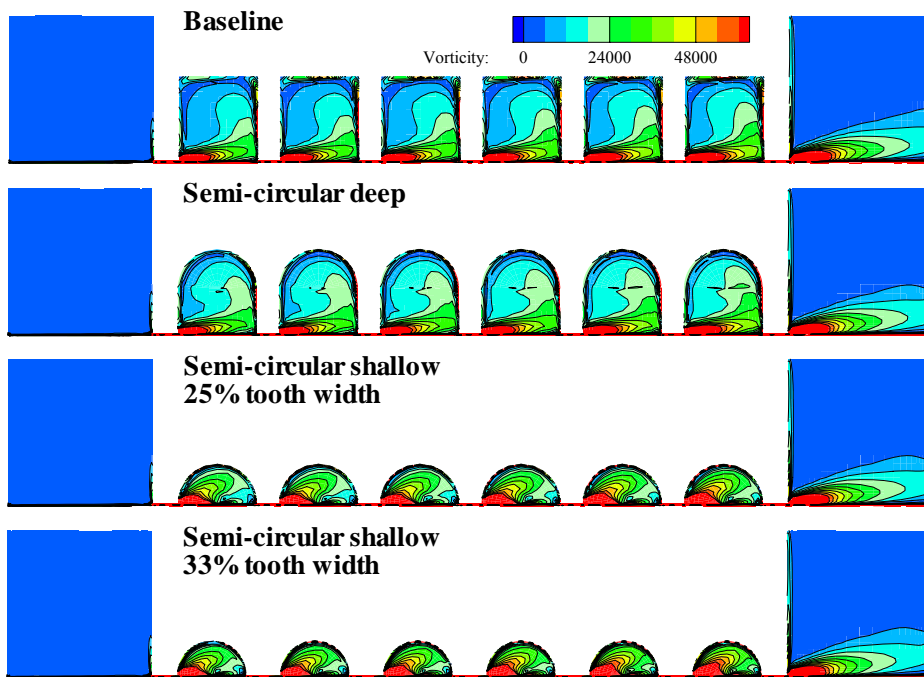
Figure B33. Vorticity magnitude contours of labyrinth seals with three different cavity shapes, c=101.6 μm, Ω=15,000 rpm, ΔP=34.47 kPa
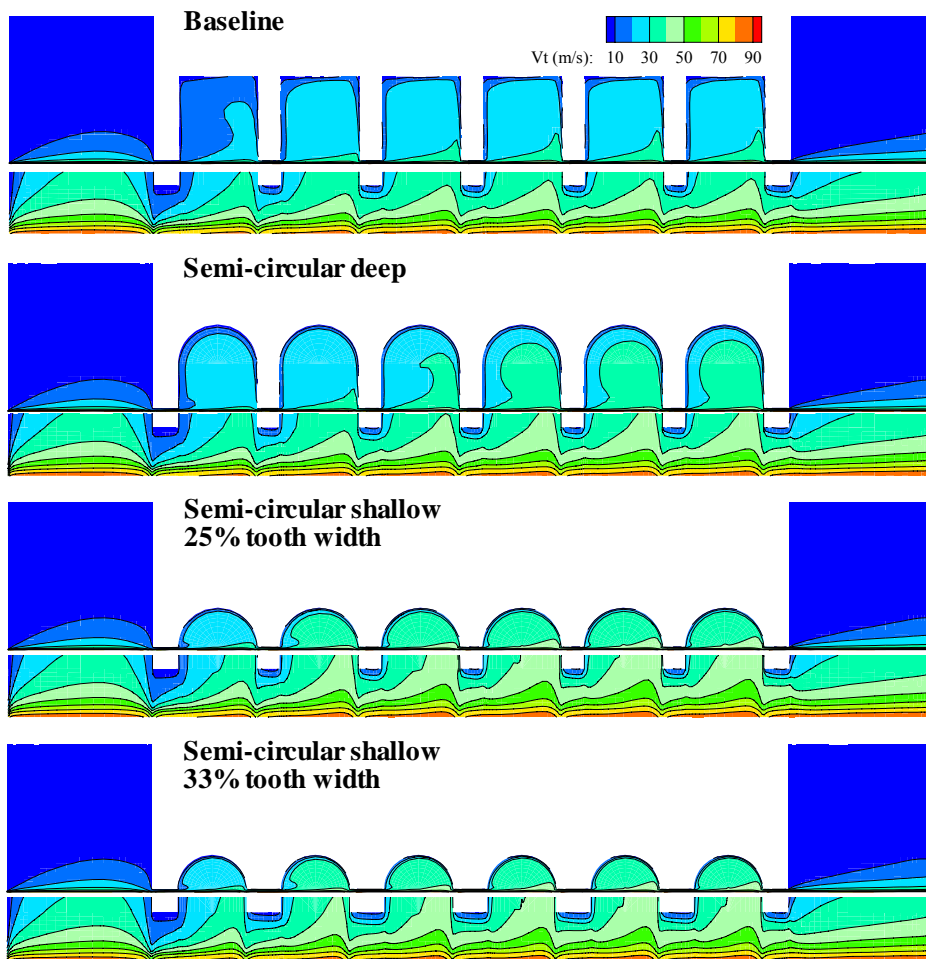
Figure B34. Tangential velocity contours of labyrinth seals with three different cavity shapes, c=101.6 μm, Ω=15,000 rpm, ΔP=34.47 kPa
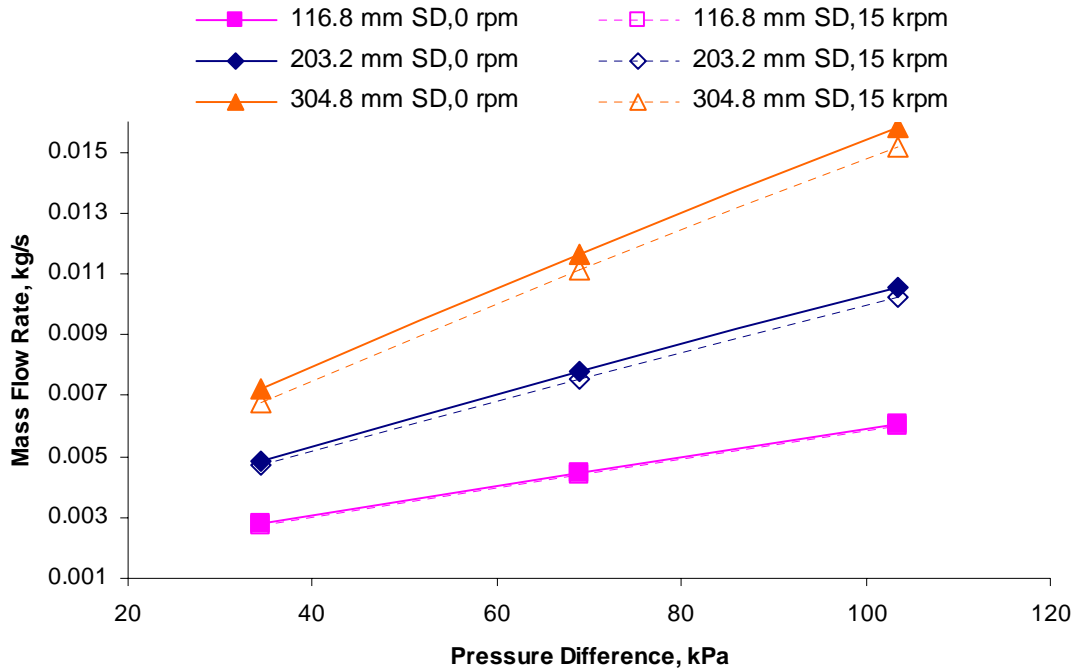
Figure B35. Leakage mass flow rate of labyrinth seal vs. differential pressure for three shaft diameters, Ω=0 and 15,000 rpm, c=101.6 µm
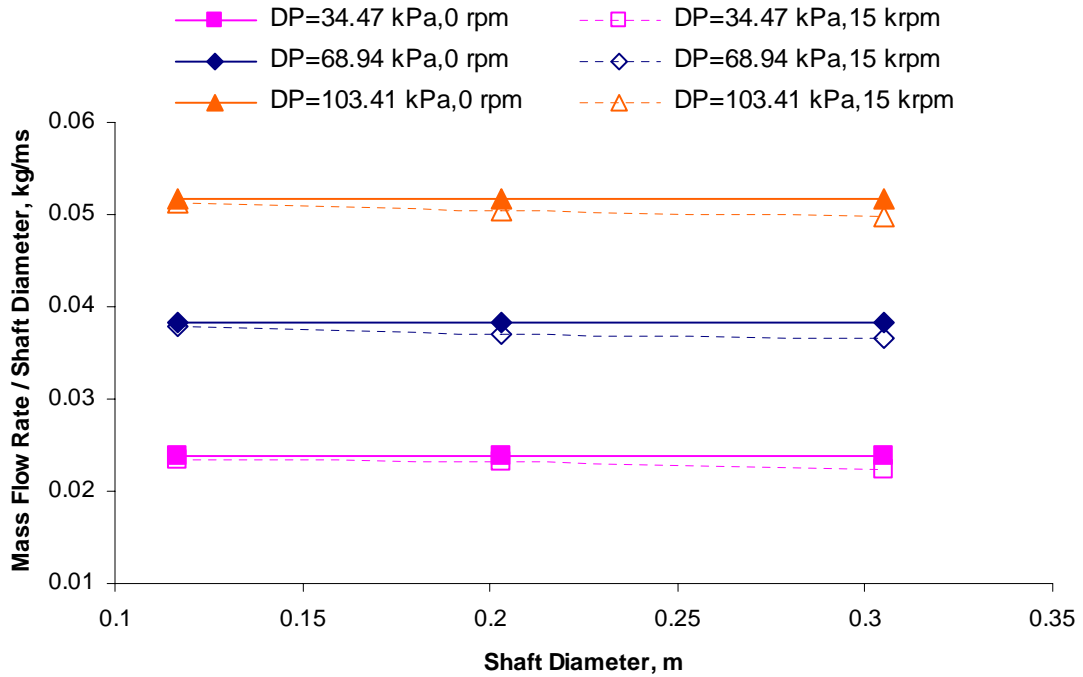
Figure B36. Leakage mass flow rate of labyrinth seal / shaft diameter vs. shaft diameter for shaft diameter dependence, Ω=0 and 15,000 rpm, c=101.6 µm
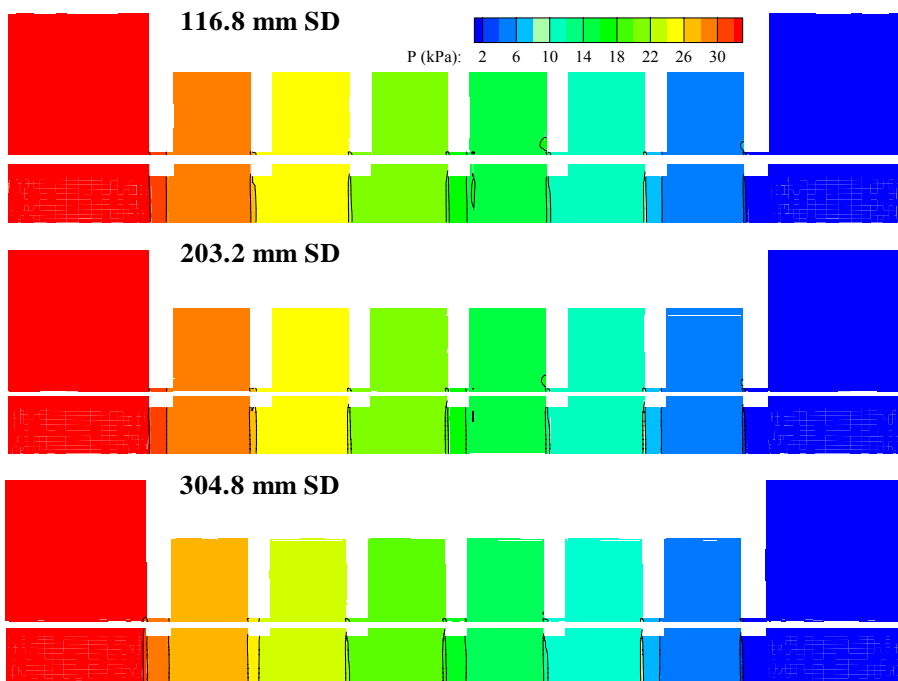
Figure B37. Pressure contours of labyrinth seals with three different shaft diameters, c=101.6 µm, Ω=15,000 rpm, ΔP=34.47 kPa
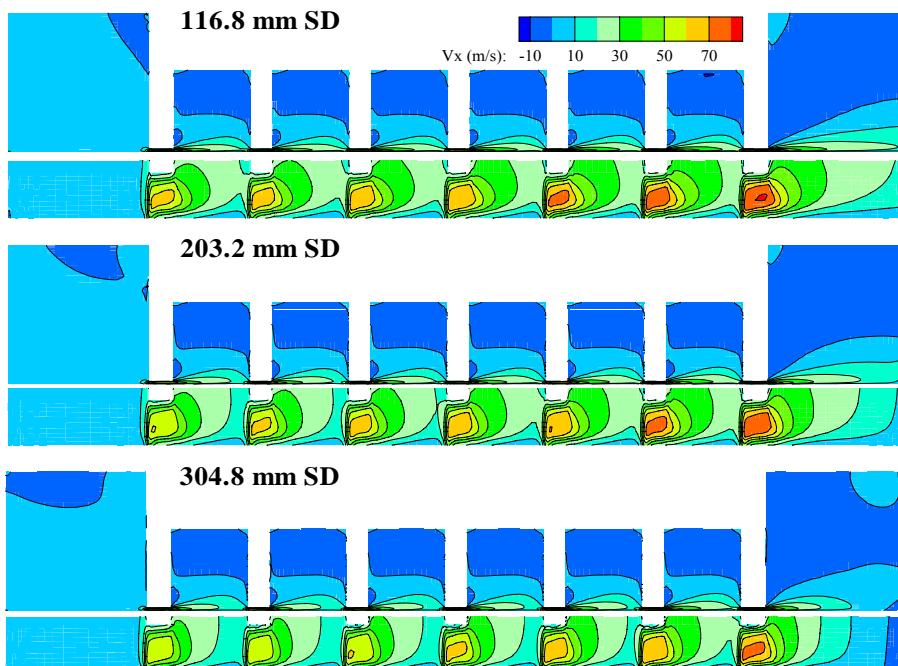
Figure B38. Axial velocity contours of labyrinth seals with three different shaft diameters, c=101.6 µm, Ω=15,000 rpm, ΔP=34.47 kPa

116.8 mm SD

Vr (m/s): -40 -30 -20 -10 0 10

203.2 mm SD

304.8 mm SD
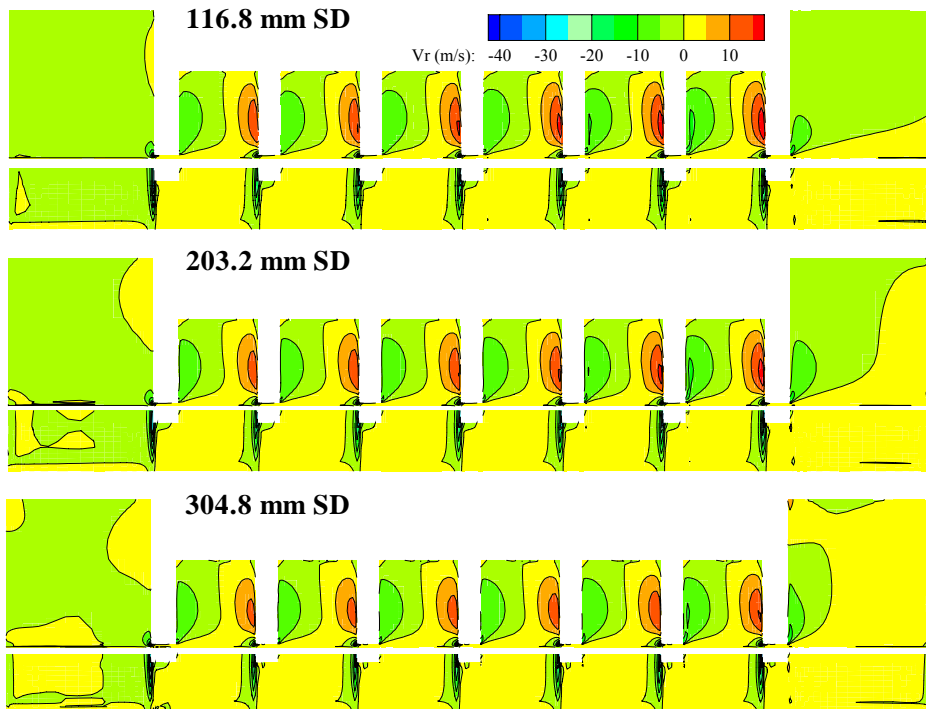
Figure B39. Radial velocity contours of labyrinth seals with three different shaft diameters, c=101.6 μm, Ω=15,000 rpm, ΔP=34.47 kPa

116.8 mm SD

Vorticity: 0 24000 48000

203.2 mm SD

304.8 mm SD
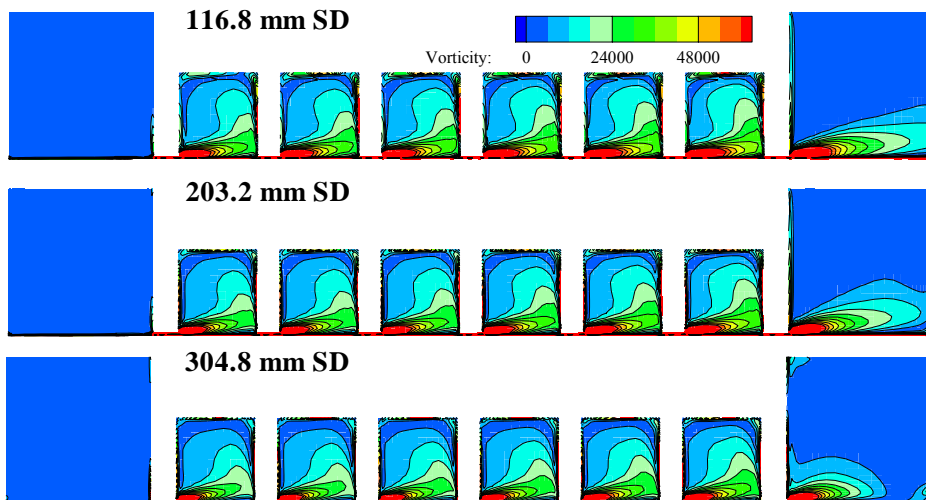
Figure B40. Vorticity magnitude contours of labyrinth seals with three different shaft diameters, c=101.6 μm, Ω=15,000 rpm, ΔP=34.47 kPa
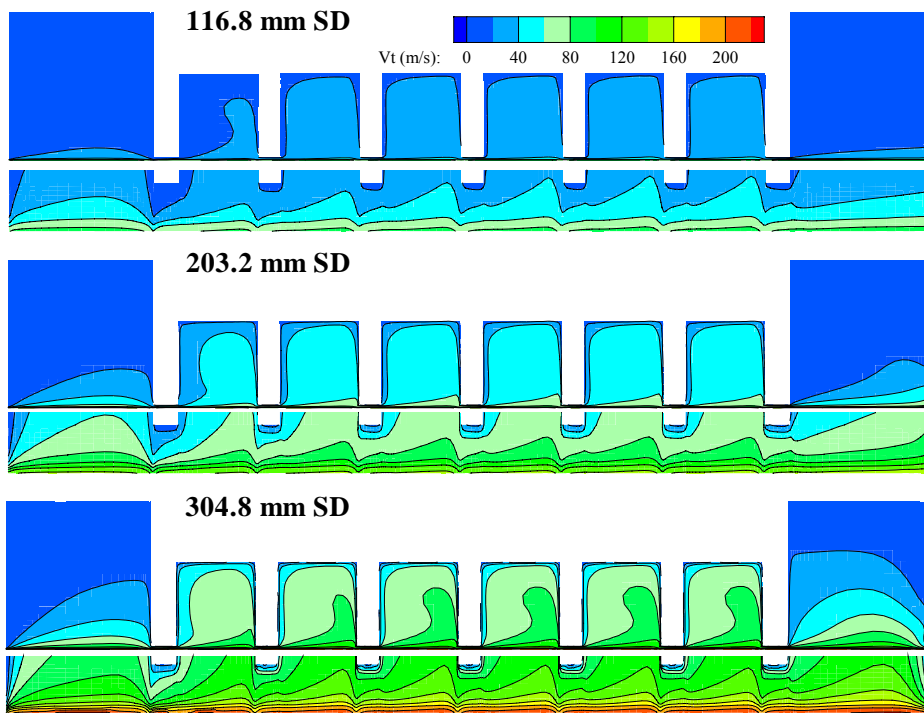
Figure B41. Tangential velocity contours of labyrinth seals with three different shaft diameters, c=101.6 μm, Ω=15,000 rpm, ΔP=34.47 kPa

APPENDIX C

Appendix C contains the plots of the leakage, pressure distribution, and velocity components for the three dimensional simulations with the air.
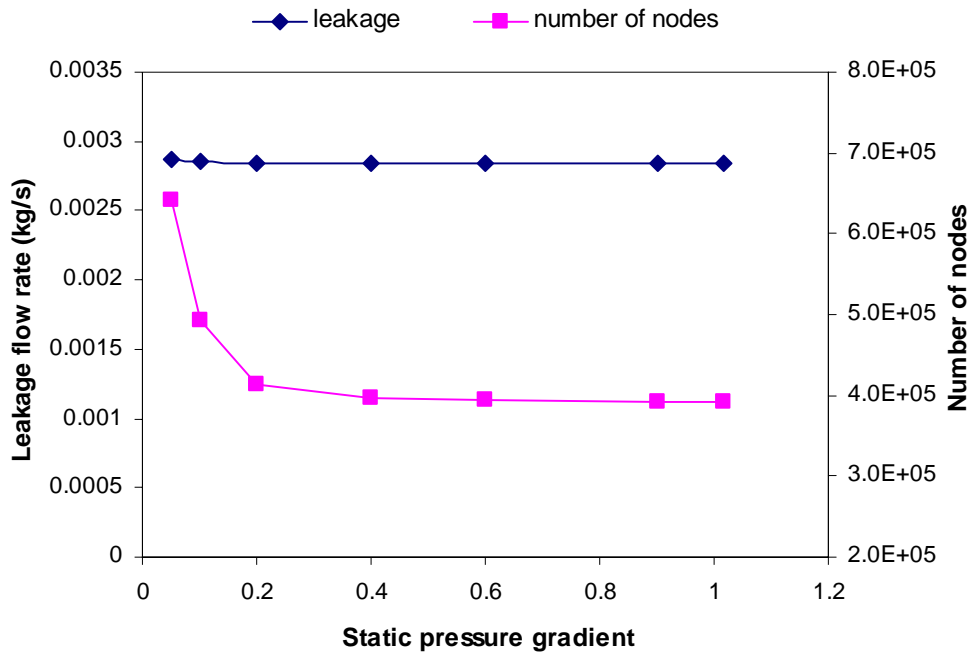
Figure C1. Leakage flow rate and number of nodes vs. static pressure gradient in the two-dimensional baseline seal
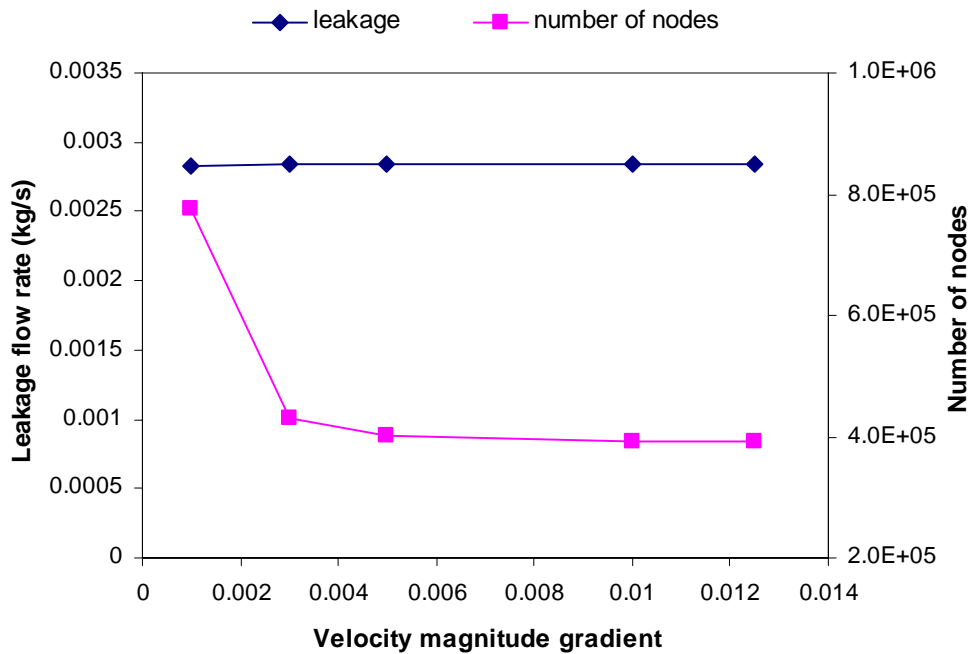
Figure C2. Leakage flow rate and number of nodes vs. velocity magnitude gradient in the two-dimensional baseline seal
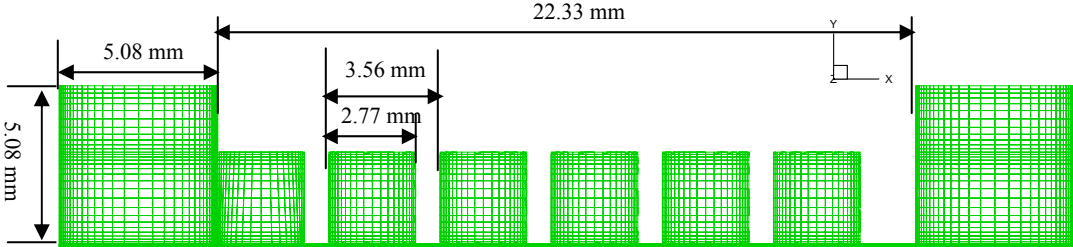
Figure C3. Overall layout labyrinth seal grid and geometry
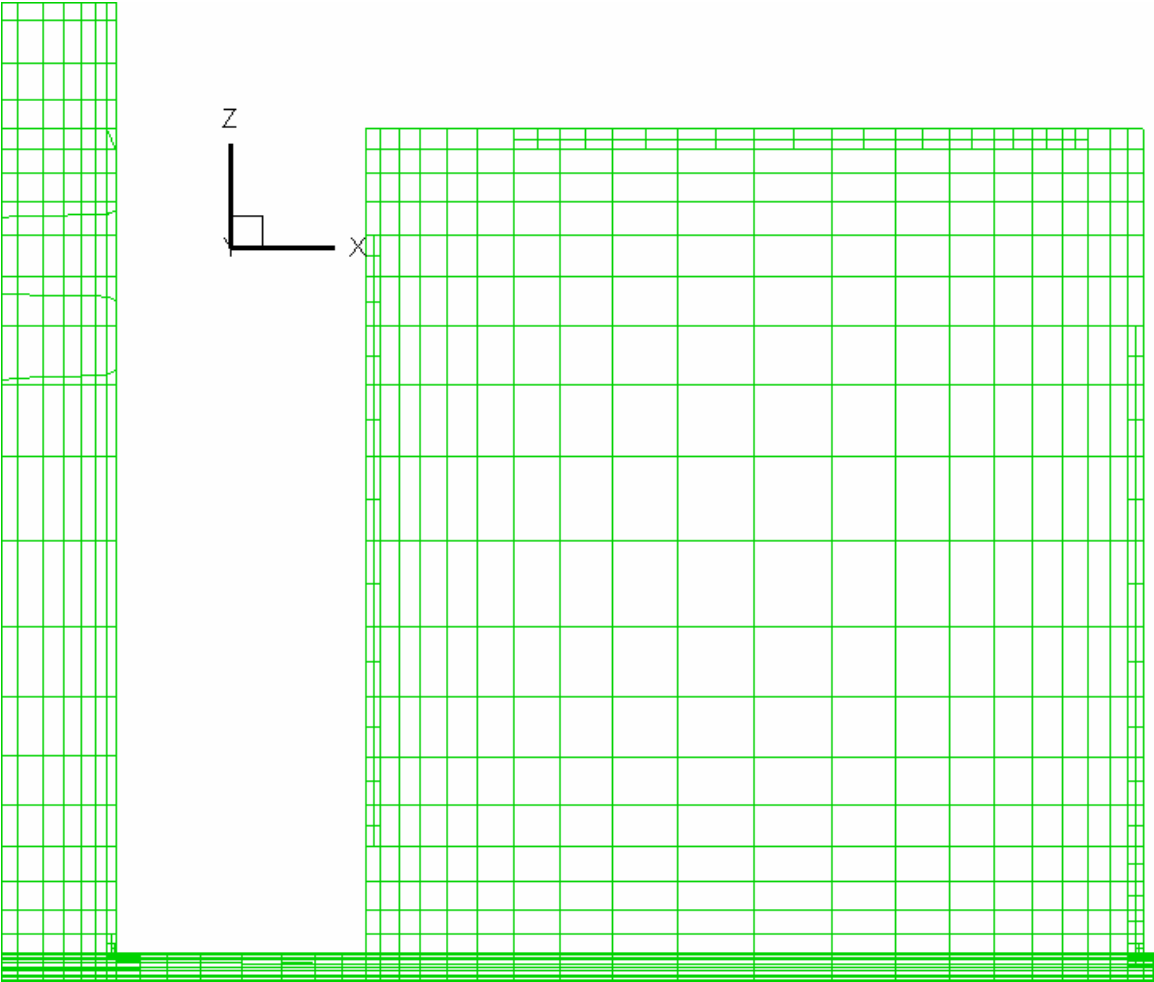
Figure C4. Cross section of grid refinement in the entrance region and first groove of the baseline windback seal
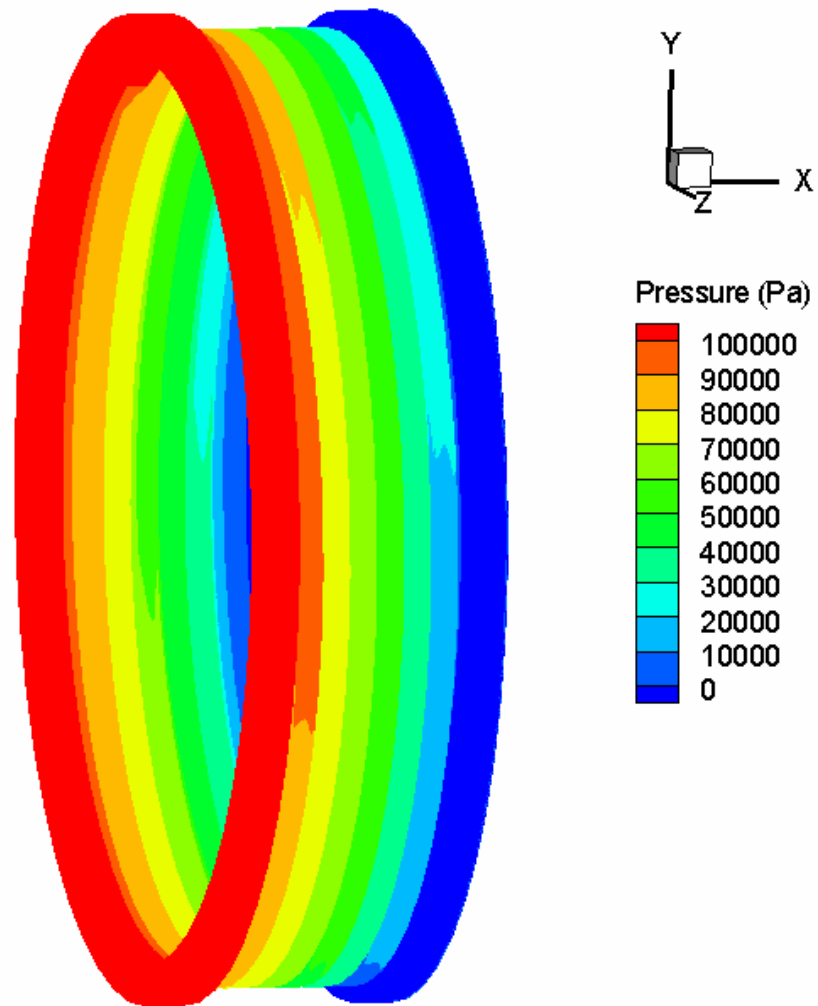
Figure C5. Overall view of pressure contour for three-dimensional windback seal, c=0.1016 mm, Ω=15,000 rpm, ΔP=103.42 kPa, helix angle=0.871°
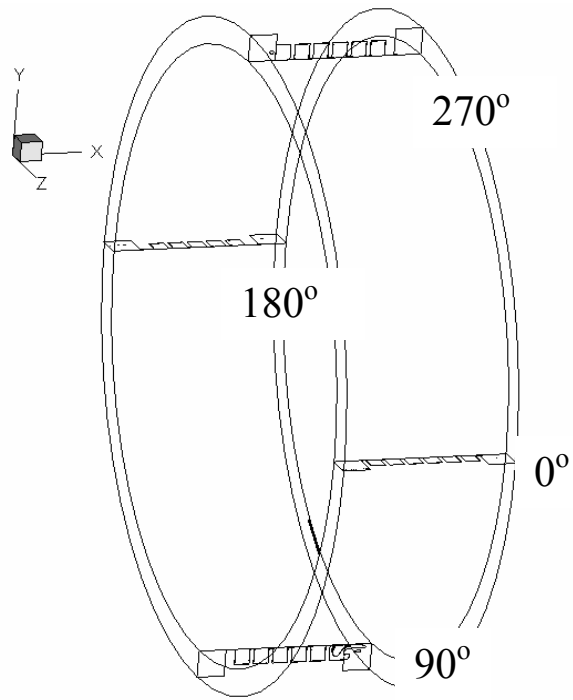
Figure C6. Four sliced angular view for the centered windback seal
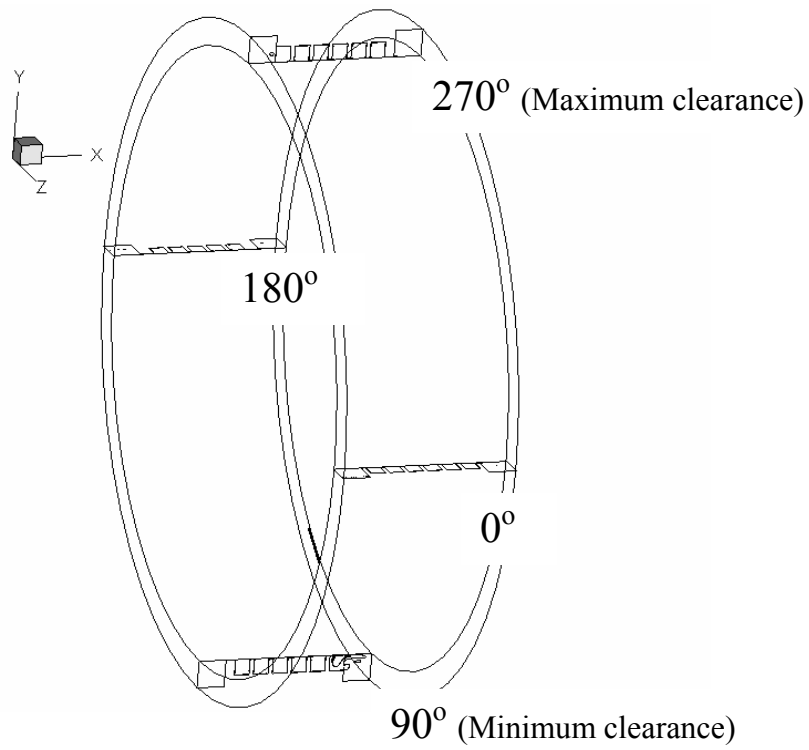
Figure C7. Four sliced angular view for the 25% eccentric windback seal
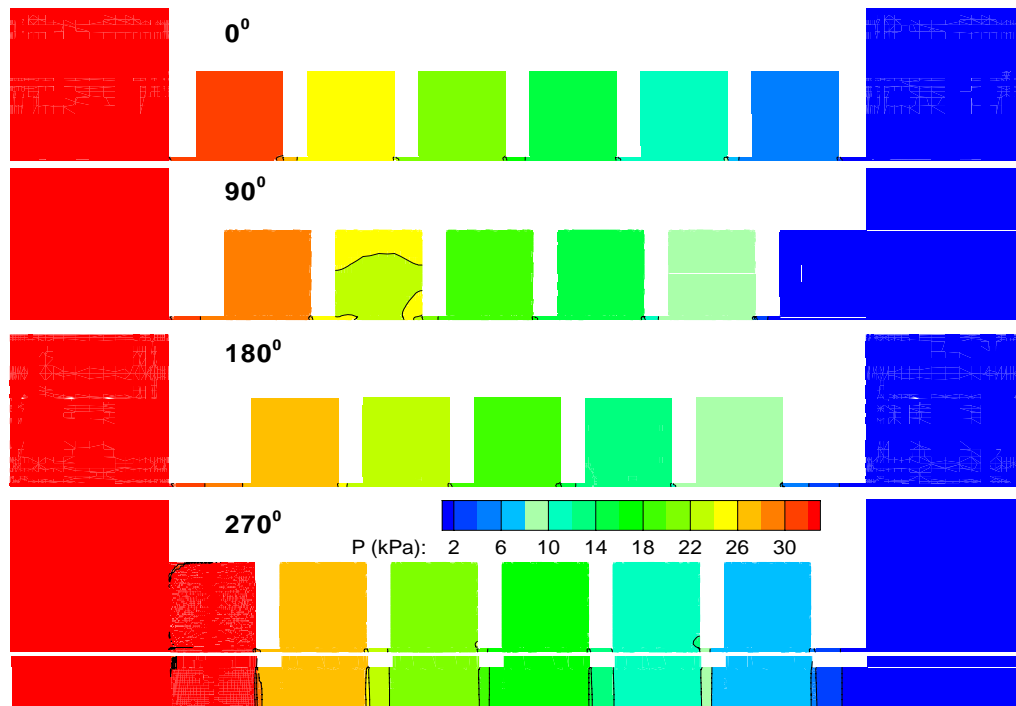
Figure C8. Pressure contours of windback seal, e=0, Ω=0 rpm, c=0.1016 mm, DP=34.47 kPa, helix angle=0.871°
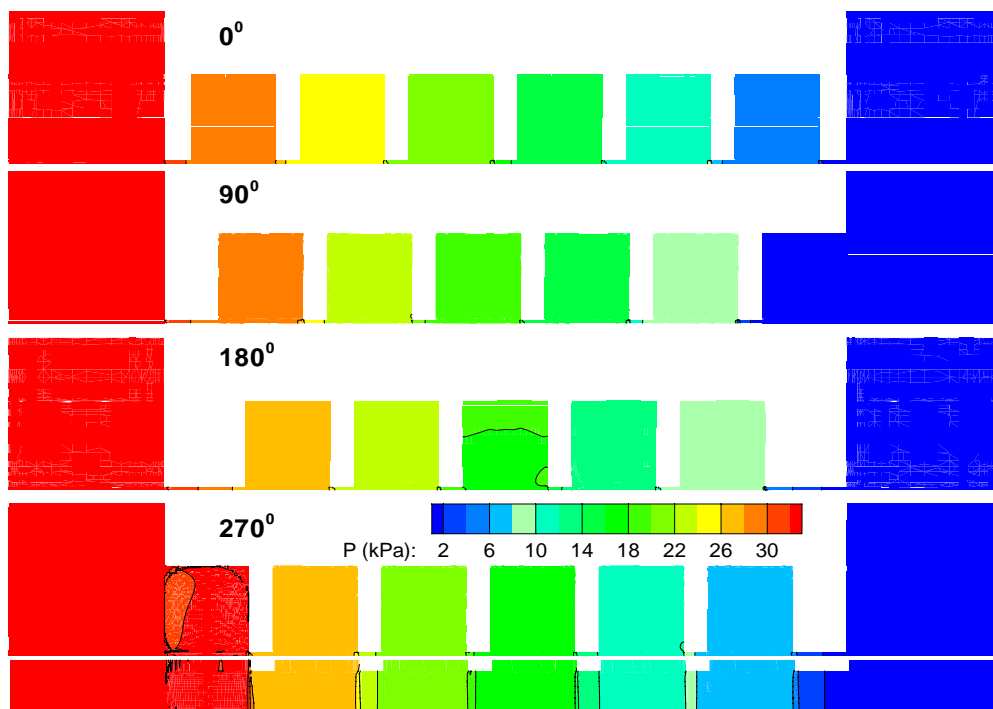
Figure C9. Pressure contours of windback seal, e=0, Ω=15,000 rpm, c=0.1016 mm, DP=34.47 kPa, helix angle=0.871°, e=0, helix angle=0.871°
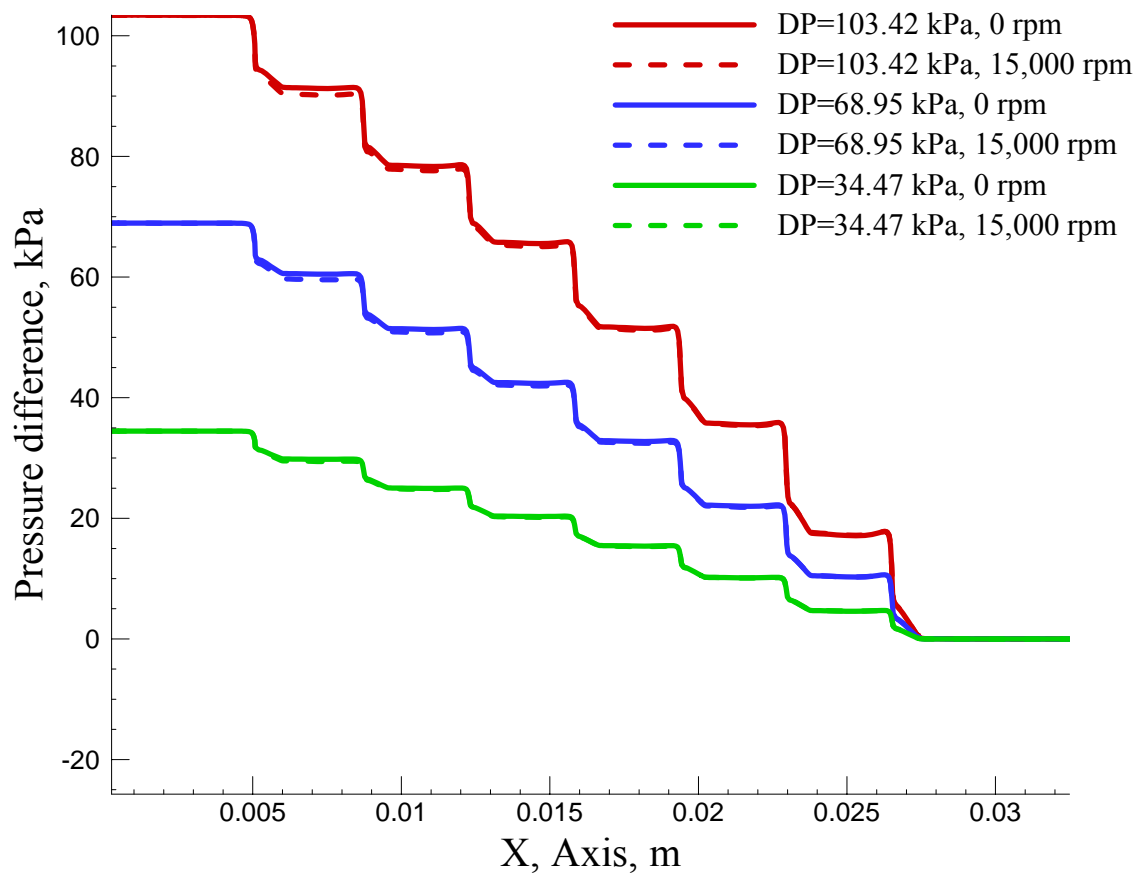
Figure C10. Axial pressure distributions along the middle of clearance for the windback seal with three differential pressure in the 0 degree sliced plane, e=0, c=0.1016 mm
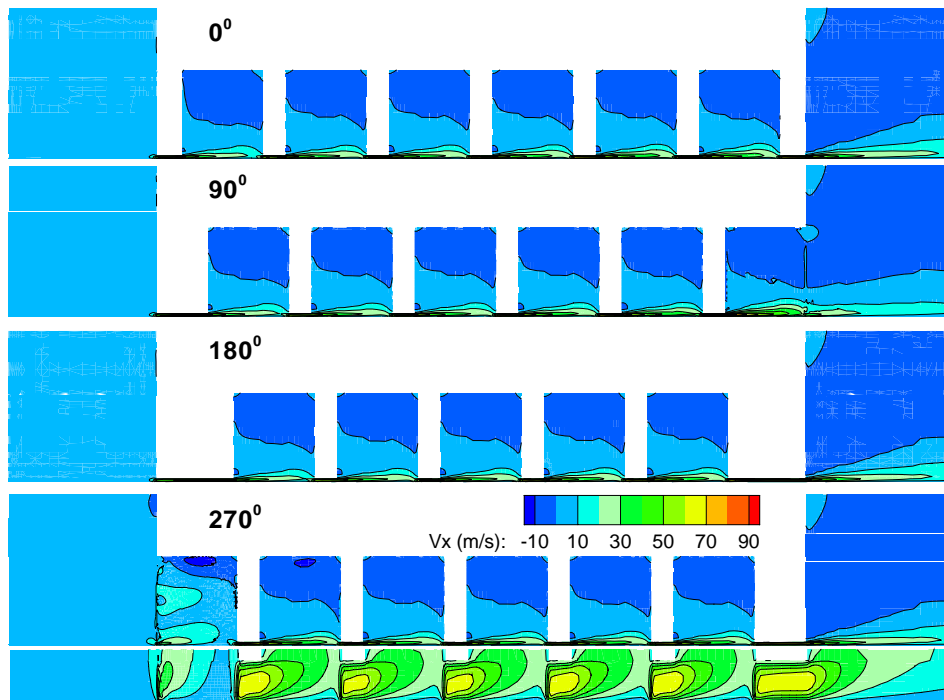
Figure C11. Axial velocity contours of windback seal, e=0, Ω=0 rpm, c=0.1016 mm, DP=34.47 kPa, helix angle=0.871°
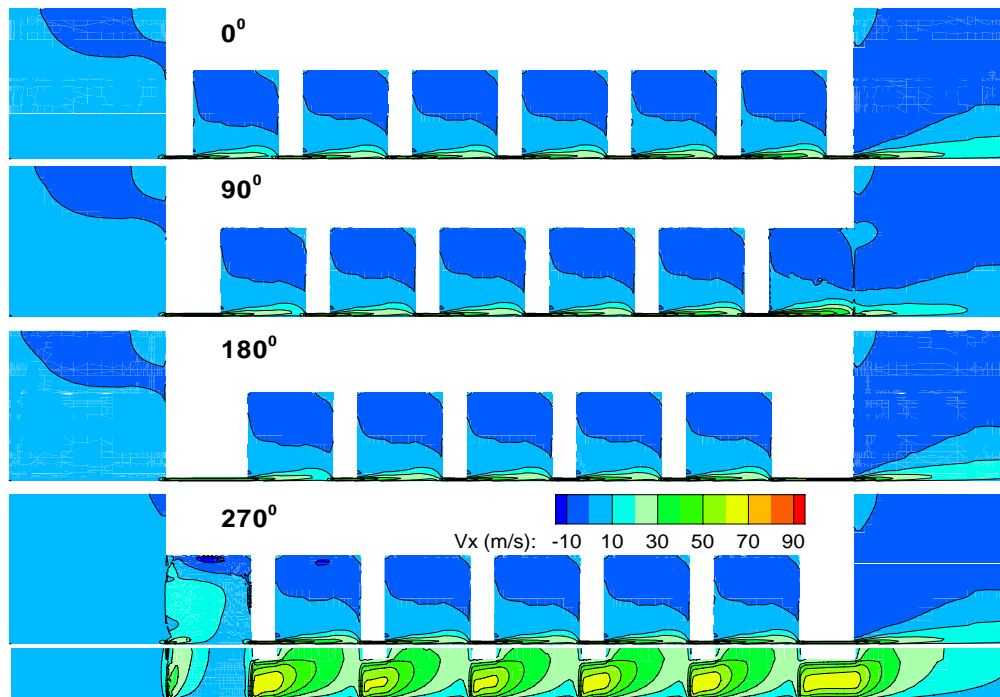
Figure C12. Axial velocity contours of windback seal, e=0, Ω=15,000 rpm, c=0.1016 mm, DP=34.47 kPa, helix angle=0.871°
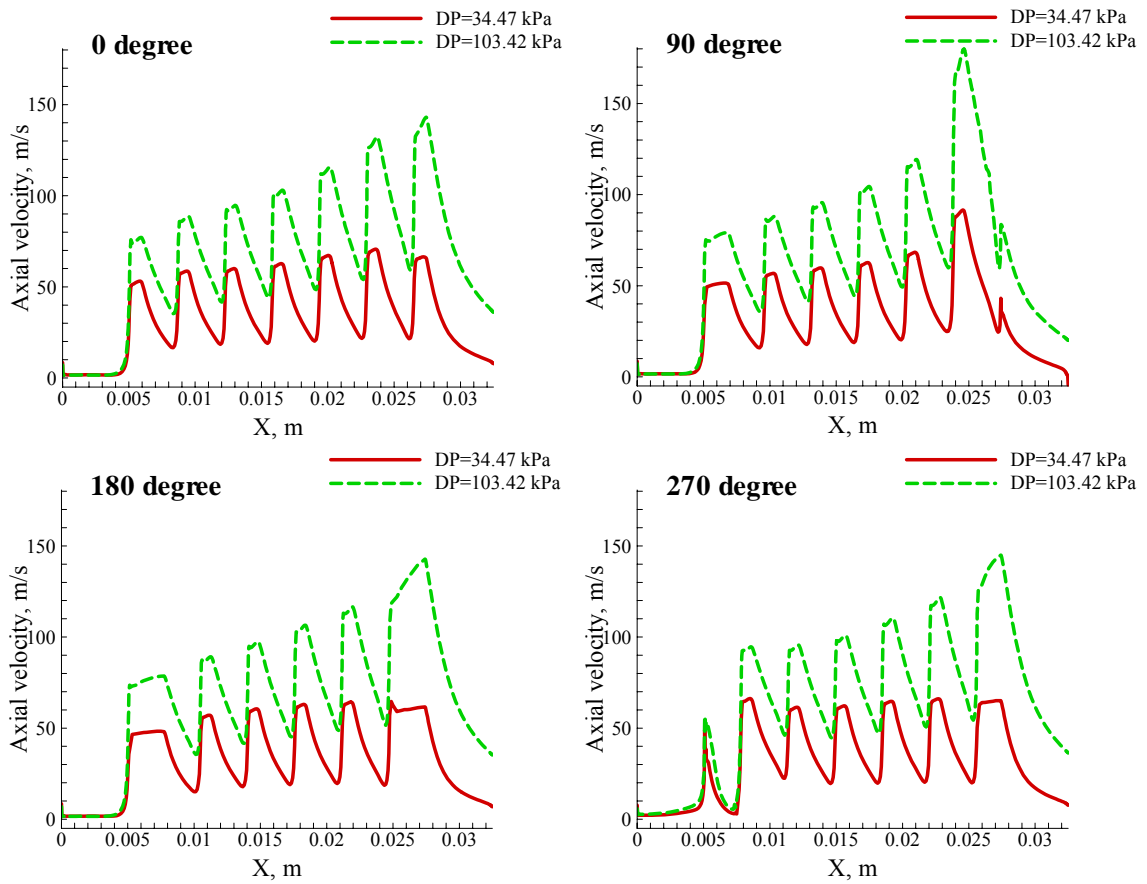
Figure C13. Axial velocity distributions of the windback seal along the middle of clearance in four different sliced planes, e=0, Ω=0 rpm, c=0.1016 mm
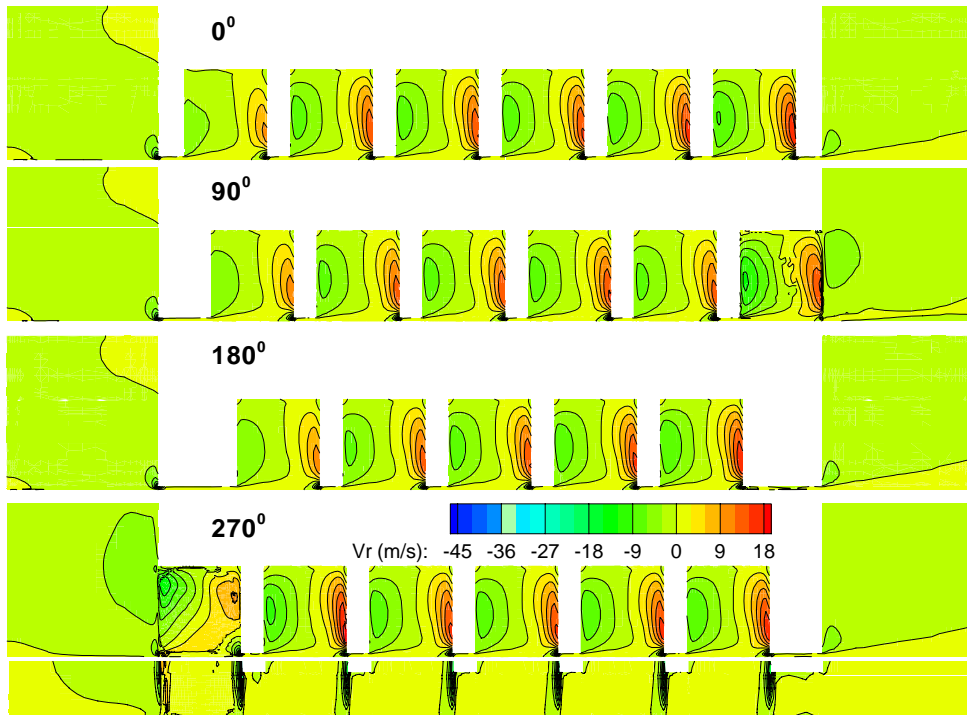
Figure C14. Radial velocity contours of windback seal, e=0, Ω=0 rpm, c=0.1016 mm, DP=34.47 kPa, helix angle=0.871°
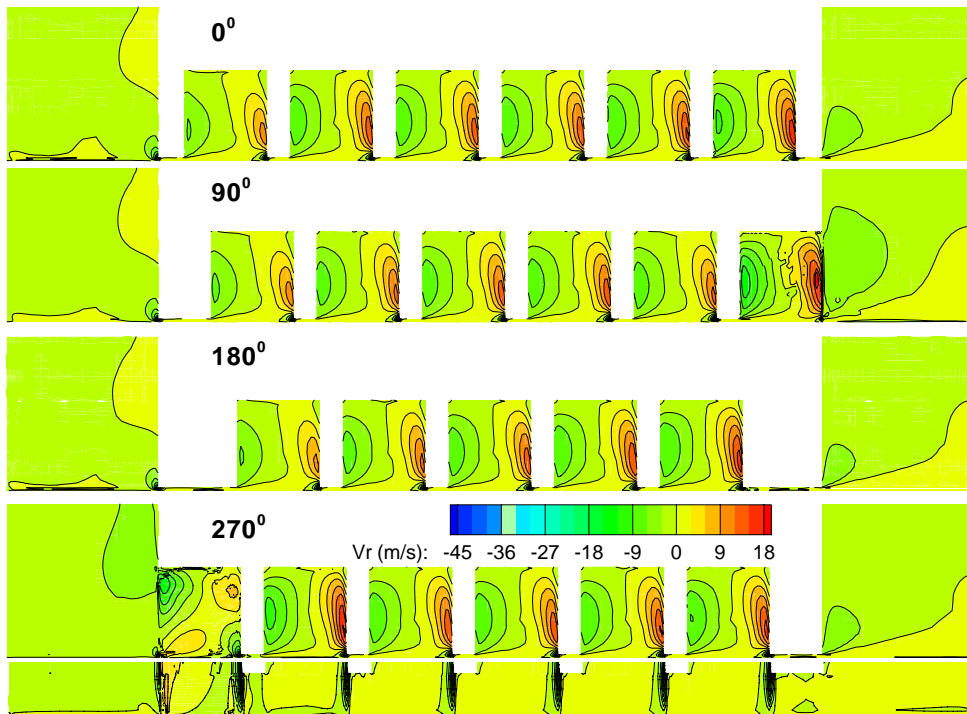
Figure C15. Radial velocity contours of windback seal, e=0, Ω=15,000 rpm, c=0.1016 mm, DP=34.47 kPa, helix angle=0.871°
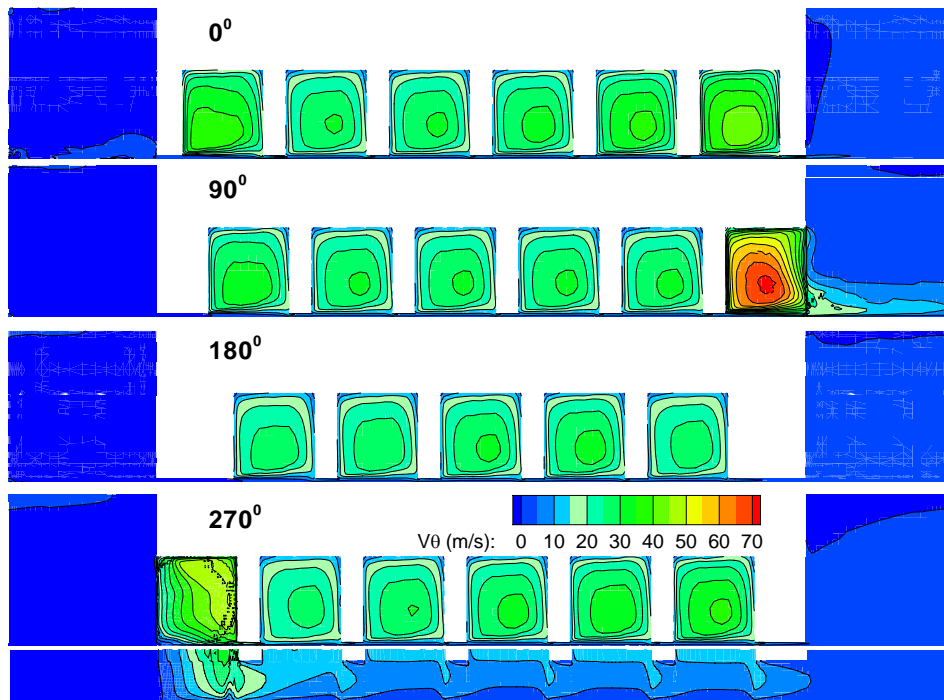
Figure C16. Circumferential velocity contours of windback seal, e=0, Ω=0 rpm, c=0.1016 mm, DP=34.47 kPa, helix angle=0.871°
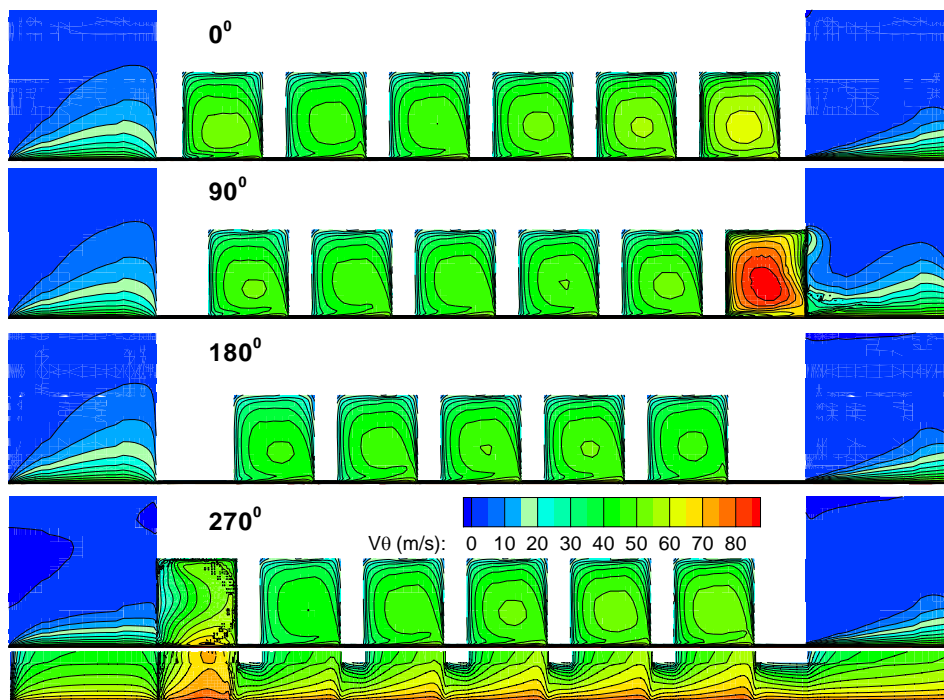
Figure C17. Circumferential velocity contours of windback seal, e=0, Ω=15,000 rpm, c=0.1016 mm, DP=34.47 kPa, helix angle=0.871°
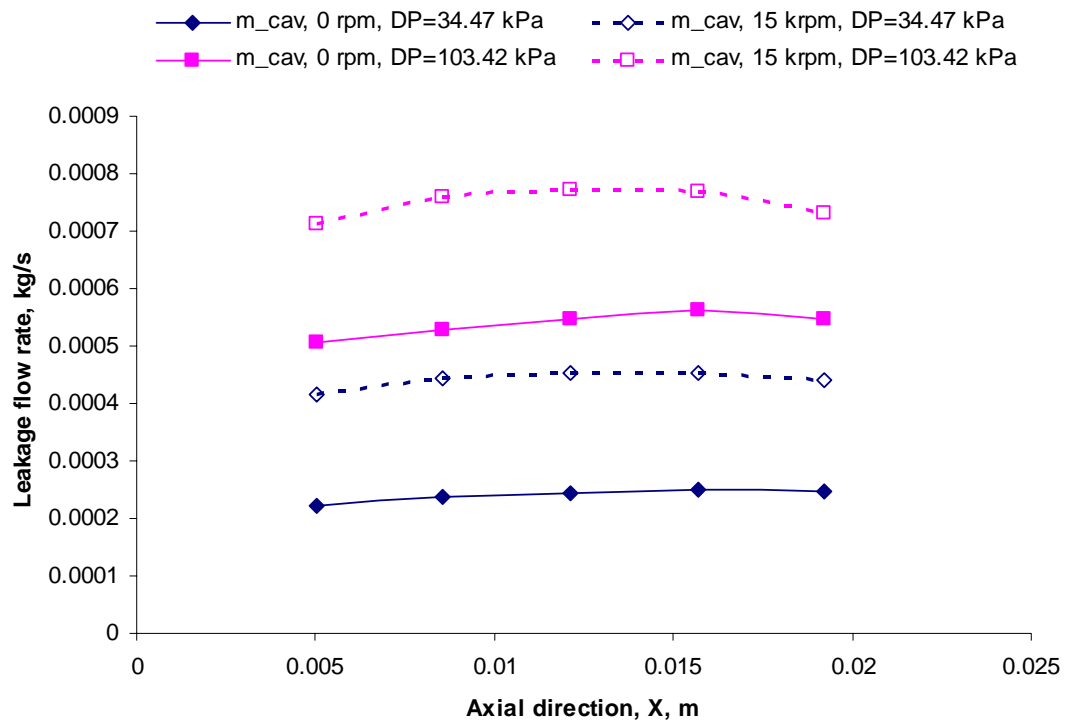
Figure C18. Leakage flow rate through the cavity along the axial direction for the baseline design
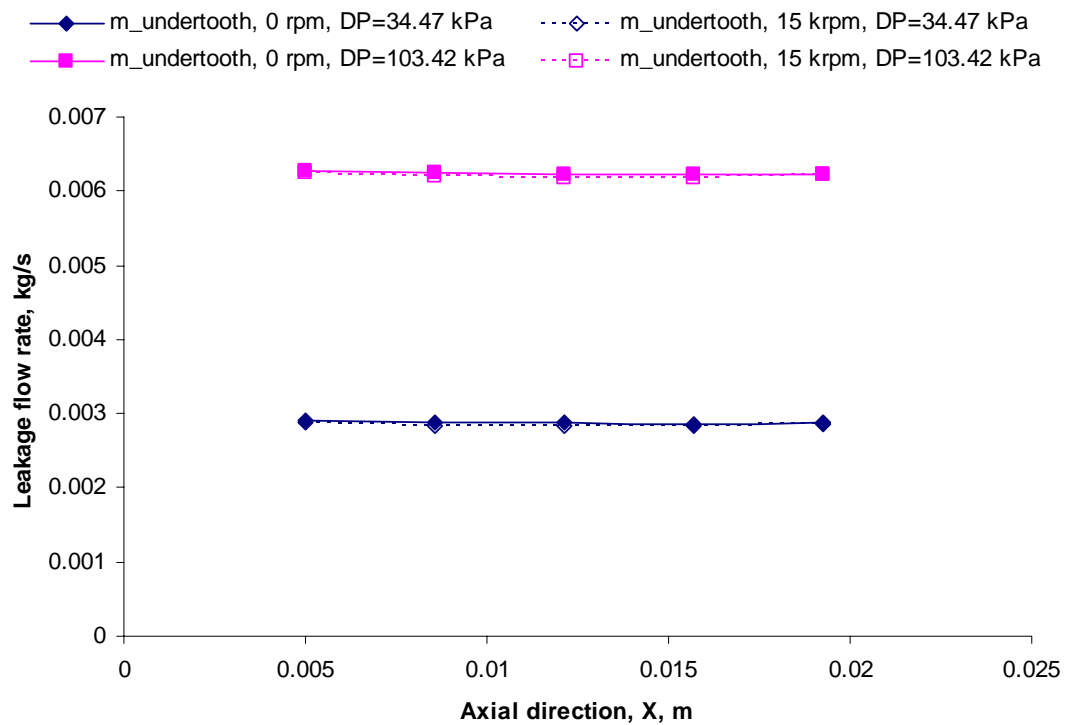
Figure C19. Leakage flow rate under the tooth along the axial direction for the baseline design
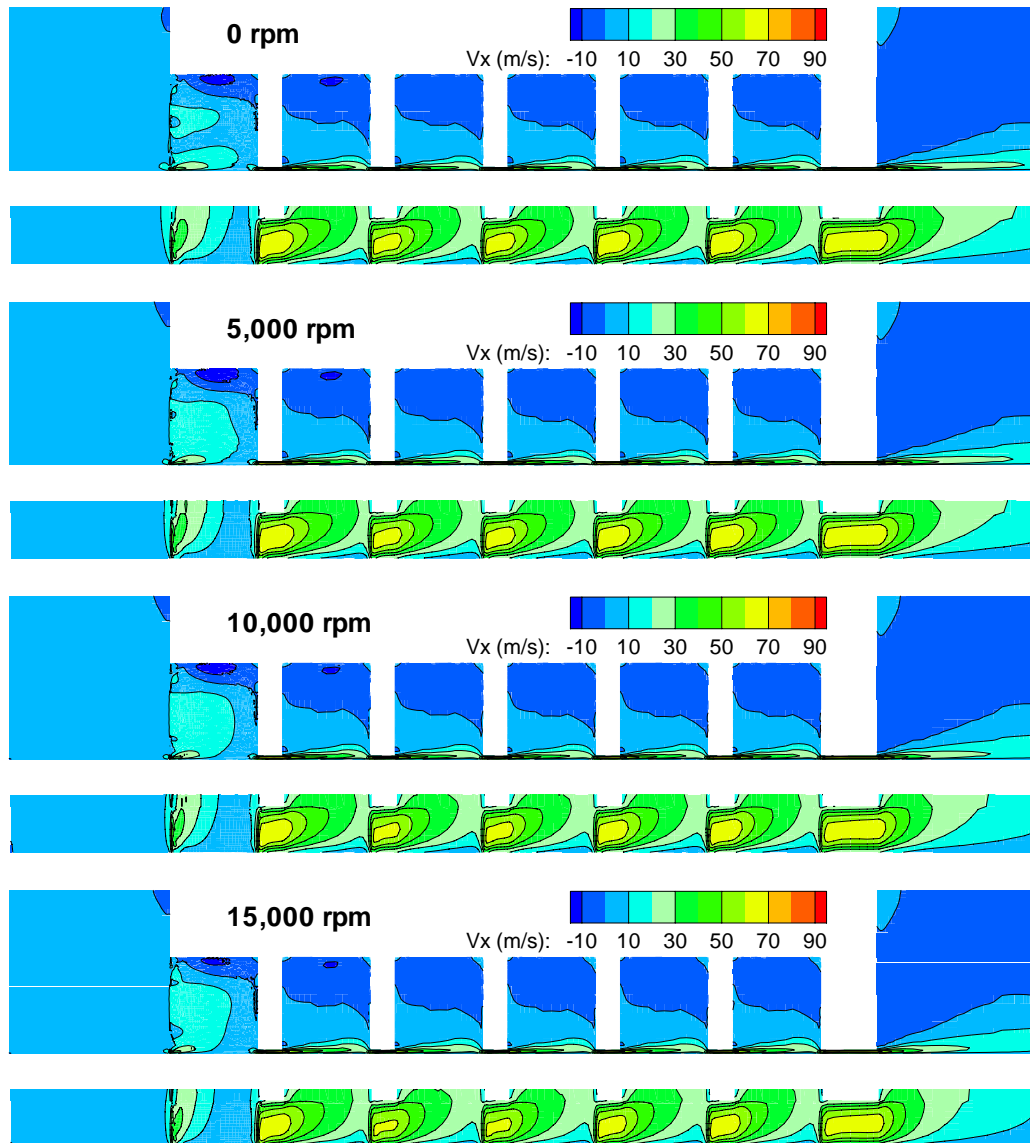
Figure C20. Axial velocity contours of windback seal for four rotor speeds, e=0, c=0.1016 mm, DP=34.47 kPa, helix angle=0.871°
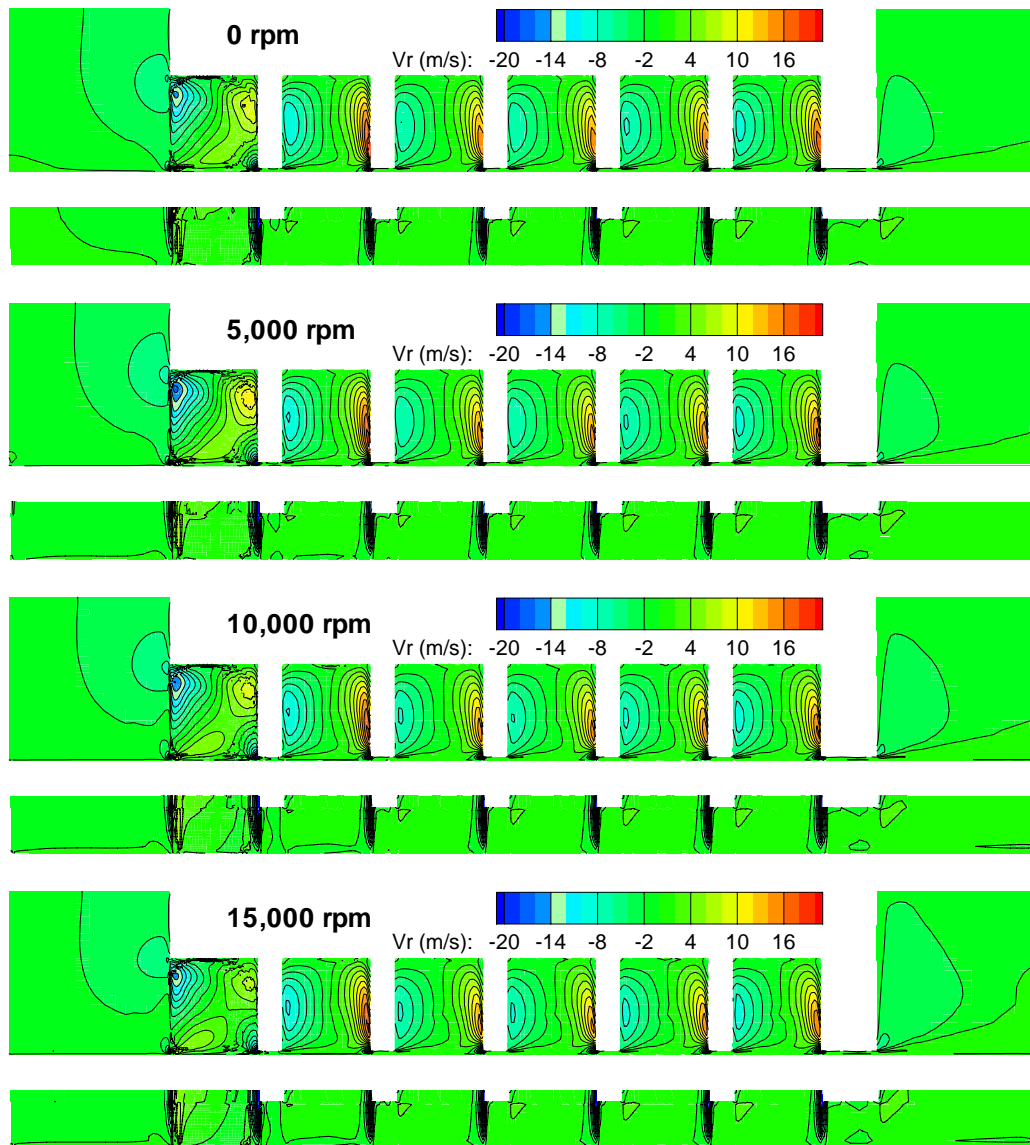
Figure C21. Radial velocity contours of windback seal for four rotor speeds, e=0, c=0.1016 mm, DP=34.47 kPa, helix angle=0.871°
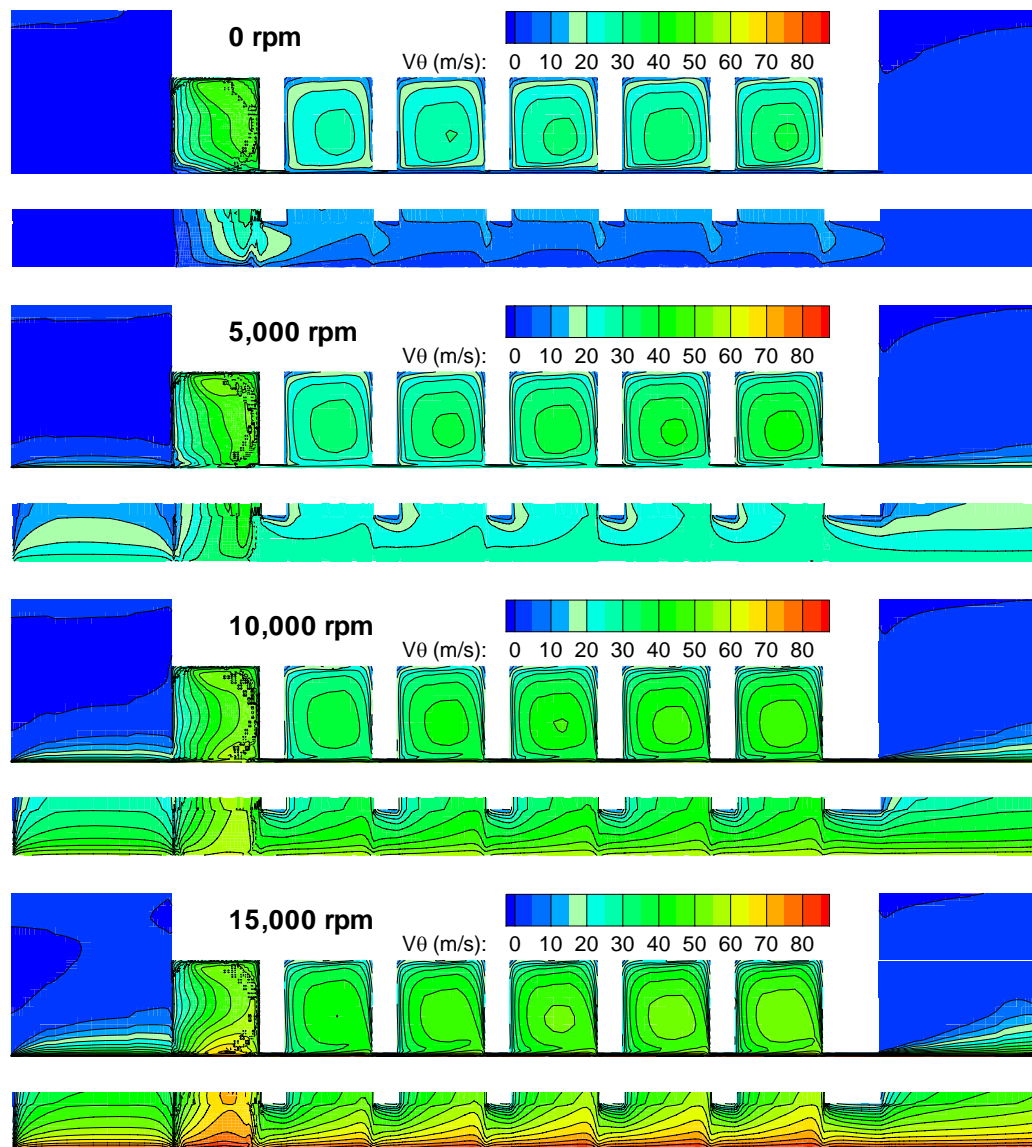
Figure C22. Circumferential velocity contours of windback seal for four rotor speeds, e=0, c=0.106 mm, DP=34.47 kPa, helix angle=0.871°
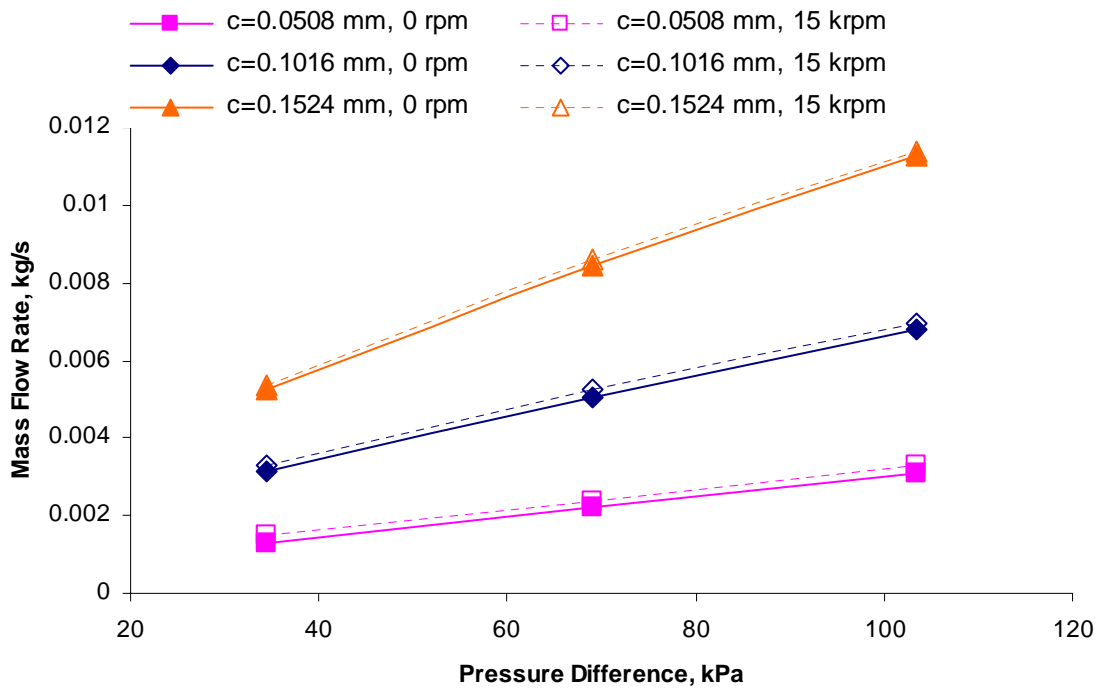
Figure C23. Leakage mass flow rate vs. differential pressure for windback seals with three different clearances at rotor speeds of 0 rpm, and 15,000 rpm, helix angle=0.871°
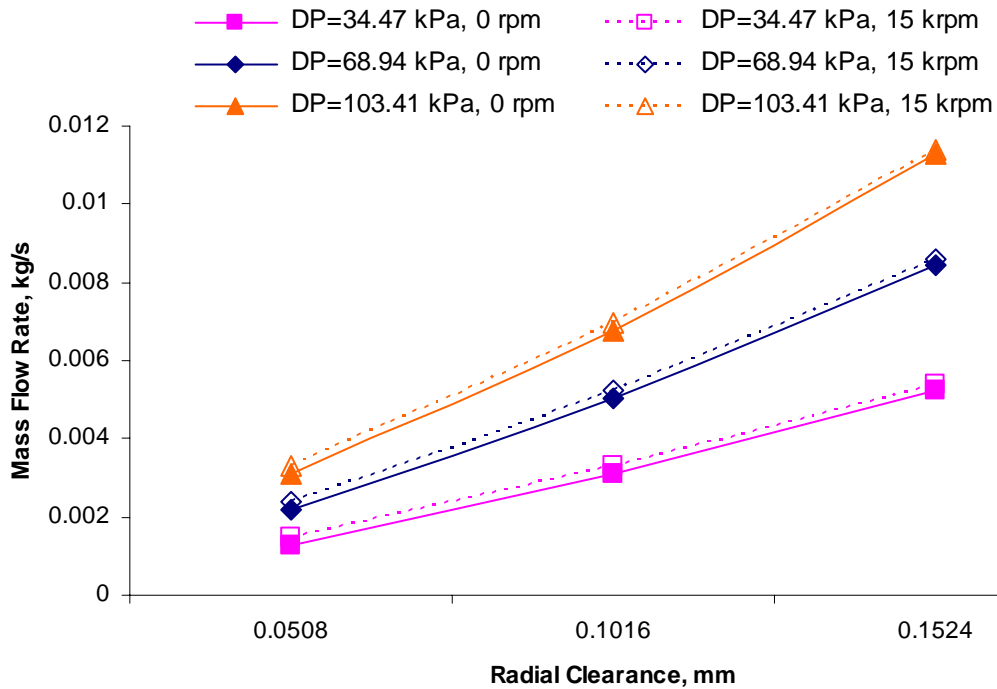
Figure C24. Leakage mass flow rate vs. radial clearance for windback seals with three differential pressures at rotor speeds of 0 rpm, and 15,000 rpm, helix angle=0.871°
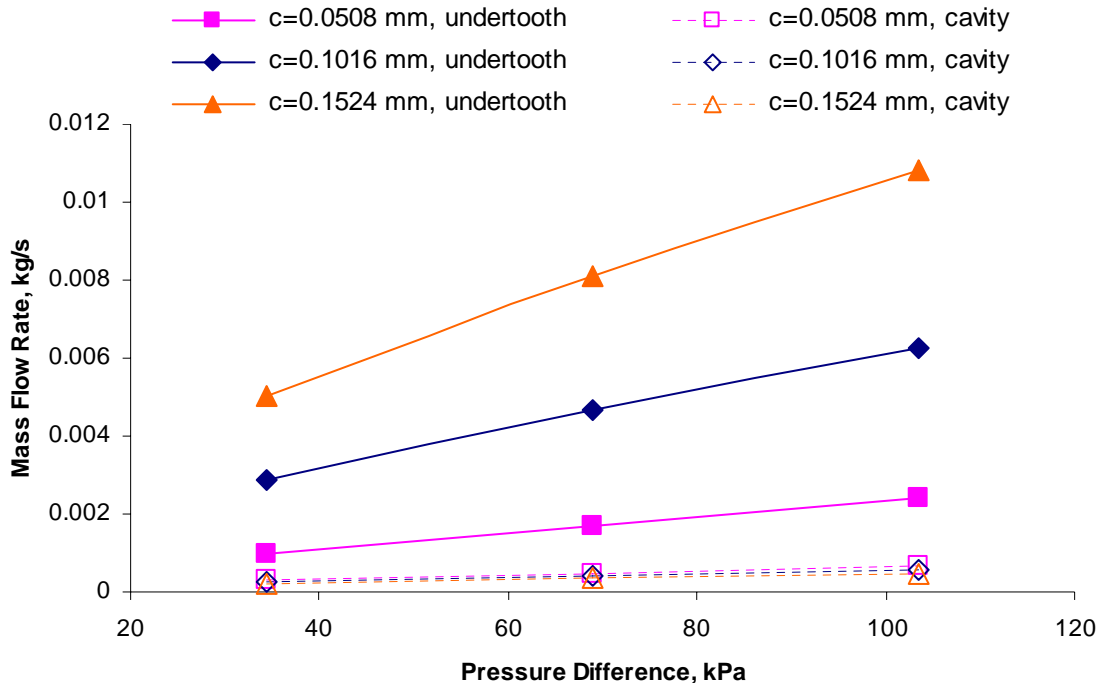
Figure C25. Leakage flow rate for two leakage paths for windback seals with three clearances e=0, Ω=0 rpm, helix angle=0.871°
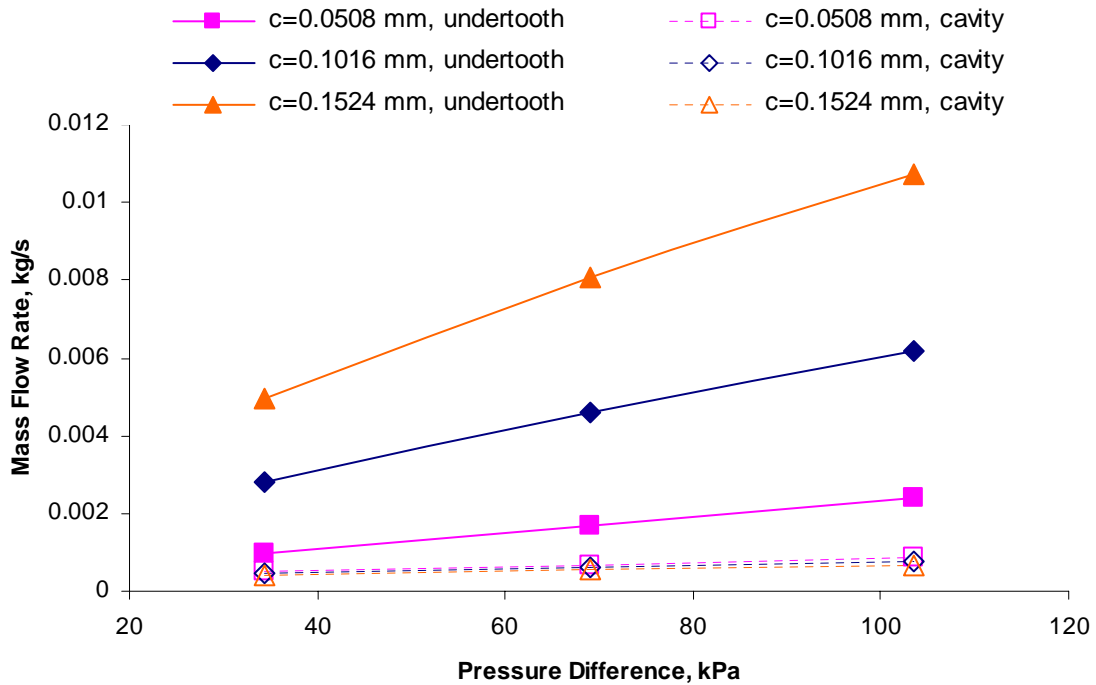
Figure C26. Leakage flow rate for two leakage paths for windback seals with three clearances e=0, Ω=15,000 rpm, helix angle=0.871°
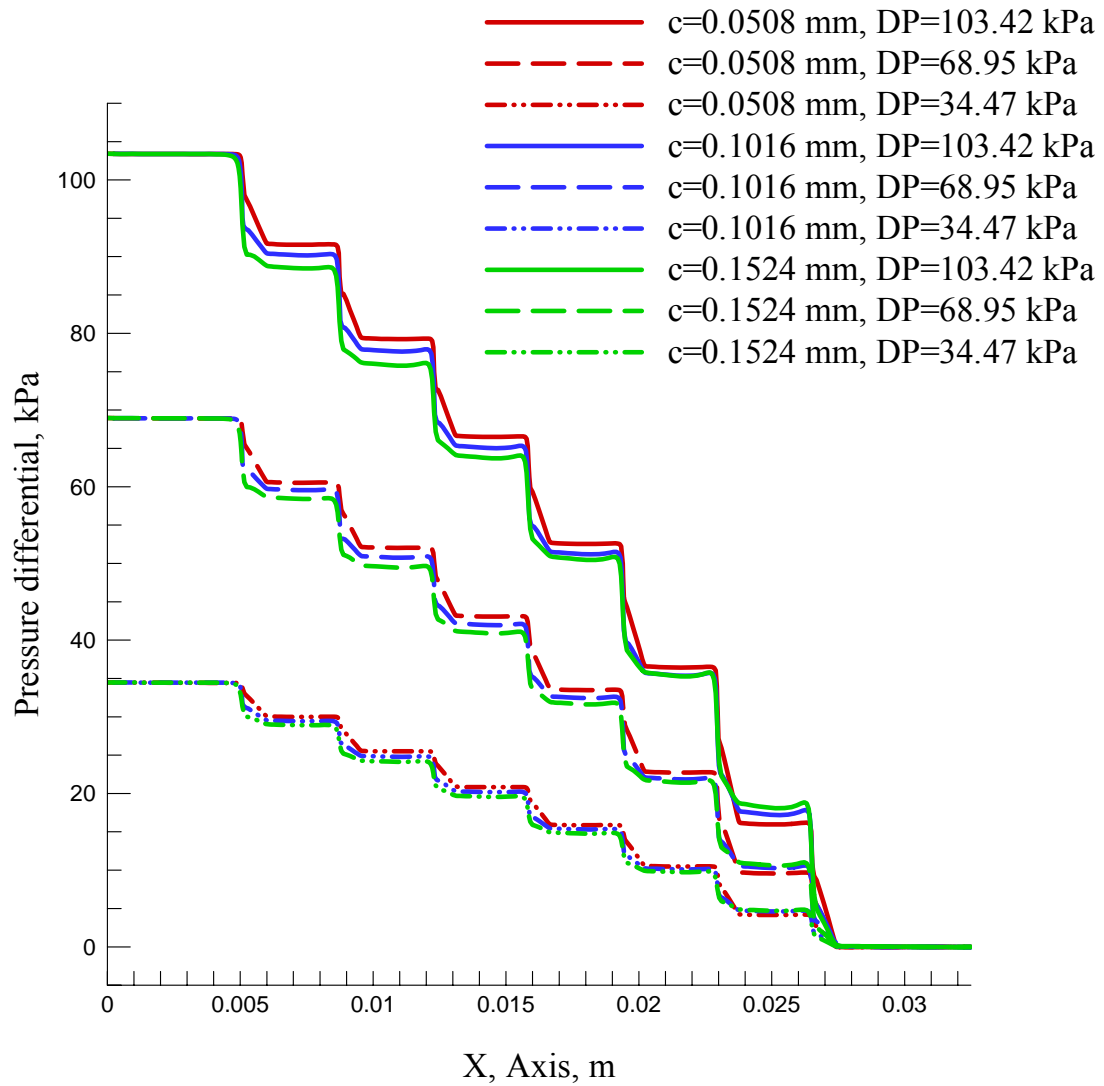
Figure C27. Axial pressure distribution of the windback seal along the middle of clearance for three different clearances at the rotor speed of 15,000 rpm in the 0 degree sliced plane
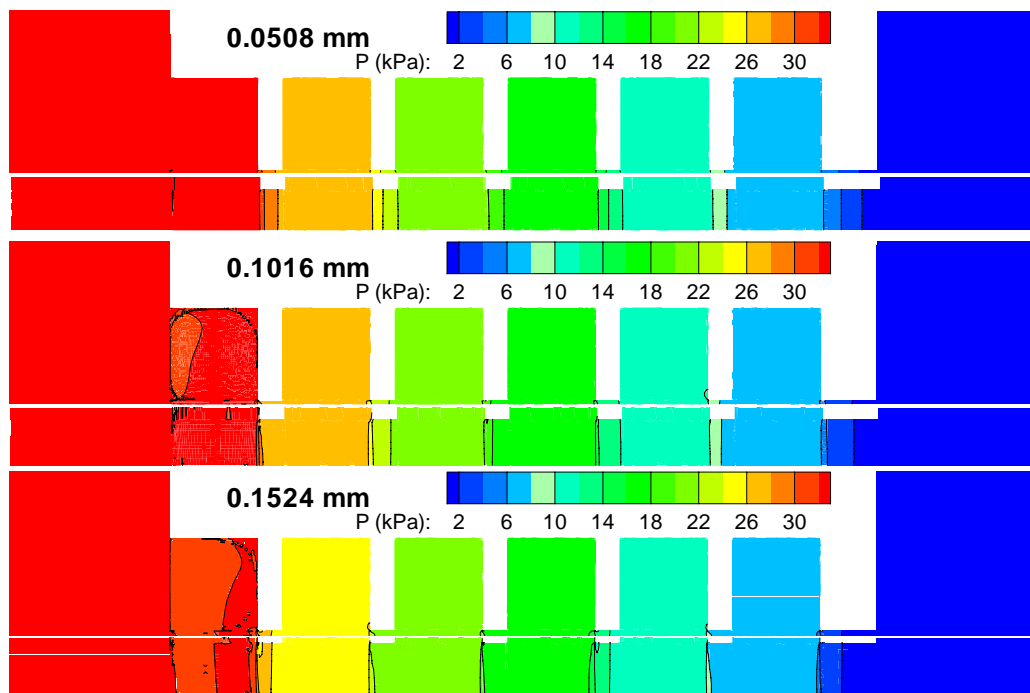
Figure C28. Pressure contours of windback seals with three different clearances in the 270° sliced plane, e=0, Ω=15,000 rpm, DP=34.47 kPa, helix angle=0.871°
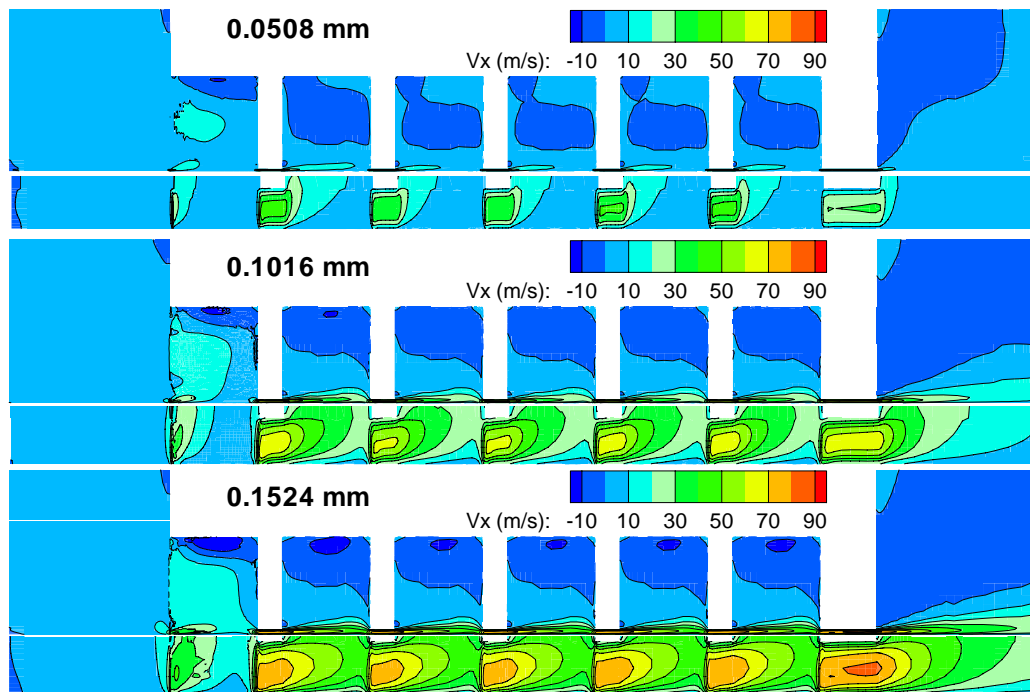
Figure C29. Axial velocity contours of windback seals with three different clearances in the 270° sliced plane, e=0, Ω=15,000 rpm, DP=34.47 kPa, helix angle=0.871°
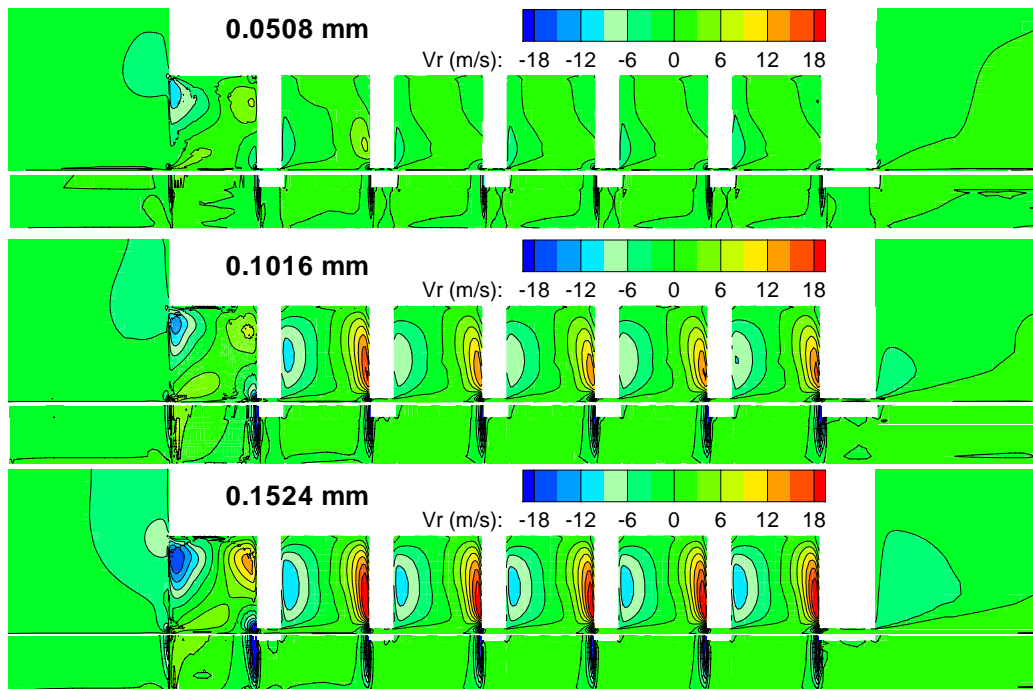
Figure C30. Radial velocity contours of windback seals with three different clearances in the270° sliced plane, e=0, Ω=15,000 rpm, DP=34.47 kPa, helix angle=0.871°
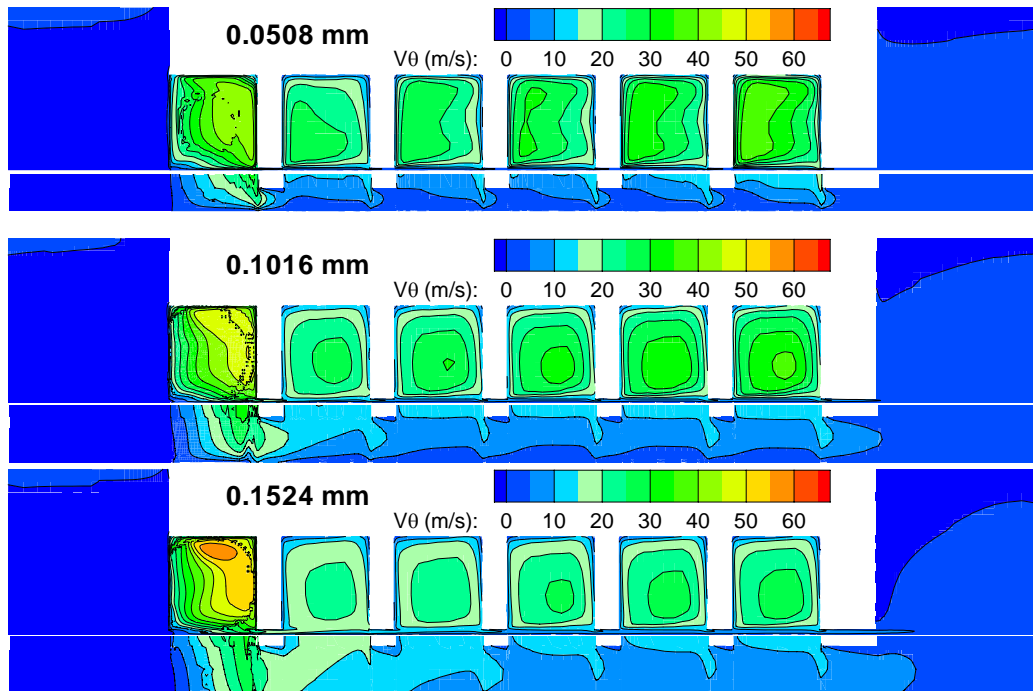
Figure C31. Circumferential velocity contours of windback seals with three different clearances in the 270° sliced plane, e=0, Ω=15,000 rpm, DP=34.47 kPa, helix angle=0.871°
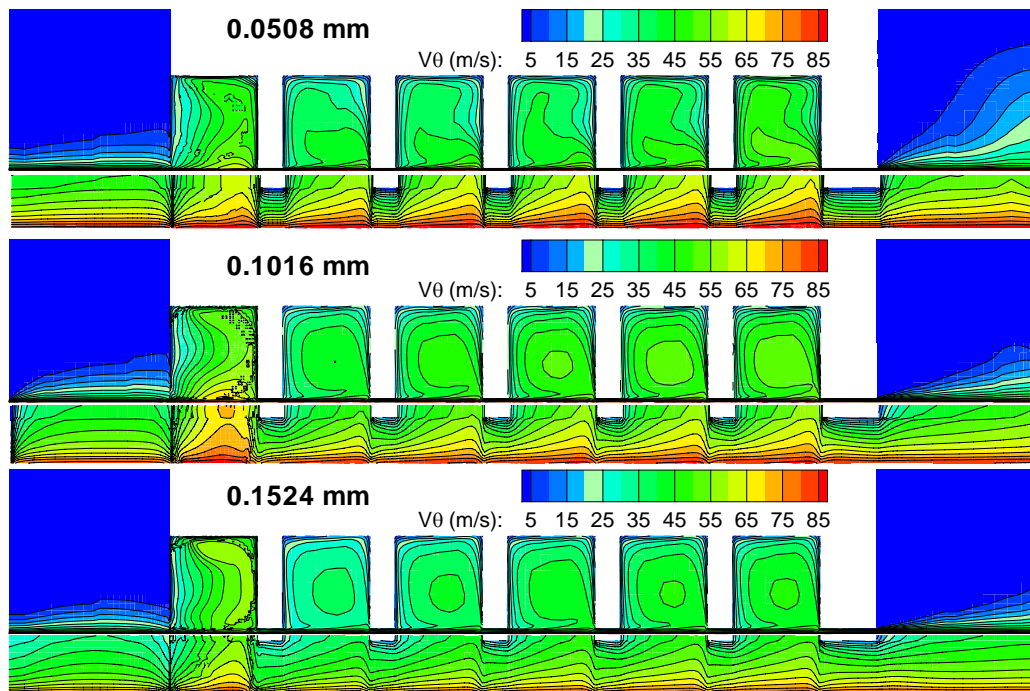
Figure C32. Circumferential velocity contours of windback seals with three different clearances in the 270° sliced plane, e=0, Ω=15,000 rpm, DP=34.47 kPa, helix angle=0.871°
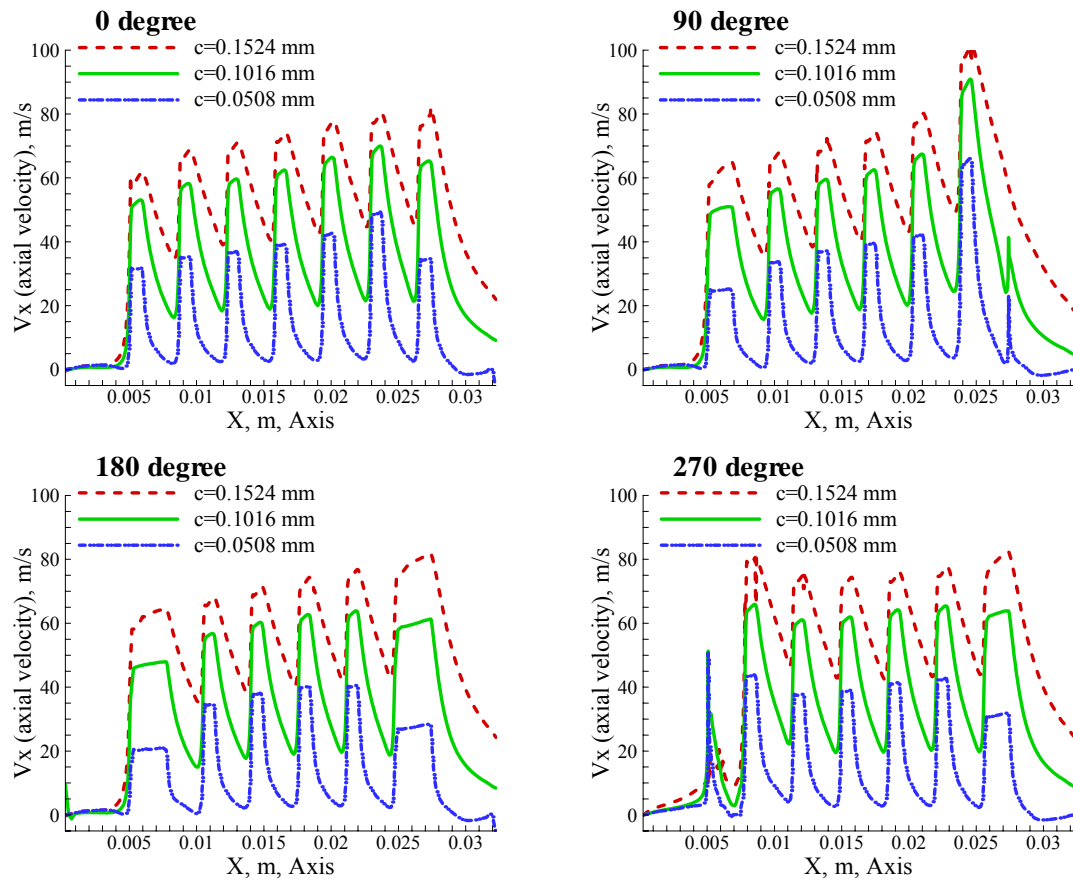
Figure C33. Axial velocity distributions for four angular planes along the middle of clearance with e=0, Ω=15,000 rpm, DP=34.47 kPa, helix angle=0.871°
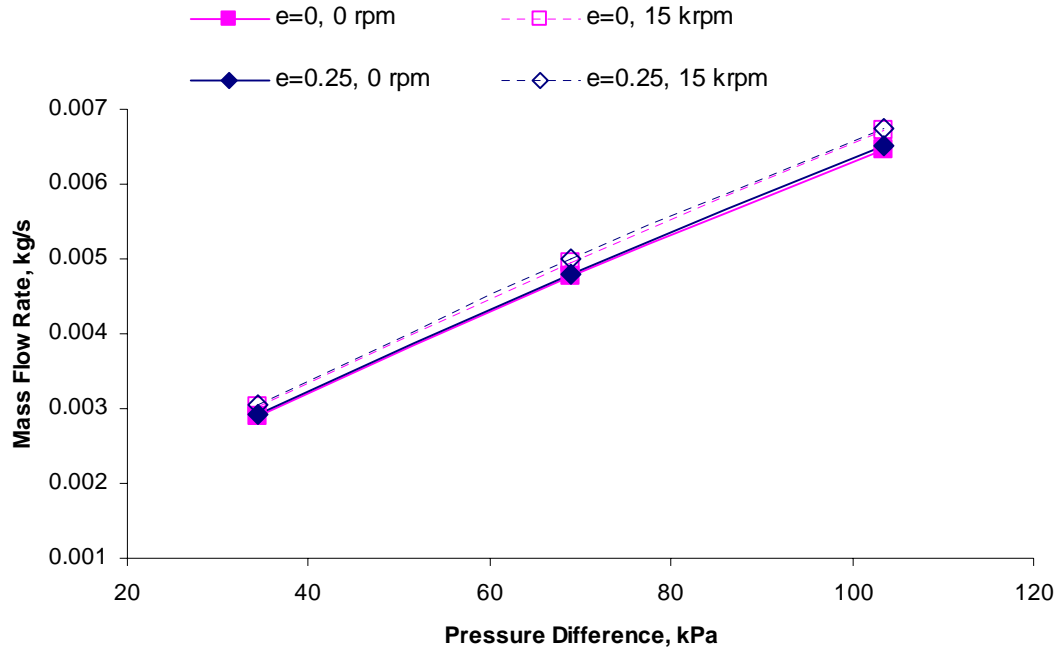
Figure C34. Effect of rotor eccentricity on the leakage rate with three differential pressures at the rotor speed of 0, and 15,000 rpm
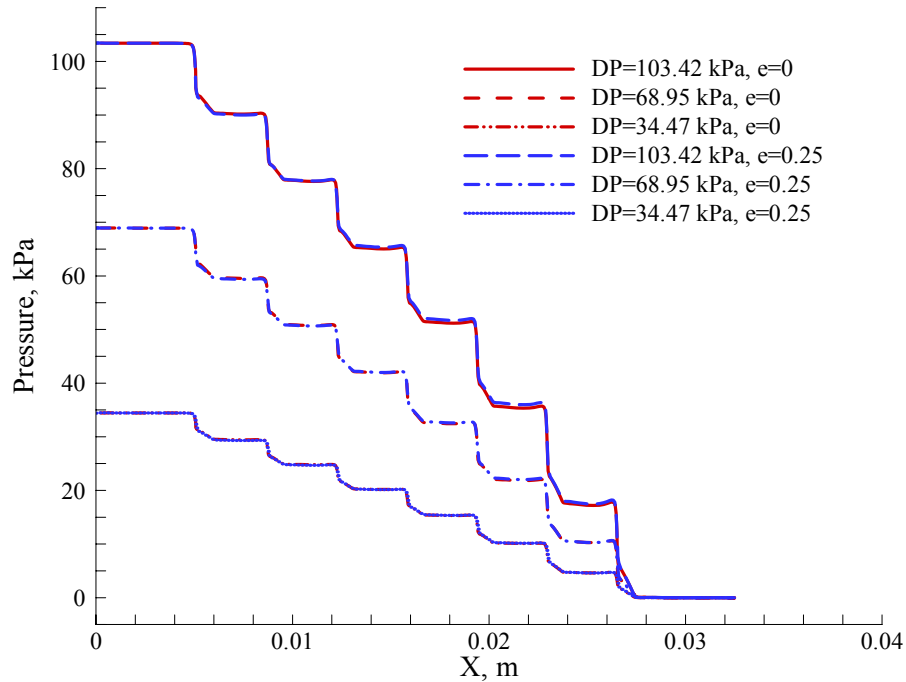
Figure C35. Pressure distribution for rotor eccentricity effect along the middle of clearance in 0 degree plane at the rotor speed of 15,000 rpm
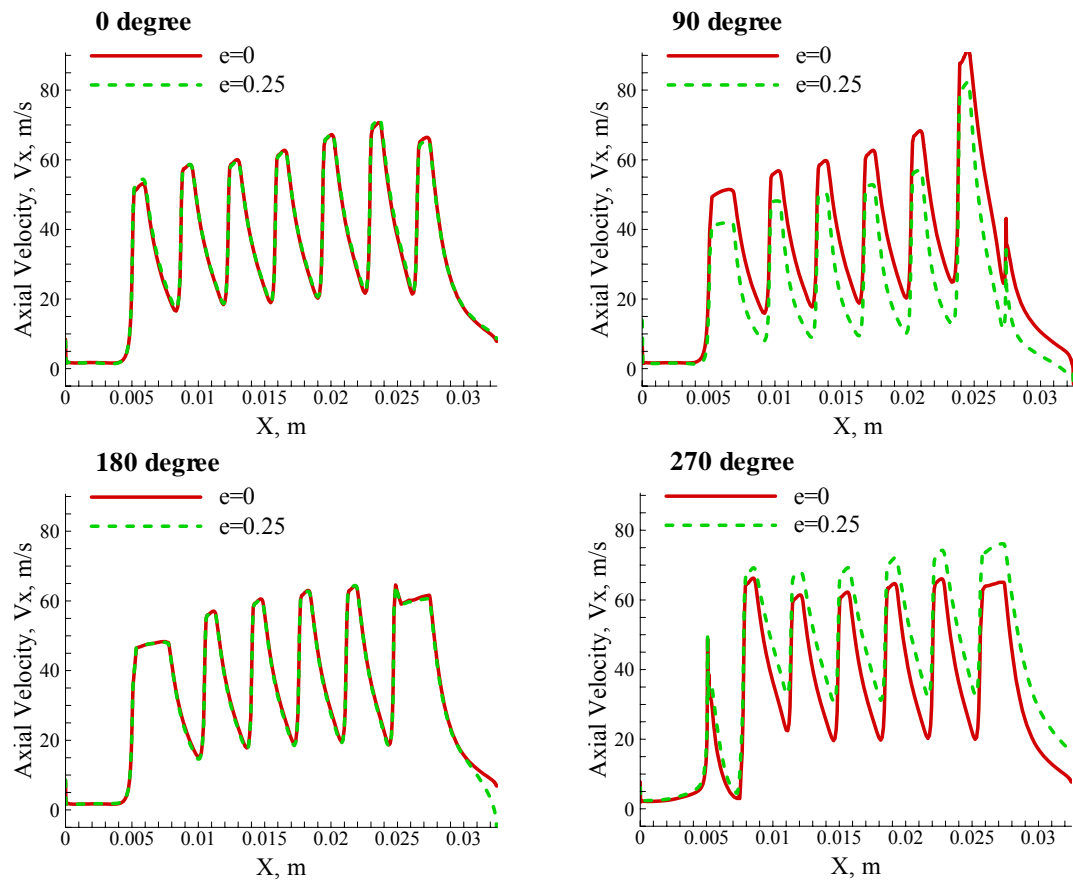
Figure C36. Axial velocity distribution for rotor eccentricity effect along the middle of clearance at four different angle planes at the rotor speed of 15,000 rpm, DP=34.47 kPa
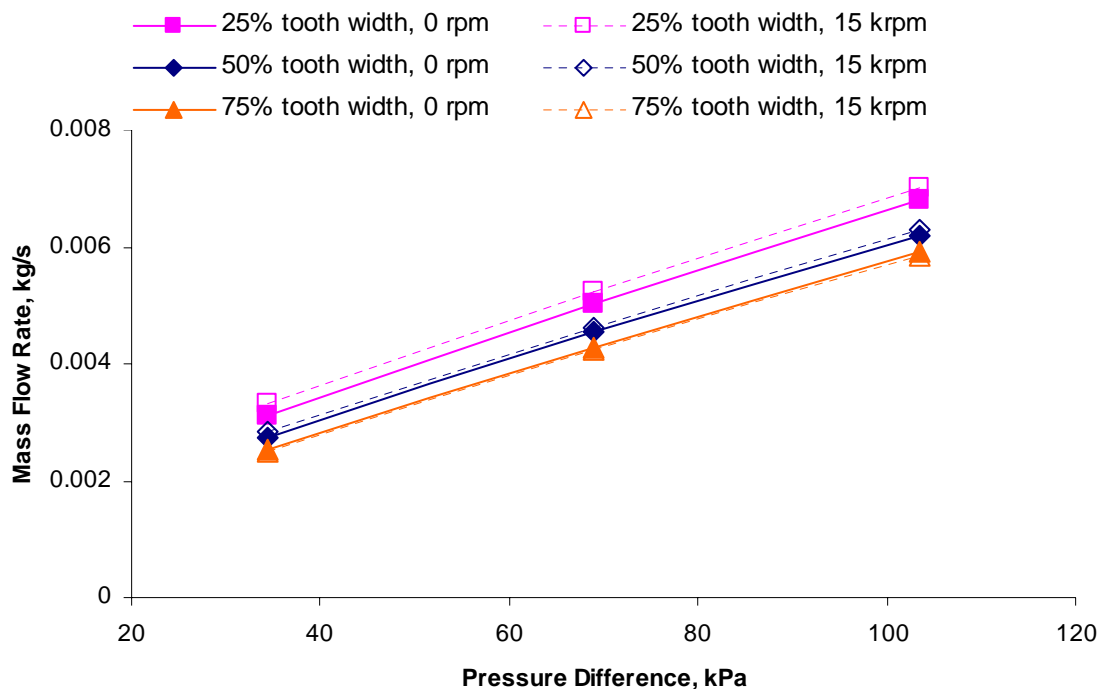
Figure C37. Leakage mass flow rate vs. pressure difference for windback seals with three different tooth widths and eccentricity of 0.25 at the rotor speeds of 0 and 15,000 rpm
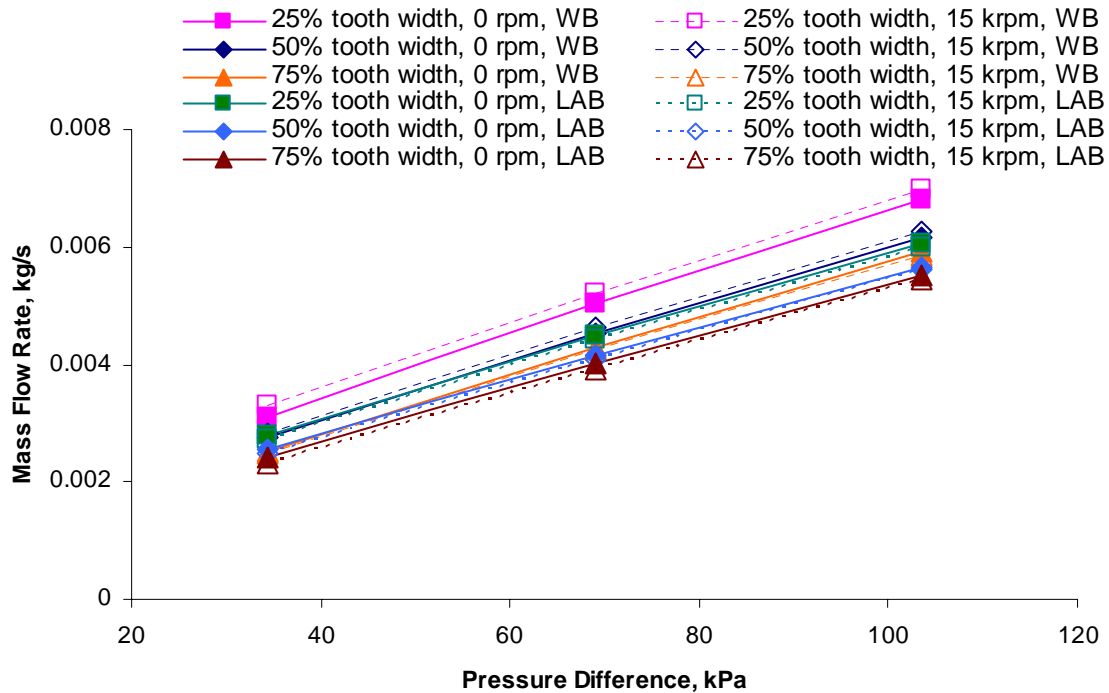
Figure C38. Leakage mass flow rate vs. pressure difference for windback and labyrinth seals with three different tooth widths at the rotor speeds of 0 and 15,000 rpm
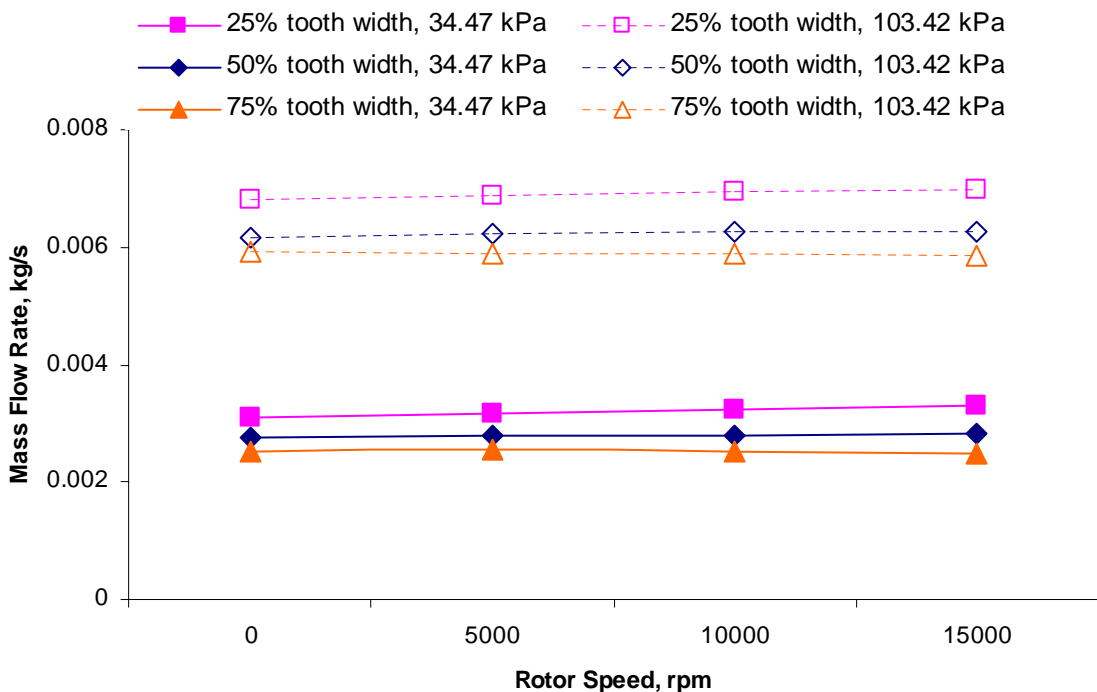
Figure C39. Leakage mass flow rate vs. rotor speed for windback seals with three different tooth widths and eccentricity of 0.25 at pressure differentials of 34.47, and 103.42 kPa
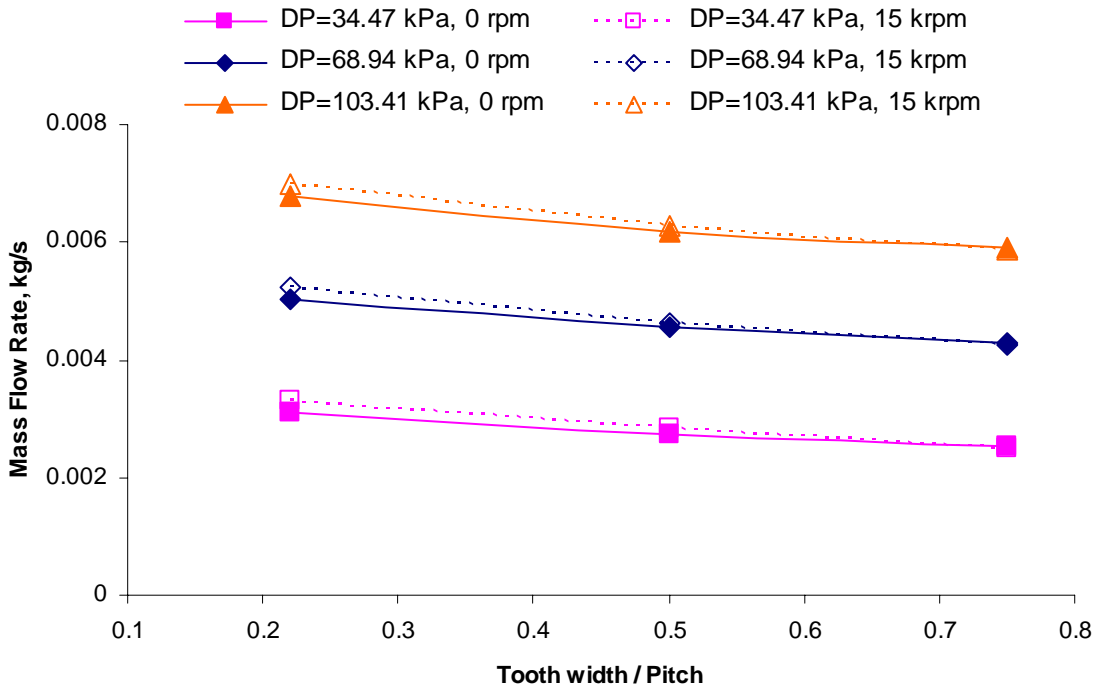
Figure C40. Effect of tooth width of pitch for windback seals with three pressure differentials at the rotor speeds of 0 rpm and 15,000 rpm
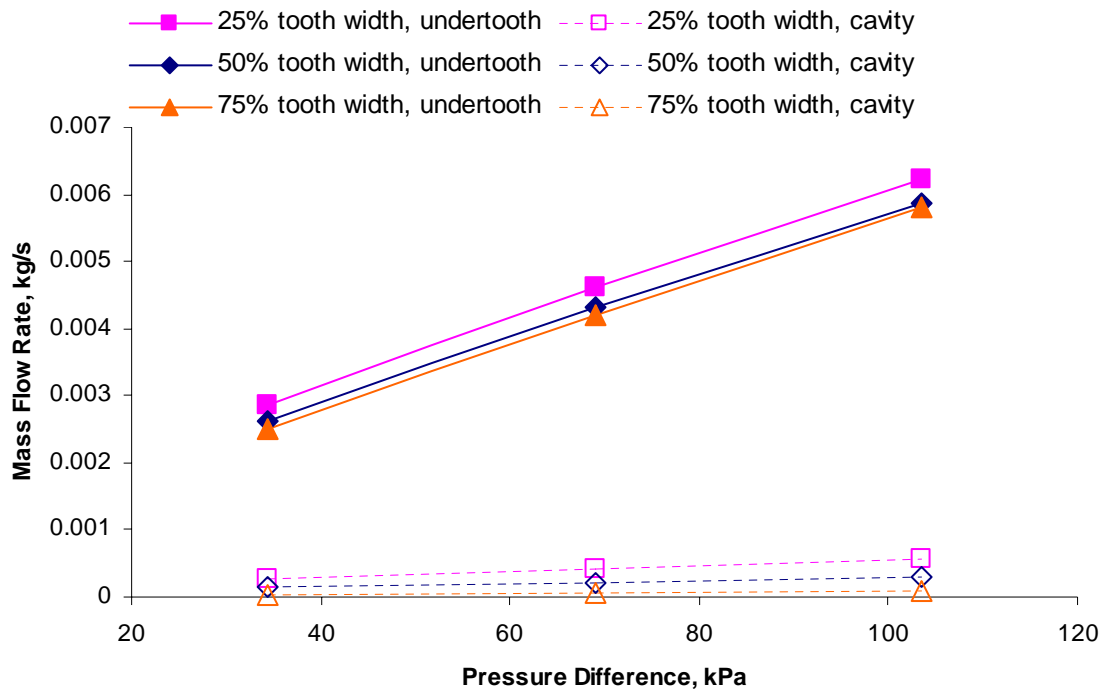
Figure C41. Leakage flow rate for two leakage paths for windback seals with three different tooth width of pitch at 0 rpm
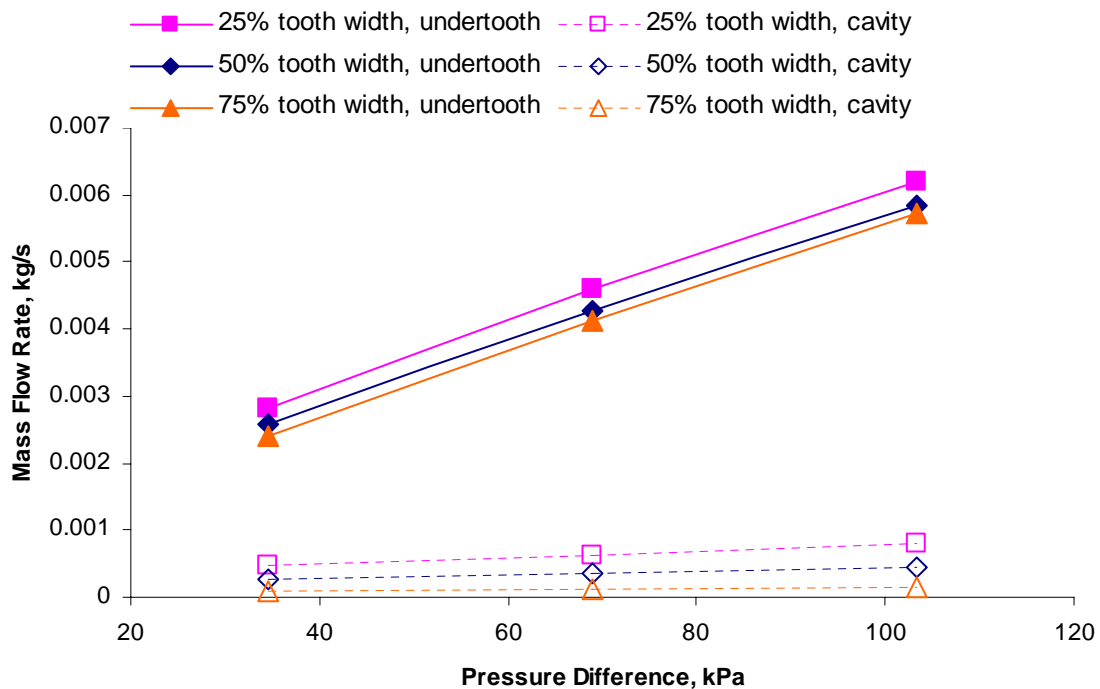
Figure C42. Leakage flow rate for two leakage paths for windback seals with three different tooth width of pitch at 15,000 rpm
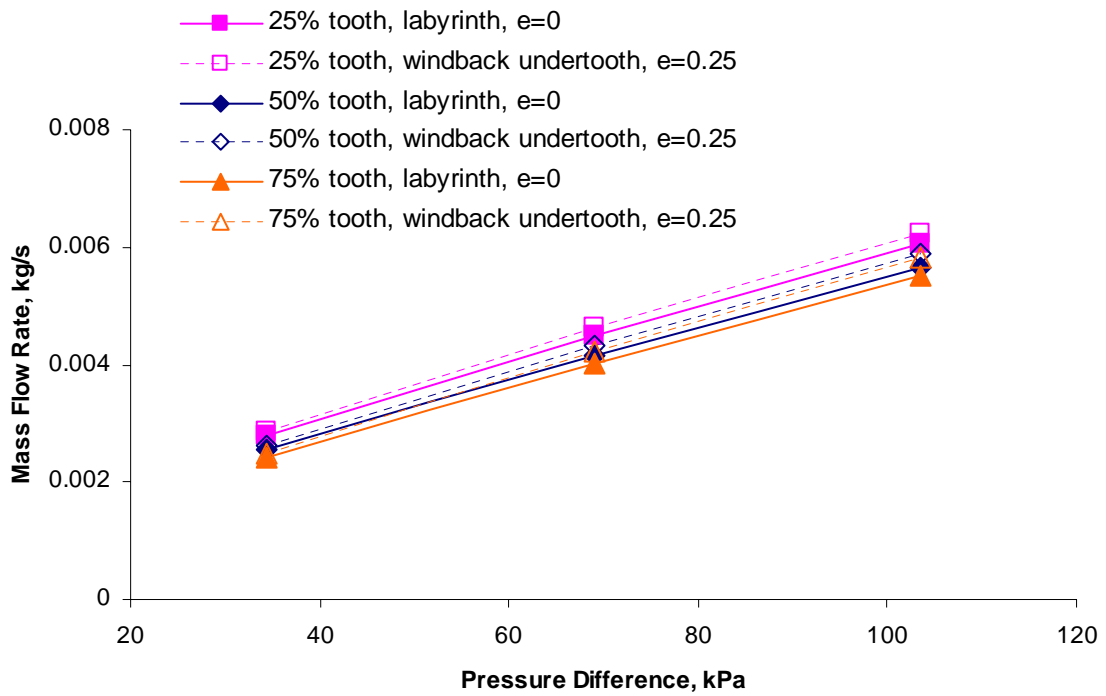
Figure C43. Leakage flow rate for the labyrinth seal and under tooth of baseline windback seal at 0 rpm
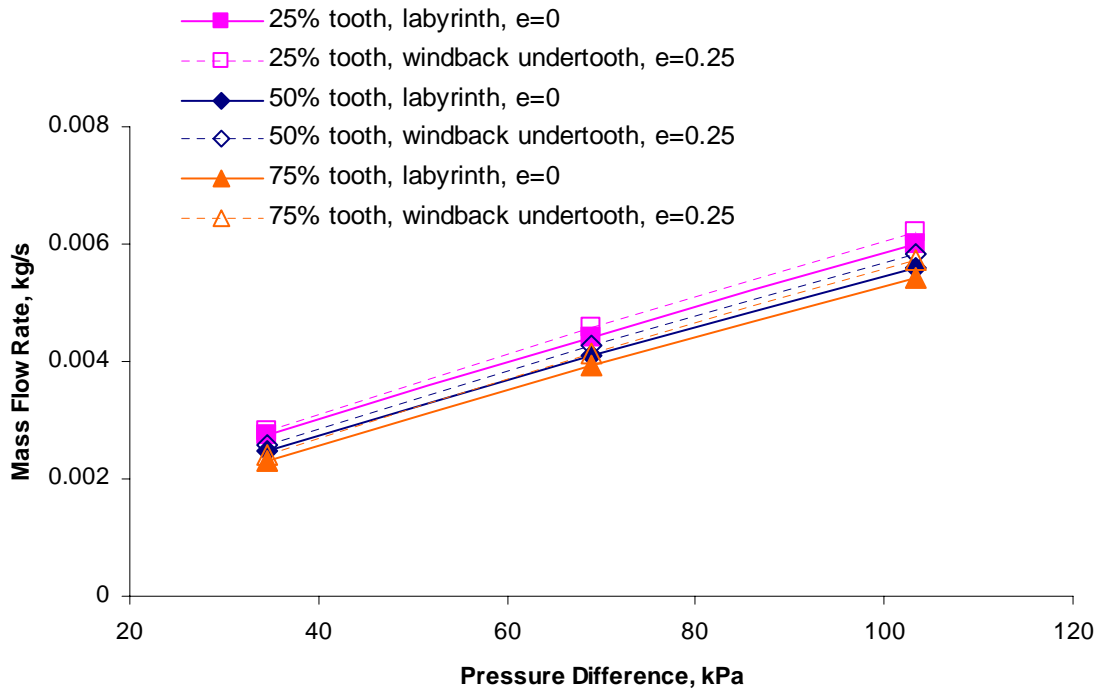
Figure C44. Leakage flow rate in the labyrinth seal and under tooth of baseline windback seal at 15,000 rpm
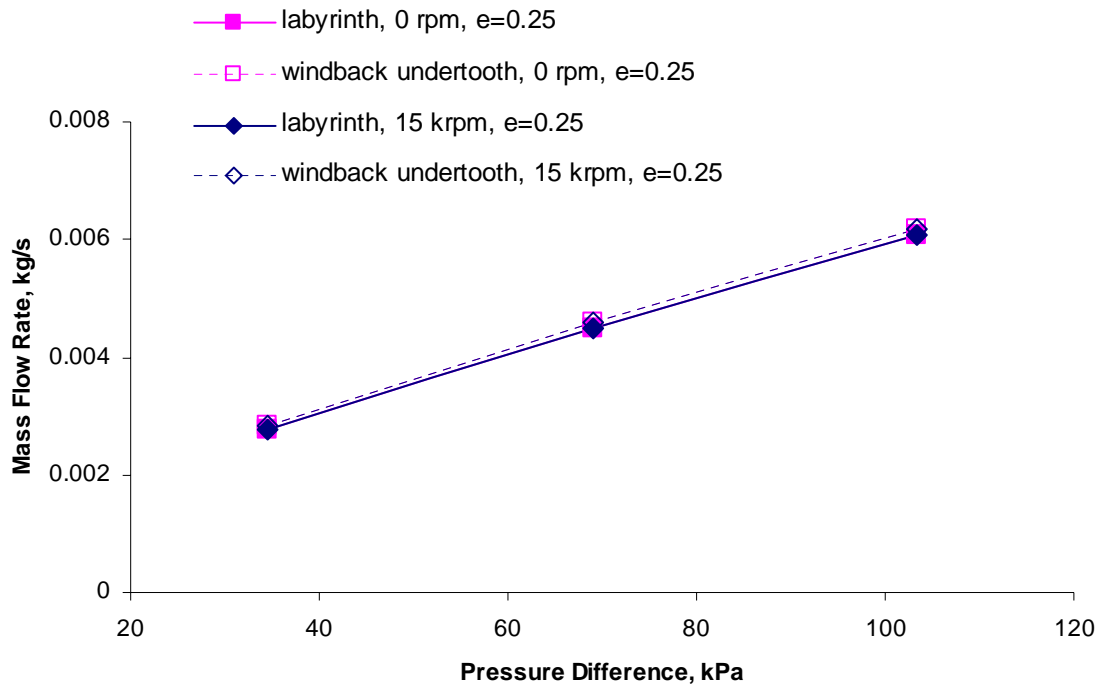
Figure C45. Leakage flow rate in the 25% rotor eccentric labyrinth seal and under the tooth of the baseline windback seal
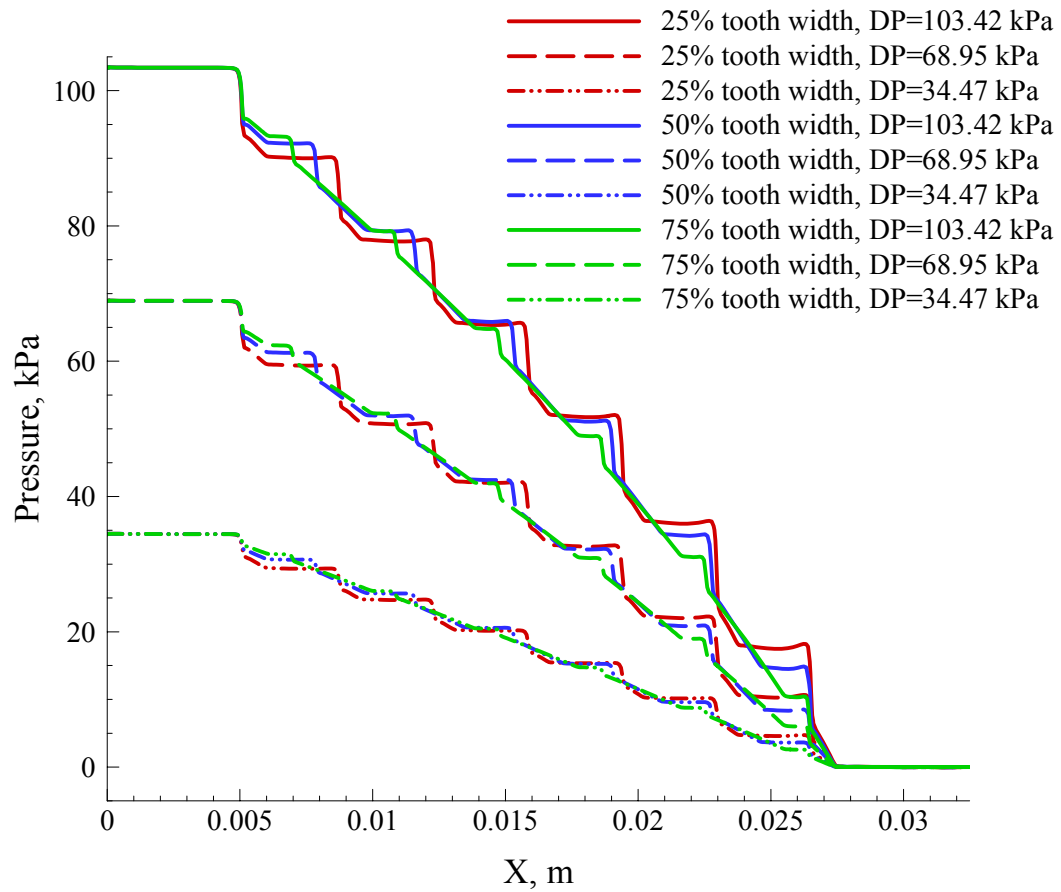
Figure C46. Pressure distribution along the middle of clearance for windback seals with three different tooth widths at 15,000 rpm
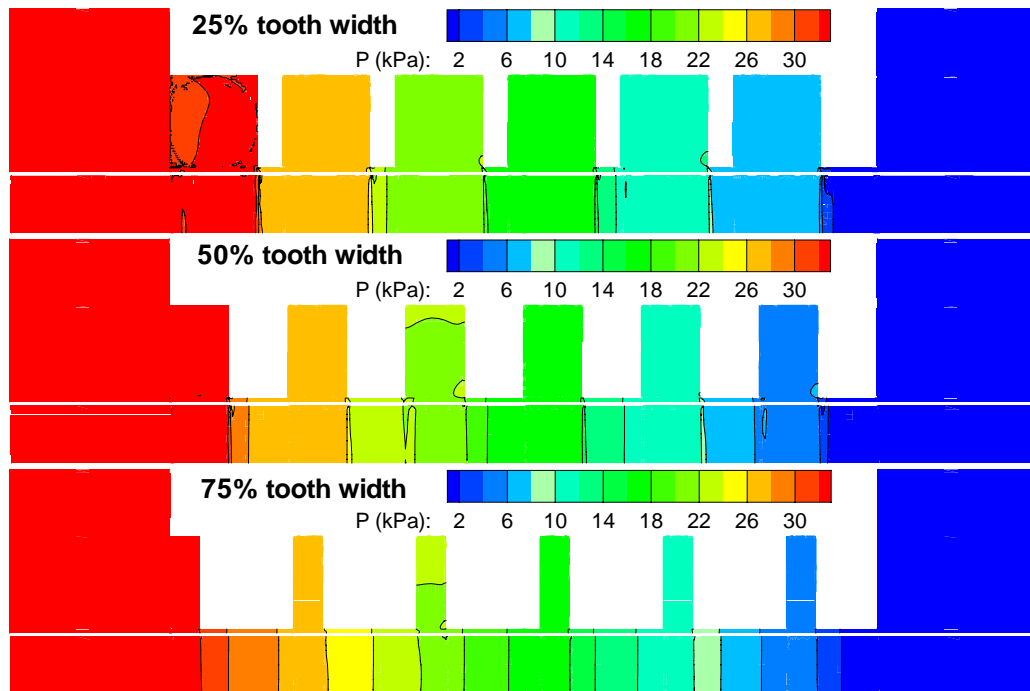
Figure C47. Pressure contours of windback seals with three different tooth widths, e=0.25, Ω=15,000 rpm, DP=34.47 kPa
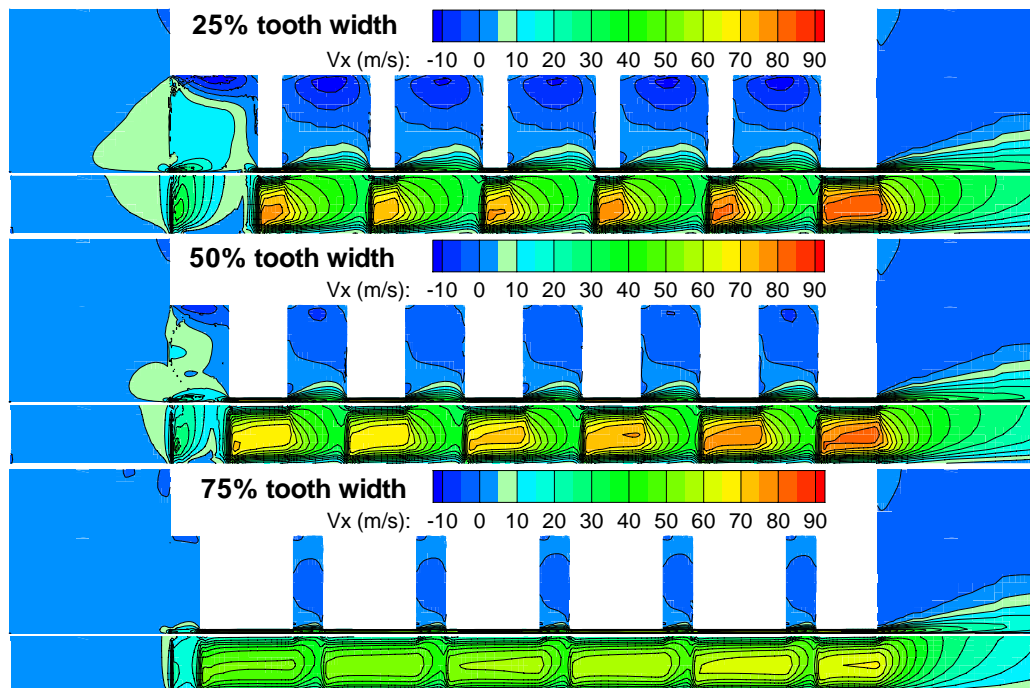
Figure C48. Axial velocity contours of windback seals with three different tooth widths, e=0.25, Ω=15,000 rpm, DP=34.47 kPa
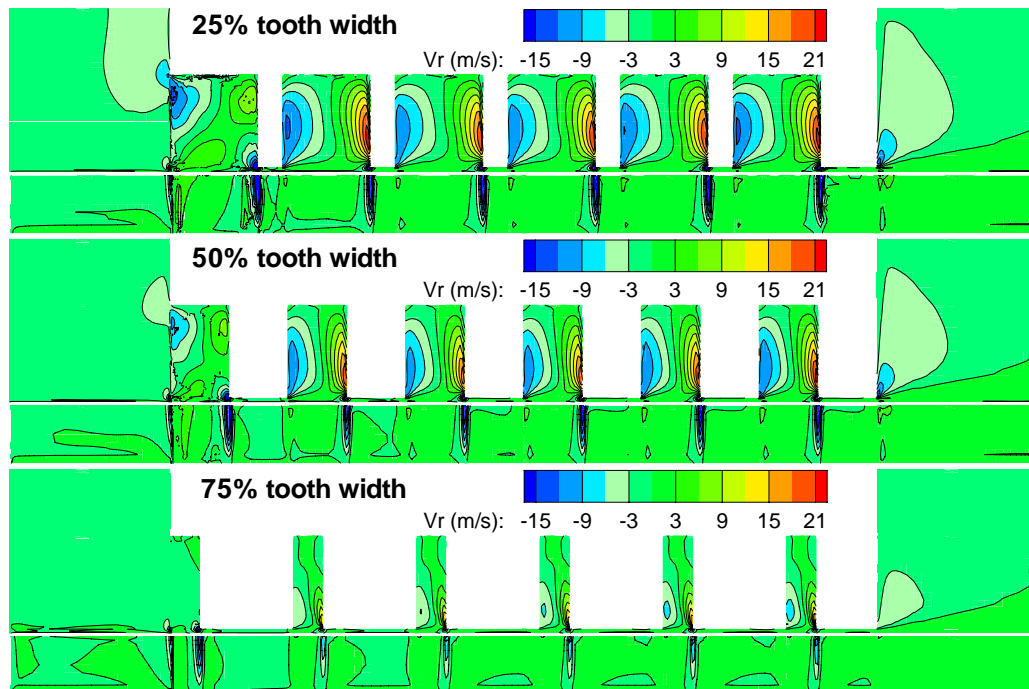
Figure C49. Radial velocity contours of windback seals with three different tooth widths, e=0.25, Ω=15,000 rpm, DP=34.47 kPa
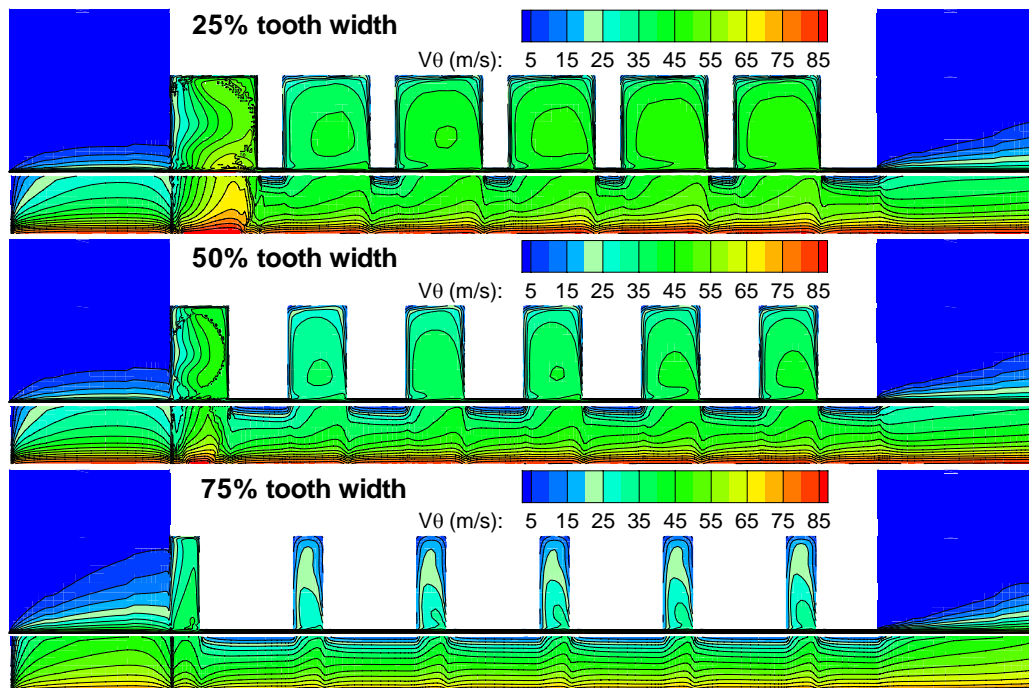
Figure C50. Circumferential velocity contours of windback seals with three different tooth widths, e=0.25, Ω=15,000 rpm, DP=34.47 kPa
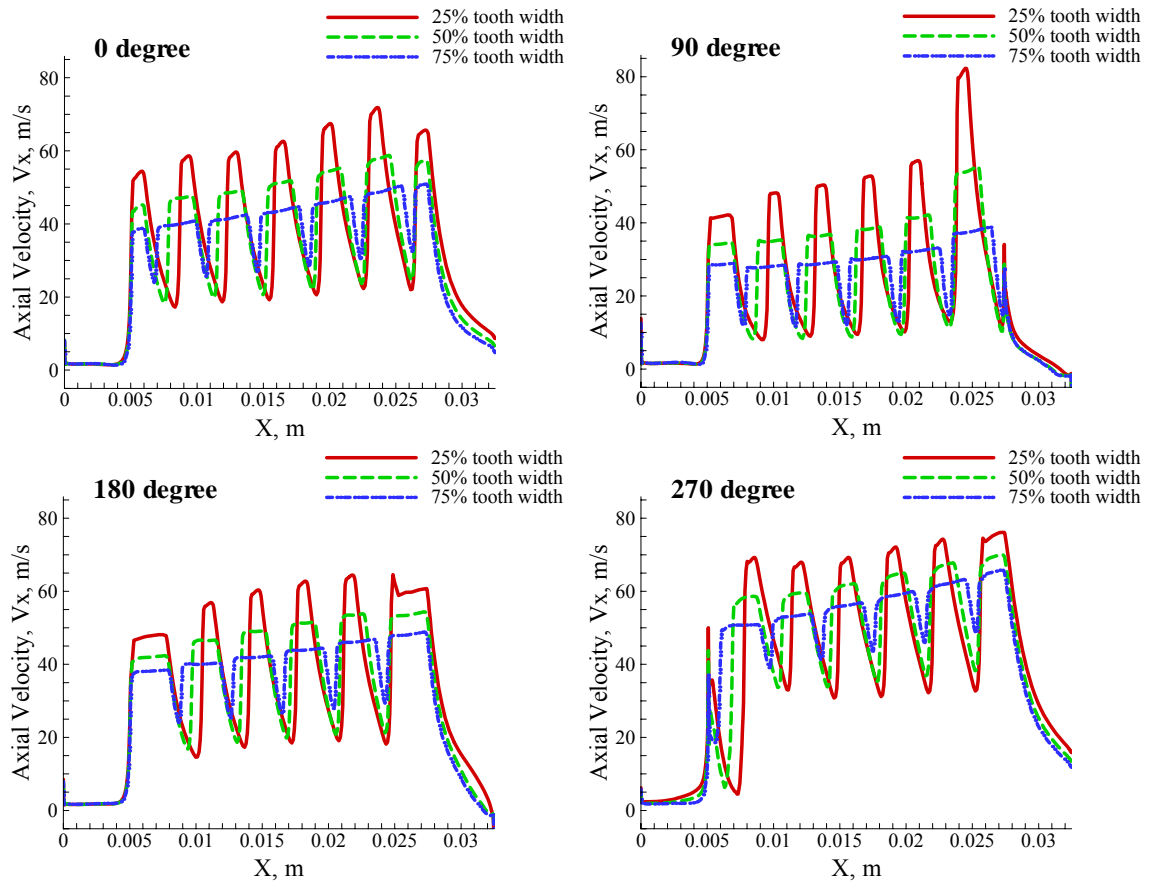
Figure C51. Axial velocity distributions along the middle of clearance for windbacks seals with three different tooth widths in four angular sliced planes at 15,000 rpm
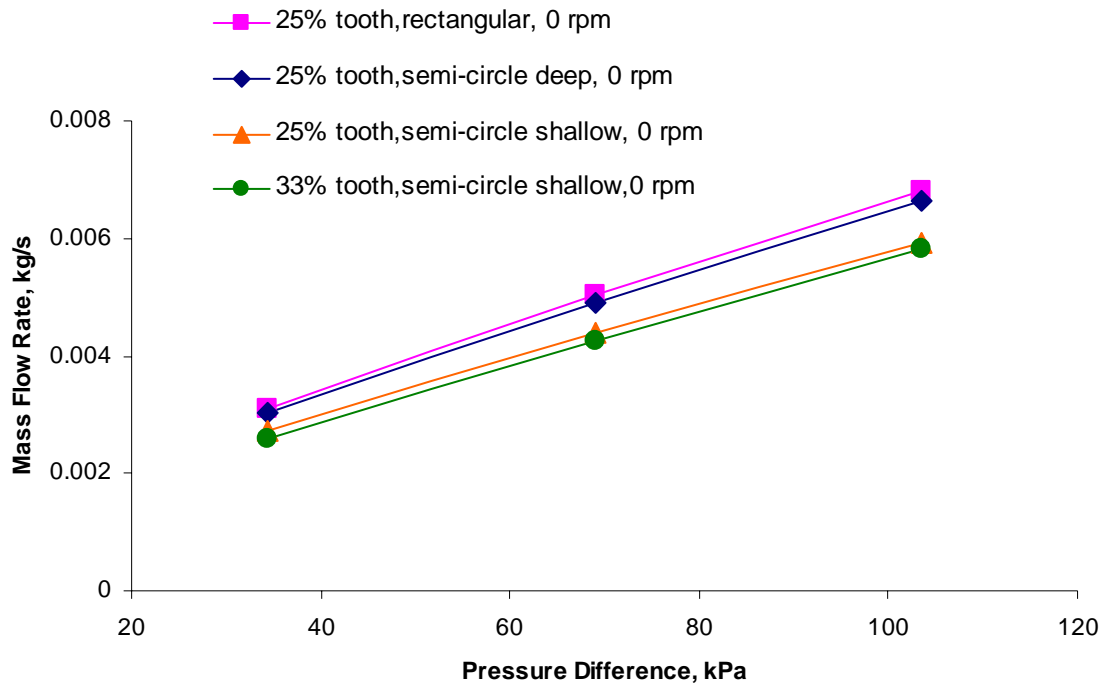
Figure C52. Leakage mass flow rate vs. pressure difference for windback seals with four different cavity shapes at the rotor speed of 0 rpm
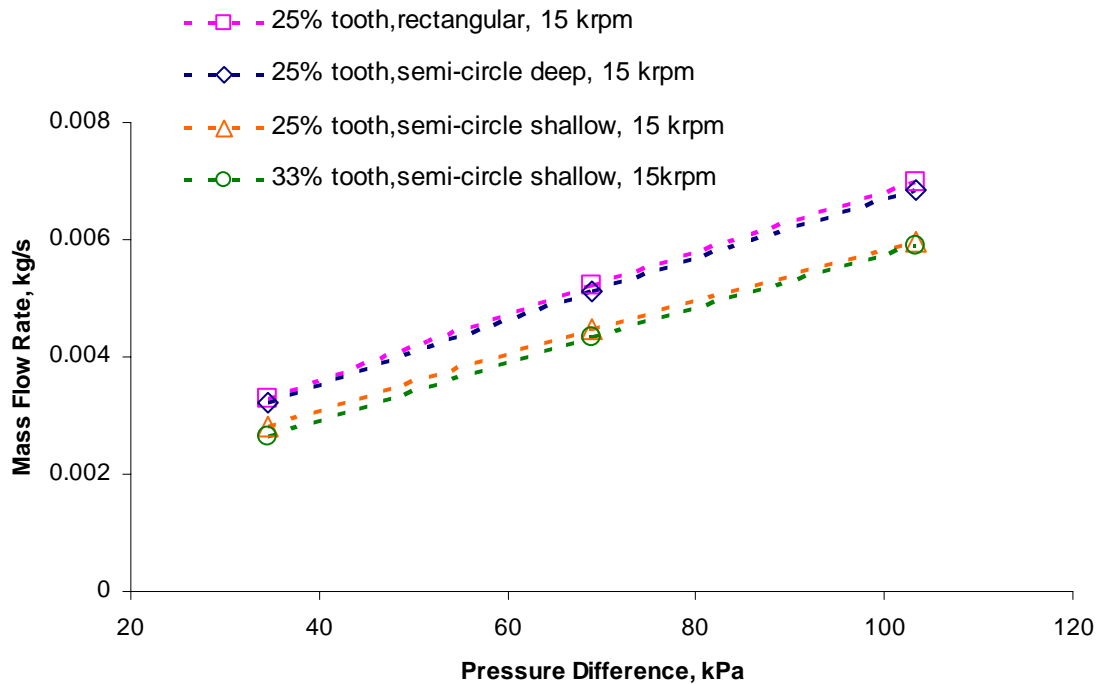
Figure C53. Leakage mass flow rate vs. pressure difference for windback seals with four different cavity shapes at the rotor speed of 15,000 rpm
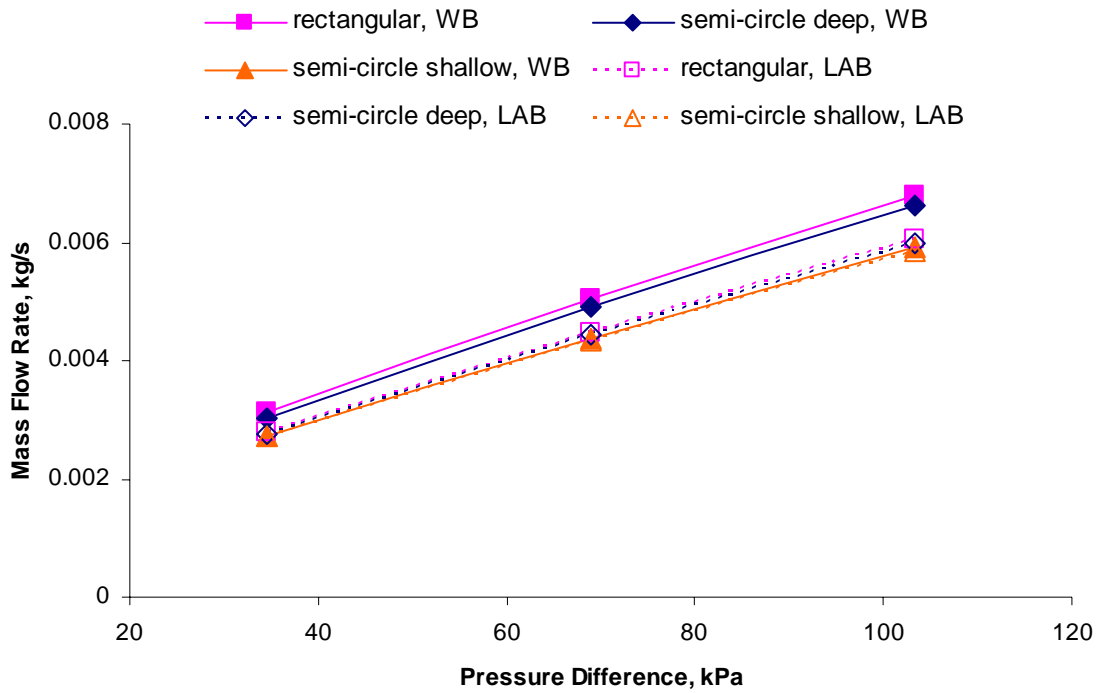
Figure C54. Leakage mass flow rate vs. pressure difference for windback and labyrinth seals with three different cavity shapes at 0 rpm
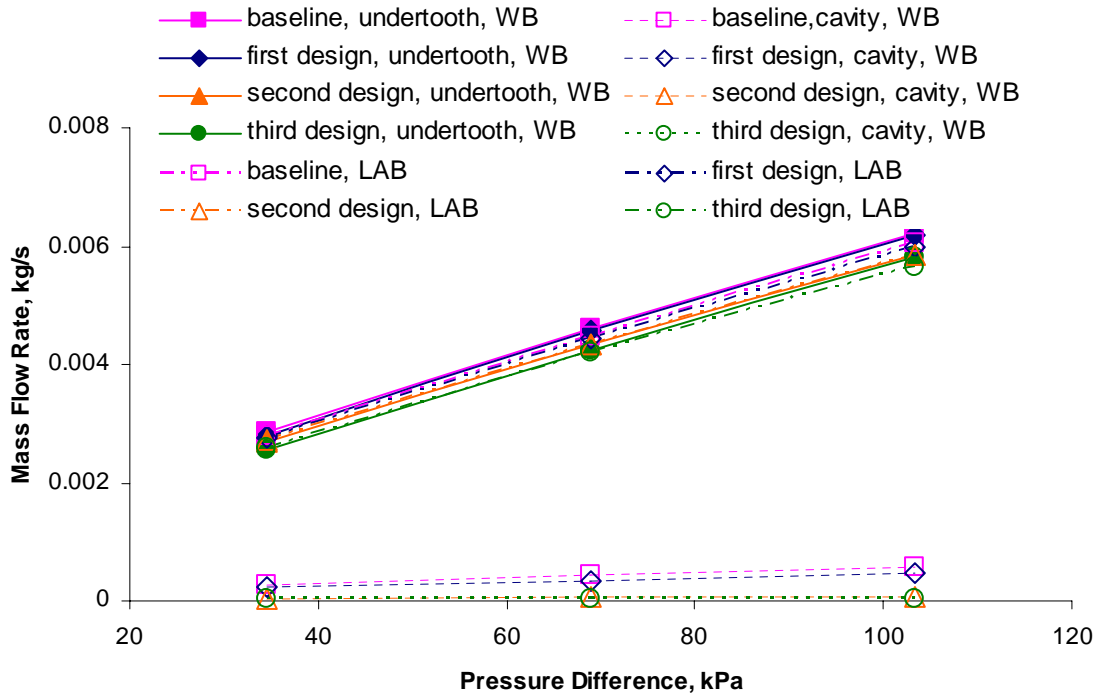
Figure C55. Leakage flow rate for two leakage paths for windback seals and for labyrinth seals with four different cavity shapes at 0 rpm
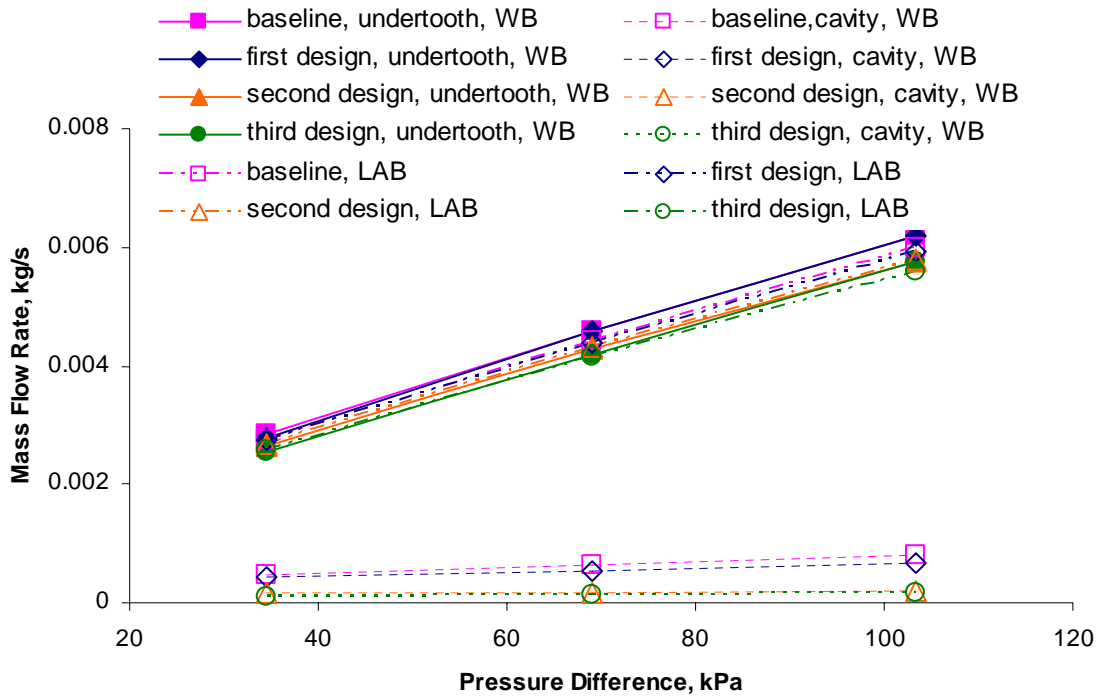
Figure C56. Leakage flow rate for two leakage paths for windback seals and for labyrinth seals with four different cavity shapes at 15,000 rpm
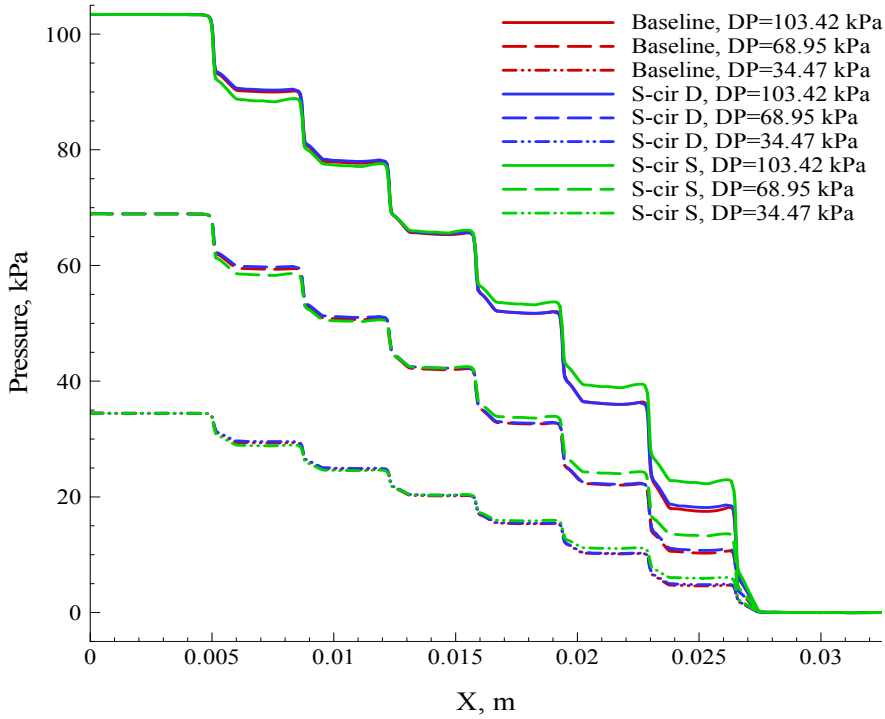
Figure C57. Pressure distribution along the middle of clearance for 25% tooth width windback seals with rectangular, semi-circular deep, and semi-circular shallow, Ω=15,000 rpm, e=0.25
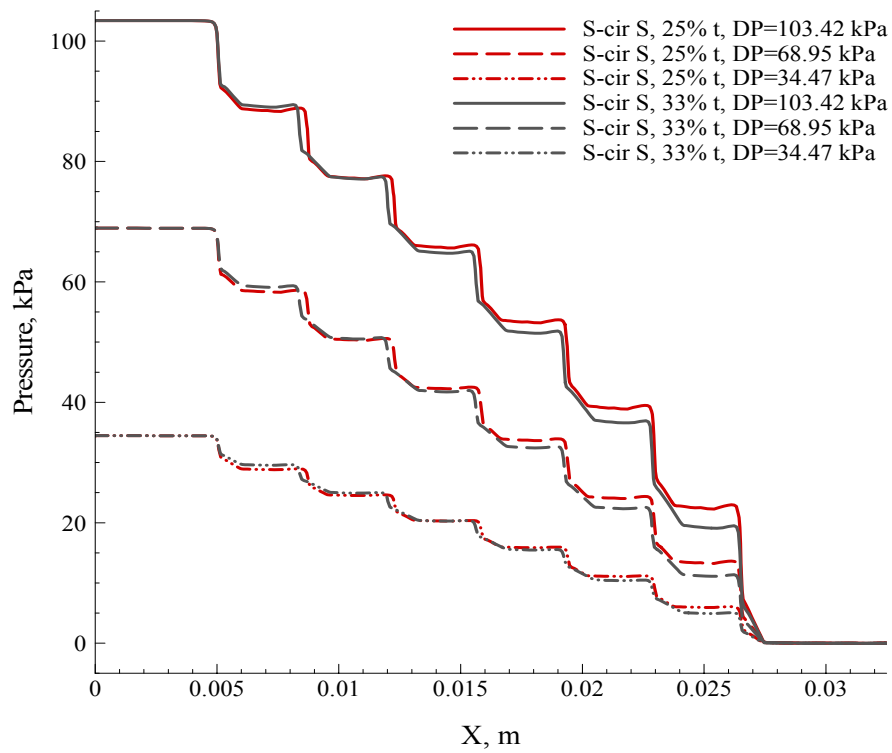
Figure C58. Pressure distribution along the middle of clearance for windback seals with 25% tooth width semi-circular and 33% tooth width semi-circular shallow, Ω=15,000 rpm, e=0.25
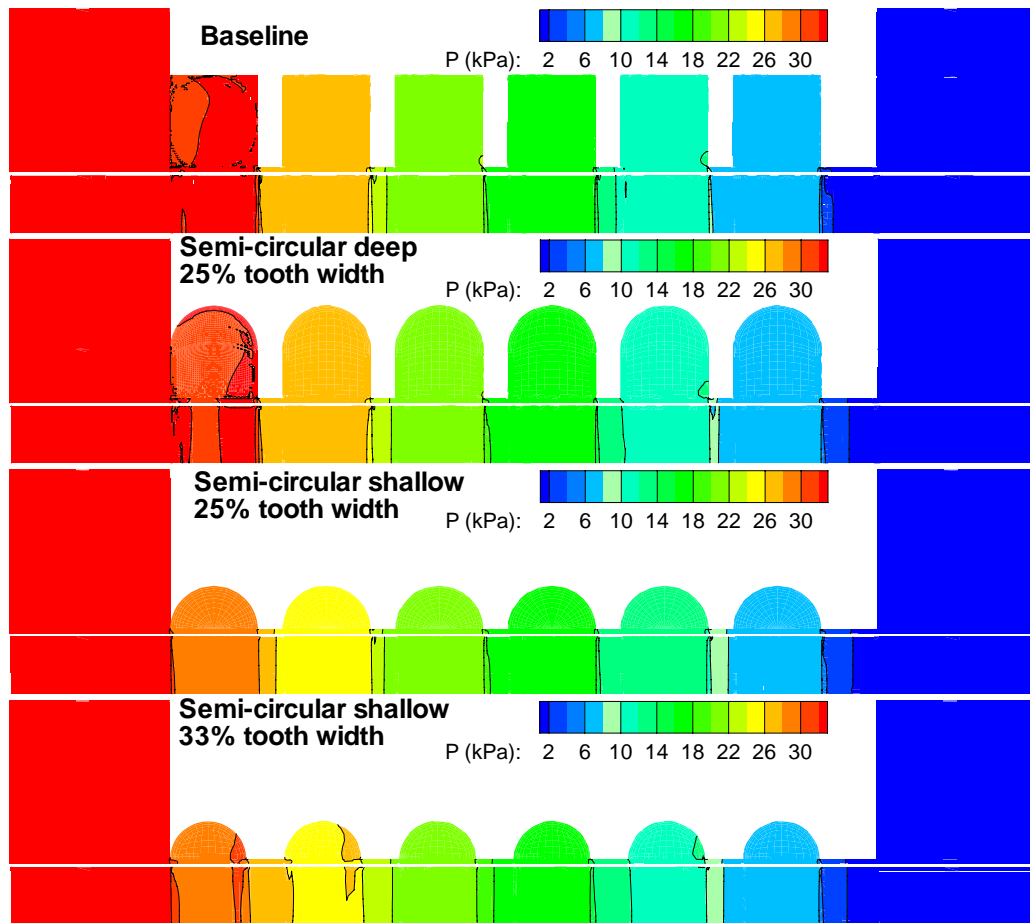
Figure C59. Pressure contours of windback seals with four different cavity shapes, e=0.25, c=0.1016 mm, Ω=15,000 rpm, DP=34.47 kPa
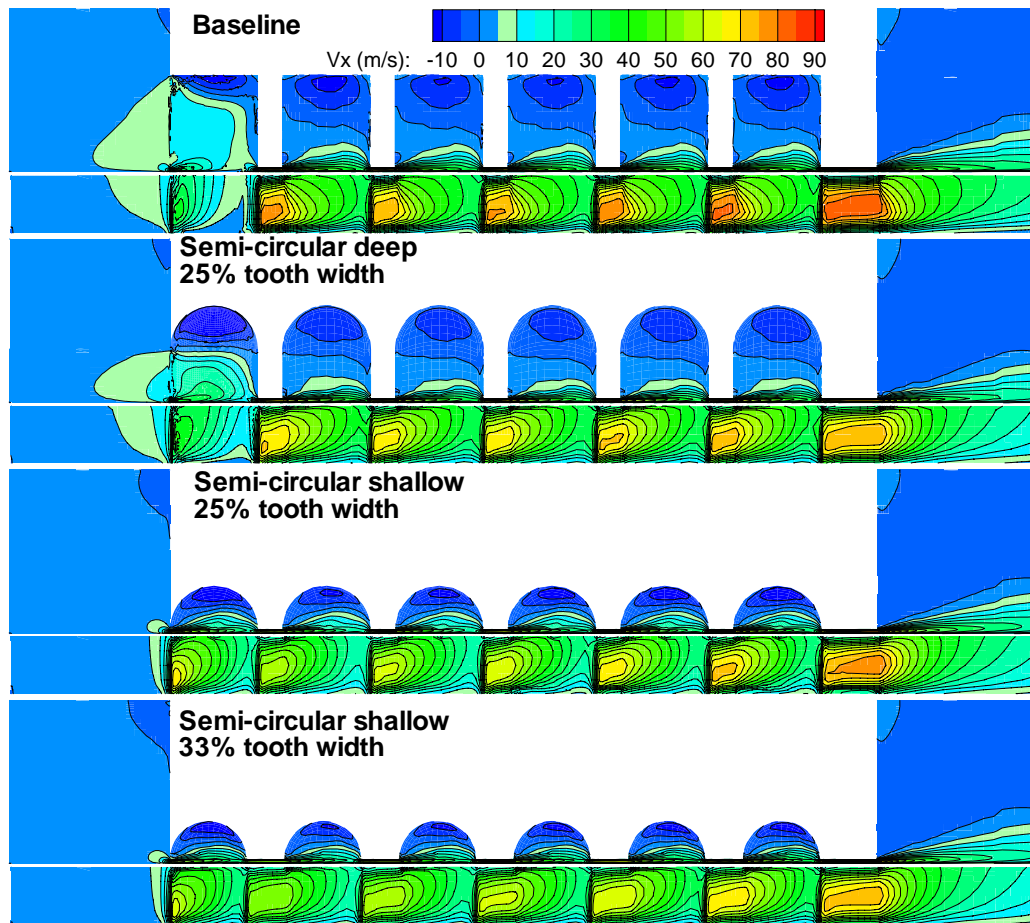
Figure C60. Axial velocity contours of windback seals with four different cavity shapes, e=0.25, c=0.1016 mm, Ω=15,000 rpm, DP=34.47 kPa
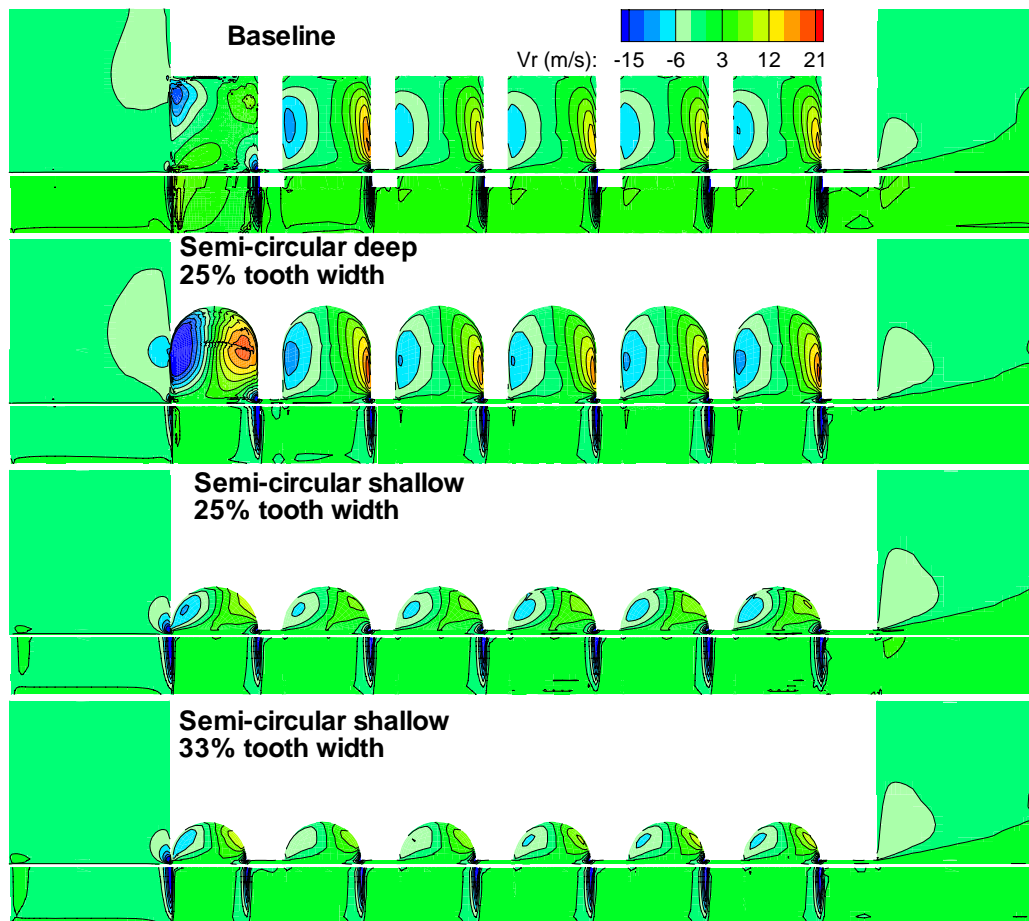
Figure C61. Radial velocity contours of windback seals with four different cavity shapes, e=0.25, c=0.1016 mm, Ω=15,000 rpm, DP=34.47 kPa
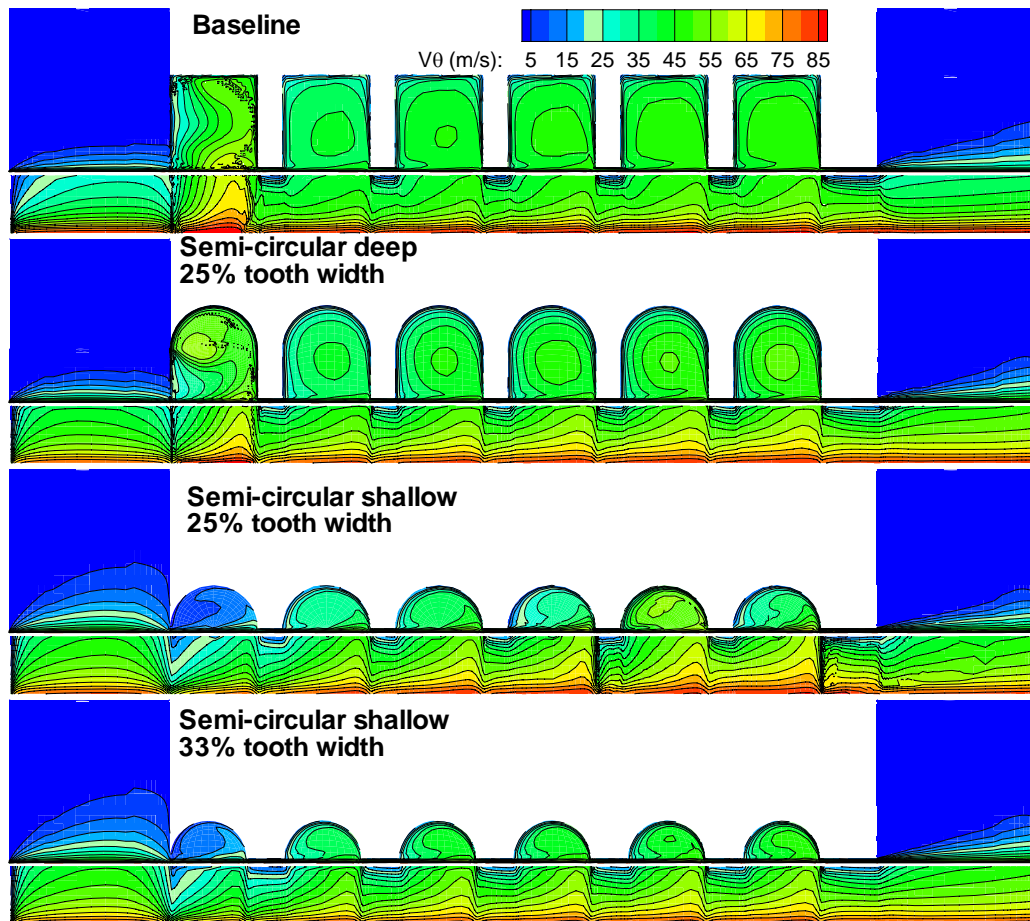
Figure C62. Circumferential velocity contours of windback seals with four different cavity shapes, e=0.25, c=0.1016 mm, Ω=15,000 rpm, DP=34.47 kPa
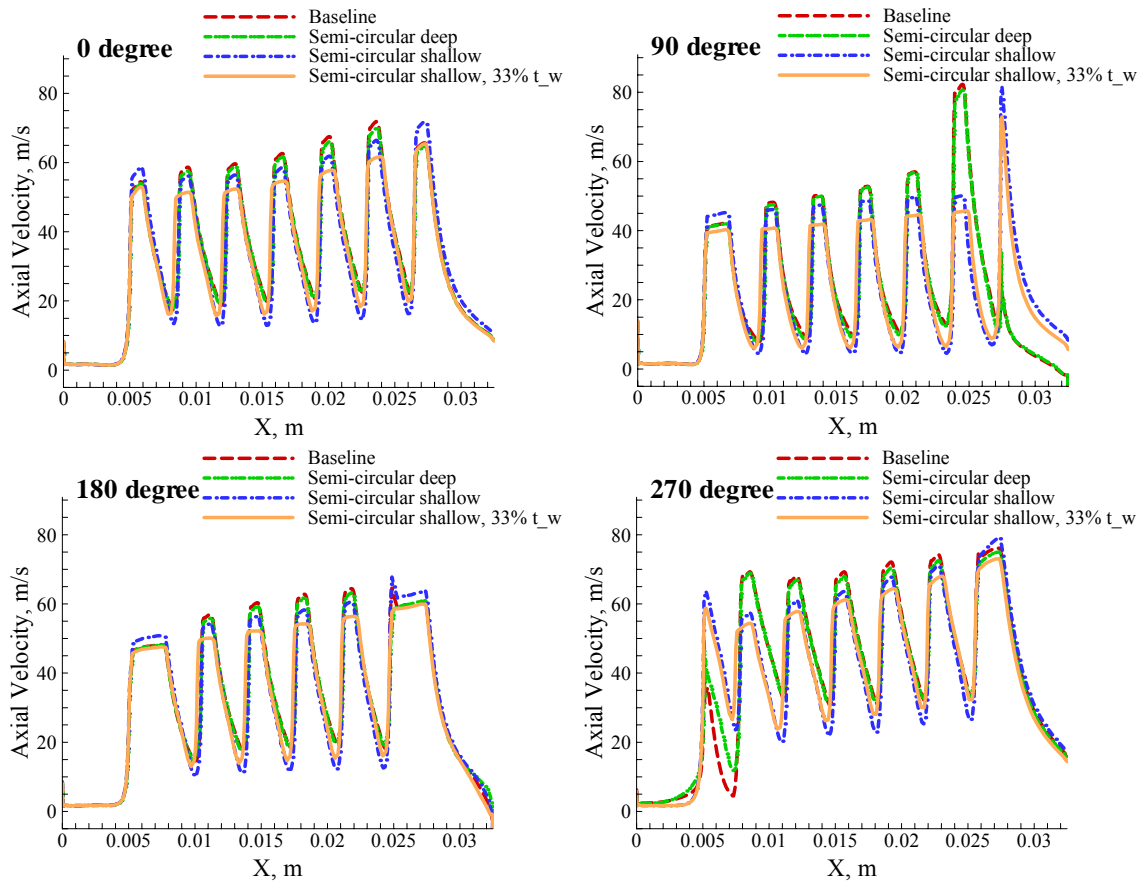
Figure C63. Axial velocity distributions along the middle of clearance for four different cavity shapes of the windback seal in four angular sliced planes, e=0, Ω=15,000 rpm, c=0.106 mm, DP=34.47 kPa
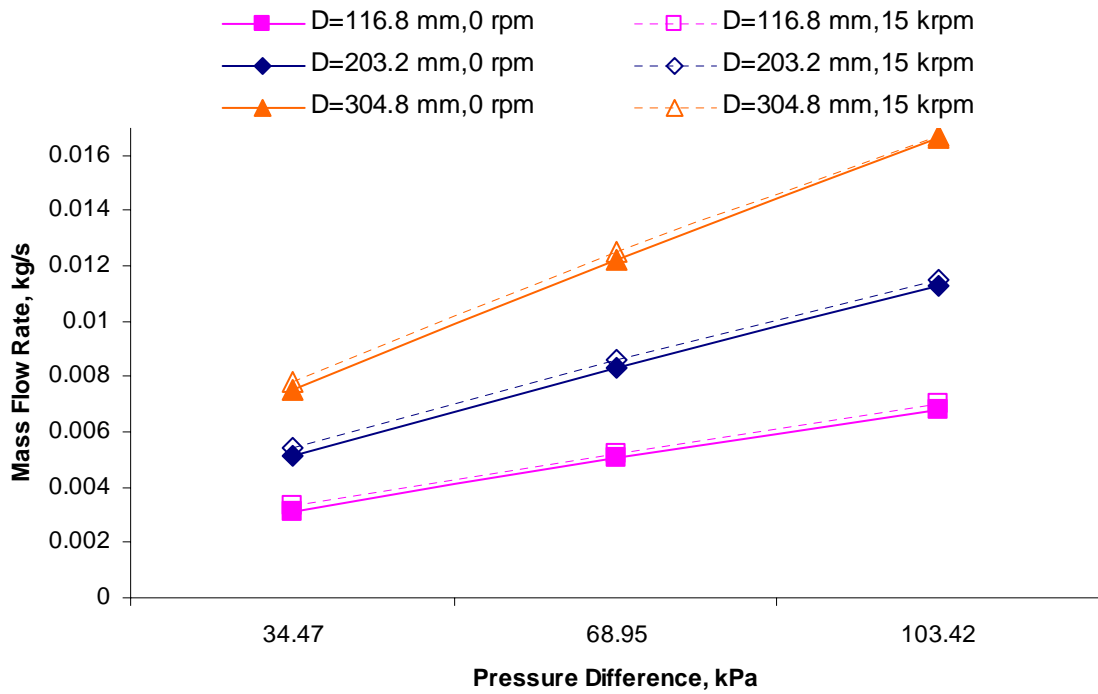
Figure C64. Leakage mass flow rate vs. differential pressure for windback seals with three shaft diameters at the rotor speed of 0 and 15,000 rpm
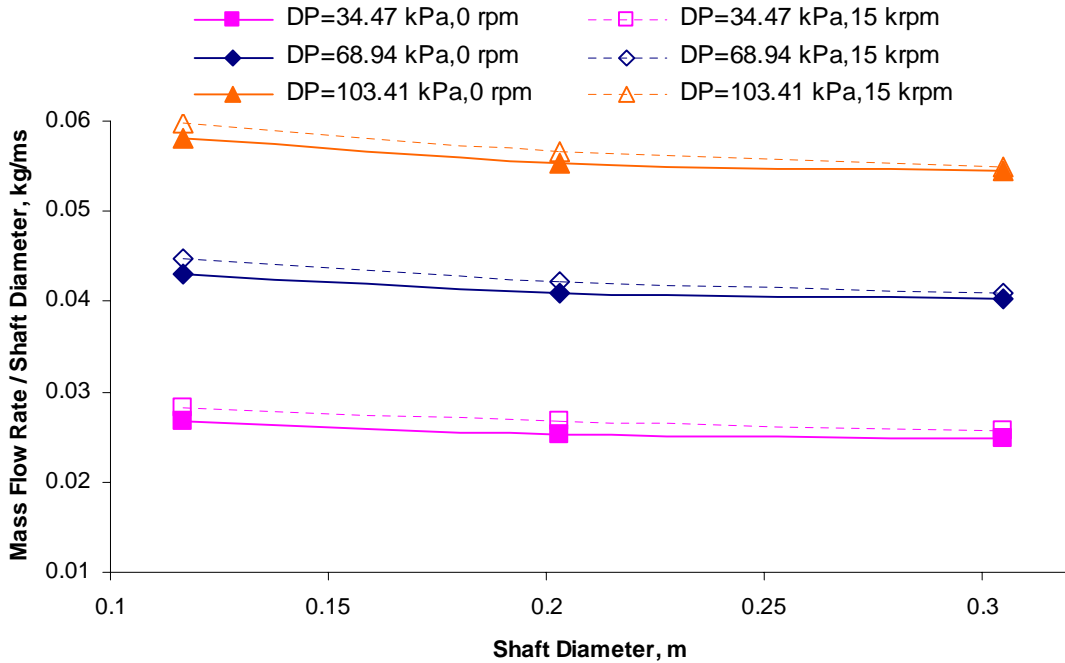
Figure C65. Leakage mass flow rate/shaft diameter vs. shaft diameter for windback seals with three shaft diameters at the rotor speed of 0 and 15,000 rpm
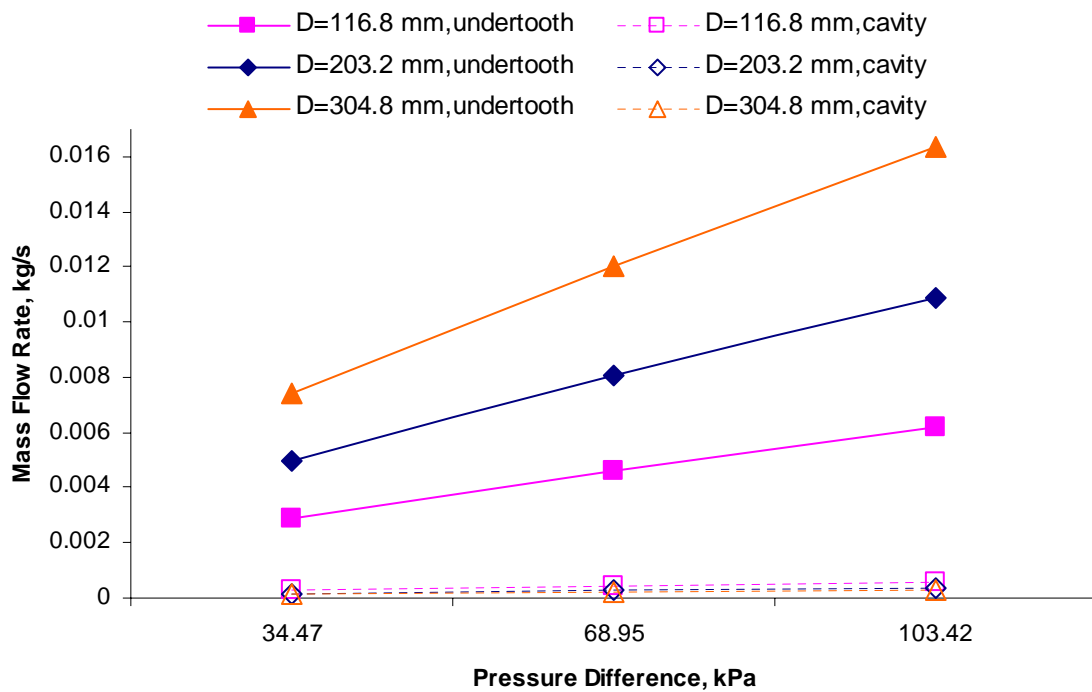
Figure C66. Leakage flow rate for two leakage paths for windback seals with three different shaft diameters at 0 rpm
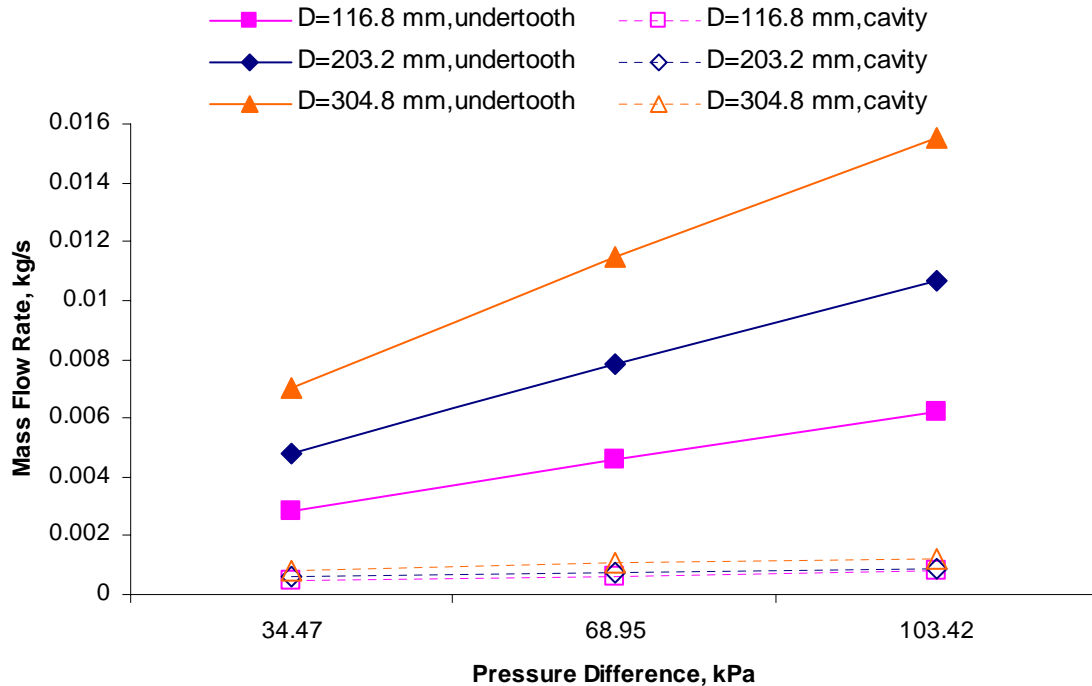
Figure C67. Leakage flow rate for two leakage paths for windback seals with three different shaft diameters at 15,000 rpm
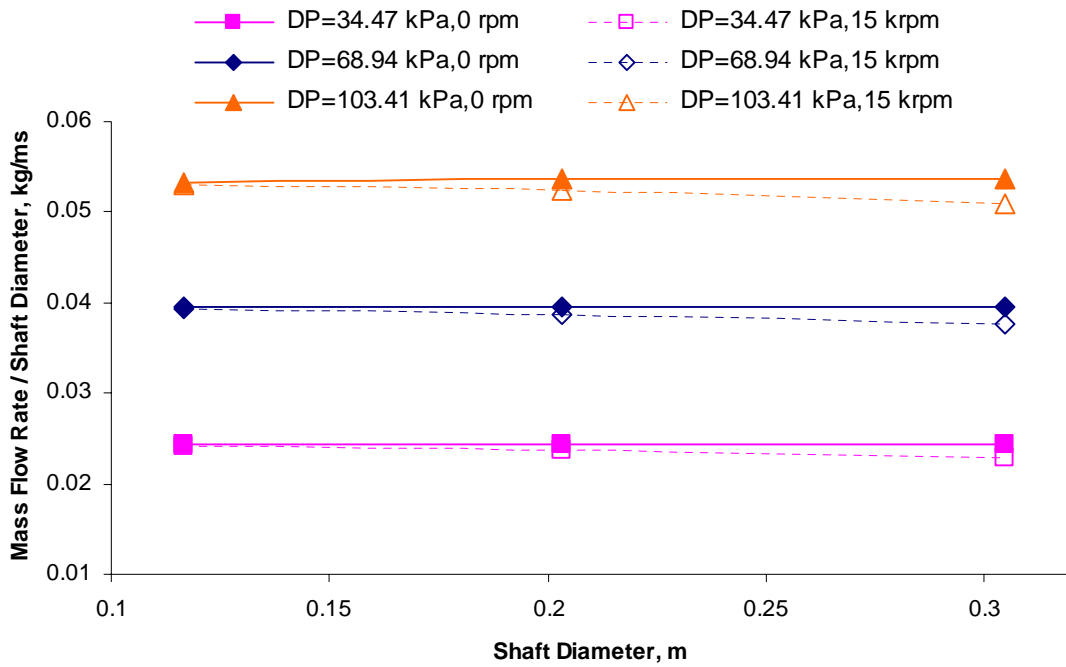
Figure C68. Leakage mass flow rate under the tooth /shaft diameter vs. shaft diameter for windback seals with three shaft diameters at the rotor speed of 0 and 15,000 rpm
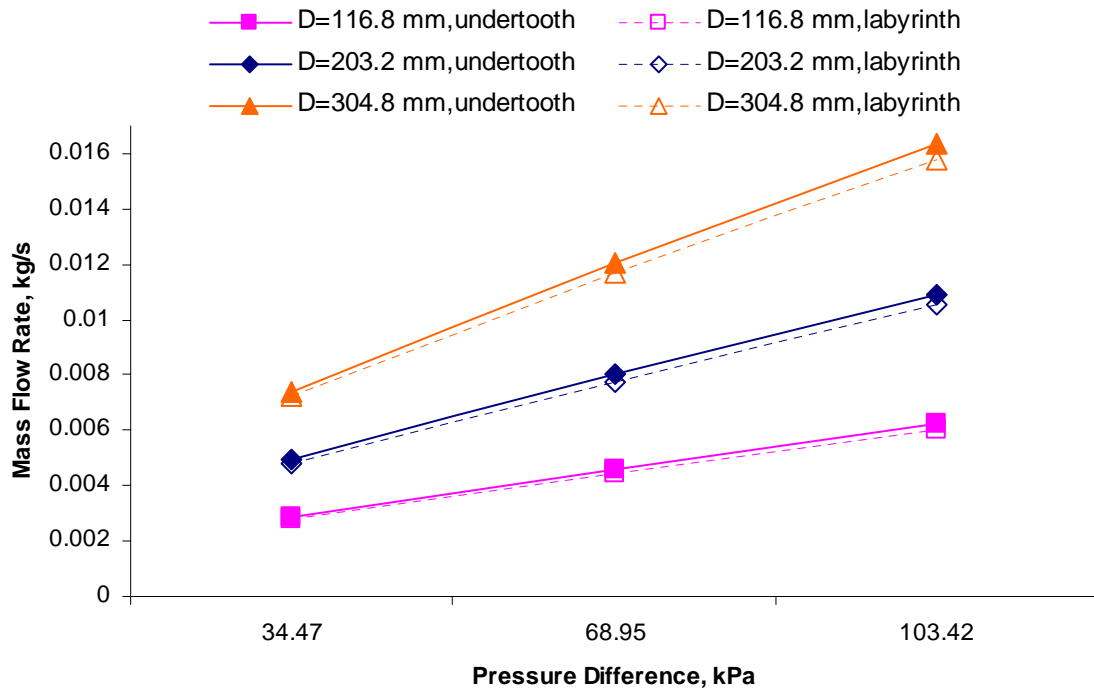
Figure C69. Leakage flow rate for the labyrinth seal and under tooth of baseline windback seal at 0 rpm
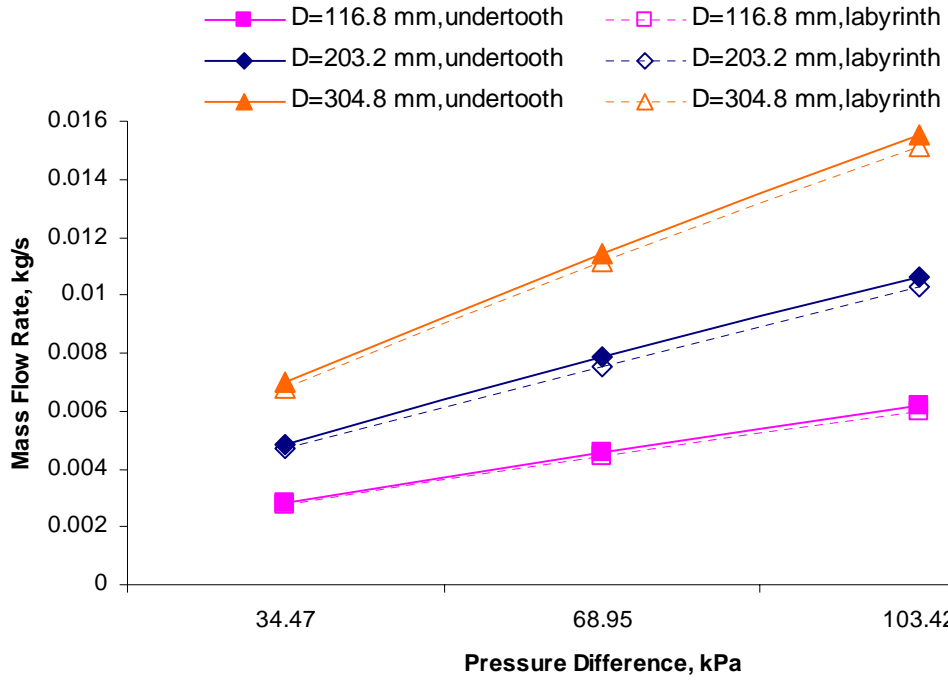
Figure C70. Leakage flow rate for the labyrinth seal and under tooth of baseline windback seal at 15,000 rpm
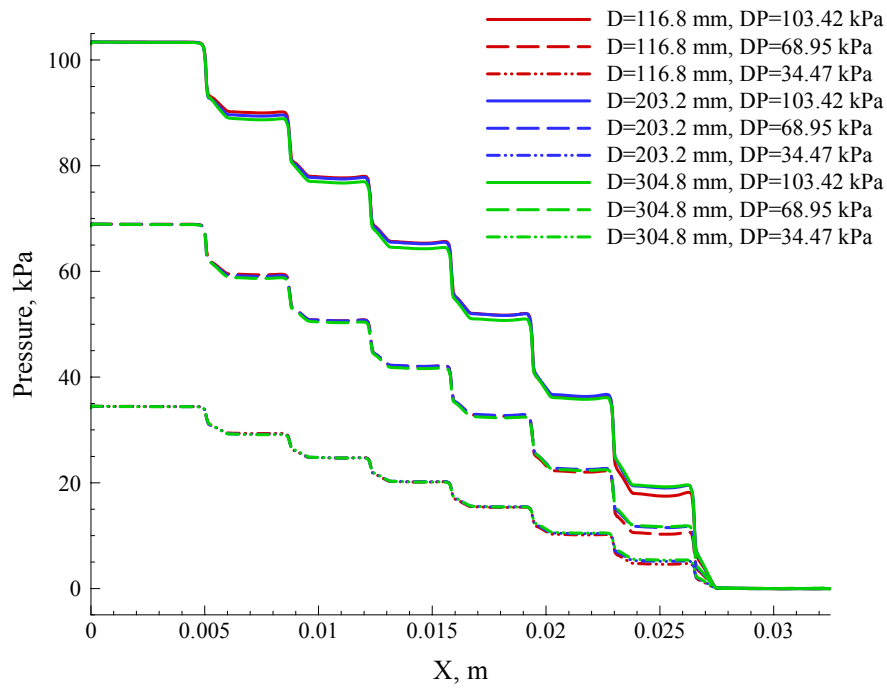
Figure C71. Pressure distribution along the middle of clearance for windback seals with three different shaft diameters, Ω=15,000 rpm, e=0.25
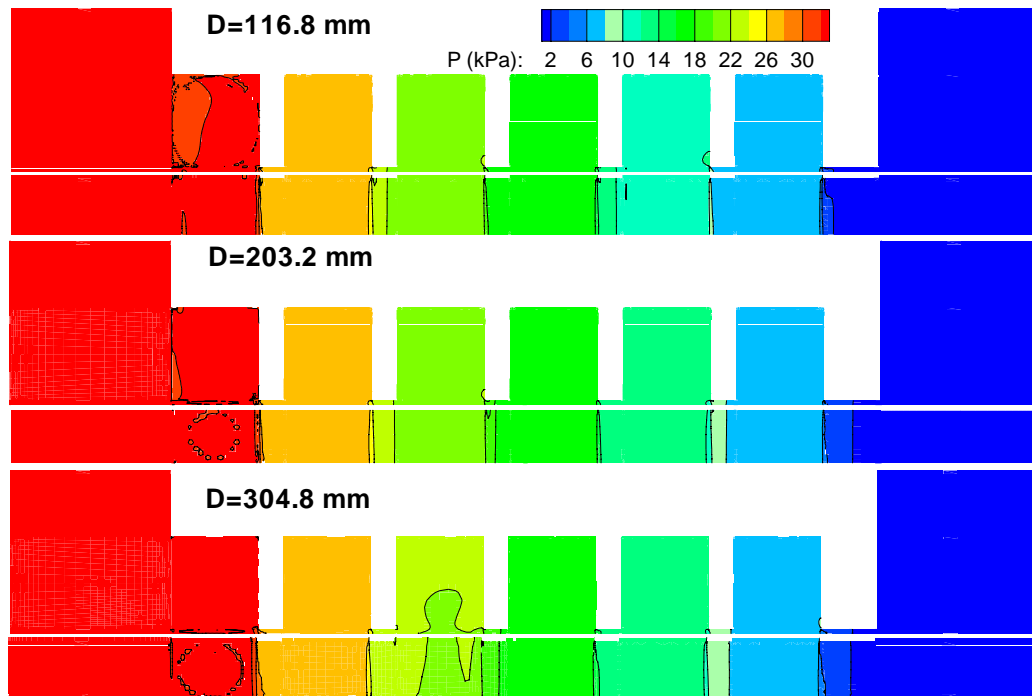
Figure C72. Pressure contours of windback seals with three different shaft diameters, e=0.25, c=0.1016 mm, Ω=15,000 rpm, DP=34.47 kPa
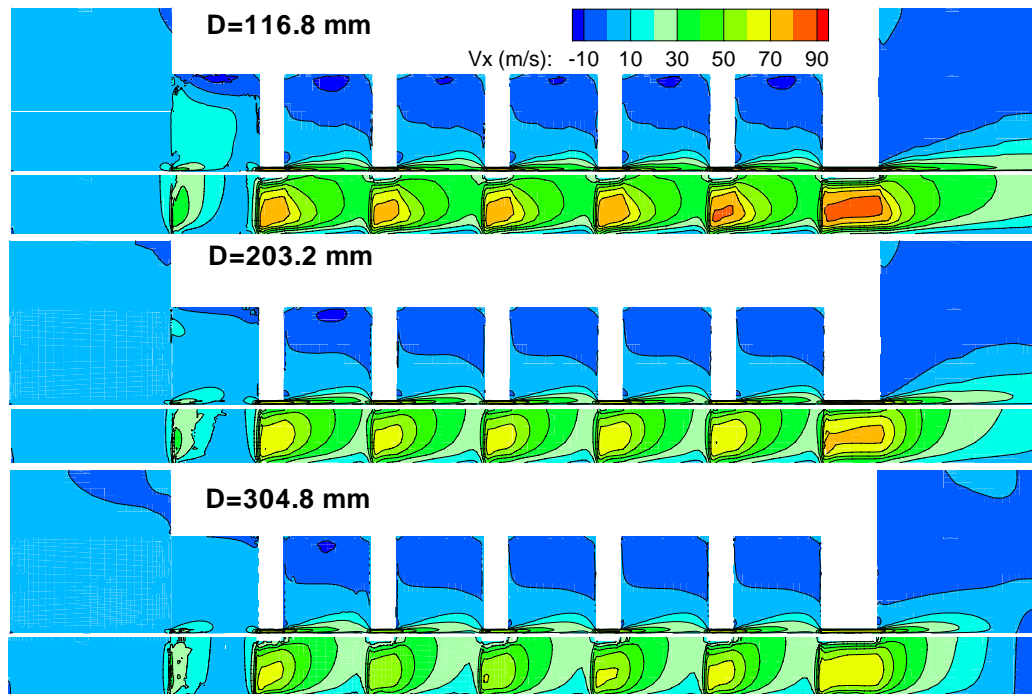
Figure C73. Axial velocity contours of windback seals with three different shaft diameters, e=0.25, c=0.1016 mm, Ω=15,000 rpm, DP=34.47 kPa
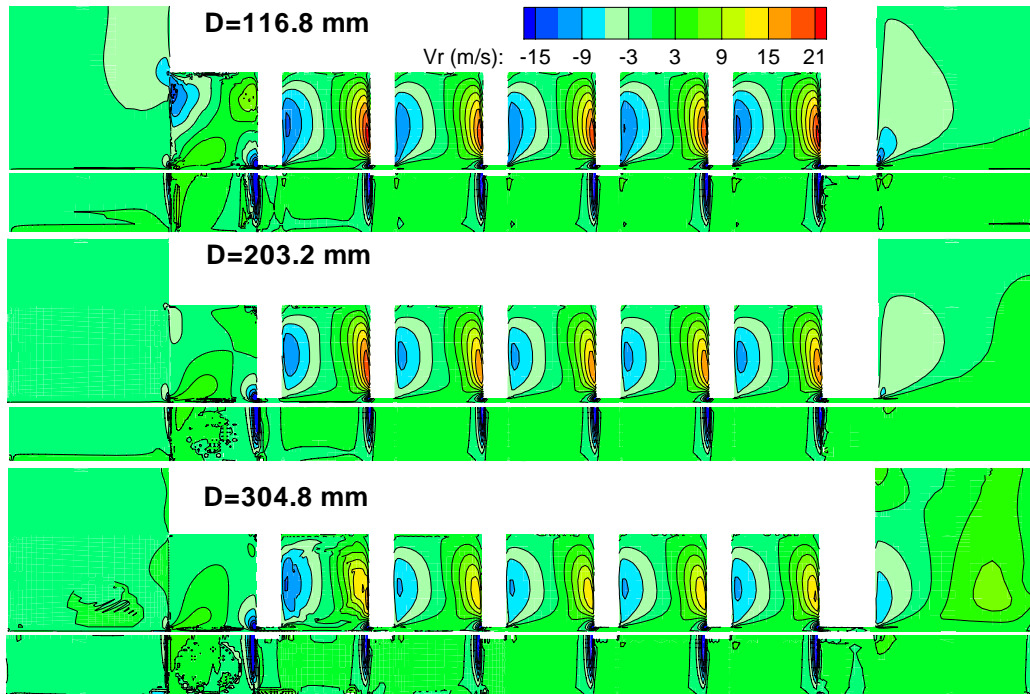
Figure C74. Radial velocity contours of windback seals with three different shaft diameters, e=0.25, c=0.1016 mm, Ω=15,000 rpm, DP=34.47 kPa
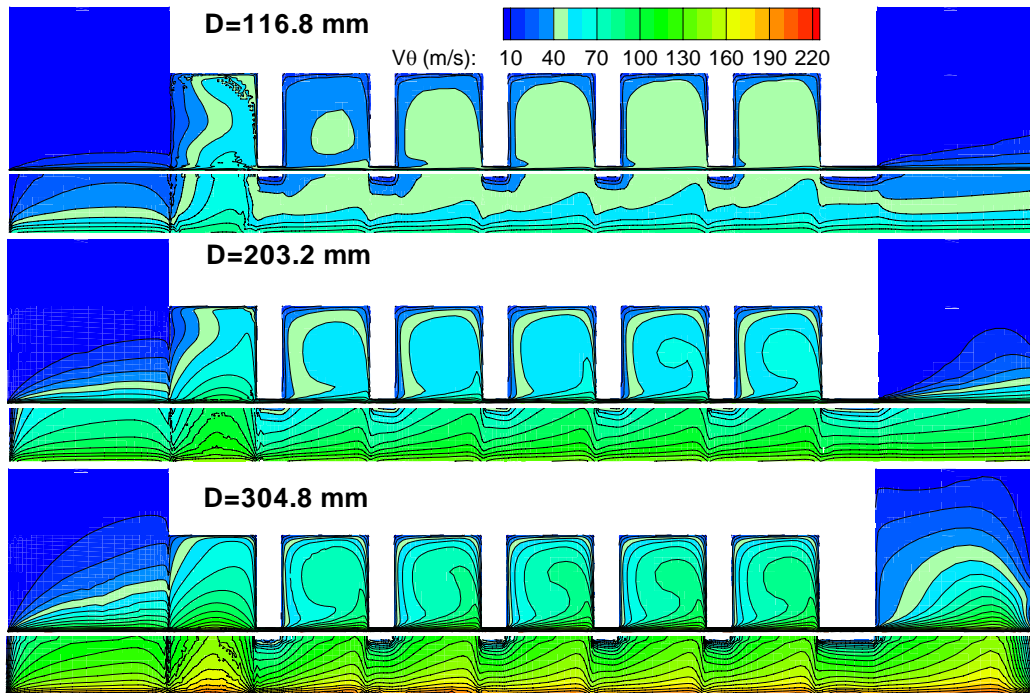
Figure C75. Circumferential velocity contours of windback seals with three different shaft diameters, e=0.25, c=0.1016 mm, Ω=15,000 rpm, DP=34.47 kPa
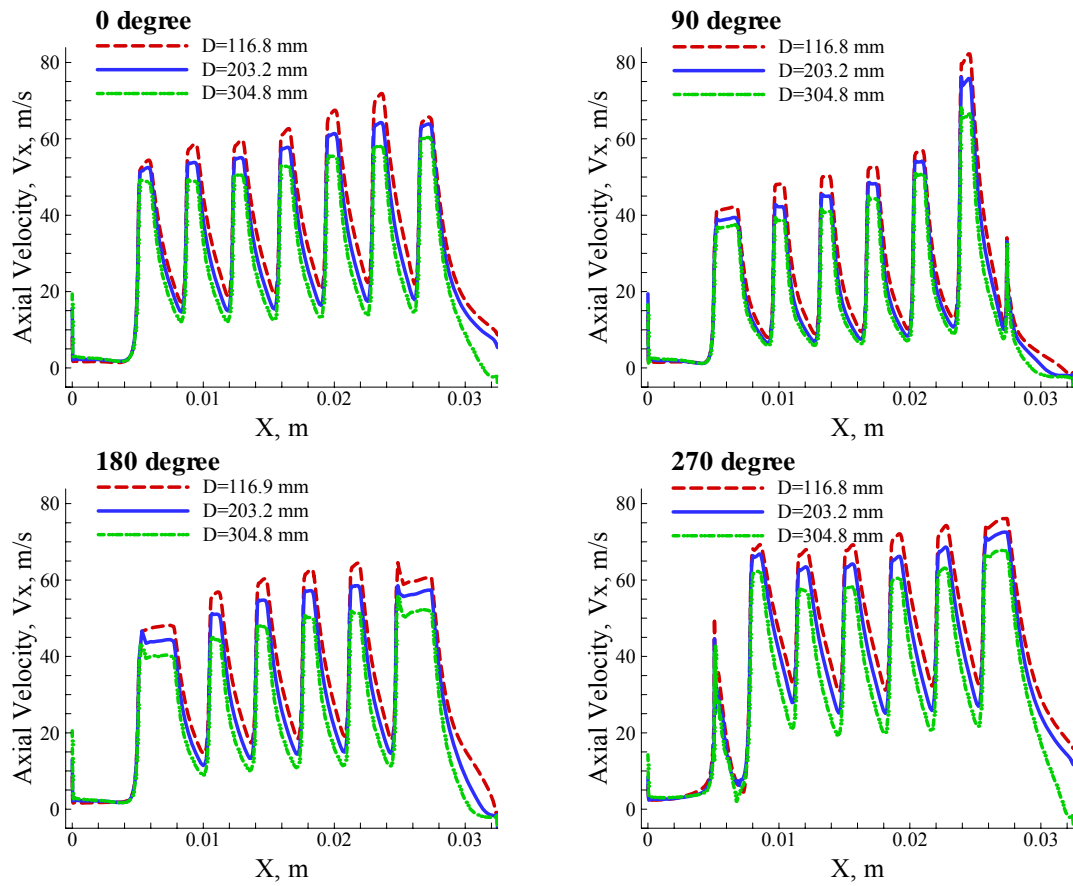
Figure C76. Axial pressure distributions along the middle of clearance for three different shaft diameters of the windback seal, e=0.25, Ω=15,000 rpm, c=0.1016 mm, DP=34.47 kPa
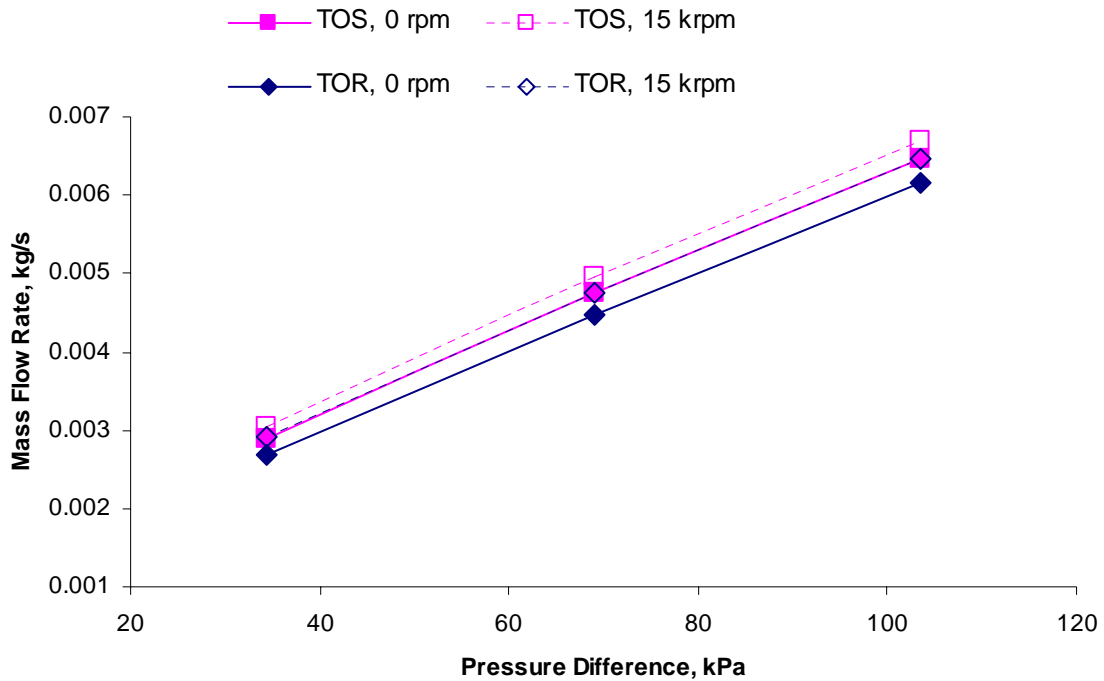
Figure C77. Leakage mass flow rate vs. differential pressure for TOS and TOR windback seals at the rotor speed of 0 and 15,000 rpm
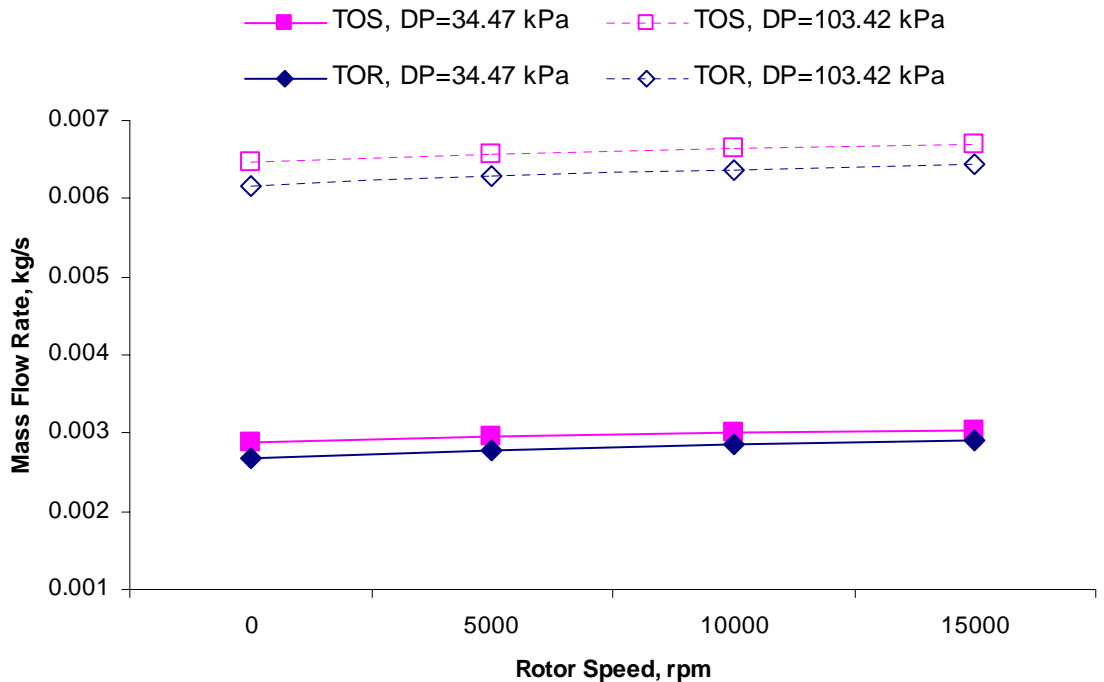
Figure C78. Leakage mass flow rate vs. rotor speed for TOS and TOR windback seals at the differential pressure of 34.47 and 103.42 kPa
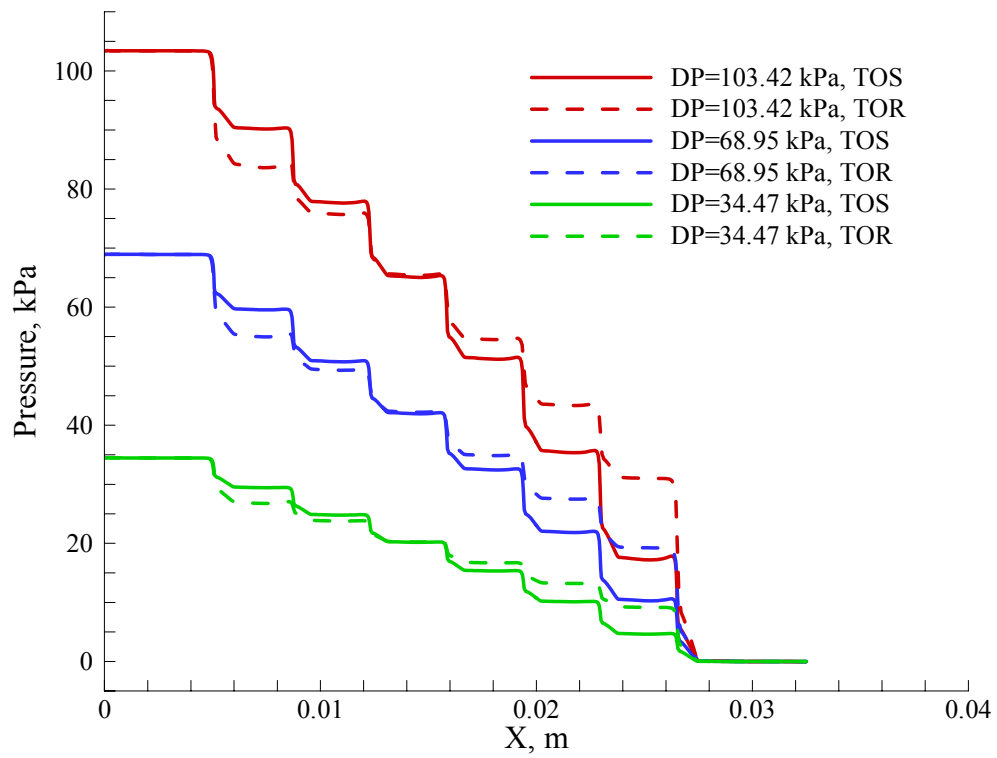
Figure C79. Axial pressure distributions along the middle of clearance for tooth locations of the windback seal with three differential pressure, e=0, Ω=15,000 rpm, c=0.106 mm
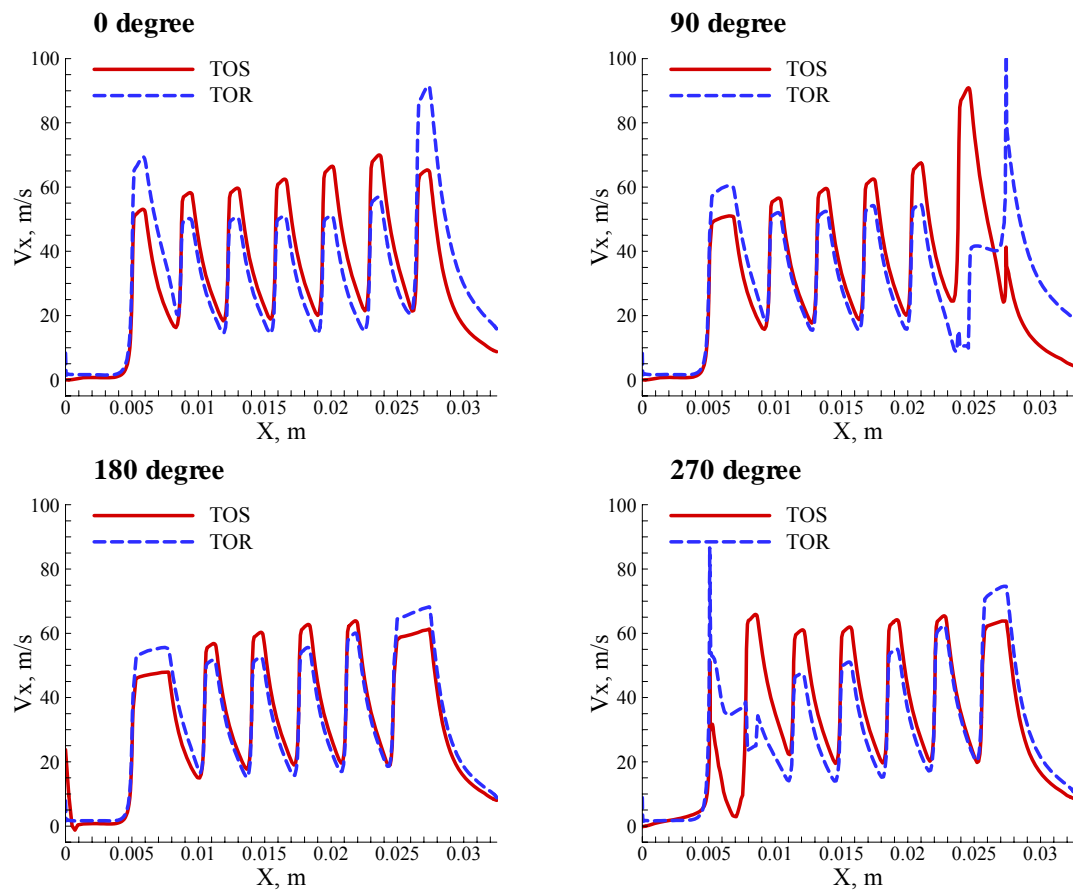
Figure C80. Axial velocity distributions along the middle of clearance for tooth locations of the windback seal in four angular sliced planes, e=0, Ω=15,000 rpm, c=0.106 mm, DP=34.47 kPa

APPENDIX D

Appendix D contains the plots of the leakage, pressure distribution, and velocity components for the three dimensional simulations with the oil.
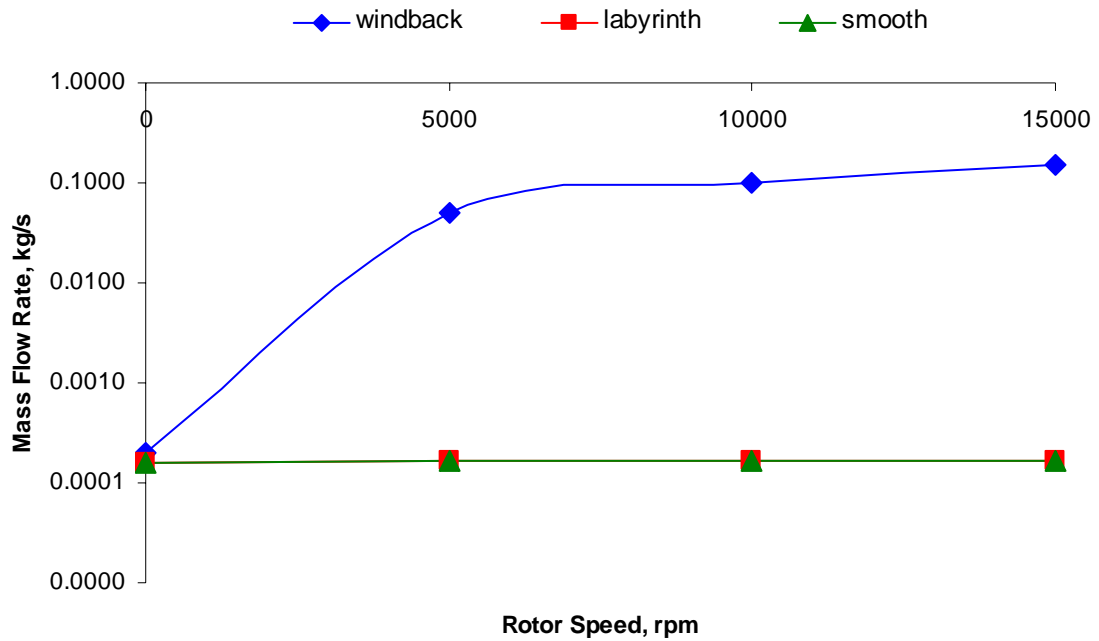
Figure D1. Oil leakage flow rate for smooth, labyrinth, and windback seal at the pressure differential of 34.47 kPa
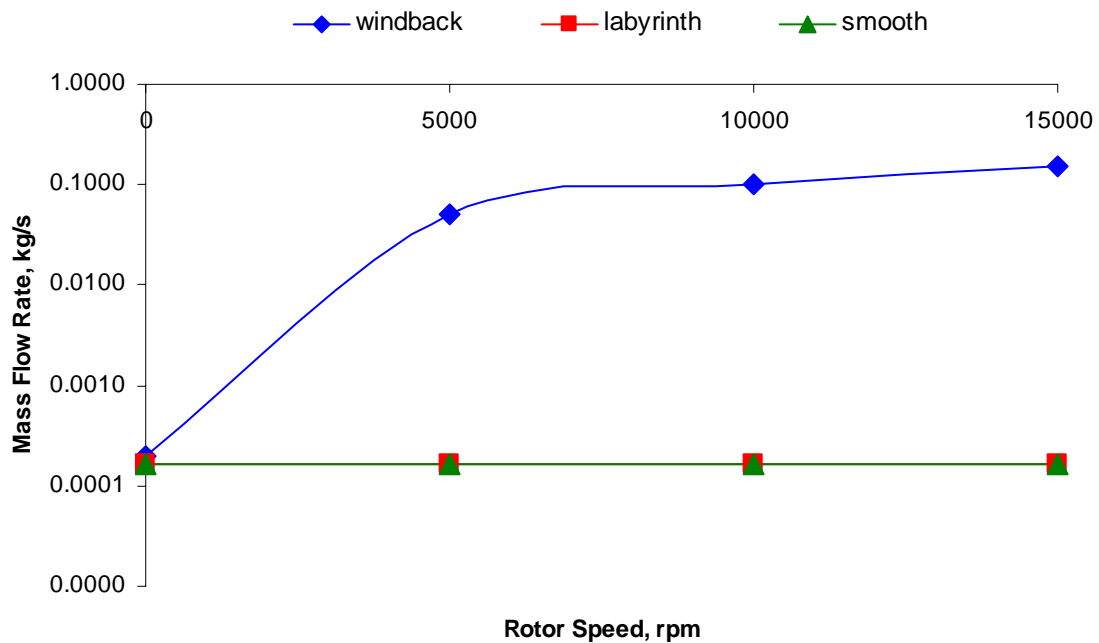
Figure D2. Oil leakage flow rate for smooth, labyrinth, and windback seal at the pressure differential of 103.42 kPa
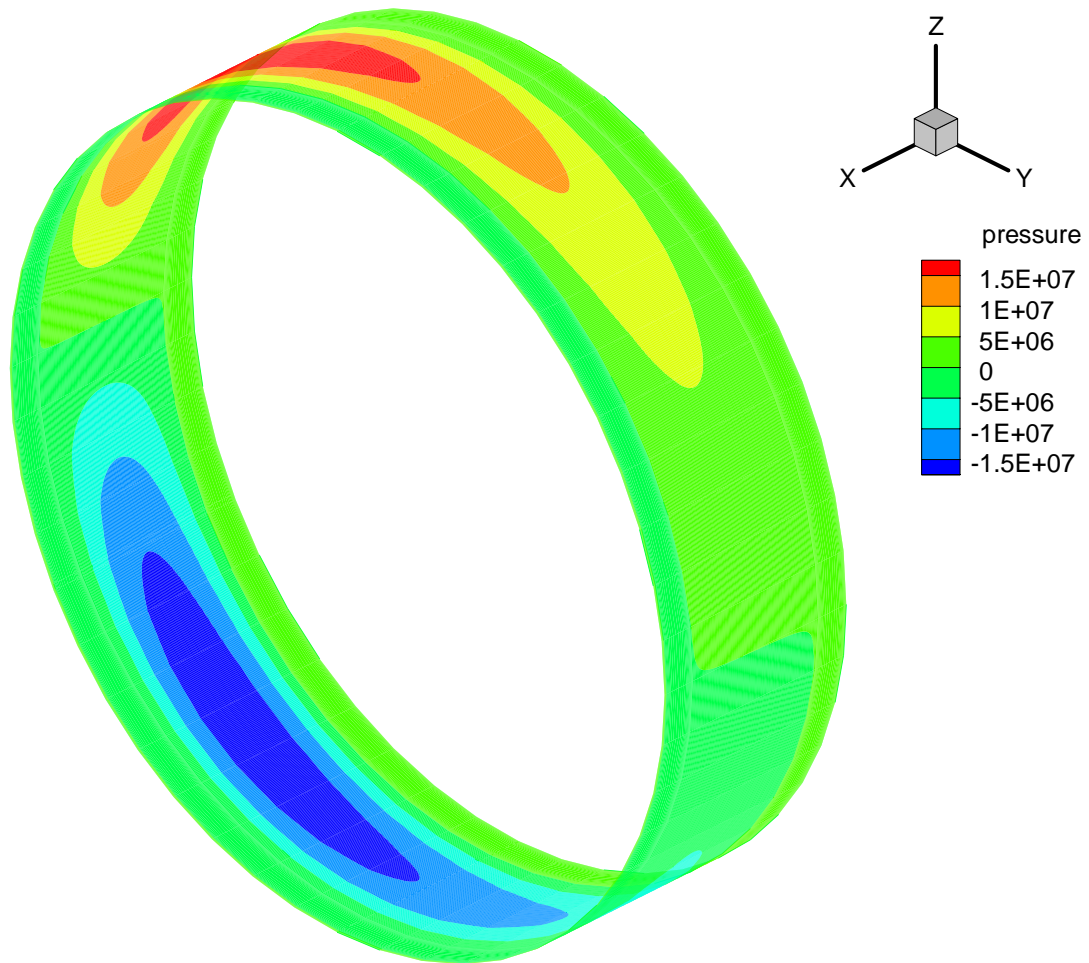
Figure D3. Oil pressure contour on the middle of clearance for the smooth seal, DP=103.42 kPa, Ω=15,000 rpm, e=0.25, c=0.1016 mm
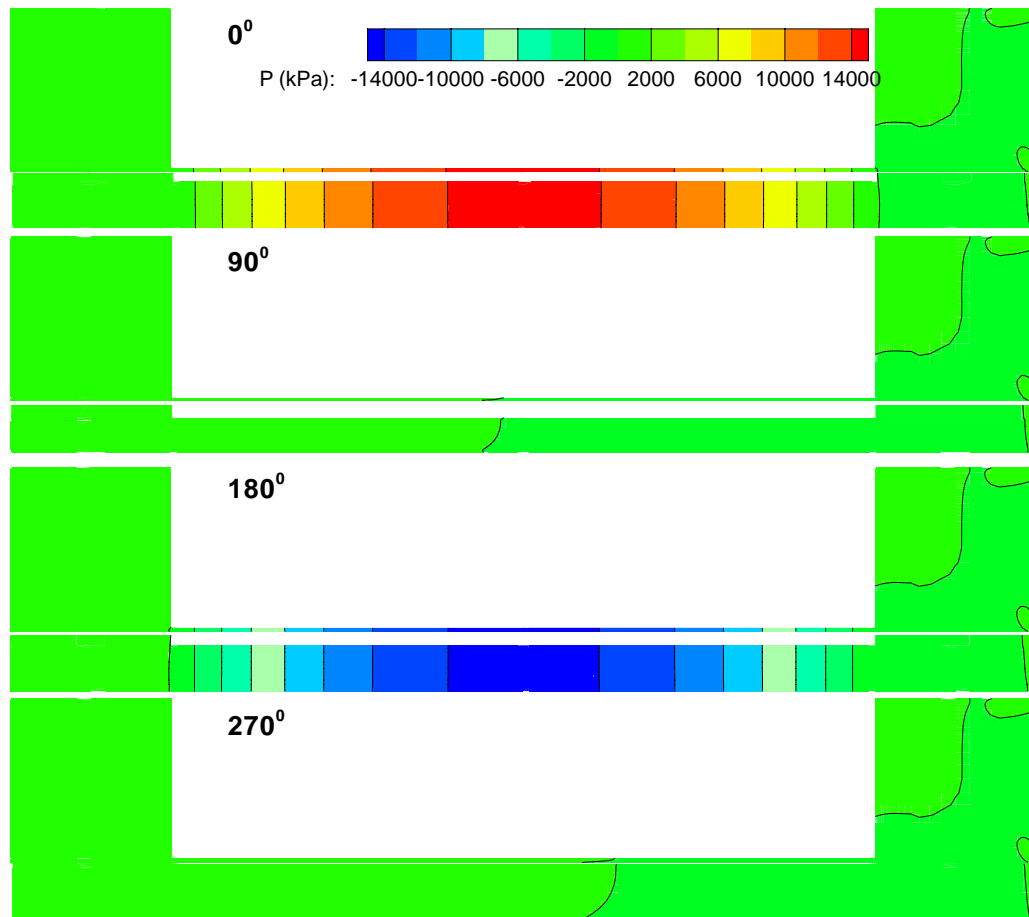
Figure D4. Oil pressure contours for the smooth seal in four angular sliced planes, DP=103.42 kPa, Ω=15,000 rpm, e=0.25, c=0.1016 mm
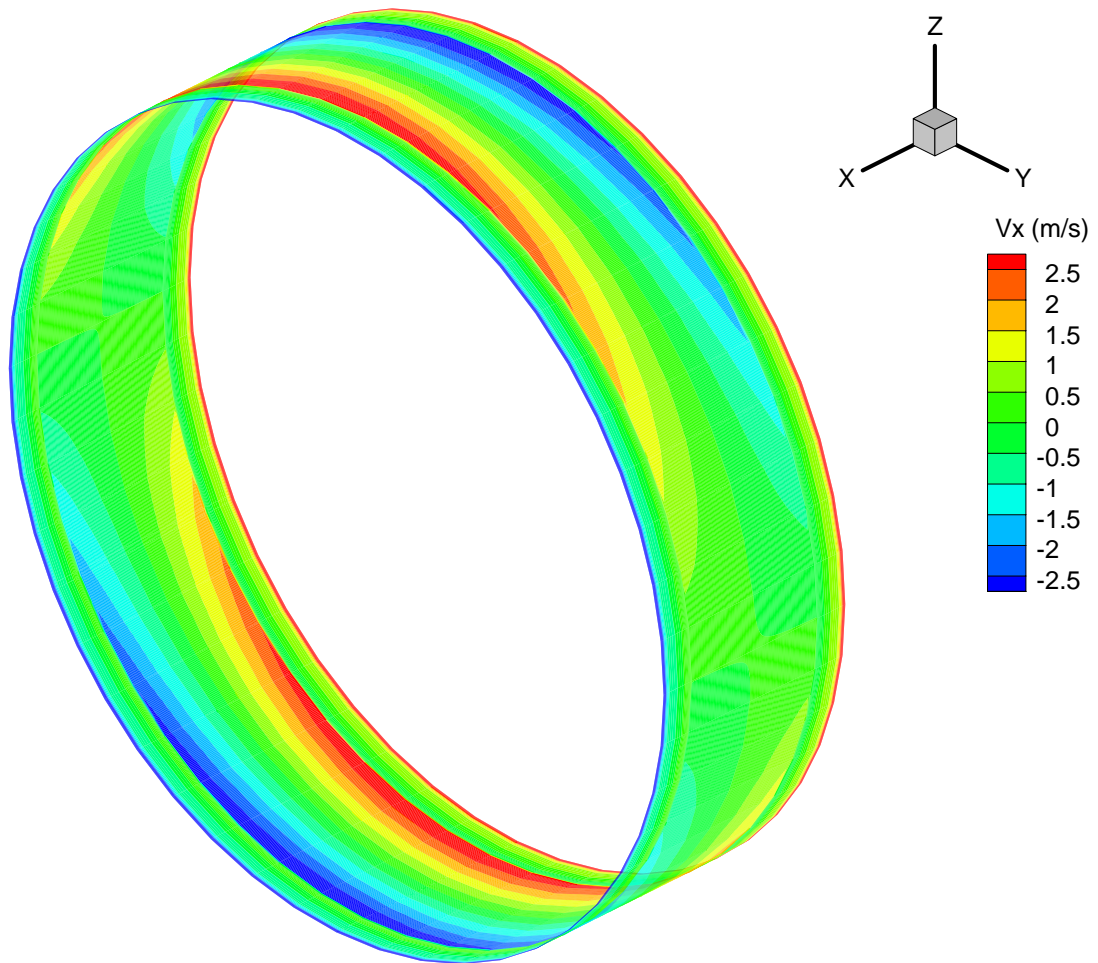
Figure D5. Oil axial velocity contour on the middle of clearance for the smooth seal, DP=103.42 kPa, Ω=15,000 rpm, e=0.25, c=0.1016 mm
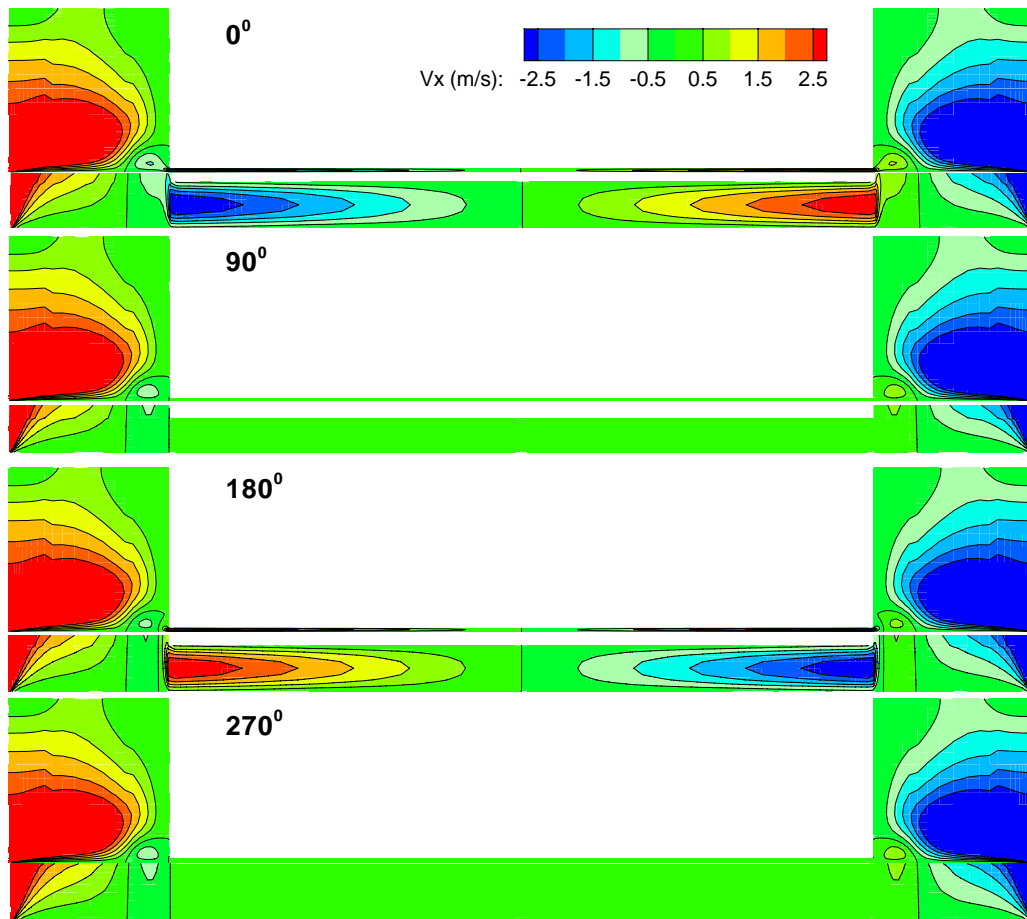
Figure D6. Oil axial velocity contour for the smooth seal in four angular sliced planes, DP=103.42 kPa, Ω=15,000 rpm, e=0.25, c=0.1016 mm
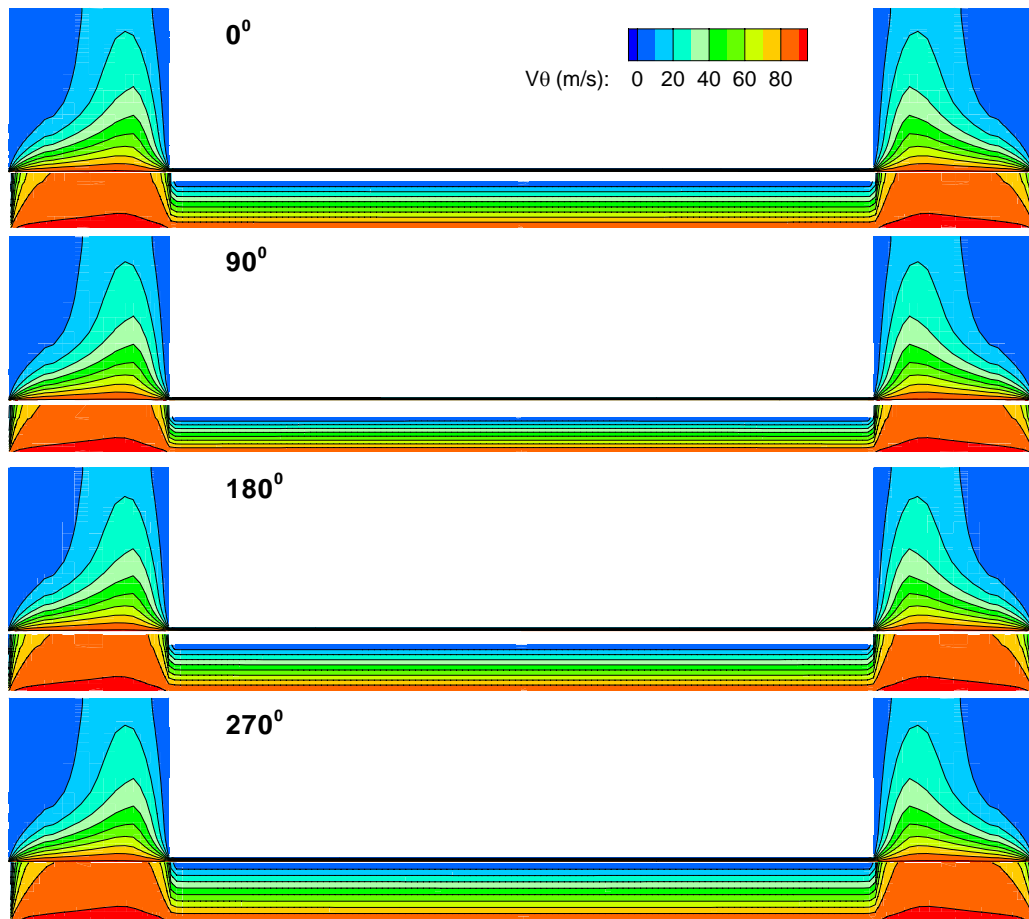
Figure D7. Oil circumferential velocity contour for the smooth seal in four angular sliced planes, DP=103.42 kPa, Ω=15,000 rpm, e=0.25, c=0.1016 mm
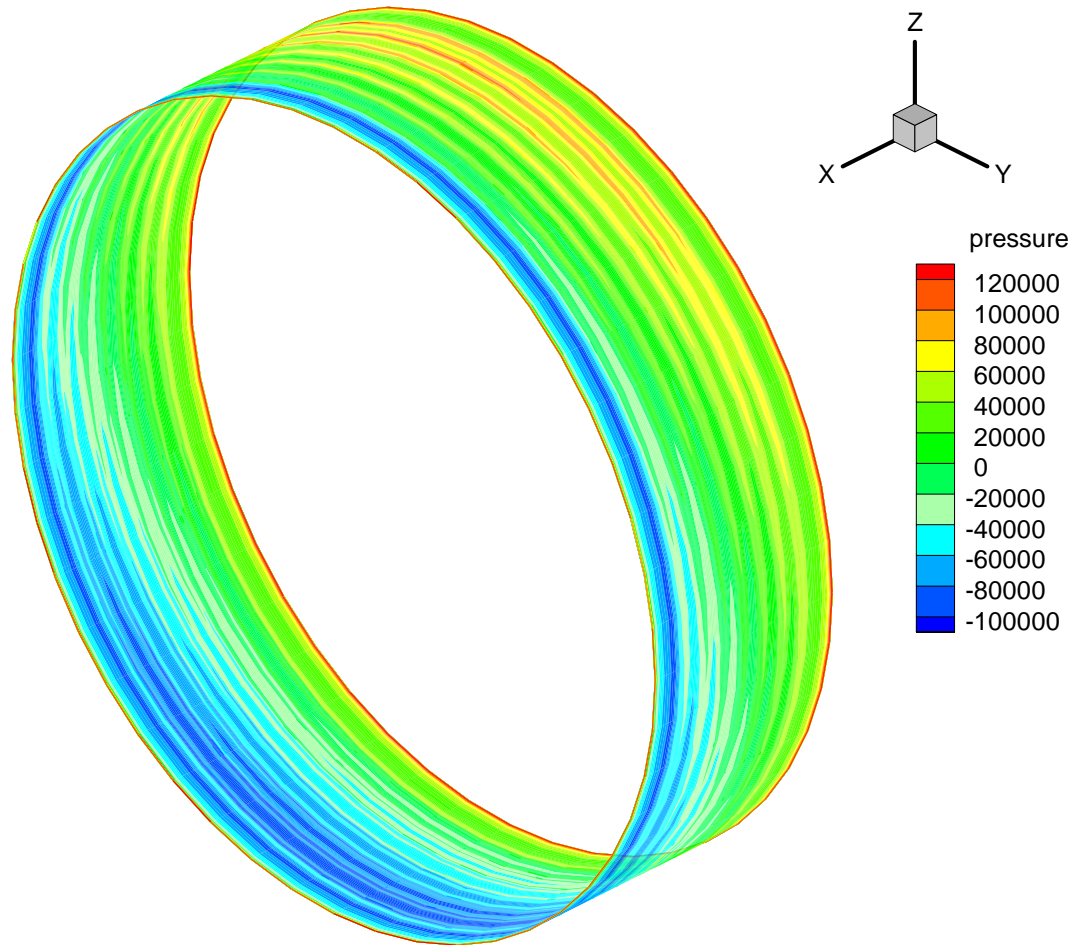
Figure D8. Oil pressure contour on the middle of clearance for the labyrinth seal, DP=103.42 kPa, Ω=15,000 rpm, e=0.25, c=0.1016 mm
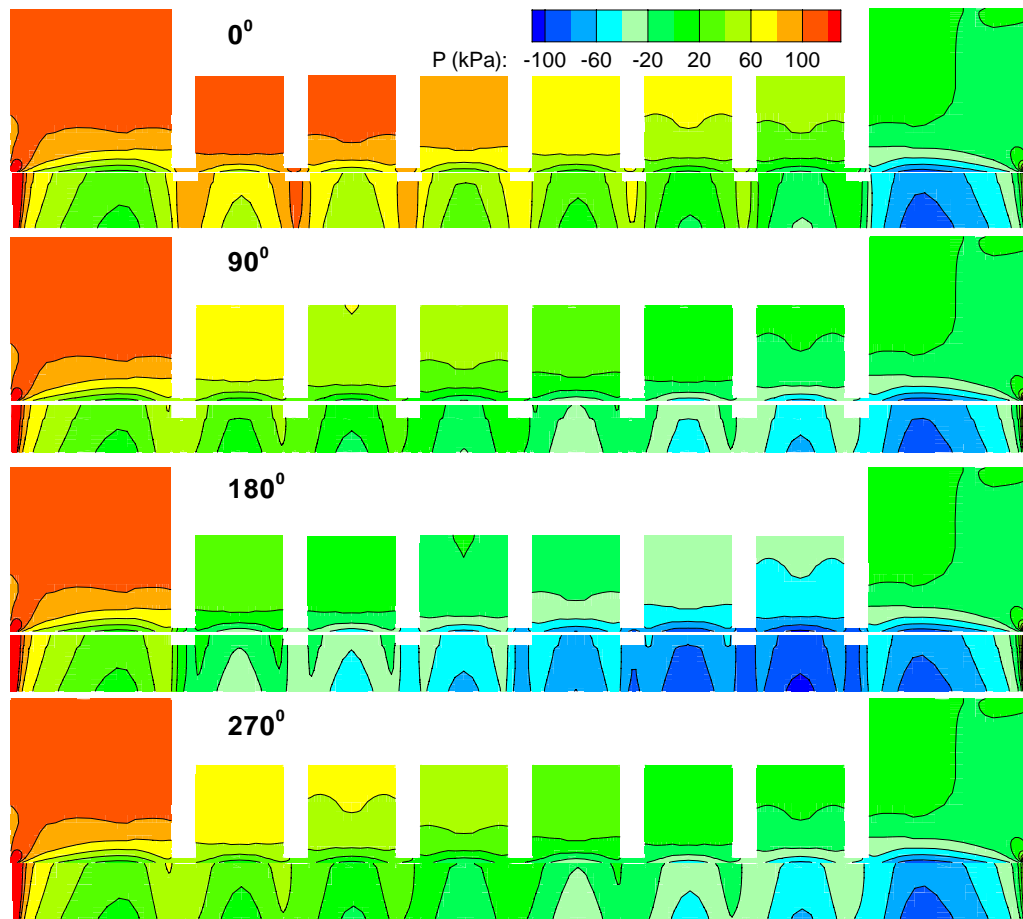
Figure D9. Oil pressure contour for the labyrinth seal in four angular sliced planes, DP=103.42 kPa, Ω=15,000 rpm, e=0.25, c=0.1016 mm
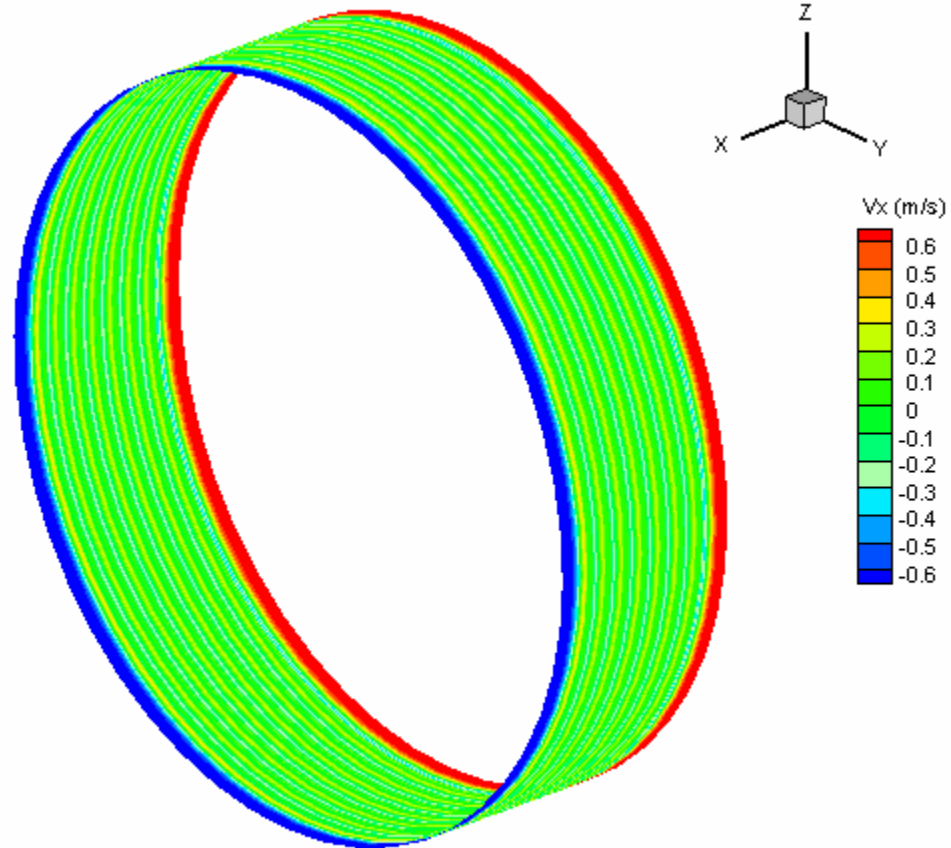
Figure D10. Axial velocity contour on the middle of clearance for the labyrinth seal operating with oil at 103.42 kPa, and 15,000 rpm
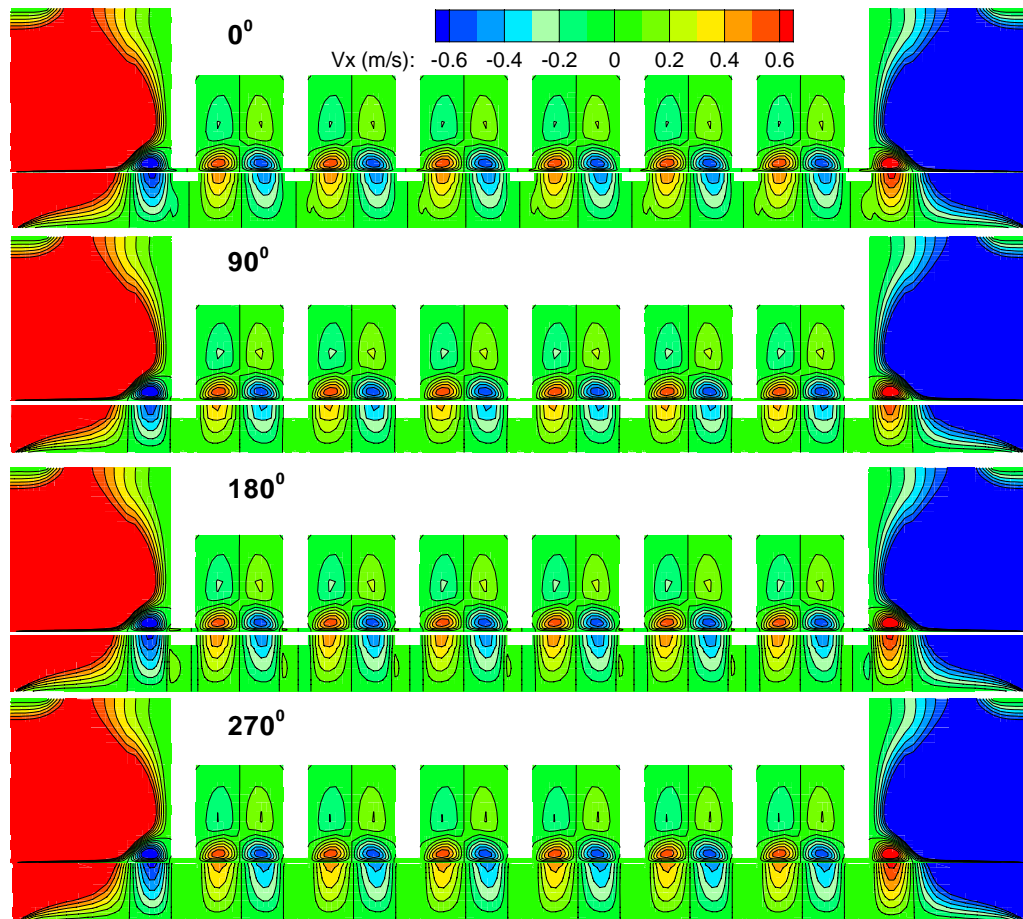
Figure D11. Axial velocity contour for the labyrinth seal in four angular sliced planes operating with the oil, DP=103.42 kPa, Ω=15,000 rpm, e=0.25, c=0.1016 mm
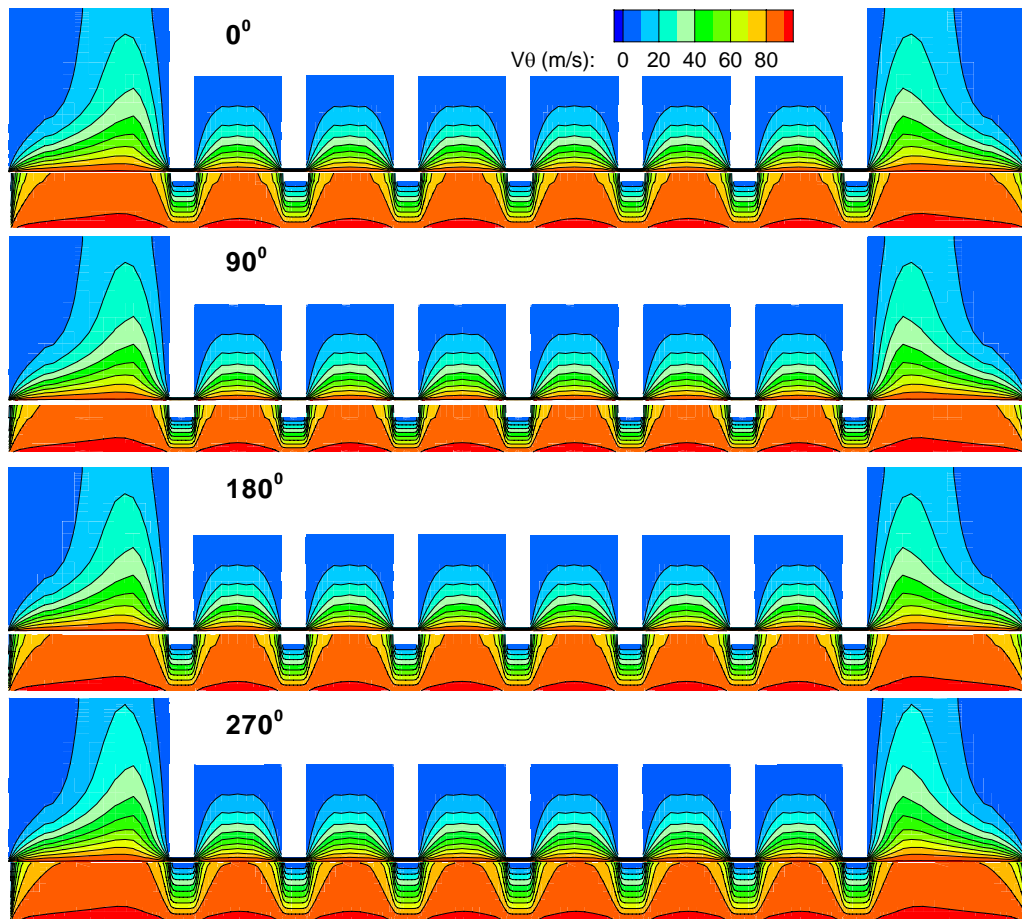
Figure D12. Circumferential velocity contour for the labyrinth seal in four angular sliced planes operating with the oil, DP=103.42 kPa, Ω=15,000 rpm, e=0.25, c=0.1016 mm
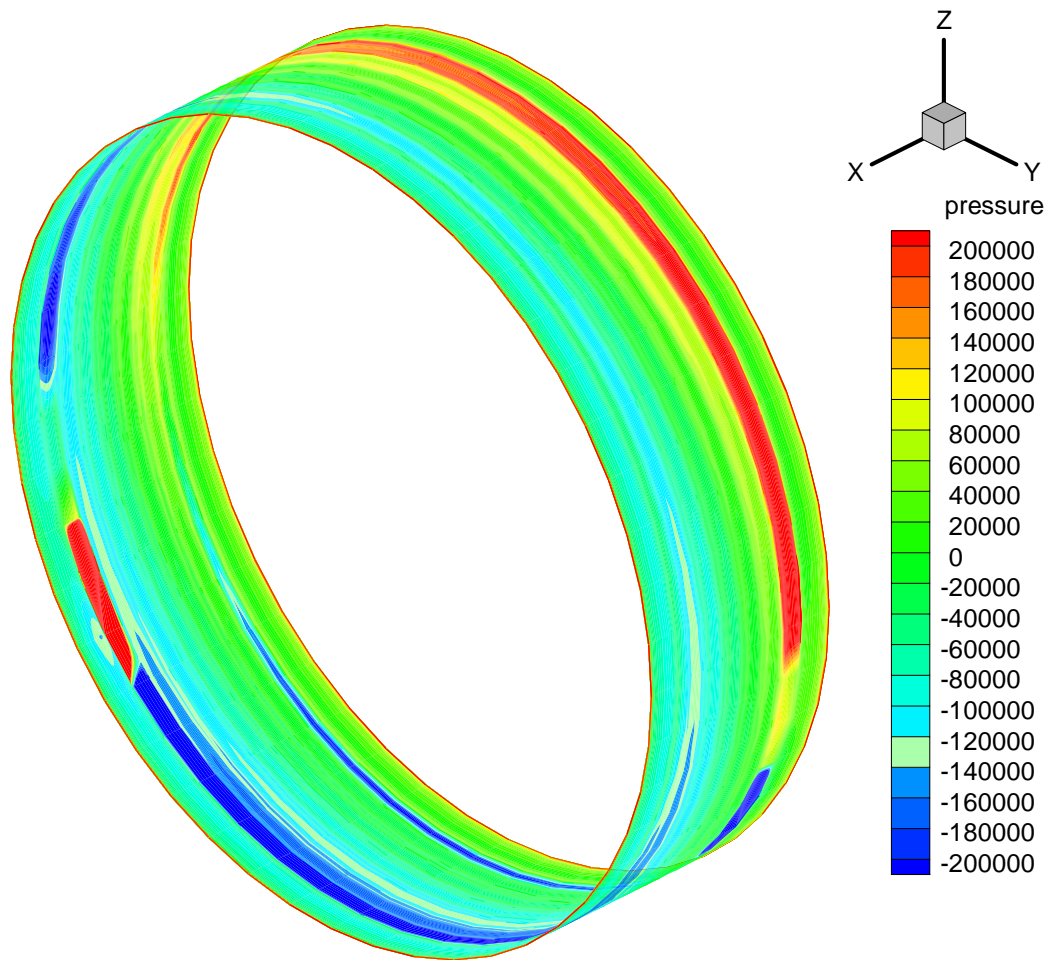
Figure D13. Pressure contour on the middle of clearance for the windback seal operating with the oil, DP=103.42 kPa, Ω=15,000 rpm, e=0.25, c=0.1016 mm
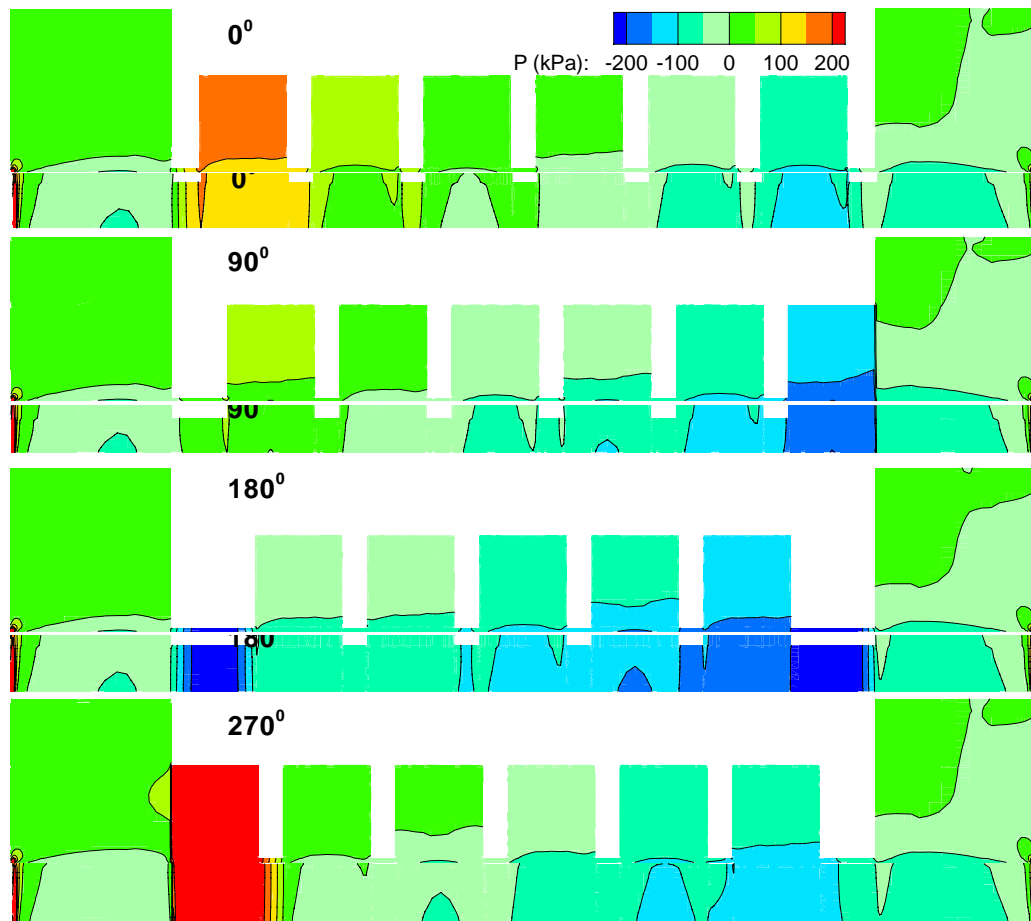
Figure D14. Pressure contour for the windback seal in four angular sliced planes operating with the oil, DP=103.42 kPa, Ω=15,000 rpm, e=0.25, c=0.1016 mm
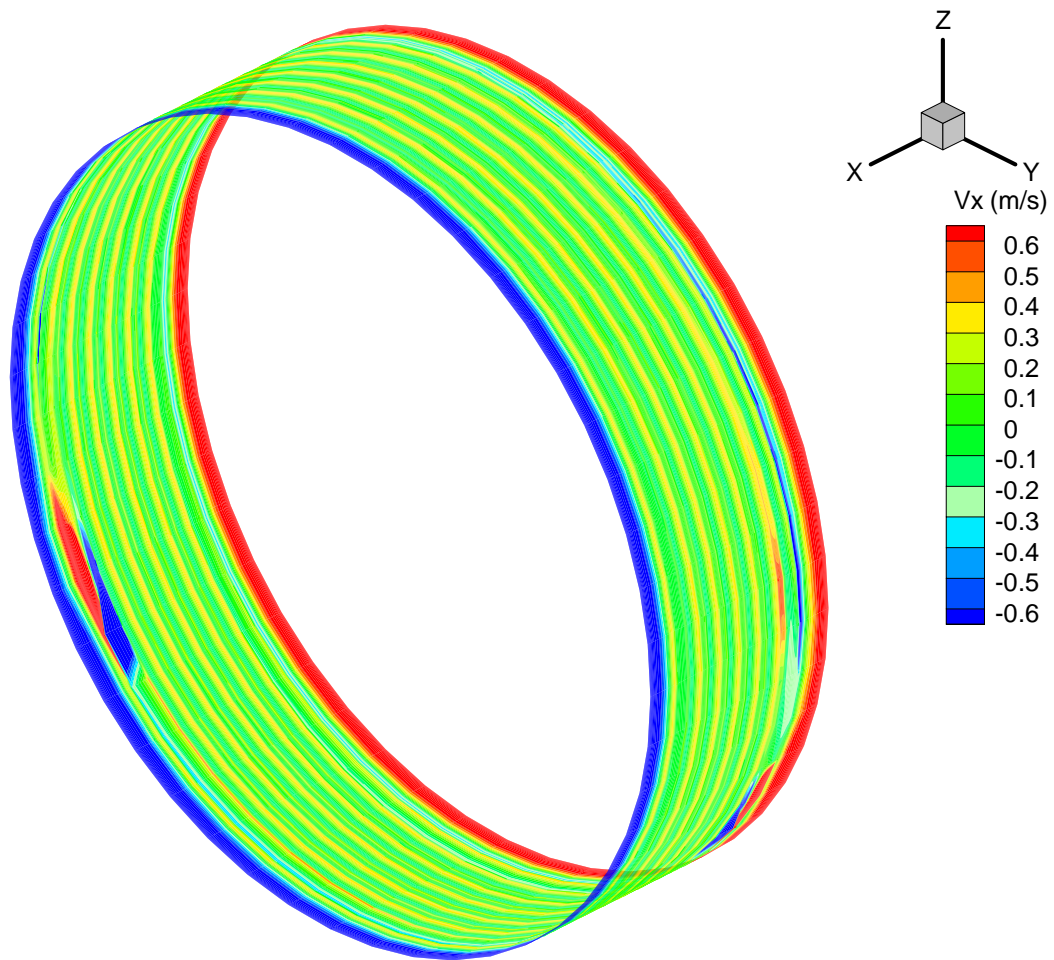
Figure D15. Axial velocity contour on the middle of clearance for the windback seal operating with the oil, DP=103.42 kPa, Ω=15,000 rpm, e=0.25, c=0.1016 mm
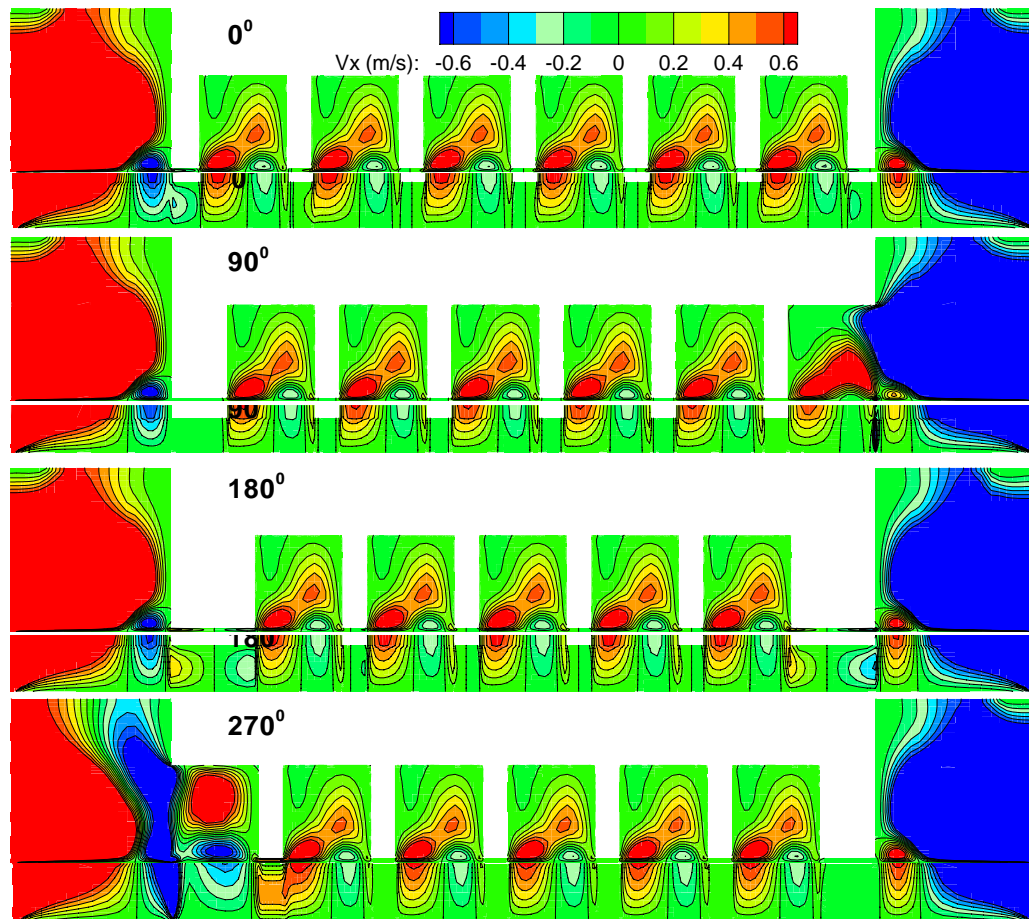
Figure D16. Axial velocity contour for the windback seal in four angular sliced planes operating with the oil, DP=103.42 kPa, Ω=15,000 rpm, e=0.25, c=0.1016 mm
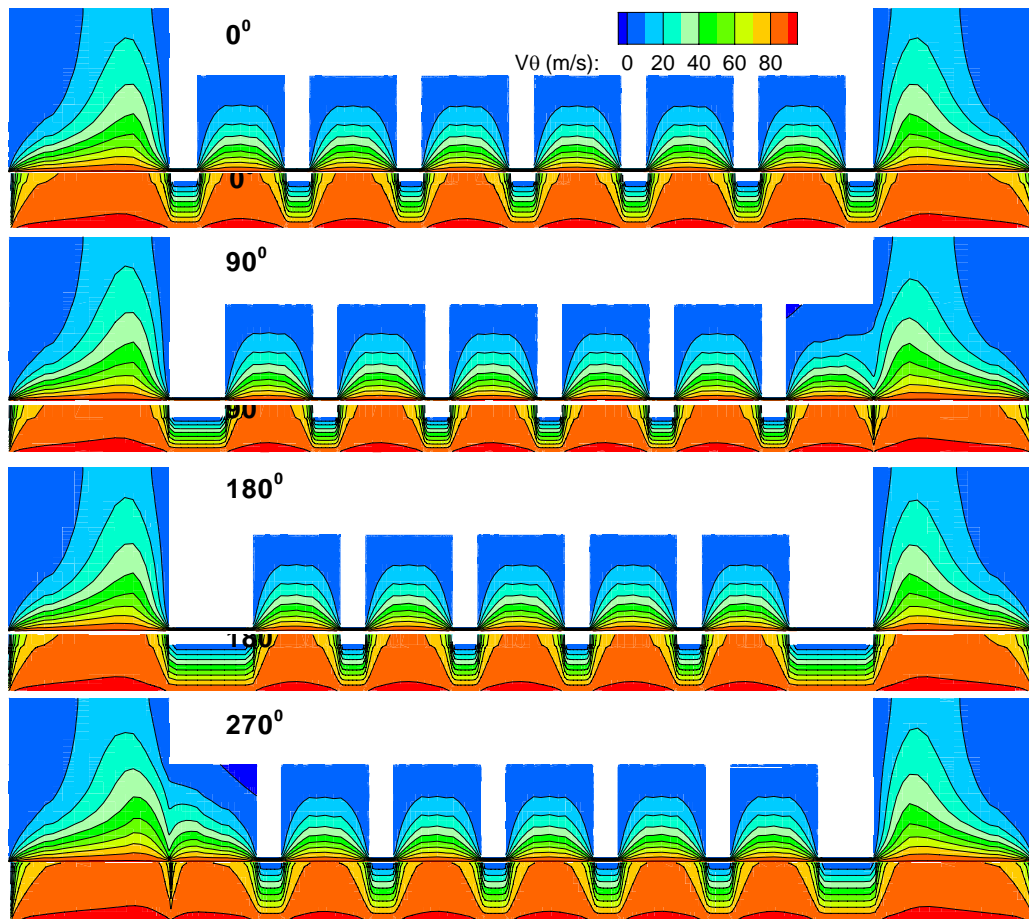
Figure D17. Circumferential velocity contour for the windback seal in four angular sliced planes operating with the oil, DP=103.42 kPa, Ω=15,000 rpm, e=0.25, c=0.1016 mm
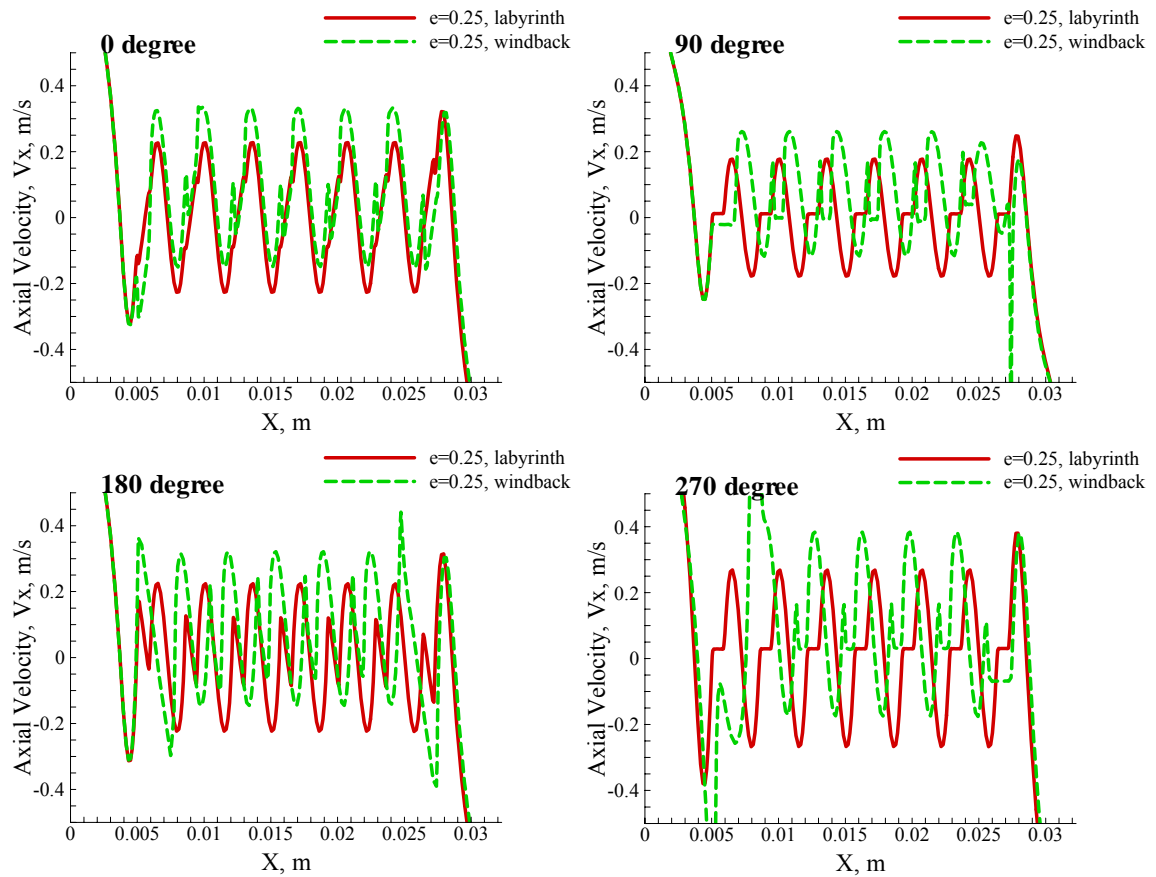
Figure D18. Axial velocity distribution along the middle of clearance for labyrinth and windback seals in four angular views operating with the oil at 103.42 kPa, and 15,000 rpm
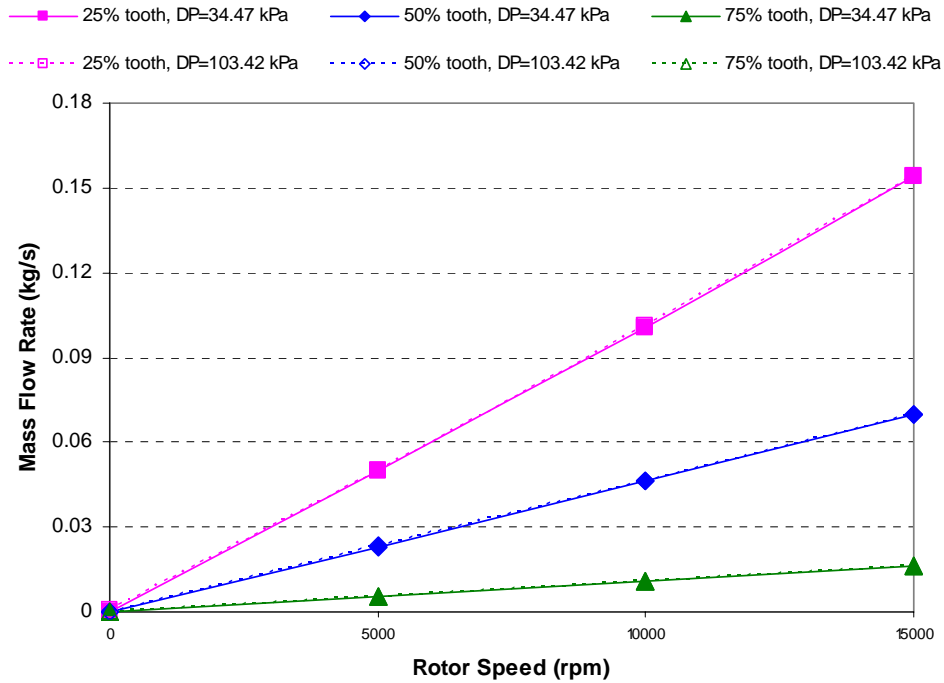
Figure D19. Oil leakage flow rate for windback seal with three tooth widths at 34.47 kPa and 103.42 kPa
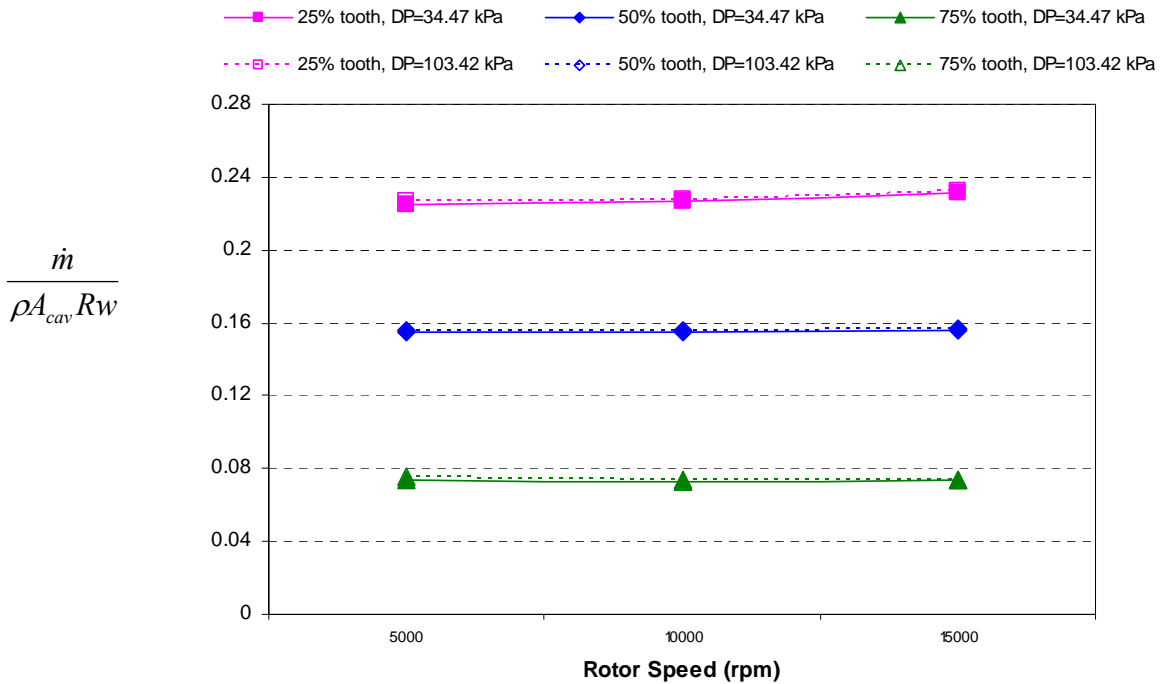
Figure D20. Oil leakage flow rate for windback seal with three tooth widths at 34.47 kPa and 103.42 kPa
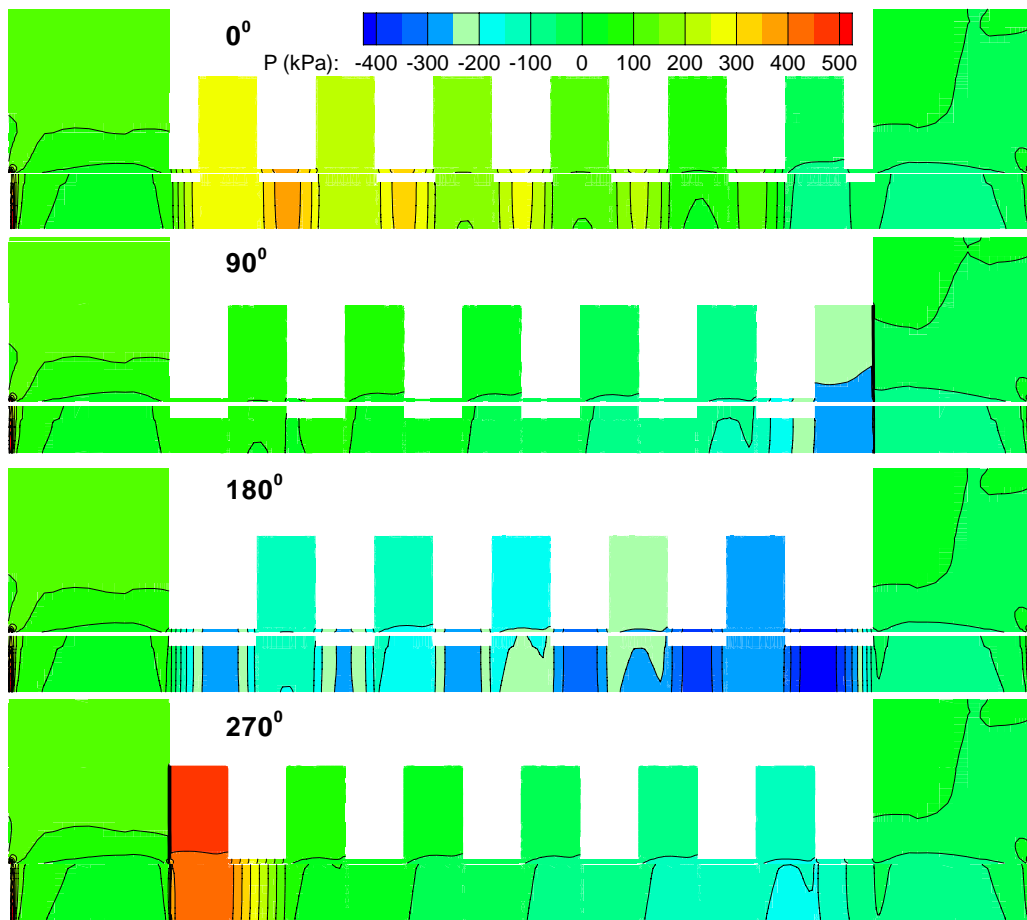
Figure D21. Pressure contours for the 25% eccentric windback seal with 50% tooth width of pitch in four angular sliced planes operating with the oil at 103.42 kPa, and 15,000 rpm
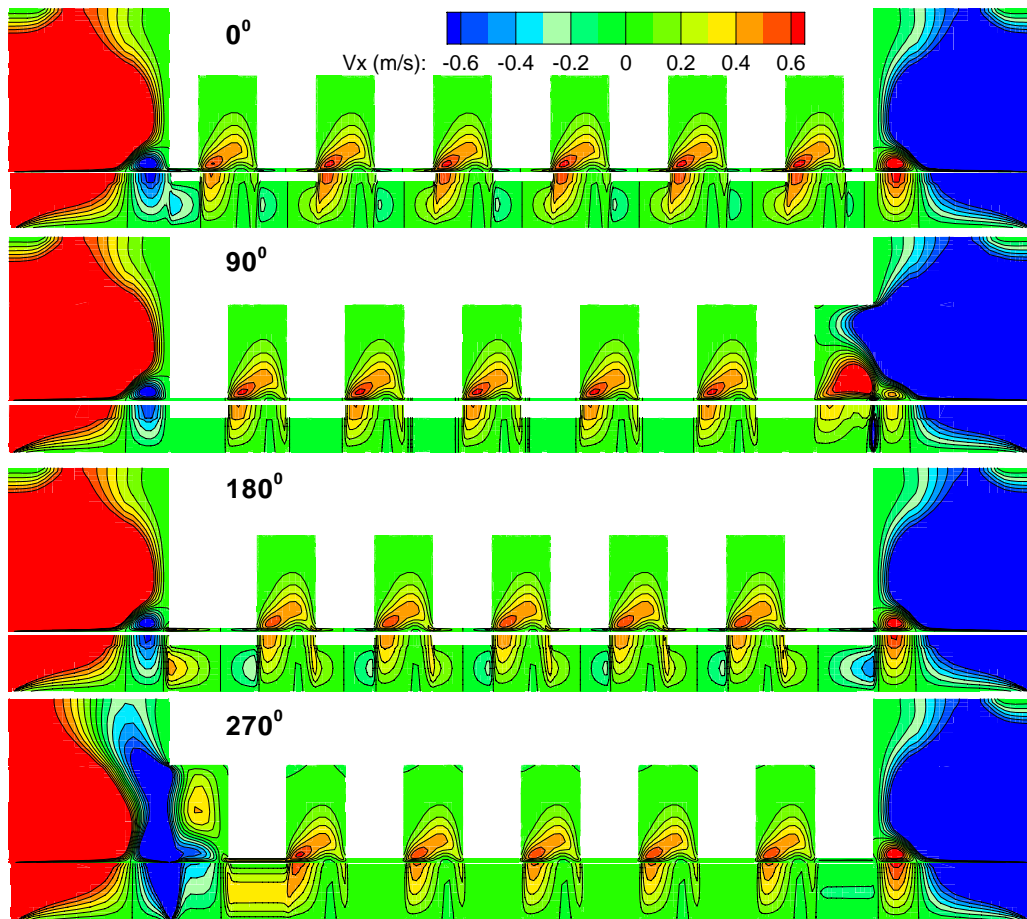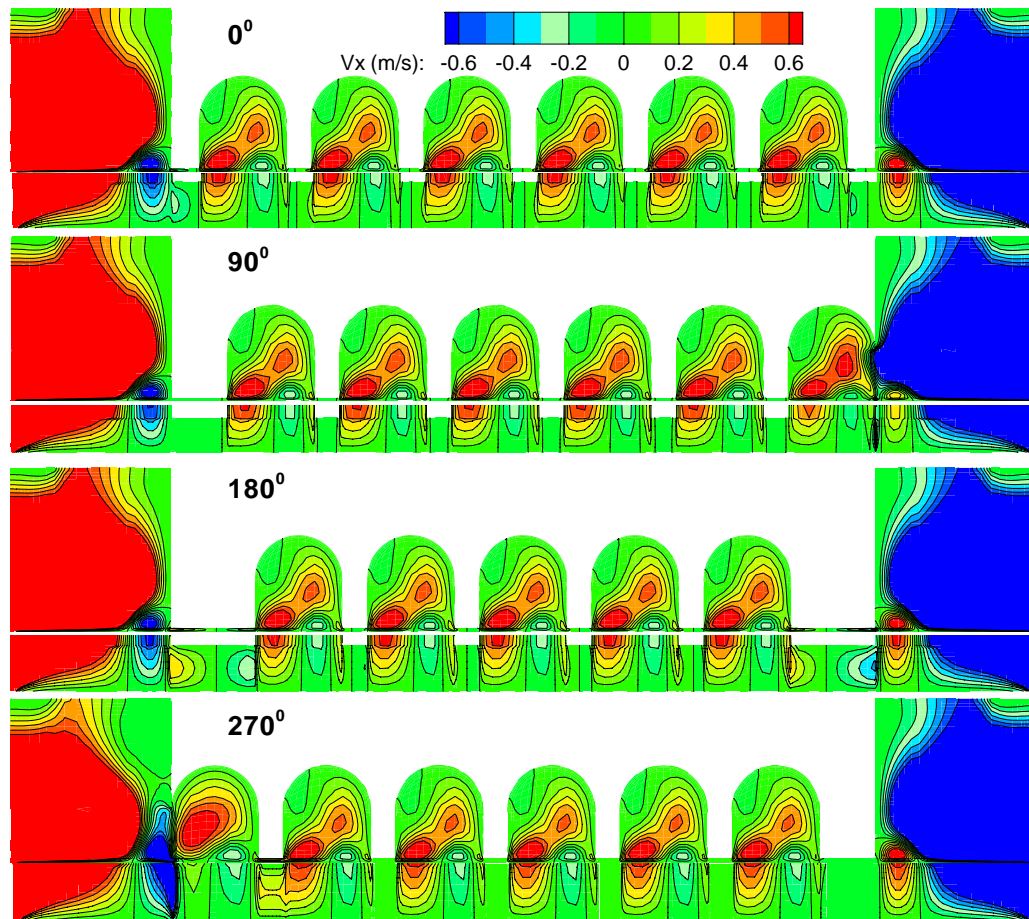
Figure D22. Axial velocity contour for the 25% rotor eccentric windback seal with 50% tooth width of pitch in four angular sliced planes operating with the oil, DP=103.42 kPa, Ω=15,000 rpm, e=0.25, c=0.1016 mm
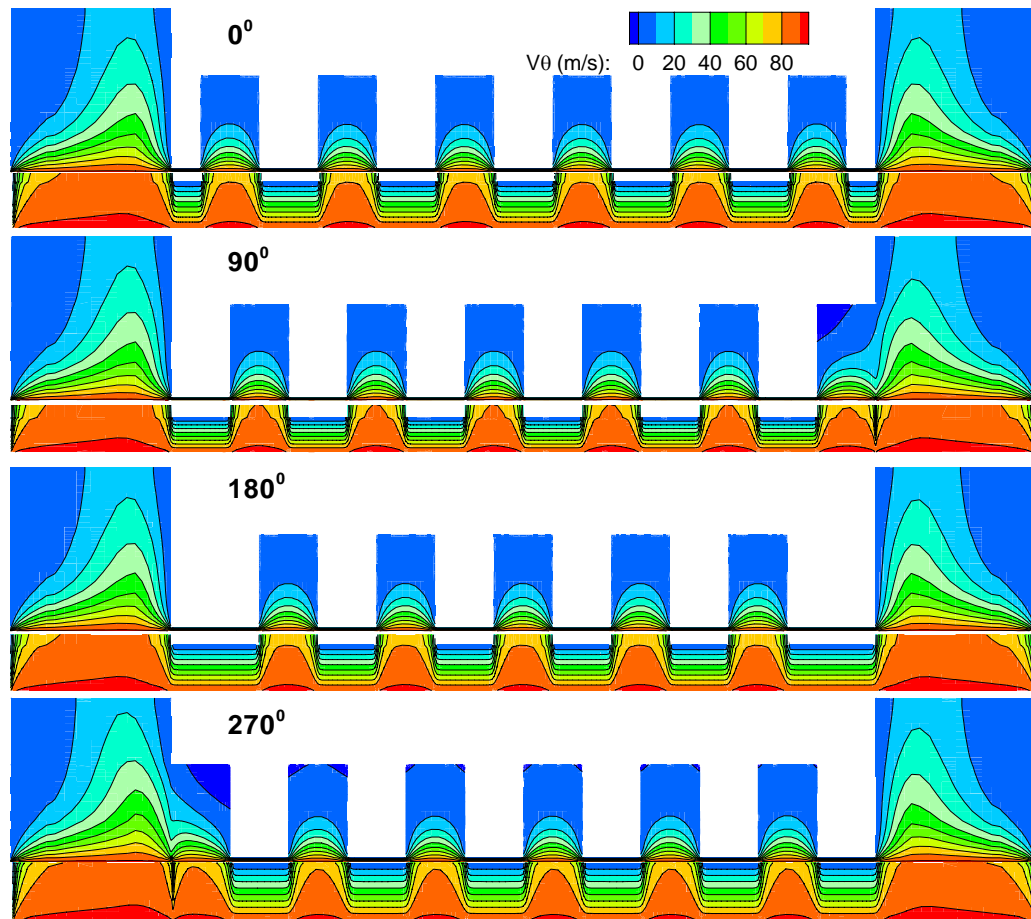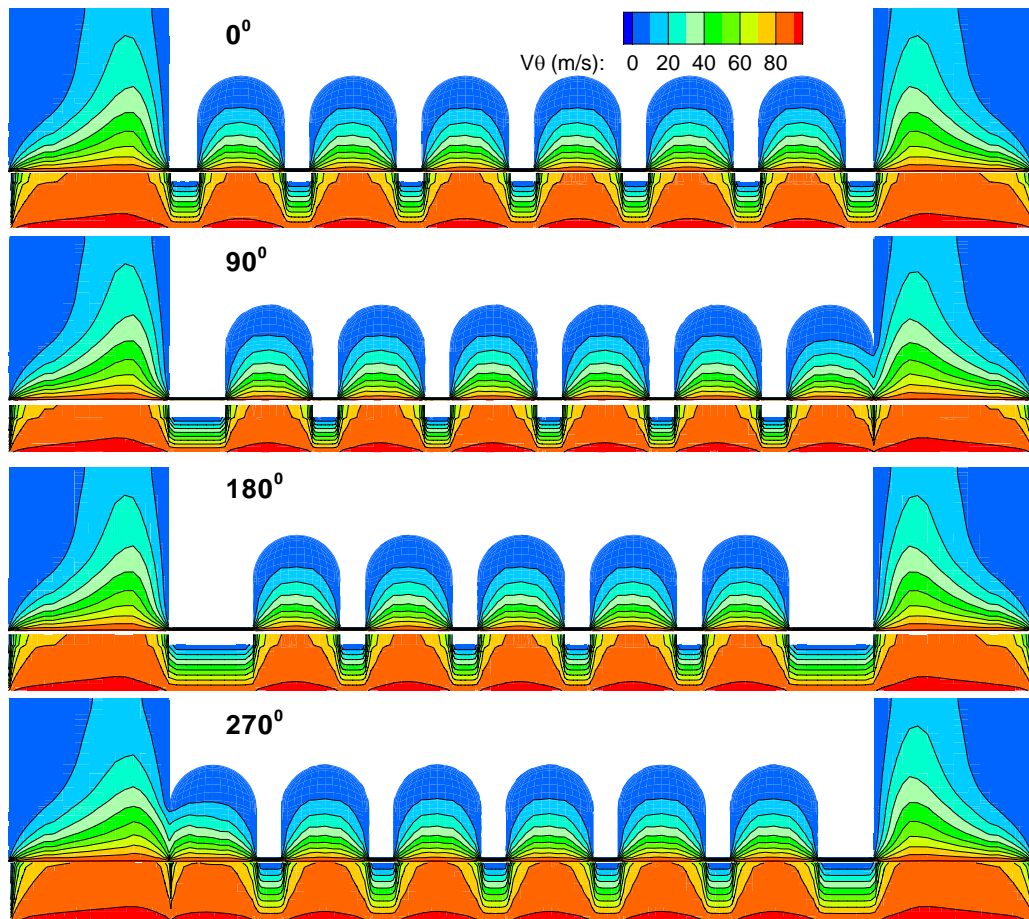
Figure D23. Circumferential velocity contour for the 25% rotor eccentric windback seal with 50% tooth width of pitch in four angular sliced planes operating with the oil, DP=103.42 kPa, Ω=15,000 rpm, e=0.25, c=0.1016 mm
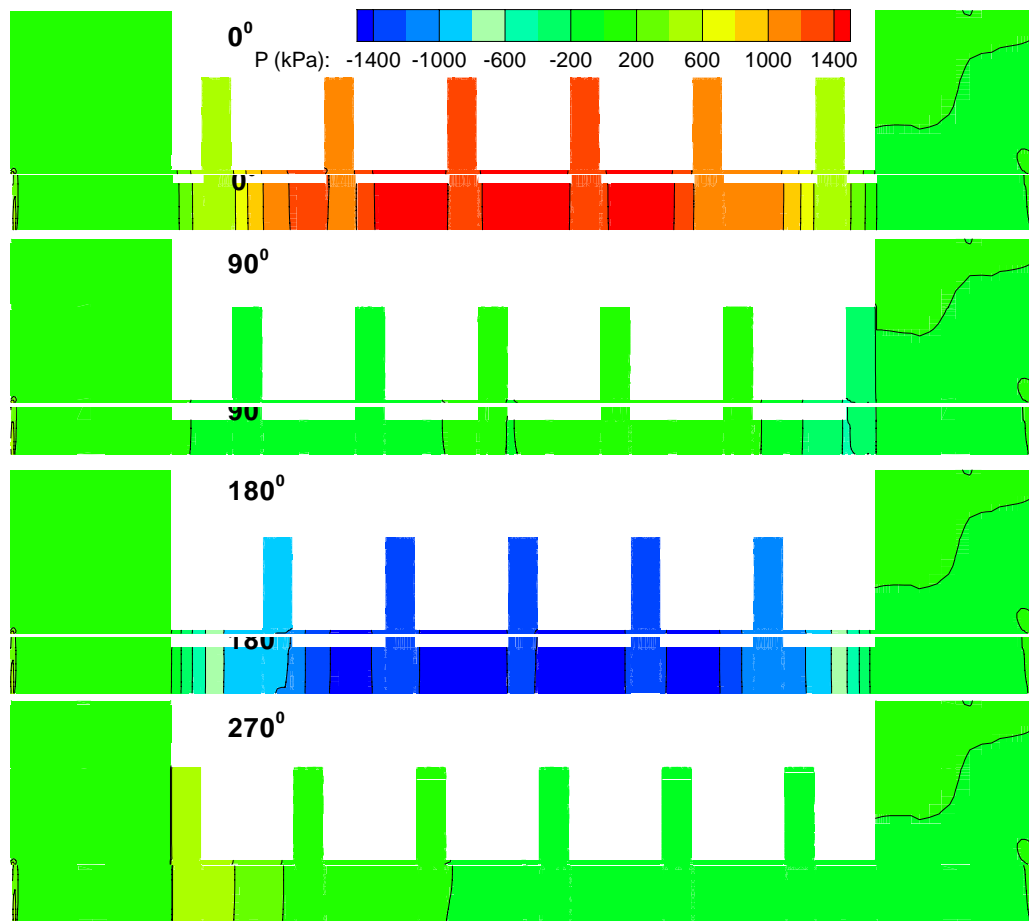
Figure D24. Pressure contour for the 25% eccentric windback seal with 75% tooth width of pitch in four angular sliced planes operating with the oil, DP=103.42 kPa, Ω=15,000 rpm, e=0.25, c=0.1016 mm
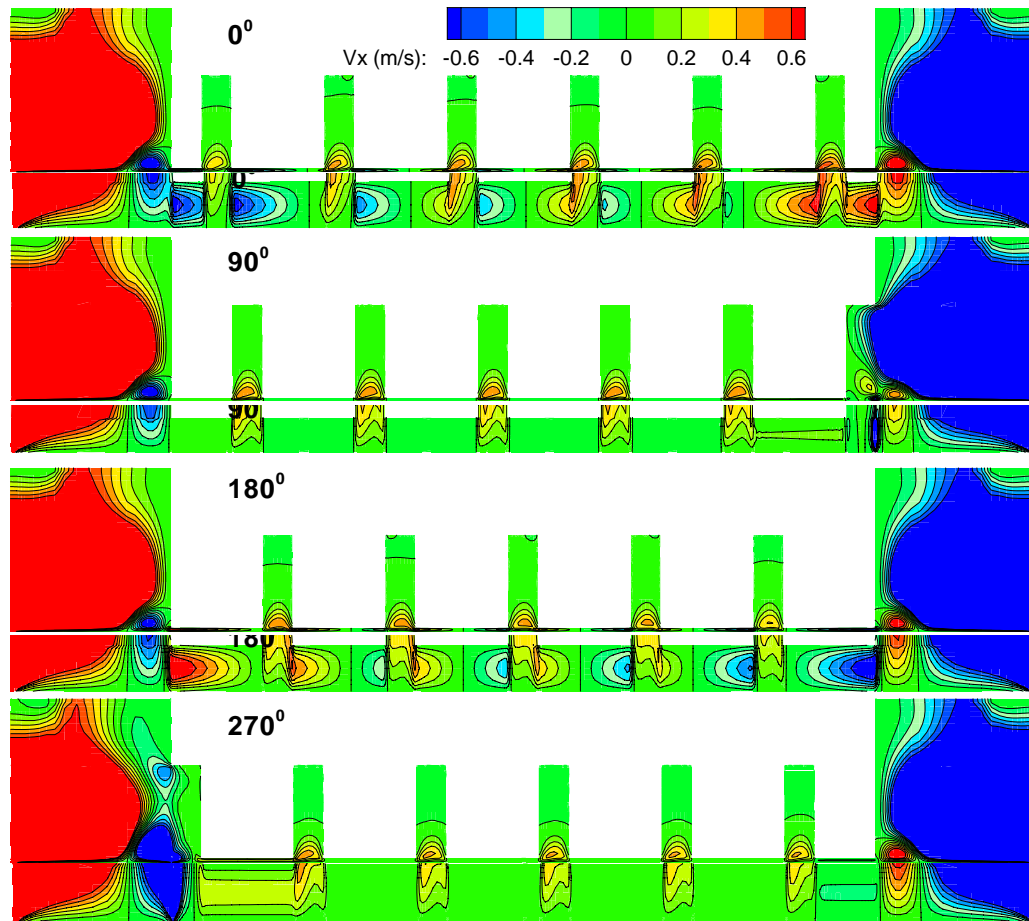
Figure D25. Axial velocity contour for the 25% eccentric windback seal with 75% tooth width of pitch in four angular sliced planes operating with the oil, DP=103.42 kPa, Ω=15,000 rpm, e=0.25, c=0.1016 mm
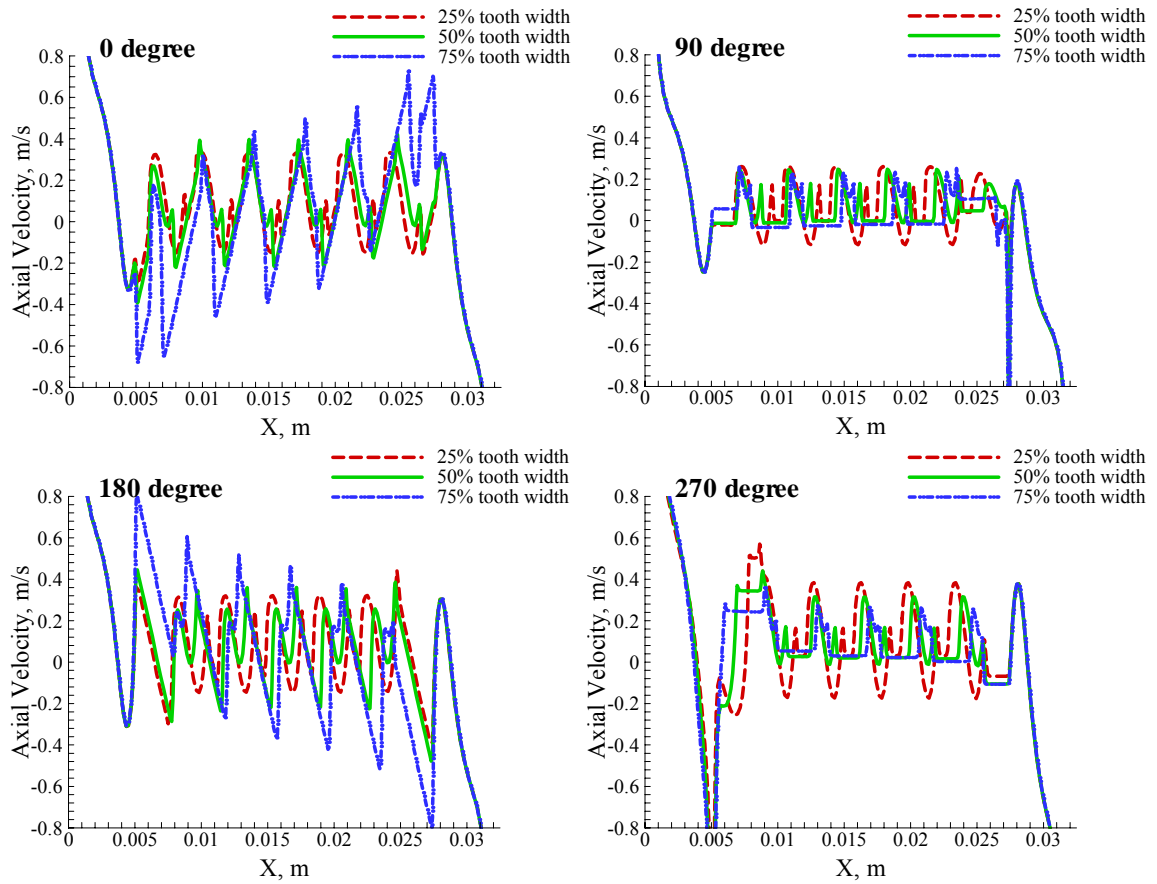
Figure D26. Axial velocity distribution along the middle of clearance for three tooth width windback seals in four angular views operating with the oil, DP=103.42 kPa, Ω=15,000 rpm, e=0.25, c=0.1016 mm
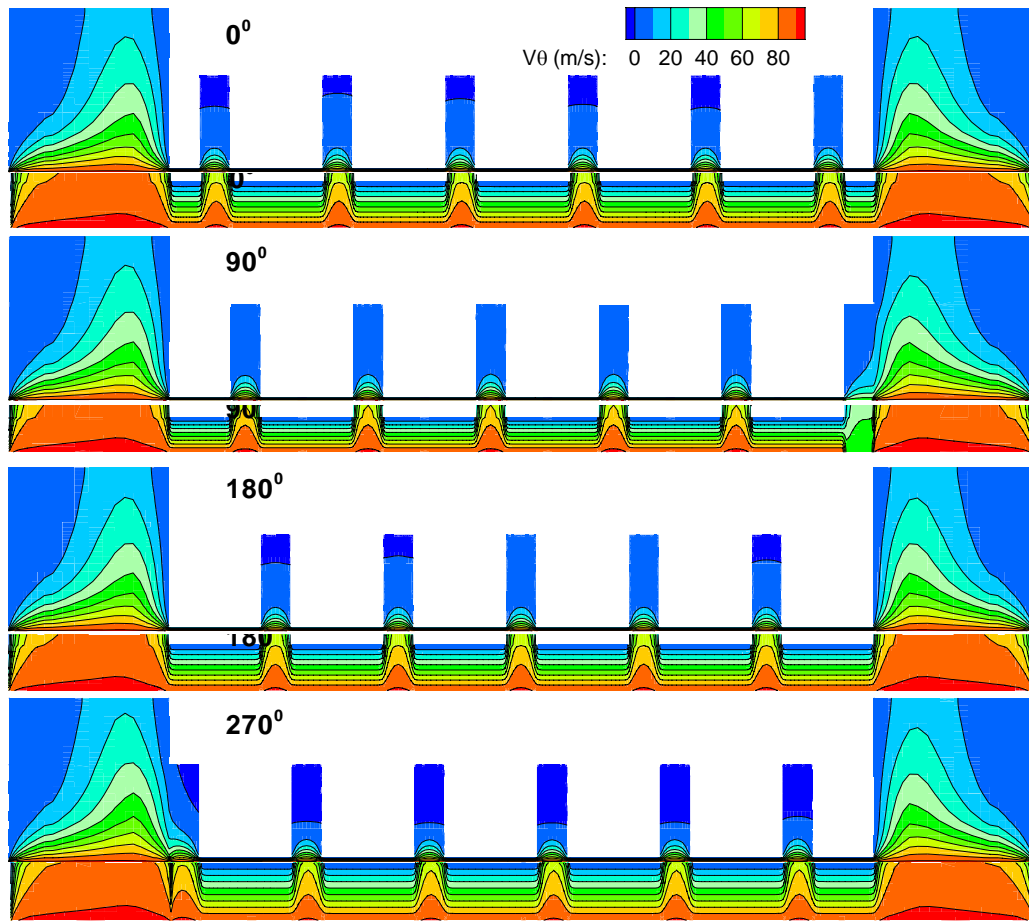
Figure D27. Circumferential velocity contour for the 25% eccentric windback seal with 75% tooth width of pitch in four angular sliced planes operating with the oil, DP=103.42 kPa, Ω=15,000 rpm, e=0.25, c=0.1016 mm
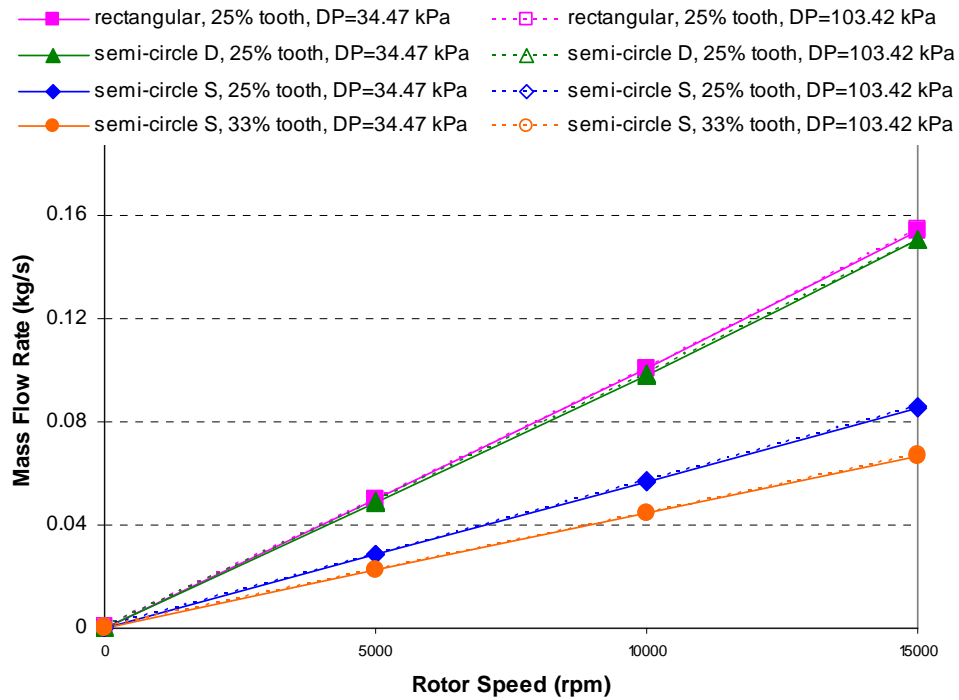
Figure D28. Oil leakage flow rate for the 25% eccentric windback seal with different cavity shapes, DP=34.47 kPa, 103.42 kPa, e=0.25, c=0.1016 mm
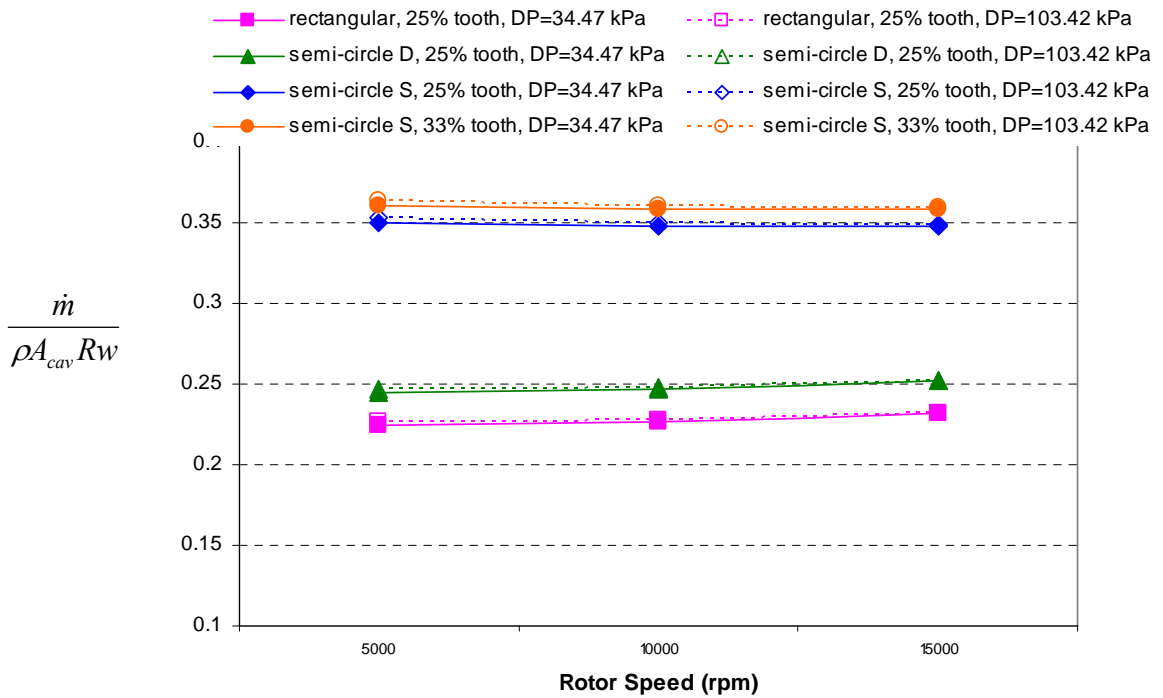
Figure D29. Oil leakage flow rate for the 25% eccentric windback seal with different cavity shapes, DP=34.47 kPa, 103.42 kPa, e=0.25, c=0.1016 mm
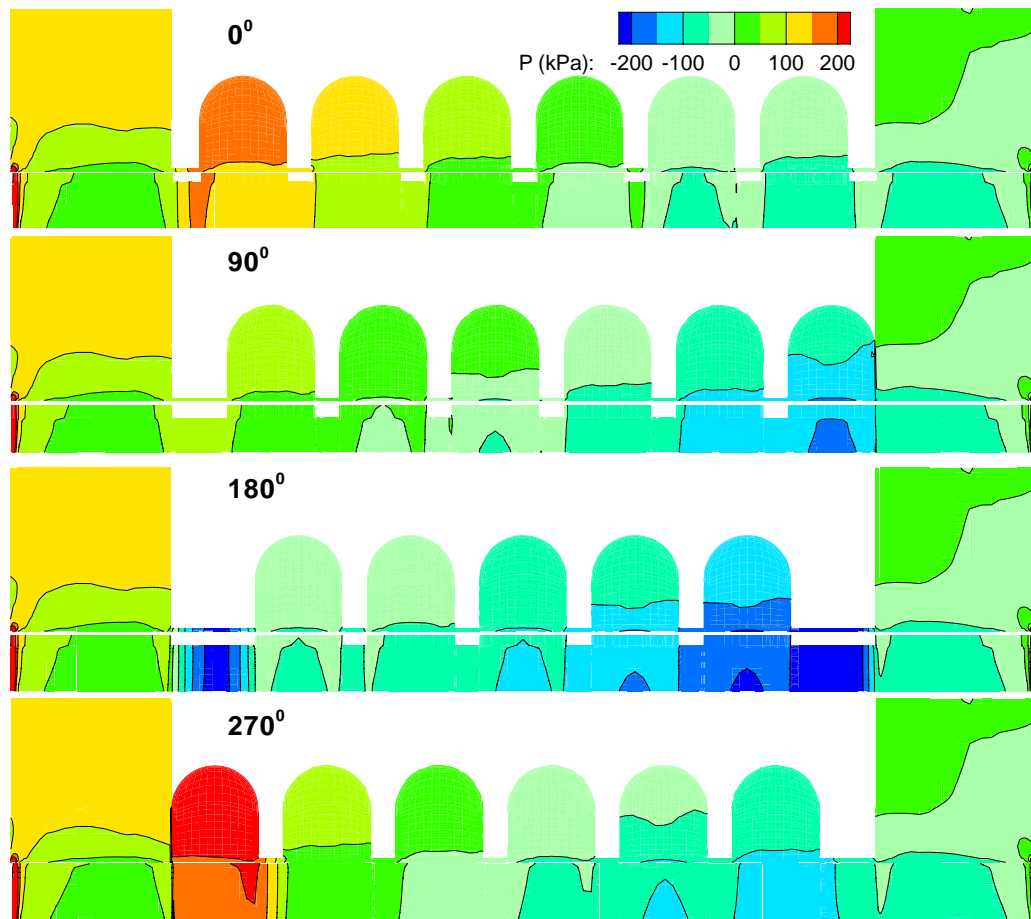
Figure D30. Pressure contours for the 25% rotor eccentric windback seal with 25% tooth width of pitch and semi-circular deep groove in four angular sliced planes operating with the oil, DP=103.42 kPa, Ω=15,000 rpm, e=0.25, c=0.1016 mm
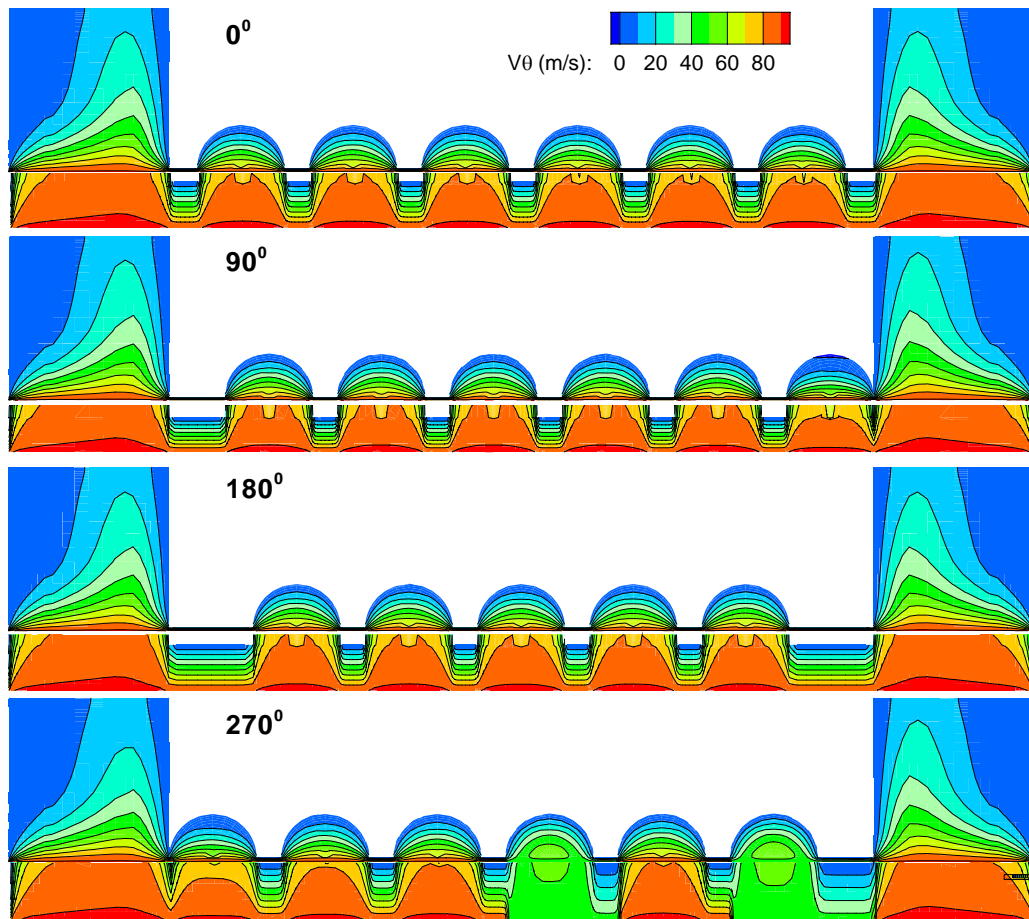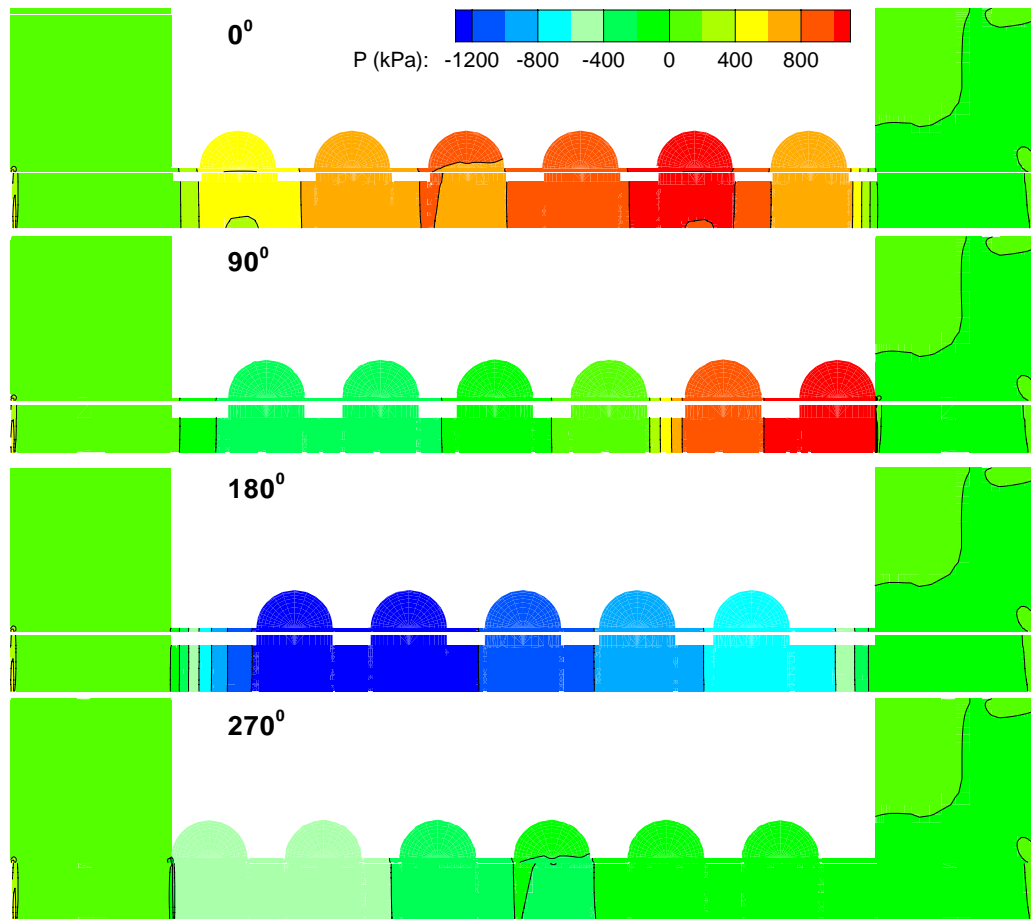
Figure D31. Axial velocity contours for the 25% rotor eccentric windback seal with 25% tooth width of pitch and semi-circular deep groove in four angular sliced planes operating with the oil, DP=103.42 kPa, Ω=15,000 rpm, e=0.25, c=0.1016 mm

Figure D32. Circumferential velocity contours for the 25% rotor eccentric windback seal with 25% tooth width of pitch and semi-circular deep groove in four angular sliced planes operating with the oil, DP=103.42 kPa, Ω=15,000 rpm, e=0.25, c=0.1016 mm
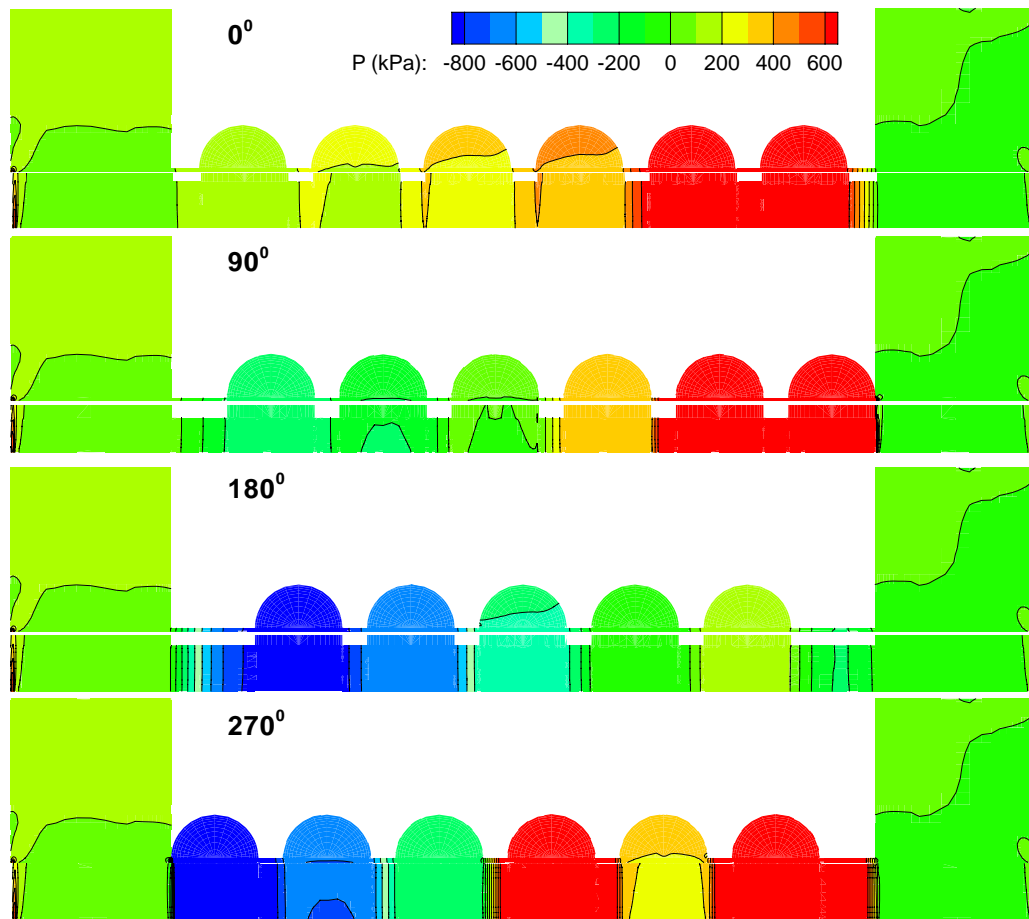
Figure D33. Pressure contours for the 25% rotor eccentric windback seal with 25% tooth width of pitch and semi-circular shallow groove in four angular sliced planes operating with the oil, DP=103.42 kPa, Ω=15,000 rpm, e=0.25, c=0.1016 mm
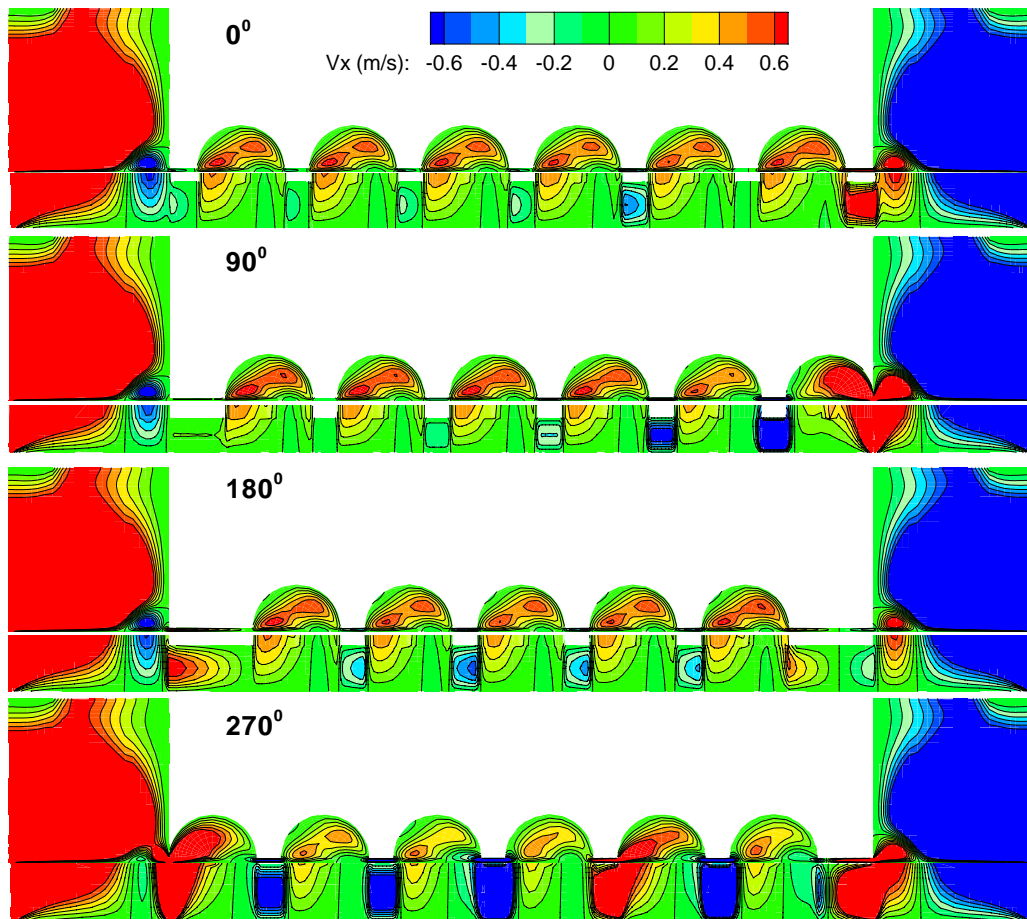
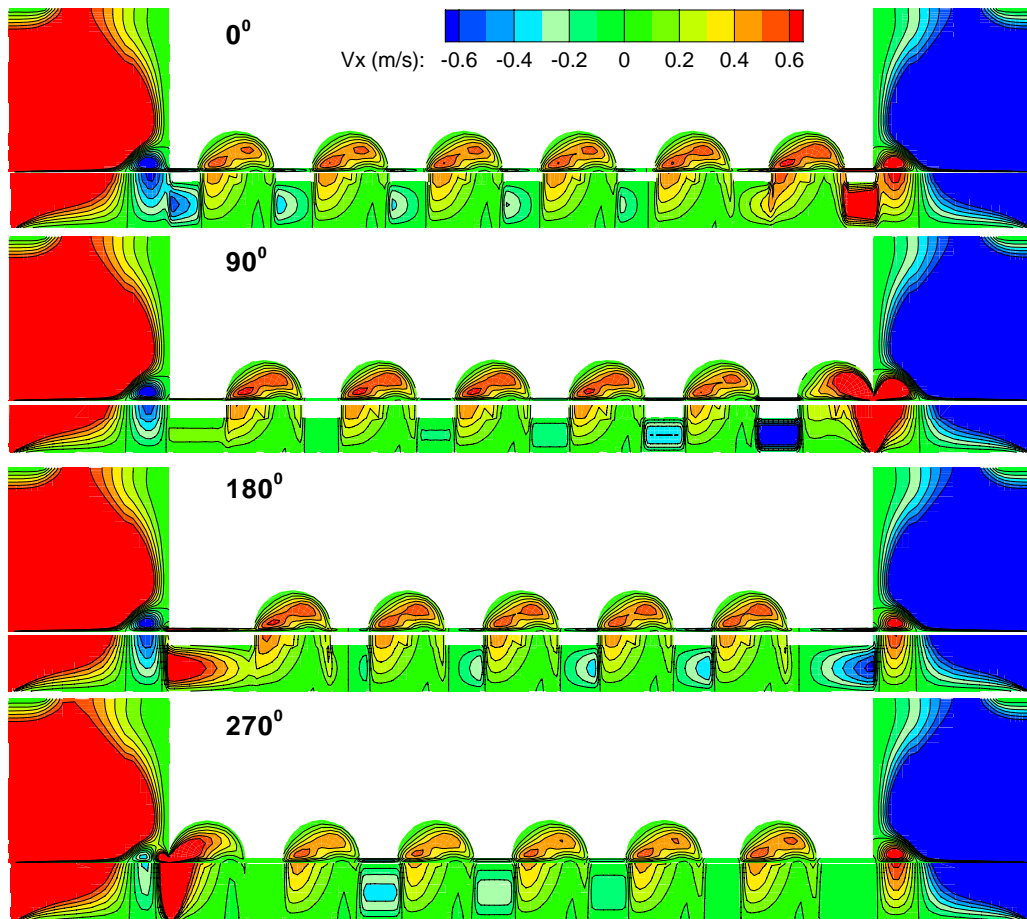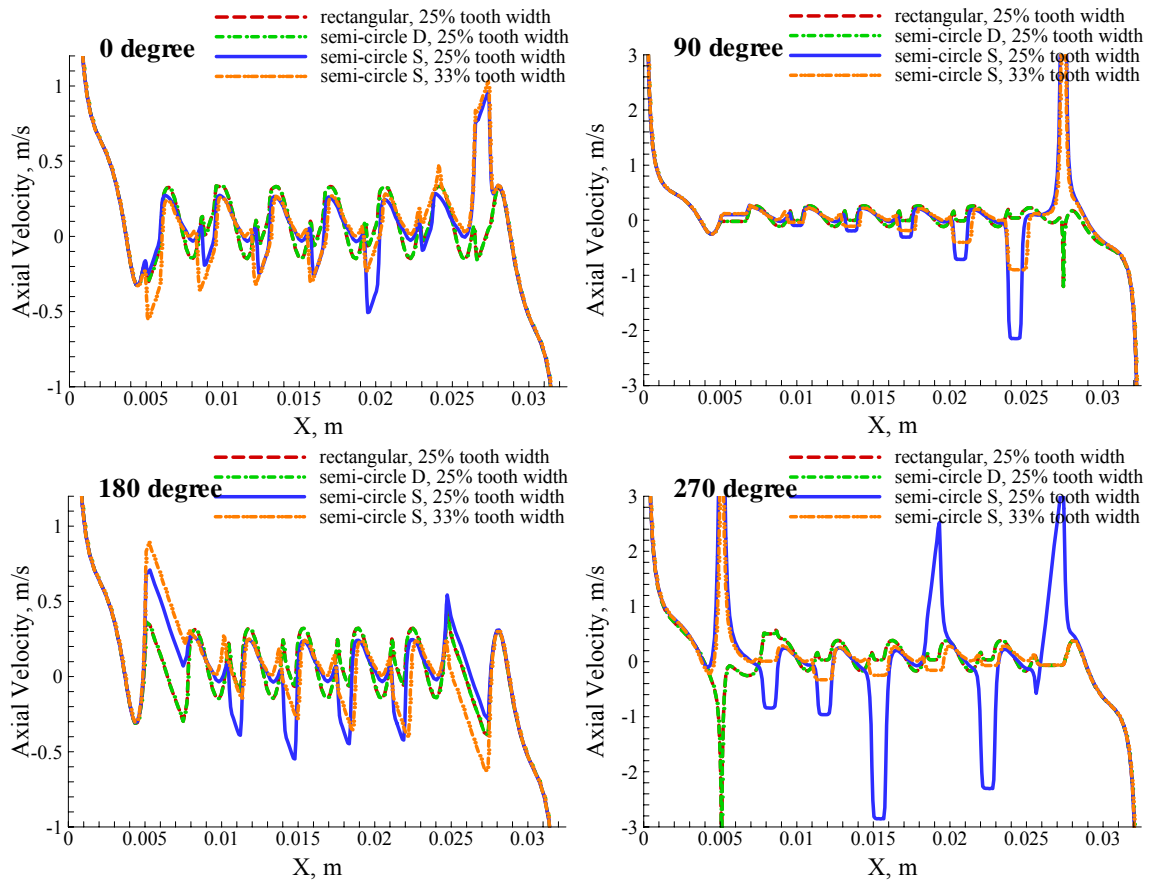Figure D34. Axial velocity contours for the 25% rotor eccentric windback seal with 25% tooth width of pitch and semi-circular shallow groove in four angular sliced planes operating with the oil, DP=103.42 kPa, Ω=15,000 rpm, e=0.25, c=0.1016 mm

Figure D35. Circumferential velocity contours for the 25% rotor eccentric windback seal with 25% tooth width of pitch and semi-circular shallow groove in four angular sliced planes operating with the oil, DP=103.42 kPa, Ω=15,000 rpm, e=0.25, c=0.1016 mm
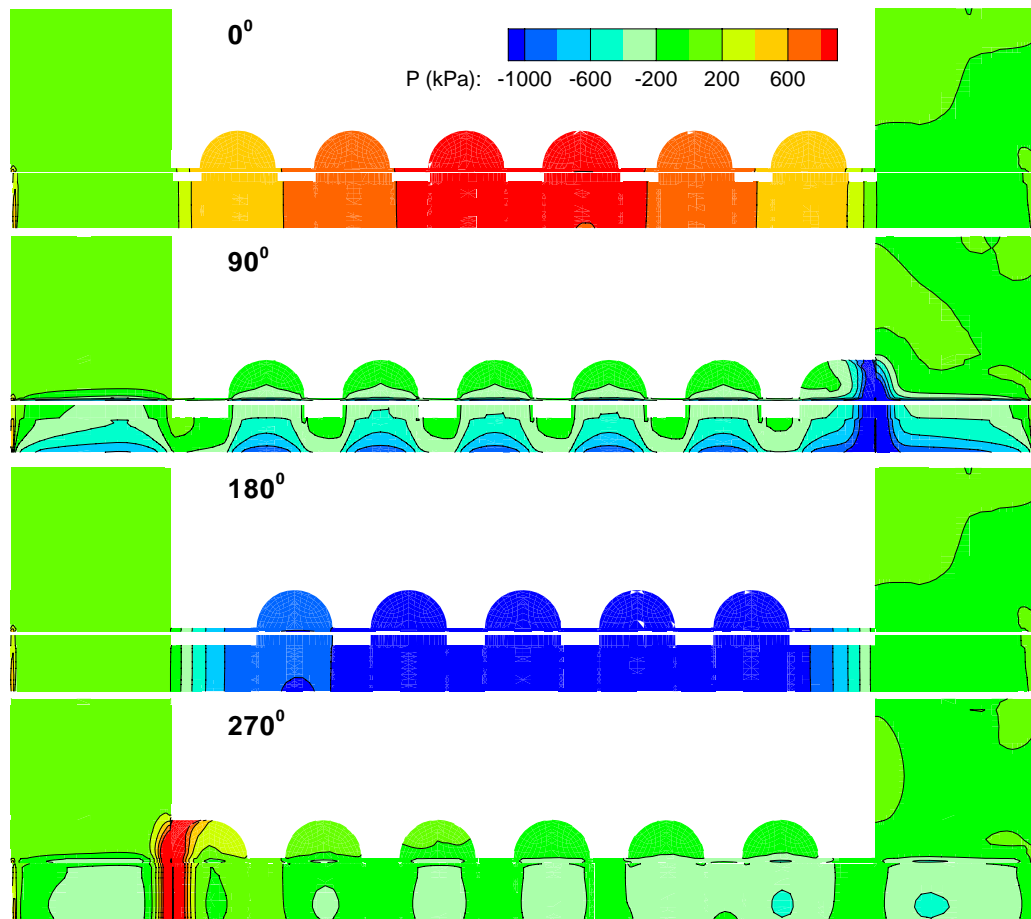
Figure D36. Pressure contour for 25% rotor eccentric windback seal with 33% tooth width of pitch and semi-circular shallow groove in four angular sliced planes operating with the oil, DP= 103.42 kPa, Ω=15,000 rpm, e=0.25, c=0.1016 mm

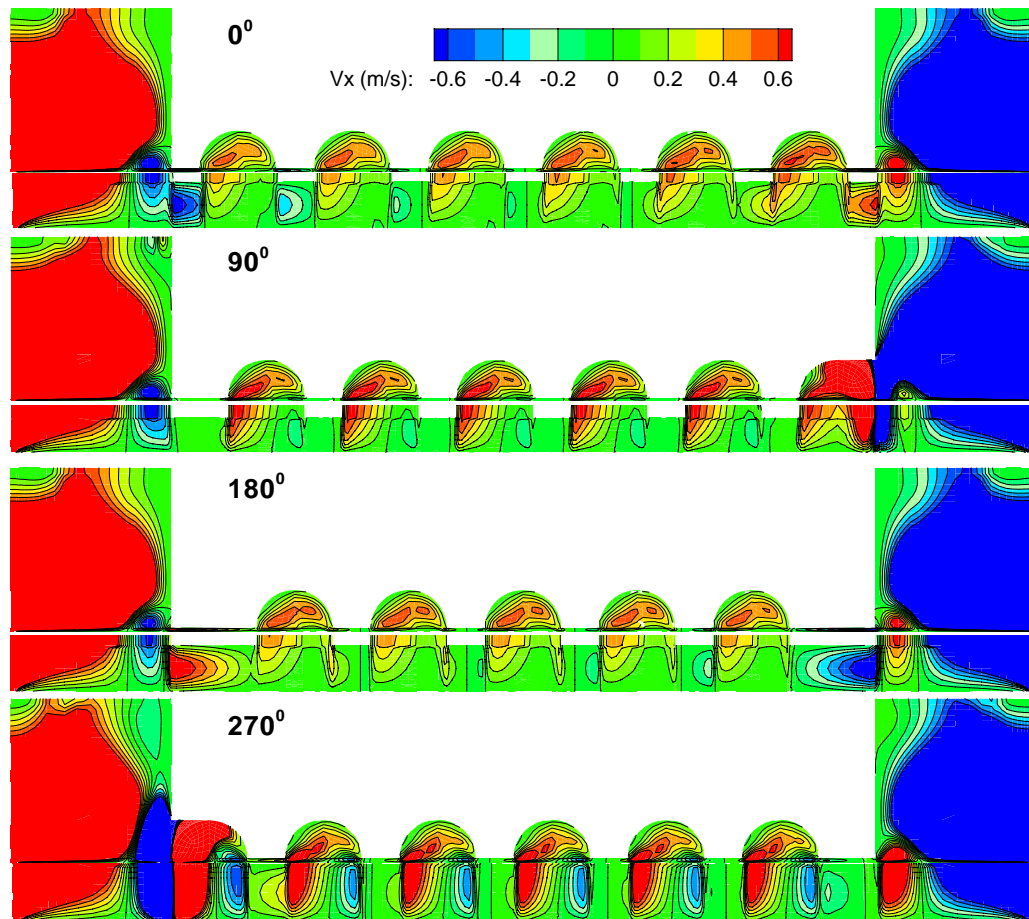Figure D37. Axial velocity contour for the windback seal with 33% tooth width of pitch and semi-circular groove in four angular sliced planes operating with the oil, DP= 103.42 kPa, Ω=15,000 rpm, e=0.25, c=0.1016 mm

Figure D38. Axial velocity distribution along the middle of clearance for four different cavity shape windback seals in four angular views operating with the oil at 103.42 kPa, and 15,000 rpm

234
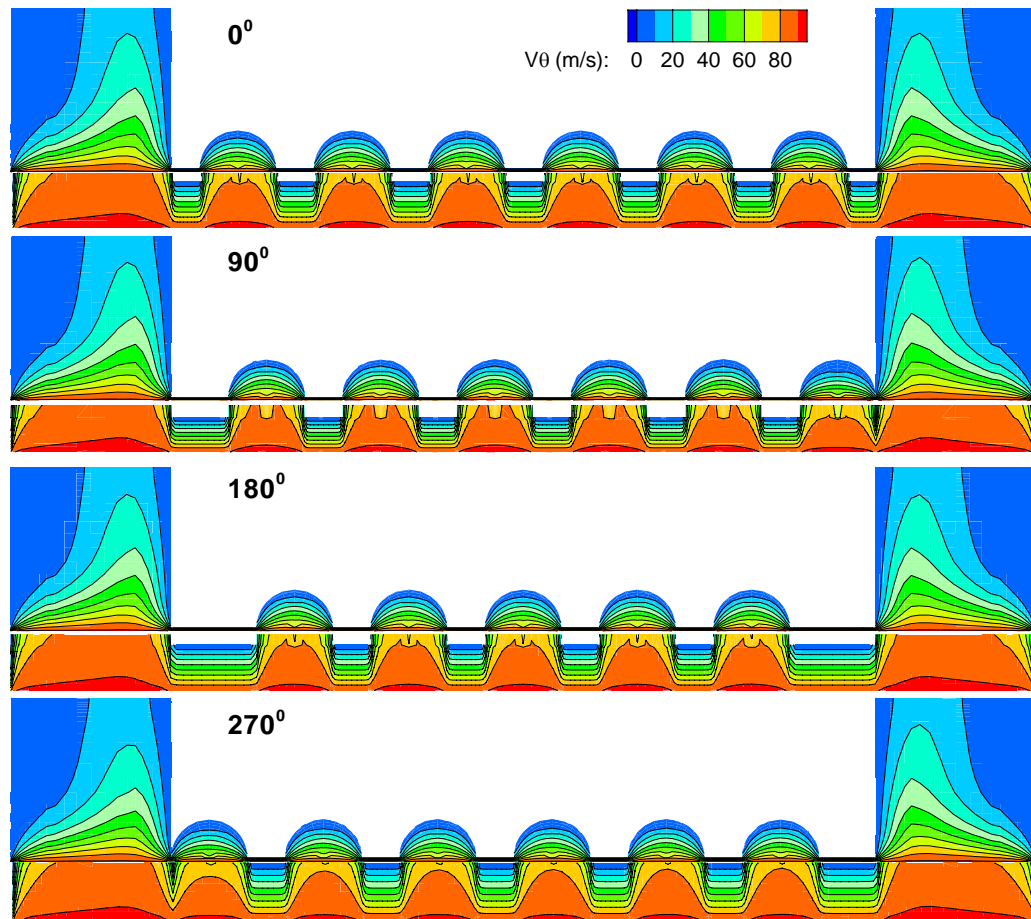
Figure D39. Circumferential velocity contour for the windback seal with 33% tooth width of pitch and semi-circular groove in four angular sliced planes operating with the oil, DP= 103.42 kPa, Ω=15,000 rpm, e=0.25, c=0.1016 mm

Figure D40. Pressure contour for 25% eccentric windback seal with 33% tooth width of pitch and modified semi-circular shallow groove in four angular sliced planes operating with the oil, DP=103.42 kPa, Ω=15,000 rpm, e=0.25, c=0.1016 mm
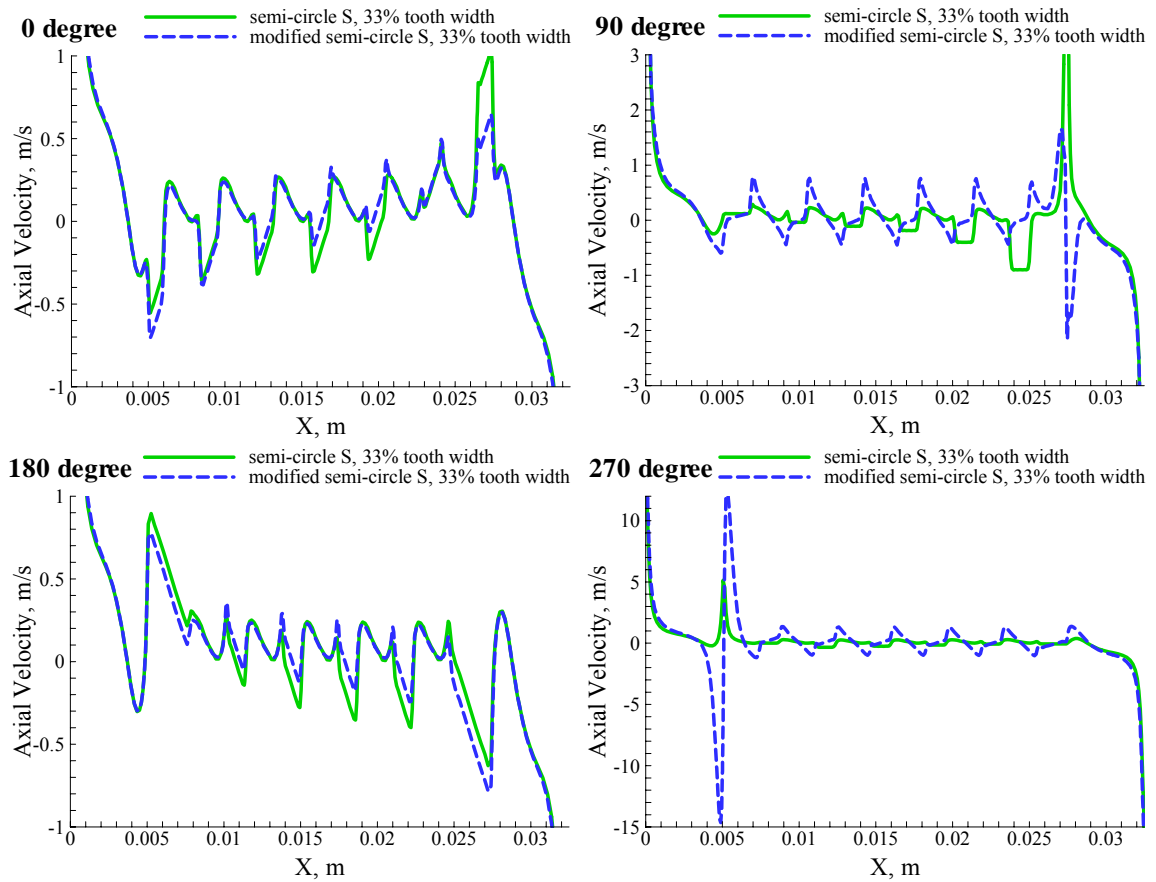
Figure D41. Axial velocity contour for 25% eccentric windback seal with 33% tooth width of pitch and modified semi-circular shallow groove in four angular sliced planes operating with the oil, DP=103.42 kPa, Ω=15,000 rpm, e=0.25, c=0.1016 mm

Figure D42. Axial velocity distribution along the middle of clearance for the semi-circular shallow windback seals with the 33% tooth width with two different open regions in four angular views operating with the oil at 103.42 kPa, and 15,000 rpm

APPENDIX E

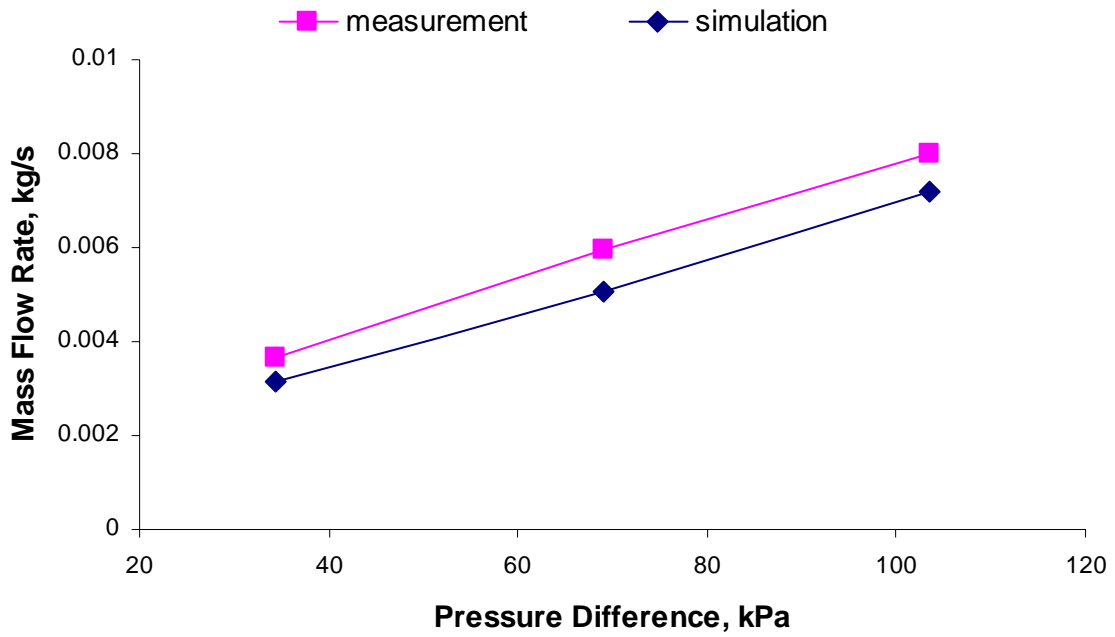This Appendix E contains the plots for the experimental results and empirical model.

Figure E1. Leakage flow rate versus pressure differential for the measurement and prediction
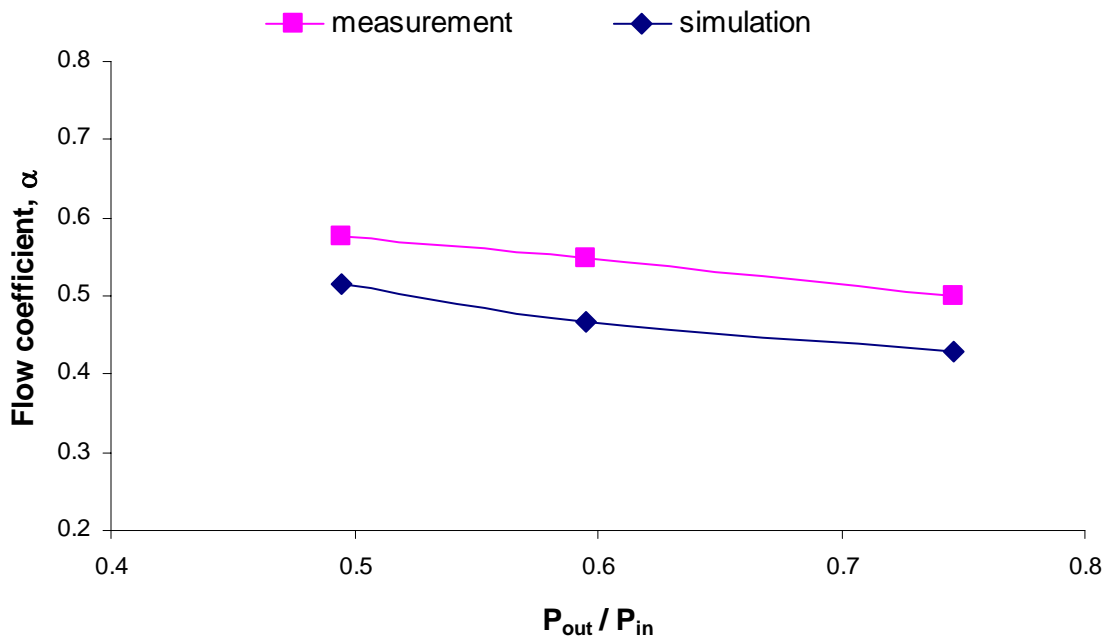

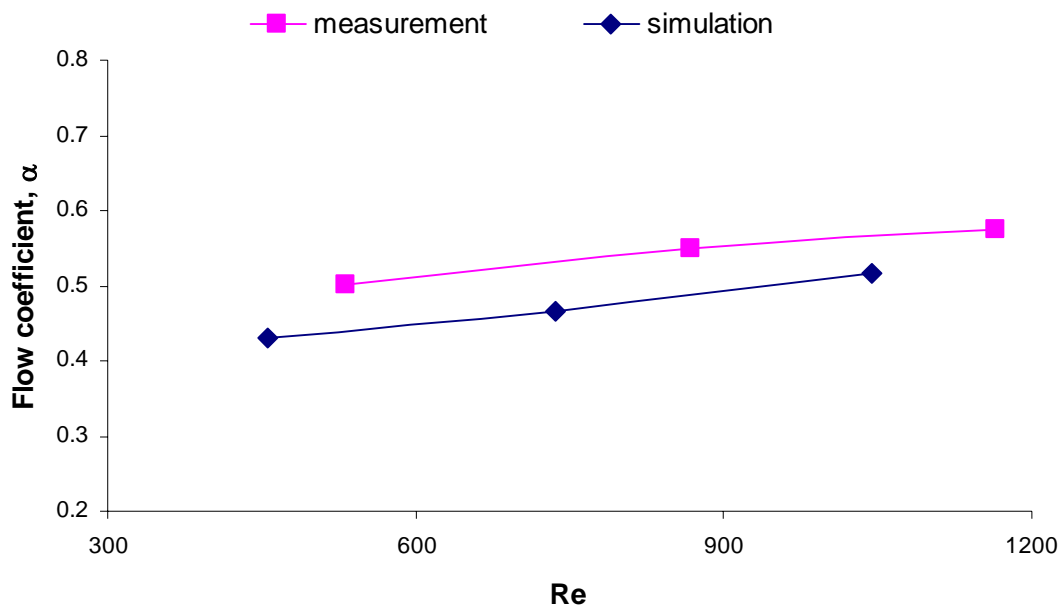Figure E2. Flow coefficient versus pressure ration for the measurement and prediction

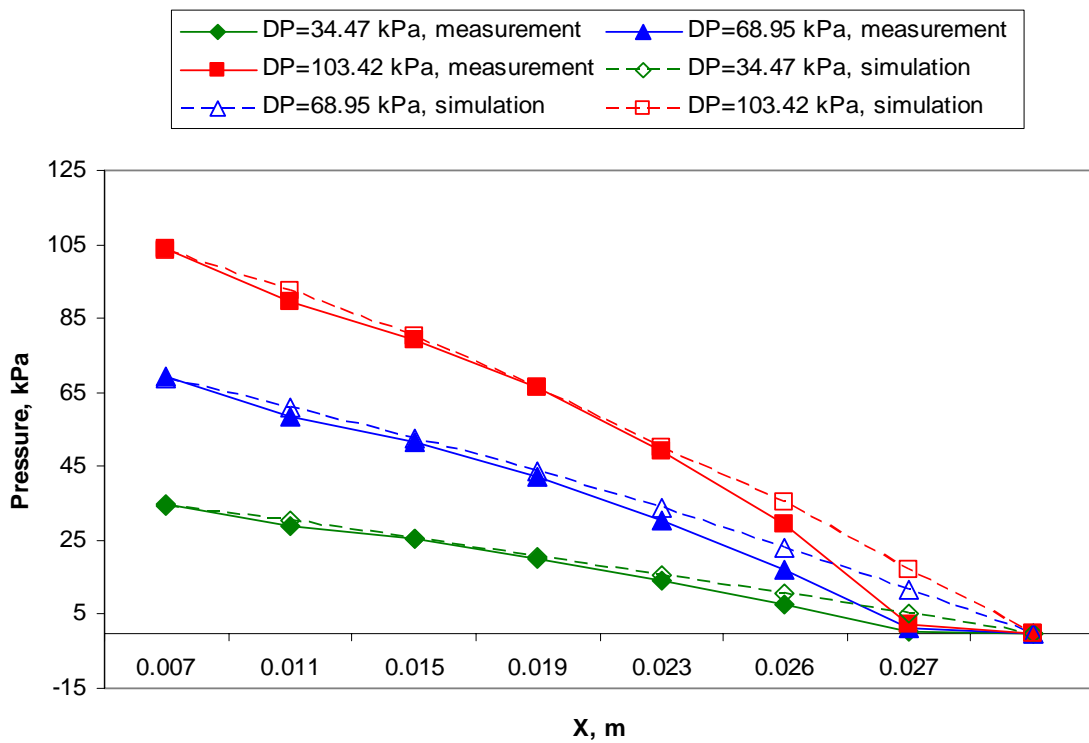Figure E3. Flow coefficient versus the axial Reynolds number for the measurement and prediction.

Figure E4. Pressure distribution for the measurement and simulation with three differential pressures and no rotation
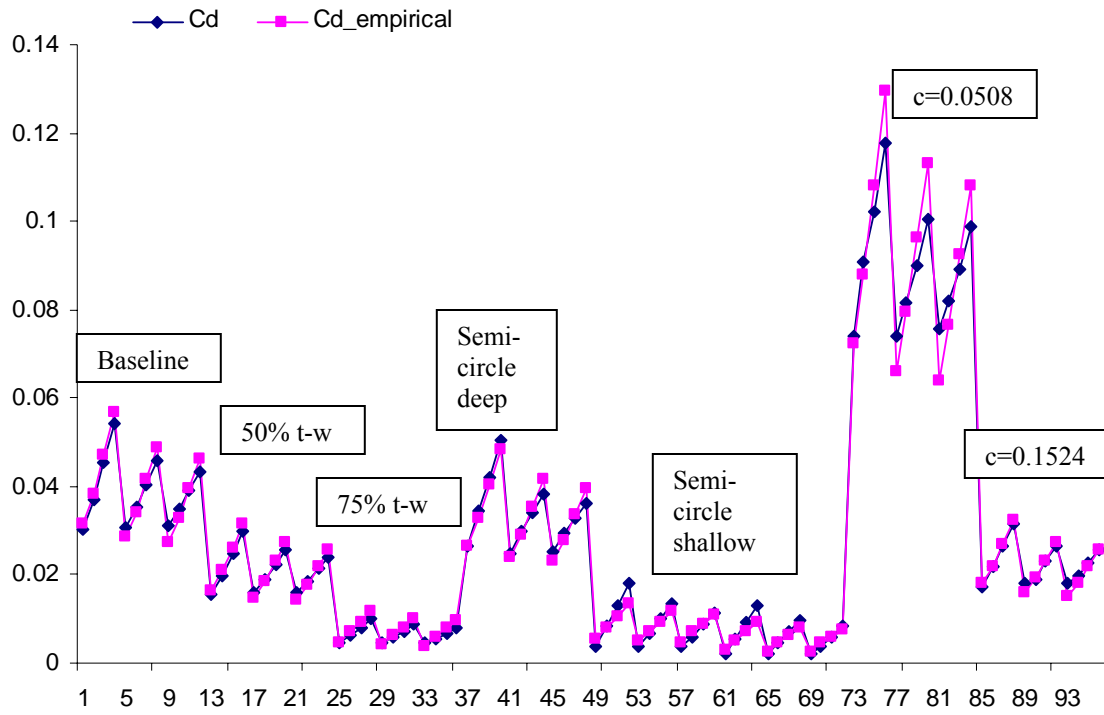
Figure E5. Comparison of the discharge coefficients from the numerical simulations and the empirical model for the cavity flow

VITA

Chae Hwan Lim was born in Seoul, Korea. In March 1990, he was admitted to Sungkyunkwan University in Seoul, Korea. He graduated with a B.S. degree in mechanical engineering in February 1994. He was an officer in the Korean Air Force from 1994 to 1998 and worked as a research engineer at the Hyundai Space & Aircraft Company from 1998 to 1999.

In September 1999, Chae Hwan Lim was admitted to Texas A&M University in the Department of Mechanical Engineering. He graduated with an M.S. degree in August 2004.

Chae Hwan Lim married in July 1999 and is blessed with a wonderful son, Alex, born in July 2002.

Chae Hwan Lim is reached at Department of Mechanical Engineering, c/o Dr. Gerald Morrison, Texas A&M University, College Station, TX 77843-3123. His email address is peterlim98@hotmail.com.